

The potential of nanoscale carriers for drug delivery to intestinal mucosa and skin

Dissertation
zur Erlangung des Grades
des Doktors der Naturwissenschaften
der Naturwissenschaftlich-Technischen Fakultät III
Chemie, Pharmazie, Bio- und Werkstoffwissenschaften
der Universität des Saarlandes

von
Barbara Weiß

Saarbrücken
2007

Tag des Kolloquiums: 1. März 2007

Dekan: Prof. Dr. Kaspar Hegetschweiler

Mitglieder des Prüfungsausschusses:

Vorsitzender:	Prof. Dr. Rolf Hempelmann
1. Gutachter:	Prof. Dr. Claus-Michael Lehr
2. Gutachter:	Prof. Dr. Udo Bakowsky

Akademischer Mitarbeiter: Dr. Ulrich Schäfer

Abstract

The subjects of the present thesis are the formulation and evaluation of poly(lactide-co-glycolide) (PLGA) based nanoparticles addressing the biological barriers intestine and skin. Fluorescence labelled PLGA nanoparticles were developed and characterized to visualize and study interactions with such anatomical sites. Stable fluorescence labelling was accomplished by a covalent polymer modification with fluoresceinamine and the potential of these nanoparticles to investigate penetration and storage in hair follicles was examined *in vitro* and *in vivo*. Additionally, fundamental research has been carried out that proves that they represent powerful tools to study accumulation and retention in inflamed intestinal mucosa in inflammatory bowel diseases in future clinical studies. Subsequently, the fluorescence labelled nanoparticles were advanced to dually fluorescence labelled nanoparticles by incorporation of a fluorescence dye as model drug. Those nanoparticles were applied to demonstrate the impact of multiphoton microscopy to simultaneously study penetration and drug release on excised human skin. Employing flufenamic acid as hydrophilic model drug, the influence of nanoencapsulation on drug penetration into the skin was studied using PLGA nanoparticles as drug carriers. Finally, a technique to surface functionalize preformed PLGA nanoparticles was developed. This approach may allow subsequent versatile binding of proteins (targeting moieties, drugs) and dyes for various applications of interest like targeting the intestinal mucosa.

Kurzzusammenfassung

Das Thema der vorliegenden Dissertation ist die Formulierung und Evaluierung von Nanopartikeln aus Polymilchsäure-co-glykolsäure (PLGA), die an der Darmschleimhaut und auf der Haut zum Einsatz kommen sollen. Zunächst wurden fluoreszenz-markierte PLGA Nanopartikel hergestellt und charakterisiert, um damit Wechselwirkungen mit diesen biologischen Barrieren zu visualisieren und zu erforschen. Zur stabilen Fluoreszenzmarkierung wurde PLGA kovalent mit Fluoreszeinamin modifiziert. Im Rahmen dieser Arbeit wurden diese Nanopartikel verwendet, um Transport und Deposition in Haarfollikeln *in vitro* und *in vivo* zu untersuchen. Des Weiteren erwiesen sie sich als viel versprechend, um künftig eine Anreicherung und Retention in entzündeter Darmschleimhaut bei Patienten mit chronisch entzündlichen Darmerkrankungen im Rahmen einer klinischen Studie zu überprüfen.

Die beschriebene Nanopartikel-Formulierung wurde weiter entwickelt, indem zusätzlich ein Fluoreszenzfarbstoff inkorporiert wurde, um als Modellarzneistoff zu dienen. An derartig modifizierten Nanopartikeln konnte gezeigt werden, dass es Multiphotonen-Mikroskopie ermöglicht, simultan Penetration und Arzneistofffreisetzung aus Nanopartikeln auf exzidierter Humanhaut zu visualisieren. Des Weiteren wurden PLGA Nanopartikel eingesetzt, um den Einfluss einer Verkapselung des lipophilen Modellarzneistoffs Flufenaminsäure auf den Transport in die Haut zu untersuchen.

Abschließend wurde eine Technik entwickelt, mit Hilfe derer die Oberfläche von PLGA Nanopartikeln nach ihrer Formierung modifiziert werden kann. Dadurch können vielseitig Proteine wie „Targeting“-Komponenten oder Proteinarzneistoffe und Fluoreszenzfarbstoffe an Nanopartikel gebunden werden.

Table of contents

Abstract / Kurzzusammenfassung	3
Table of contents.....	5
1 General introduction	7
2 Objectives.....	15
3 Essential experimental aspects of the present study.....	17
3.1 Poly(lactic acid-co-glycolic acid) as polymer for pharmaceutical applications.....	17
3.2 Preparation techniques of poly(lactic acid-co-glycolic acid) nanoparticles.....	18
3.2.1 Solvent evaporation and solvent extraction process.....	19
3.2.2 Salting-out.....	21
3.2.3 Nanoprecipitation.....	21
3.3 Loading of active compounds in poly(lactic acid-co-glycolic acid) nanoparticles and their release	22
3.4 Characterization techniques for nanoparticles.....	23
3.4.1 Photon correlation spectroscopy.....	24
3.4.2 Laser doppler electrophoresis.....	25
3.4.3 Scanning probe microscopy.....	26
3.4.4 Nuclear magnetic resonance spectroscopy.....	27
3.4.5 Differential scanning calorimetry.....	27
4 Results and discussion.....	29
4.1 Preparation, characterization, and evaluation of fluoresceinamine labelled PLGA nanoparticles.....	29
4.2 Application of fluorescent and drug containing nanoparticles to investigate skin permeation and penetration.....	33
4.2.1 Nanoparticles – an efficient carrier for drug delivery into the hair follicles.....	33
4.2.2 Multiphoton microscopy for the investigation of dermal penetration of nano- particle-borne drugs.....	36
4.2.3 Influence of nanoencapsulation on human skin transport of flufenamic acid.....	39
4.3 Surface biotinylated nanoparticles for coupling of versatile ligands.....	41
5 References.....	45

6	Forthcoming publications.....	57
6.1	Nanoparticles made of fluorescence-labelled poly(L-lactide-co-glycolide): preparation, stability, and biocompatibility.....	59
6.2	Nanoparticles – an efficient carrier for drug delivery into hair follicles.....	79
6.3	Multiphoton microscopy for the investigation of dermal penetration of nano- particle-borne drugs.....	103
6.4	Influence of nanoencapsulation on human skin transport of flufenamic acid.....	113
6.5	Coupling of biotin-(polyethyleneglycol)amine to poly(D,L-lactide-co-glycolide) nanoparticles for versatile surface modification.....	121
7	Summary / Zusammenfassung.....	163
	Publication list.....	175
	Curriculum vitae.....	177

1 General introduction

In the past 30 years, the explosive growth of nanotechnology has burst into challenging innovations in pharmacology with tremendous impact on both therapeutics and diagnostics.¹⁻¹³ In this context, colloidal systems are in the current limelight of interest due to their outstanding potential to target physiological sites, organs, tissues, or cells where the pharmacological activity of a drug is required or where physiological conditions have to be examined.

The concept of targeted drug delivery was already proposed by the immunologist Nobel laureate Paul Ehrlich in the beginning of the 20th century as so called “magic bullet”.¹⁴ However, today’s demands on colloidal targeted drug delivery devices have even become more complex: in addition, new systems should be non-toxic, biocompatible and biodegradable, the carrier core itself should be shielded by a protective layer against harmful environmental effects and/or charged for adsorption of active compounds or to facilitate tissue approach; frequently, they should also exhibit attributes like antigen detection, fluorescence labelling and shape/surface recognition. Thereby, the active compound is, preferentially, either entrapped in the core or specifically bound to linker groups on the particle surface (Figure 1).²

Nowadays, delivery technologies are still far away from the realization of such perfect systems, however, research is in continuous progress.¹⁵⁻²¹

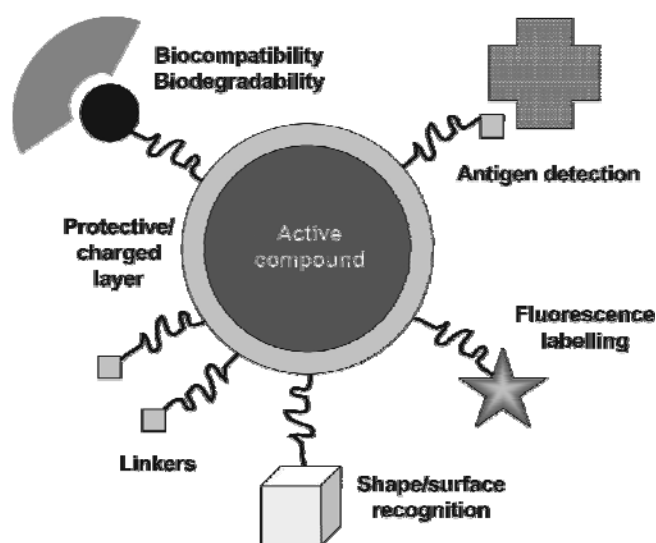


Figure 1: Approaches to the construction of an ideal colloidal drug delivery system²

Colloidal systems are generally defined to be in a size below 1 μm . Consequently, in literature, one can find an ocean of materials and formulations in this size range for potential applications in diagnostics and therapy: colloidal gold,²² iron oxide crystals,²³ and quantum dot semiconductor nanocrystals²⁴ as examples of promising diagnosis tools in medicine, and nanosuspensions,^{25, 26} nanoparticles,^{3, 4} nanoemulsions,²⁷ liposomes,²⁸ and micelles²⁹ as examples of approaches for drug delivery.

Solid nanoparticles (NP) are of special impact for targeted drug delivery since exhibiting significant interactions with various tissues of interest e.g. accumulation in tumors,^{6, 7} penetration into skin,^{8, 30} overcoming membrane barriers, particularly in the nose^{31, 32} and in the gastrointestinal tract,^{10, 33, 34} and improvement of drug transport over the blood brain barrier.^{9, 31}

Major subjects of this thesis are the formulation of NP with specific properties and investigations of interactions with the biological barriers skin and intestine. Hence, the subsequent part of this chapter aims current advances of research in these fields and represents a placement of present work.

Interactions of nanoparticles with the skin

Structure and composition of the skin provide an excellent barrier which confines percutaneous drug delivery.^{35, 36} Many approaches have been introduced in order to enhance transdermal delivery such as increasing the drug concentration in the vehicle, improving the partitioning between the vehicle and the skin, chemical penetration enhancers, and physical enhancement methods like iontophoresis and electroporation.³⁷⁻⁴¹ In the recent years, NP have attracted considerable interest as penetration enhancers not only for topical administration but also as an alternative route for the systemic drug administration.

Different penetration pathways into and through the stratum corneum, the main barrier of the skin, are known: the transepidermal pathway which means mainly intercellular penetration (the transcorneocyte is only of minor relevance) and the transappendageal routes i.e. via sweat glands and hair follicles. Different approaches have been undertaken in order to distinguish between follicular and intercellular penetration. E.g. Alvarez-Román et al.⁴² used confocal laser scanning microscopy for more

semiquantitative studies of the distribution of topically applied substances in different skin layers and appendages, Toll et al.⁴³ performed histological investigations, and Teichmann et al.⁴⁴ closed hair follicles artificially to investigate their influence on the penetration process of hydrophilic compounds.

Although comprising only 0.1% of the total skin surface, hair follicles⁴⁵ in particular have recently moved into the centre of interest for the topical application of free and NP associated drugs.^{3, 30, 45, 46} Different research groups showed that hair follicles provide a pathway for the penetration of NP,^{8, 46} thereby also acting as long-term reservoir.³⁰ In contrast, in the stratum corneum NP are stored mainly in the upper cell layers of corneocytes being quickly depleted by normal desquamation, textile contact, and washing.³⁰

However, as with most other biological barriers, the use of NP as drug carriers is strongly size-dependent. Here, NP were shown to penetrate better, the smaller the particle size.^{8, 46} Interestingly, large particles (> 5 µm) acted as highly efficient follicle blockers.⁴⁵

Besides nanoparticulate microfine metallic oxides used as powerful agents in sunscreens, NP described in literature for topical administration of cosmetics and drugs can be assigned to polymeric NP and solid lipid nanoparticles (SLN). A limited number of polymeric NP have been investigated with respect to their potential for transdermal drug administration. Hereby, biodegradable polymeric NP have clearly shown to significantly enhance the penetration of highly lipophilic compounds, when compared to non-particulate formulations.^{3, 46} Moreover, bioadhesive polymer NP have been studied as a sustained drug delivery system offering the possibility of improving the therapeutic index and the frequency of treatment.⁴⁷

During the past twenty years, SLN have been introduced as an alternative topical carrier system to traditional carriers, such as emulsions and liposomes. They have been studied to exhibit numerous advantages like protection of labile compounds from chemical degradation,⁴⁸ occlusion effects which can increase the water content in the skin, thus favouring drug penetration,^{49, 50} sustained release,^{51, 52} reduced systemic absorption,⁵³ and reduction of skin irritations.⁴⁹ Moreover, SLN are frequently described to act as UV sunscreen systems in cosmetics.^{54, 55} Especially in the last decade, intense research was focused on the use of SLN for the delivery of pharmaceutical compounds,

either topical (e.g. podophyllotoxin,⁵⁶ triptolide⁵⁷) or transdermal (e.g. insulin⁵⁸ and flurbiprofen⁵²).

However, facing problems like polymorphic transformations of the lipid matrix, low drug pay-load and drug expulsion during storage, nanostructured lipid carriers (NLC) have been recently introduced as new generation of SLN.^{59, 60} The concept is based on a blending of solid with liquid lipids, thus giving the lipid matrix a certain nanostructure and excluding the obstacles as with SLN.⁶¹

Transcutaneous vaccination represents a rather new concept of NP application to the skin; it has been evaluated as an attractive alternative to subcutaneous injection due to a high population of dendritic cells in the skin.⁶²⁻⁶⁴ However, this field appears to be rather unexplored so far, and mainly NP-based DNA vaccine systems facilitating DNA penetration into the skin have been studied.^{63, 64} Recently, Lademann's group found a size effect with 40 nm particles showing best properties for transcutaneous vaccine delivery.⁶²

Interactions of nanoparticles with the intestine

NP uptake from the gut is important as an additional route of entry to the systemic circulation⁶⁵ with high potential as a means of drug and vaccine delivery. Several studies have been done at cellular and tissue level in order to illuminate the way of particle uptake.⁶⁶⁻⁶⁸ Particles are described to be taken up either at the level of Peyer's patches (i.e. follicle-associated epithelium and M cells) or through the enterocytes (persorption).⁶⁸ In literature, it is clearly stated that neither of the possible ways of particle uptake is exclusive,^{69, 70} and conditions favouring one or the other are still subject to present investigations. Particle uptake is supposed to be greatly influenced by physicochemical properties such as size, zeta potential and hydrophobicity. In general, the absorption of particles is promoted by a smaller size.^{71, 72} Desai et al.⁶⁸ studied poly(lactic acid-co-glycolic acid) (PLGA) NP in the size range from 100 nm to 10 μ m in a rat intestinal model and found a significantly increased uptake in case of the 100 nm particles. Furthermore, they found that particle uptake of all sizes was to a higher extent mediated by Peyer's patch tissue than by nonpatch tissue, whereas both tissues had comparatively higher uptake when collected from the ileum than from the duodenum. Shakweh et al.⁷⁰ investigated influences of particle size and zeta potential

on the uptake of fluorescent PLGA NP by means of histological localization in intestinal tissue in mice. They saw that particles (300 nm; 1 μ m and 3 μ m) were taken up by Peyer's patches as well as bound to nonpatch tissue. They showed that smaller particles are taken up into the deep region of Peyer's patches and at greater rate than microparticles, which were found to remain localized in the dome region. In addition to particle size effects, they also found an influence of surface charge on the uptake via Peyer's patches: particles of negative or neutral zeta potential exhibited higher affinity than positively charged particles. The authors hypothesized that this finding is an effect of electrostatic interactions between the positively charged particles and the negative charged mucus gel layer slowing down the penetration of those particles and thus reducing the uptake. In contrast, other authors stated a preferred uptake of positively charged NP as consequence of NP interactions with negatively charged intestinal epithelial cells and mucus.^{73, 74}

Absorption of NP made of diverse materials has been enhanced by coupling the particles to molecules like lectins⁷⁵⁻⁷⁷ or invasins.^{78, 79} As consequence, the site of particle uptake shifts from the Peyer's patches to the nonpatch tissue, greatly augmenting the effective surface area, and thus increasing absorption.⁶⁹ Mucoadhesion represents another approach to improve drug absorption from orally administered NP; NP of different materials^{80, 81} and with diverse surface modifications^{33, 82} have been studied to exhibit mucoadhesive properties. Sandri et al.⁸³ investigated strong mucoadhesion with NP made of a chitosan modification. They also found that mucoadhesion delayed the absorption of NP, though, they produced an increase in contact time with the intestinal epithelia, hence offering a better chance for internalization.

Research on the use of NP for the oral route of administering active compounds, the most convenient way of delivering drugs, has shown that nanoencapsulation can protect active compounds from harmful attacks in the gastrointestinal milieu⁸⁴ and, conversely, also improve gastric tolerance of agents irritant to the stomach.⁸⁵ Moreover, nanoencapsulation can enhance drug absorption and bioavailability of entrapped or adsorbed molecules.^{33, 34} This is especially valuable with respect to the delivery of peptide and protein drugs with particular instability in the gastrointestinal tract and low permeability through the intestinal mucosa.⁸⁶ Intense research has been done on the oral delivery of nanoencapsulated insulin; in comparison to non-encapsulated orally

administered insulin, several authors showed an improvement in oral absorption and prolongation of the hypoglycaemic effect.⁸⁷⁻⁸⁹ Luo et al.⁹⁰ studied an increased absorption and a significant (4.17-fold) improve in the oral bioavailability of vinpocetine when entrapped into SLN in comparison to a solution of the free drug. Hariharan et al.⁷³ encapsulated the well absorbable but poorly bioavailable drug estradiol into NP from PLGA demonstrating sustained release from those formulations up to 7 days; in comparison, a steep fall in blood levels was observed in oral and i.v. administration of pure drug within a period of 2 h.

The feature of being adsorbed via Peyer's patches is the rationale of using NP for the development of formulations for mucosal immunization. Thereby, major interest of mucosal vaccination is that the resulting immunity will be expressed at the level of all mucosae, independently of where it has been induced.⁹¹ However, as with transcutaneous vaccination, the application of NP does not appear as well-investigated in this field up to now; only few studies can be found describing the development and evaluation of NP-based antigen (e.g. deriving from *Bordetella pertussis*⁹² or *Toxoplasma gondii*⁹³) and DNA vaccines⁹⁴ for oral administration.

Of special interest for an oral delivery of NP is the effect of gastrointestinal disease on important features of the intestinal barrier like mucus layer, epithelial permeability and capillary innervations; they can be changed, thus altering NP uptake pathways and processes.⁹⁵ Recently, new experimental therapeutic strategies have been described using particles as targeted drug carrier in inflammatory bowel disease (IBD). This approach is mainly based on two pathophysiological changes in inflamed tissue as under the conditions of IBD: first, a highly increased number of immune-related cells, and second, elevated mucus production allowing a higher adhesion of particulate carriers in the inflamed regions and enhanced permeability of the tissue leading to intense particle uptake.^{96, 97} This accumulation phenomenon was observed to be particle size dependent with an increasing effect for smaller particle diameters and highest efficiency in case of NP of around 100 nm.^{10, 98} Based on these results, several studies have been performed in rodent models with experimentally induced colitis comparing the effects of orally administered drugs in NP formulations with those of free drug solutions. Lamprecht et al.⁹⁶ showed the same efficiency in mitigating the inflammation, a sustained effect and a significant reduction of adverse effects after

administration of the anti-inflammatory drug rolipram encapsulated into NP. Meissner et al.⁹⁹ confirmed these results showing reduced nephrotoxicity when applying the immunosuppressive drug tacrolimus in nano-encapsulated formulation; in their case the drug effect was even increased in comparison to the free drug solution. Moreover, with the same drug tacrolimus, Lamprecht et al.⁹⁸ studied an about 3-fold higher penetration into the inflamed tissue compared to healthy tissue when using NP as drug carriers.

2 Objectives

The present work was focused on the formulation, characterization, and evaluation of PLGA based NP systems addressing the biological barriers intestine and skin. As first step, fluorescence labelled PLGA NP were developed to study and to visualise interactions with such anatomical sites. Within the scope of this work, the potential of those NP to investigate penetration and storage in hair follicles was examined *in vitro* and *in vivo*. Moreover, they may represent valuable tools in future clinical studies in inflammatory bowel diseases (IBD). Additionally incorporating a model drug compound, fluorescence labelled NP were advanced to dually fluorescence labelled NP; they were applied to demonstrate the impact of multiphoton microscopy to investigate dermal penetration and drug release. Using PLGA NP as drug carriers, their influence on drug penetration into the skin was studied employing flufenamic acid as hydrophobic model. Finally, the development of a technique to surface functionalize PLGA NP may allow subsequent versatile binding of proteins (targeting moieties, drugs) and dyes for various applications of interest e.g. targeting the intestinal mucosa.

The specific aims of each study were (the corresponding chapter is indicated within parenthesis):

- to develop and to characterize a formulation of stable fluorescence labelled non-toxic NP in order to investigate the potential of NP to target inflamed intestinal mucosa in IBD in a future clinical study. (4.1)
- to investigate the penetration and storage behaviour of fluorescence labelled NP in hair follicles in comparison to a free fluorescence dye. (4.2.1)
- to simultaneously study and visualize NP penetration and drug release in dermal administration employing a dually fluorescence labelled model system. (4.2.2)
- to investigate the effect of nanoencapsulation on the permeation and penetration of the lipophilic model drug flufenamic acid into excised human skin. (4.2.3)
- to develop a procedure to surface functionalize preformed polymeric NP for subsequent versatile conjugation of targeting ligands and fluorescence dyes under mild conditions. (4.3)

3 Essential experimental aspects of the present study

The following chapter briefly presents and discusses the principles of essential materials and methods applied in this thesis. The techniques described are focussed on the formulation and physicochemical characterization of polymeric NP.

3.1 Poly(lactic acid-co-glycolic acid) as polymer for pharmaceutical applications

Since the last three decades, synthetic biodegradable polymers have been increasingly used to deliver drugs. Amongst them the aliphatic poly(esters) poly(lactic acid) (PLA), poly(glycolic acid) (PGA), and their copolymers poly(lactic acid-co-glycolic acid) (PLGA) (Figure 2) have generated special interest due to their excellent biocompatibility and biodegradability.¹⁰⁰

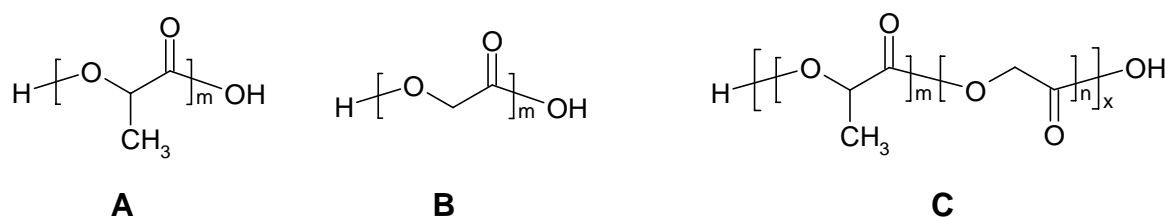


Figure 2: Chemical structures of poly(lactic acid) (A), poly(glycolic acid) (B), and poly(lactic acid-co-glycolic acid) (C)

During the late 1960s and early 1970s, pioneering work on the utility of lactide/glycolide polymers to make bioresorbable sutures/fibres was published first.¹¹ Since then, especially PGA was and still is used as biodegradable suture material. The wide acceptance of the lactide/glycolide polymers made them further attractive to various biomedical applications like tracheal replacement, vascular grafts, or dental and fracture repair.¹⁰⁰ Nowadays, because they are part of FDA approved drug products for parenteral administration, those polymers are most common for the fabrication of modern controlled release devices like microparticles, NP, films, and implants.¹⁰⁰

PLGA can be directly synthesized from monomers. However, it is also commercially available in different molar ratios of glycolic and lactic acid and in different molecular weights of the polymer chains. Thereby, the physicochemical properties of PLGA are strongly dependent on the nature of the monomers. L-PLA was generally found to be semi-crystalline in nature whereas D,L-PLA is amorphous due to irregularities in the

chain structure; PGA was reported to be highly crystalline. Lactic acid is more hydrophobic than glycolic acid, hence, by variation of the glycolic acid/lactic acid ratio important polymer features like mechanical strength, crystallinity, swelling, polymer degradation rate and hydrolysis can be controlled.^{11, 100}

Both *in vitro* and *in vivo* PLGA undergoes degradation in aqueous environment through scission of its backbone ester linkages.¹⁰¹ In general, degradation time will be shorter for low molecular weight, hydrophilic, amorphous polymers, and for copolymers with higher content of glycolide.¹⁰² E.g. the most widely used PLGA copolymer composition of 50:50 has the fastest degradation rate of the D,L-lactic acid/glycolic acid materials. This polymer degrades in about 50-60 days.¹¹ It is well known that bulk erosion is the main degradation mechanism with PLGA devices.^{18, 103} Polymer chains are cleaved randomly throughout the polymer matrix leading to a subsequent decrease of molecular weight without any appreciable weight loss. For PLGA biodegradation a three-phase mechanism has been proposed where first, a random chain scission results in a decrease in molecular weight of the polymer without any significant weight loss. Second, the decrease in molecular weight is accompanied by rapid loss of mass due to the formation of soluble degradation products. Third, soluble monomer products are formed from soluble oligomeric fragments leading to a complete polymer solubilization.¹⁰⁰ Finally, the degradation products are easily metabolized in the body via the Krebs cycle and subsequently eliminated.¹⁰⁴

In conclusion, from the toxicological point of view, PLGA represents a well characterized, biocompatible and biodegradable polymer. Its tissue response is characterized by minimal localized inflammation and a foreign body reaction that decreases with time. The monomers D,L-lactide and glycolide possess a low acute toxicity, probably as a consequence of rapid metabolism, and no apparent long-term effects.¹¹

3.2 Preparation techniques of poly(lactic acid-co-glycolic acid) nanoparticles

The choice of the process employed for NP preparation governs the formation of either nanocapsules or nanospheres. Nanocapsules are defined as hollow NP where a polymer membrane encloses a drug reservoir; nanospheres consist of a solid polymer matrix in which the active compound is embedded.

Several methods have been developed to obtain polymeric particles in the nanosize range. Roughly, they can be categorized into two main strategies: formation of NP by emulsion polymerization of monomers and preparation of NP from preformed polymers.¹¹ Nowadays, the use of preformed polymers is first choice for the preparation of PLGA NP due to a good commercial availability of diverse PLGA polymers with standardized physicochemical characteristics. The following overview of the basic methods of NP preparation from preformed polymers provides some background information about the applicability and the mechanism from a physicochemical point of view.

Generally, NP preparation methods have to meet the following requirements:

- No adverse effect on stability and biological activity of the encapsulated active compound
- Reproducible quality and drug release profile of the NP within specified limits
- High encapsulation efficiency
- High yield of NP in the desired size range; narrow size distribution
- Stability of the NP in aqueous medium or as lyophilized product

3.2.1 Solvent evaporation and solvent extraction process

Single emulsion process

The preformed polymer is dissolved in an organic volatile solvent (e.g. dichloromethane¹⁰⁵, ethyl acetate¹⁰⁶); the drug is added to the polymer solution to further produce a solution or dispersion of the drug. The organic phase is emulsified in a larger volume of aqueous solution (with appropriate stirring and temperature conditions) in presence of a stabilizer (e.g. poly(vinyl alcohol)¹⁰⁶, didodecyl dimethyl ammonium bromide),¹¹ to yield an oil-in-water (o/w) emulsion. The emulsion is then subjected to a solvent displacement and a subsequent hardening of the oil droplets (Figure 3).

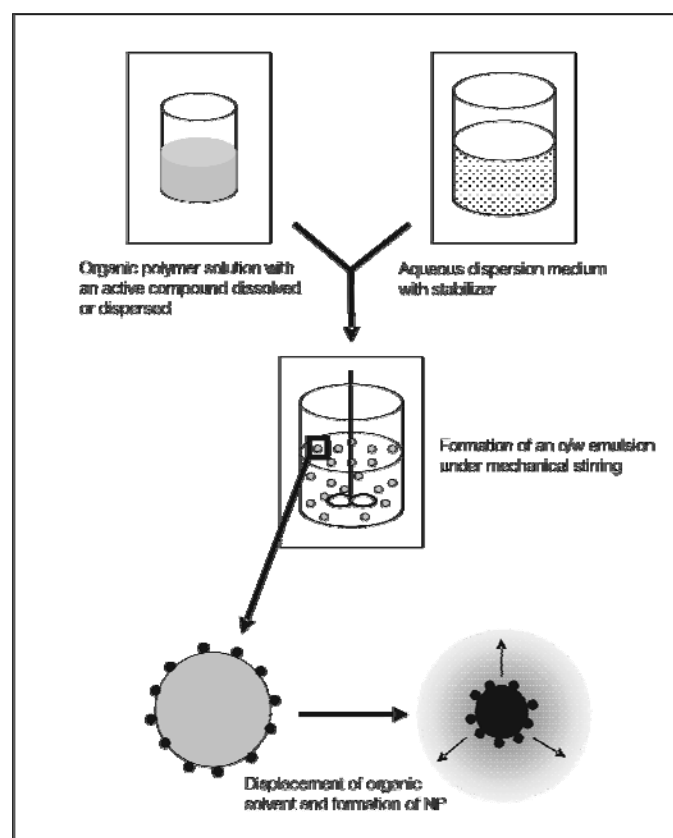


Figure 3: General procedure of a solvent displacement process used for NP preparation

In case of a water-immiscible organic solvent, the emulsion is maintained at reduced pressure¹⁰⁷ or at atmospheric pressure and the stir rate is reduced to enable the organic solvent to evaporate (solvent evaporation). In case of a partially water-miscible organic solvent, the emulsion is transferred into a large quantity of aqueous medium into which the solvent associated with the oil droplets can diffuse (solvent extraction).^{11, 108} The single emulsion process is ideal for the encapsulation of water insoluble drugs such as steroids.^{12, 100}

Double (multiple) emulsion process

The single emulsion method is confined to the entrapment of lipophilic compounds; hydrophilic compounds tend to show diffusion and partitioning from the dispersed oil phase into the continuous aqueous phase. Therefore, for an encapsulation of hydrophilic agents, the single emulsion method has to be upgraded to a double emulsion process. A buffered or plain aqueous solution of the compound, additionally

containing a viscosity building and/or stabilizing agent if necessary, is added to the organic polymer solution under vigorous stirring to form the first microfine water-in-oil (w/o) solution. This emulsion is added gently with stirring into a second aqueous phase containing stabilizers to form a water-in-oil-in-water (w/o/w) emulsion. As described above, the organic solvent is removed by evaporation or extraction.

This double emulsion process is best suited to encapsulate hydrophilic drugs like peptides and proteins, also in terms of protein stability.^{19, 105, 109}

3.2.2 Salting-out

This technique can be considered as a special version of the emulsion method: the polymer and the active compound dissolved in a water-miscible organic solvent (e.g. acetone) are added to an aqueous solution of a stabilizer and the salting-out agent (e.g. $MgCl_2$) in saturation under vigorous mechanical stirring. Thereby, diffusion of the water-miscible organic solvent in the outer aqueous phase is inhibited by the presence of the saturated salt solution (salting-out effect) until the volume of the aqueous phase is increased leading to subsequent formation of NP.^{13, 20, 110}

3.2.3 Nanoprecipitation

The nanoprecipitation method was first developed and patented by Fessi and co-workers.¹¹¹ It gives the advantage of a rapid, easy, and reproducible performance and it is best valuable for the entrapment of lipophilic compounds. In contrast to the emulsion processes, two miscible solvents are employed, only one of them being also a solvent for the polymer (e.g. water containing stabilizers and acetone). Briefly, both the polymer and the active compound are dissolved; nanoprecipitation occurs by a rapid desolvation of the polymer when the polymer solution is added to the non-solvent, thereby encapsulating the drug. The rapid NP formation is governed by the Marangoni effect, which describes turbulences at the interface of the solvent and the non-solvent.^{111, 112} As for the emulsion process, first steps have already been made to adapt this technique for the entrapment of hydrophilic drugs. This is especially relevant for the encapsulation of hydrophilic proteins which might suffer from solvent interfaces, high shear rates, and hydrolytic degradation when employing the double emulsion process.¹¹³

All methods described above require purification of the NP to remove residual organic solvent, stabilizer, or non-encapsulated free drug. The purification method has to be selected carefully to avoid NP aggregation or drug loss; commonly applied techniques are ultracentrifugation, ultrafiltration, dialysis or cross-flow filtration.

Due to the immense surface area and the resulting energetic and thermodynamic instability, NP tend to agglomerate during storage especially in liquid formulations; to overcome this problem lyophilization is best established.^{11, 114, 115}

3.3 Loading of active compounds in poly(lactic acid-co-glycolic acid) nanoparticles and their release

The encapsulation capacity of NP and the release kinetics of active compounds are major criteria in the development of NP formulations.

A successful NP system is considered to be the one, which has a high loading capacity to reduce the quantity of the carrier required for application. Thereby, the encapsulation efficiency depends on the preparation method, NP size and the nature of the polymer and drug. Generally, loading of active compounds into NP is achieved by two methods. First, agents can be incorporated at the time of NP preparation, i.e. during polymerization process or when the preformed polymer is dissolved (as described in chapter 3.2). Second, drugs can be physically adsorbed after formulation of the NP. Adsorption isotherms for the respective system give vital information on the best possible formulation; normally, adsorption of active compounds onto NP follows the Langmuir mechanism.¹¹⁶ Consequently, it is evident that a large amount of drug can be entrapped by the incorporation method when compared to the adsorption.¹¹⁷ In addition to the common methods adsorption and incorporation of drugs, new techniques of drug loading have been developed. Yoo et al.¹¹⁸ proposed a technique where the drug was chemically conjugated to the polymer PLGA prior to NP formation. However, this method is only applicable for compounds with active sites for chemical modifications. In order to enable a more versatile binding of substances to the surface of NP, various techniques have been developed recently where for instance polymers have been chemically linked with biotin. After NP preparations, those systems exhibit biotin surface groups for the binding of avidin (or homologues) which can be further conjugated to other compounds.^{15, 16, 21}

Release profiles of active substances from NP are again dependent on both the kind of NP and the preparation method applied. Generally, the smaller the NP and the larger the surface, the faster the release can be expected. In case of a NP device where the drug is uniformly distributed or dissolved in the matrix, the release occurs either by diffusion or by erosion of the matrix, or both. In case of surface bound or surface adsorbed compounds, the release is governed by drug detachment and by partitioning processes. In order to study the *in vitro* release rates of NP the technical difficulty of NP separation from the release media has to be overcome. Most common methods for that approach are: side-by-side diffusion cells with artificial membranes, dialysis bag diffusion techniques, (ultra-) centrifugation, (ultra-) filtration and centrifugal ultrafiltration techniques^{110, 117, 119, 120} combined with HPLC analysis or spectroscopic measurements of the release media.

3.4 Characterization techniques for nanoparticles

The characterization of nanoparticulate systems for pharmaceutical applications can be categorized into physicochemical and biopharmaceutical aspects. The physicochemical characterization involves the determination of parameters like particle size, size distribution, morphology, and surface properties; the biopharmaceutical characterization covers determination of drug encapsulation and release, biodistribution and bioavailability.

For the physicochemical analysis and characterization of polymeric NP the following methods are generally considered as state-of-the-art.^{11, 121}

- Photon correlation spectroscopy for the determination of particle size and size distribution
- Laser Doppler electrophoresis for the measurement of zeta potential (surface charge density)
- Scanning probe microscopy for the investigation of morphology, surface and mechanical properties
- Scanning electron microscopy and transmission electron microscopy for imaging of the particle morphology

- X-ray photoelectron spectroscopy, Fourier transform infrared spectroscopy, and nuclear magnetic resonance spectroscopy for the investigation of polymer and surface chemistry
- Differential scanning calorimetry for the determination of thermal properties of polymers and particles

Subsequently, this chapter focuses on the characterization techniques for NP applied in the course of this thesis.

3.4.1 Photon correlation spectroscopy

It is well known that NP size is a crucial factor to the release of active compounds,^{122, 123} degradation,^{103, 123, 124} deposition,¹⁰ tissue penetration¹²⁵ and even cellular uptake.^{11, 126} Furthermore, particle size is an important parameter in in-process control and quality assurance because the physical stability of particle dispersions depends on size and size distribution.¹²⁷

Photon correlation spectroscopy (PCS) represents a routine method to determine the NP mean hydrodynamic diameter and the particle size distribution (polydispersity). It is based on the scattering of a laser light employed onto a dispersion of spherical NP in Brownian motion; the light fluctuations increase as particle size decreases and Brownian motion increases. The scattered light is detected by a photomultiplier which is usually located in a 90° angle position transforming the variation of light intensity into a variation of voltage (Figure 4). Finally, PCS results derive from a correlation between the different intensities within short time intervals; generally, they determine the particle size distribution and the z-average which corresponds to the hydrodynamic diameter of the particles.¹²⁷ The hydrodynamic diameter is strongly influenced by adhesion of water molecules on the particle surface and can differ significantly from the true physical diameter. For that reason, in all cases, an additional method like scanning probe or electron microscopy should be applied.

The polydispersity index (PI) is a dimensionless measure for the broadness of a particle size distribution and can be used for the evaluation of NP preparation. In practice, NP dispersions with a PI between 0.03 and 0.06 can be denoted as mono-disperse, between 0.1 and 0.2 as narrowly distributed, and between 0.25 and 0.5 as broadly

distributed. Values above 0.5 indicate an extremely broad size distribution that can not be described by means of PI.¹²⁸

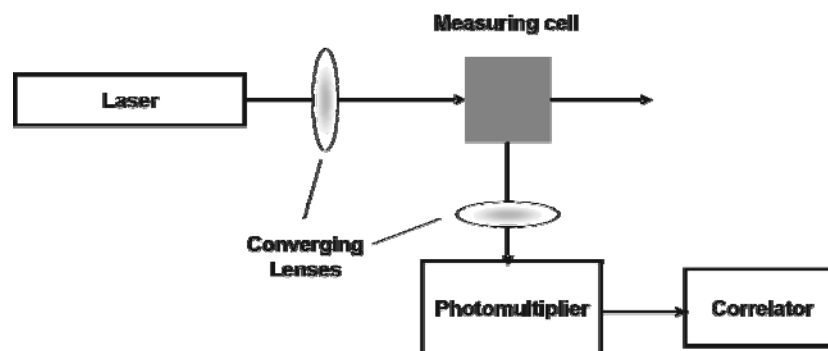


Figure 4: Schematic setup of a PCS apparatus

3.4.2 Laser doppler electrophoresis

Each non-neutral particle dispersed in a polar solution is surrounded by oppositely charged ions forming a fixed layer. Outside the fixed layer, there are ions of opposite polarities, forming cloud-like areas.¹²⁹ When the particles move relative to the suspension medium, a part of this so called diffuse double layer will attach to the particles resulting in a potential at the shear zone; this potential is called zeta potential and can be measured by laser doppler electrophoresis (LDE). The magnitude of the zeta potential is an indication of the repulsive force between NP;¹²⁹ high zeta potentials, either positive or negative, allow NP stability and avoid particle aggregation. Besides stability, the zeta potential can strongly influence parameters like mucoadhesion and intracellular trafficking of NP.¹¹

LDE applies an electrical field of known strength across the NP sample. The electrophoretic mobility of the colloid will determine the velocity of particle movement which can be measured by the frequency shift of an incident laser beam passing the sample. Using Henry's equation, the dielectric constant of the sample, the solvent viscosity, and the measured electrophoretic mobility the zeta potential of the particles can be calculated.

3.4.3 Scanning probe microscopy

Scanning probe microscopy (SPM) is a valuable tool for non-destructive three-dimensional visualization of NP. Moreover, it provides qualitative and quantitative information on various physical properties. Hence, it can be used for NP characterization and monitoring of changes in NP features e.g. due to drug loading, variation of the NP preparation method, or NP degradation.

A SPM is scanning the surface using a micro-scale cantilever with a sharp, nanoscale tip at its end. When the tip is approached to the sample surface it is subjected to attractive or repulsive forces leading to a deflection of the cantilever. The extent of deflection is determined by the reflection of a laser beam from the top of the cantilever onto an array of 4 photodiodes. In order to move the tip over the sample surface, the cantilever is mounted on a piezoelectric tube, or vice versa the sample. For scanning in xy direction and to adjust the tip-to-sample distance during scanning the cantilever position is controlled by a feedback mechanism (Figure 5).

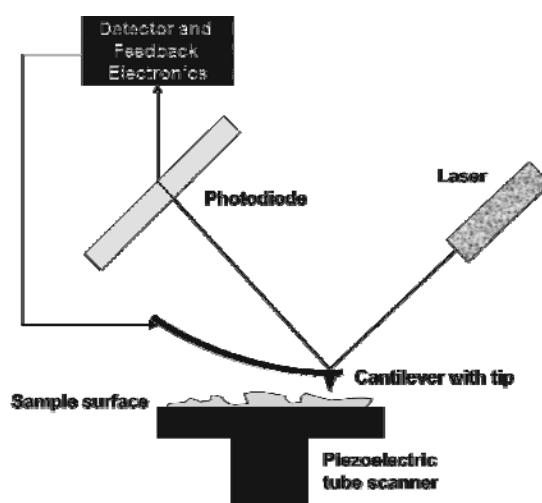


Figure 5: Schematic depiction of a basic AFM setup

In this work, Tapping ModeTM was employed to image samples. At this imaging mode, the cantilever oscillates at or close to its resonance frequency. A Tapping Mode measurement usually results in three signals: height, amplitude and phase signal. The height signal displays the topography of a sample, the amplitude signal highlights rapid changes in sample topography, and the phase signal qualitatively shows changes in the sample elasticity.

3.4.4 Nuclear magnetic resonance spectroscopy

Nuclear magnetic resonance (NMR) spectroscopy is a non-destructive spectroscopic method based upon the physical property of atoms (generally atoms with odd numbers of nuclei) to exhibit magnetic moments; the most often used nuclei are ^1H , ^2H , and ^{13}C . NMR spectroscopy studies the magnetic nucleus by alignment with a strong external magnetic field, which is perturbed by means of an electromagnetic field. The resulting change in the magnetisation of the atomic nuclei is detected to obtain detailed information about the molecular structure. In the field of NP technology, NMR spectroscopy is commonly used to characterize molecular structures of polymers,¹³⁰ to evidence their assembly in NP,^{131, 132} and to analyse their degradation products.¹³³ Moreover, NMR is a valuable tool to verify chemical integrity of drugs after nanoencapsulation.¹³⁴

3.4.5 Differential scanning calorimetry

Differential scanning calorimetry (DSC) represents a thermoanalytical method that measures the difference in the thermal energy required to increase the temperature of a sample and a reference with well-defined heat capacity as a function of the temperature. Ideally, both the sample and the reference are kept at identical temperature, while the temperature increases linearly as a function of time. As soon as the sample undergoes a physical transformation; either exothermic or endothermic, the heat flow to the sample will be decreased or increased relative to the reference, thus, resulting in a DSC signal.

In NP technology, DSC is widely used to study e.g. polymer characteristics (glass transition, melting point)^{135, 136} and ageing phenomena,¹³⁷ or to evaluate lyophilization procedures of NP.^{138, 139}

4 Results and discussion

4.1 Preparation, characterization, and evaluation of fluoresceinamine labelled PLGA nanoparticles

NP have recently been demonstrated in a rat model to be a promising tool for targeting inflamed areas of the intestinal mucosa in IBD whilst concentrating anti-inflammatory drugs at their site of action.^{4, 10, 140} Considering these promising results in animals, a proof of concept for this novel targeting approach in IBD must be provided in humans. For such purpose, drug-free but fluorescence labelled non-toxic NP are needed to show their accumulation in inflamed areas of the colonic mucosa by means of fluorescence microscopy.

As a first step, biodegradable and biocompatible fluorescent NP were prepared and characterized; fluorescein (FC) was chosen as a fluorescence marker since it is also applied even in high doses for diagnostic purposes. To achieve stable fluorescence labelling, the FC derivative 5-fluoresceinamine (FA) was covalently bound to the free carboxyl functions of the PLGA chains by a simple one-step reaction as described by Horisawa et al.¹⁴¹ ¹H NMR revealed a 65% modification rate of carboxyl-end groups of PLGA chains. The glass transition temperature of FA-PLGA was determined by DSC to roughly $T_g = 29^\circ\text{C}$.

From this modified polymer (FA-PLGA), NP (FA-PLGA NP) with a mean diameter of 270 nm were prepared via nanoprecipitation. In regard to an *in vivo* application of the NP in IBD, this size order is expected to be adequate to act as a potential drug carrier whilst still likely to display an enhanced accumulation and retention in inflamed mucosal areas. The density of FA-PLGA NP was determined to 1.46 g/ml; it did not differ significantly from the density of pure PLGA.

For the intended studies, it is crucial that the fluorescence label remains firmly associated with the NP over an appreciable period of time. In case of FA-PLGA NP, the leakage of fluorescence marker occurred in a strongly delayed manner as depicted in Figure 6. The initial burst effect led to 11.7% loss of fluorescence marker within 2 h which is most likely due to starting polymer degradation after re-hydration of the freeze dried NP. After 8 days, 60.8% of fluorescence marker was still bound to the NP. As generally known from PLGA devices, polymer swelling occurs under aqueous

conditions leading to subsequent polymer chain cleavage. By means of thin layer chromatography, it was found that polymer degradation led to different fluorescent products which were expected to be FA-linked PLGA fragments.

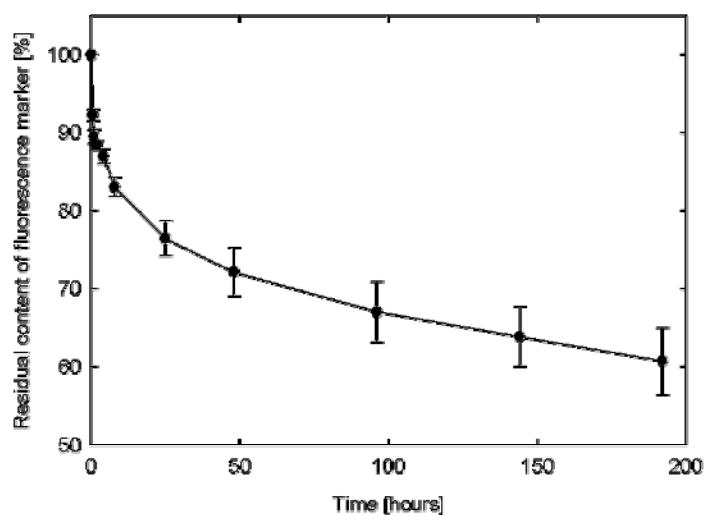


Figure 6: Relative residual content of fluorescence marker in FA-PLGA NP as a function of time (mean \pm SD).¹⁴²

Alternatively to a polymer modification, FC was entrapped into PLGA NP using the w/o/w emulsification method for the purpose of comparison with FA-PLGA NP. In contrast to FA-PLGA NP, it was shown that the release of encapsulated fluorescence marker from those particles (FC-PLGA NP) was very fast: 82.6% were already released after 30 min. This result is in accordance with literature, where hydrophilic drugs are described to be released rapidly when encapsulated into PLGA NP using the w/o/w method.¹⁴³⁻¹⁴⁵ By SPM it was studied that the FC release was not associated with any surface phenomena. Shape and surface appearance of FC-PLGA NP did not differ from those of FA-PLGA NP. Possible explanations for the fast FC release are that either the hydrophilic compound diffuses out of the core very fast or that the w/o/w emulsification method led to an imperfect encapsulation due to the instable nature of the emulsion droplets during the preparation process. In conclusion, FC-PLGA NP, in contrast to FA-PLGA NP, do not appear to be suitable for particle visualization studies over a longer period of time due to a rapid loss and a rather low and insufficient residual amount of encapsulated compound.

The zeta potential of FA-PLGA NP was -1.4 mV. Generally, highly negative zeta potential values are expected for pure polyester NP from non-end capped PLGA due to the

presence of carboxyl groups on the polymeric chain extremities.¹¹⁰ However, in this study, PLGA with around 65% of chain end groups being covalently bound to FA was used. This has possibly led to the less negative surface charge. Another factor may be residual PVA from the preparation process. It is reported that this polymer can create a shield between the NP surface and the surrounding medium, thus masking possible charged groups on the particle surface¹¹⁰ whilst protecting the NP from aggregation. Using SPM, changes in morphology and in elastic and/or adhesive properties of the FA-PLGA NP were studied within long-term degradation (Figure 7).

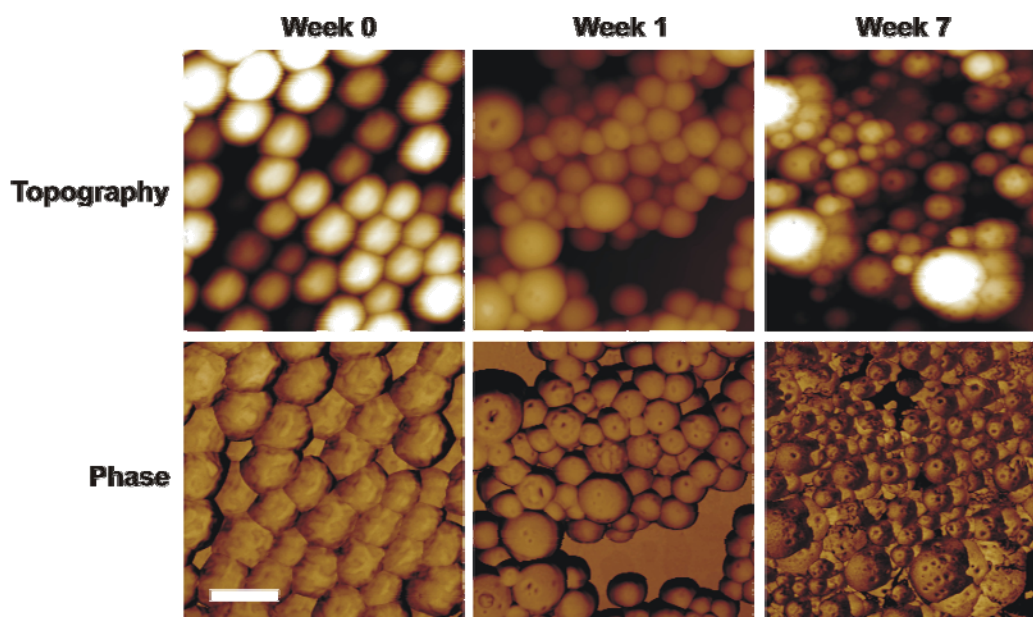


Figure 7: SPM topography and phase images of degrading FA-PLGA NP after week 0, week 1, and week 7. The size of all images is equal (bar = 500 nm).¹⁴²

NP made of PLGA have been shown to predominantly erode in bulk¹⁰³ which is characterized by the formation of pores enabling water to penetrate into the particles followed by a random cleavage of the ester bonds. During that process, the particle core and size generally remain constant. This complies with the findings in size measurements: the mean particle size did not change notably during the experiment. At the beginning of the experiment, the NP were spherical and exhibited a smooth surface. After 1 week, pore development became apparent which continuously proceeded until week 7 followed by a surface smoothing after 15 weeks. In association with pore formation and degradation, a change in the elastic and/or adhesive properties was found which can be explained by a swelling process. This might also be a possible explanation for the particle surface smoothing found after 15 weeks of degradation.

Lyophilisation is one of the most suitable methods in order to stabilize and to facilitate the handling of nanoparticulate systems which would suffer alteration in a brief period of time if stored as suspension.¹³⁸ With regard to application in a clinical study, it is highly important that lyophilised NP can be easily re-constituted before application to patients. Several authors have claimed that an addition of cryoprotectants is necessary in order to prevent PLGA NP from aggregation during lyophilisation and to maintain the integrity after re-hydration of the lyophilised samples.^{115, 138, 144, 146} However, in the present study it was found that NP from FA-PLGA maintained their size and still showed narrow size distribution when lyophilised without any additives. In literature, this behaviour was described as an effect of the stabilizer PVA used for the preparation of NP^{139, 147, 148} forming a stable thick layer on the particle surface.¹⁴⁷ Similar to other cryoprotectants, PVA is described to form a glassy state at low temperature due to hydrogen bonding between the polymer and the water molecules, thus stabilizing NP during lyophilisation and preventing particle aggregation.¹³⁹

Finally, FA-PLGA NP were applied on an *in vitro* model of the intestinal mucosa (Caco-2 cell culture) in order to evaluate the interaction with intestinal epithelial cells, addressing absorption and potential cytotoxicity. A transport of FA-PLGA NP across Caco-2 monolayers was not observed. The transport of their fluorescent degradation products ($\sim 0.02\%$ after 6 h) was even approximately 500 times smaller than that of the low permeability marker FC. This result was attributed to a high molecular weight when FA is additionally bound to short lactide-glycolide chains. No additional transport mechanism except diffusion seemed to be activated.

For an *in vivo* application in a clinical study in humans, FA-PLGA NP were assayed for their cytotoxic effects on Caco-2 cells. The IC_{50} value was shown to be 10 mg/ml. It was of the same order as found with NP from pure PLGA which is well-known for its excellent biocompatibility.¹⁴⁹ Apparently, covalent labelling of PLGA with FA did not affect the cytotoxic potential of the NP. With respect to a potential absorption of FA-PLGA NP from the lumen of the intestine, the results from the Caco-2 transport experiments indicate that only the degradation products are transported across the intestinal epithelial barrier. Even if absorption due to a compromised barrier function of the intestinal mucosa under conditions of IBD might occur to some extent, a progressive shortening of the polymer chains would facilitate their elimination.

Excised intestine from pig served as a model for a first evaluation of particle visualization and quantification in intestinal tissue. Using confocal laser scanning microscopy (CLSM), FA-PLGA NP could be well visualized in different depths of the tissue. The detection limit of such NP in the presence of tissue samples is 3 $\mu\text{g/ml}$ suggesting that extraction of biopsies taken from IBD patients may represent an additional way to quantify particle accumulation in inflamed intestinal tissue.

4.2 Application of fluorescent and drug containing nanoparticles to investigate skin permeation and penetration

4.2.1 Nanoparticles – an efficient carrier for drug delivery into the hair follicles

Follicular penetration represents an important and encouraging pathway into the skin with potential use in selective dermatotherapy and cosmetics. Several studies have shown that not only single drug molecules but also NP can use this route of penetration into the skin.^{8, 43} However, penetration and storage features of topically applied NP formulations still need to be explored in detail. The aim of the present investigations was to compare the efficacy of penetration and storage in hair follicles of compounds in free and nanoencapsulated form.

For that purpose, fluorescence labelled NP (referred to as 'dye-in-particle-form'; formulation described in chapter 4.1) and a particle-free FC formulation of the same dye concentration (referred to as 'dye-in-non-particle-form') were employed.

The penetration of the dye into the hair follicles was investigated *in vitro* using porcine ear skin, which is an appropriate model for human tissue.¹⁵⁰ The penetration depths of the fluorescence dye deriving from both formulations were determined by analyzing biopsies by means of laser scanning microscopy. It was shown that the dye-in-particle-form penetrated significantly deeper into the hair follicles than the dye-in-non-particle-form, if a massage had been applied. Without massage, similar results were obtained for both formulations. Thereby, the penetration depth was significantly decreased in comparison to the penetration depth after a massage.

Figure 8 exhibits superpositions of transmission and a fluorescence microscopy images. They demonstrate the penetration of dye-in-particle-form (A) and dye-in-non-particle-form (B) into hair follicles of porcine skin after application of a massage.

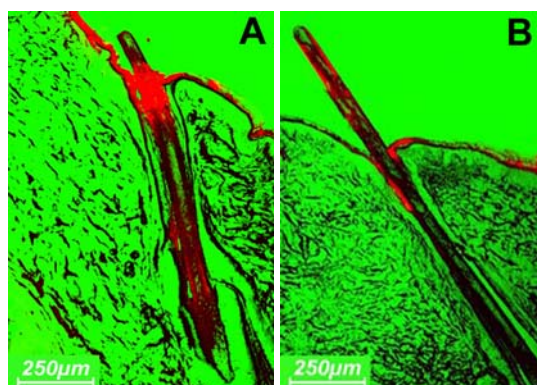


Figure 8: Superposition of a transmission and a fluorescence microscopy image showing the penetration of dye-in-particle-form (A) and dye-in-non-particle-form (B) *in vitro* into the hair follicles of porcine skin after application of a massage. The dye derived from both formulations is displayed in red.¹⁵¹

From structure analysis of hair surface and hair follicles, it is well known that the cuticle produced by keratinocyte desquamation forms a structured surface, which can be approximated by a zigzag relief.¹⁵² This relief is determined to a range of 500 to 800 nm by the thickness of the keratin cells. When the hairs are moved by a massage, the cuticle may act as a geared pump pushing particles in the size order of the surface structure of the hairs and hair follicles into the follicles. These results are in agreement with those obtained by Toll et al.⁴³ They found that particles of 750 nm penetrated better into hair follicles of excised human skin than larger particles and that the penetration could even be enhanced by a mechanical massage. Under *in vivo* conditions, the assumed pump mechanism may occur without a massage on account of the continuous movement of the body stimulating the terminal and vellus hairs.

The storage behavior of both formulations in hair follicles was analyzed *in vivo* on human skin by means of differential stripping after penetration times up to 10 days.⁴⁴ Thereby, the upper part of the stratum corneum, which serves as a reservoir for topically applied substances, was removed by tape stripping as described by Weigmann et al.,¹⁵³ and the fluorescence dye (particle-form and non-particle-form) in the hair follicle infundibula was determined semi-quantitatively by extraction of cyanoacrylate biopsies at different time points after application. As depicted in Figure 9, the concentration of the fluorescence dye in the hair follicles decreased with time. If the skin had been treated with the dye in the non-particle-form, the dye was detected only up to 4 days. However, in case of the dye-in-particle-form, fluorescence was still found 10 days after application.

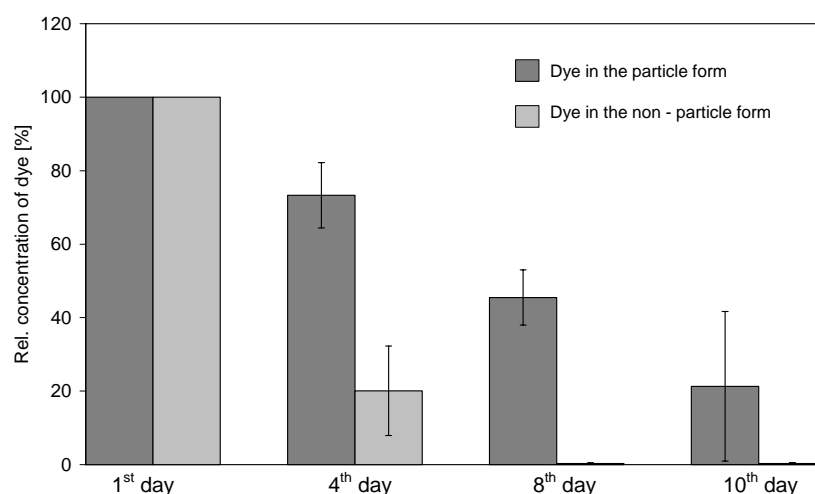


Figure 9: Semi-quantitative determination of the fluorescence dye (particle-form and non-particle-form) in the hair follicle infundibula at different time points after application (mean \pm SD).¹⁵¹

The *in vivo* storage experiments demonstrated that penetration of the fluorescence dye out of the hair follicles is a relatively slow process for both formulations, when compared to the penetration into the hair follicles. The obtained results can be explained as follows: as soon as the reservoir of the skin surface and the stratum corneum, as source of the dye penetrating into the hair follicles, is depleted by textile contact and desquamation, the sebum production seemed to be mainly responsible for the removal of the formulations out of the hair follicles. Thereby, it is assumed that the dye in non-particle form was quickly removed joining the sebum excretion, whereas the release of particles from the hair follicles was retarded by the surface structure. Considering studies on follicle penetration of TiO₂ microparticles,¹⁵⁴ it can be hypothesized that all particles larger than 100 nm, which penetrated into the hair follicles, will be removed after some time on account of the sebum production without having reached living cells.

In conclusion, by means of fluorescence labelled NP it was possible to demonstrate the superiority of a particle versus a non-particle formulation concerning penetration and storage of the delivered dye as a model for any other compound in hair follicles. It is hypothesized that these results are effects of the surface structure of the skin, in particular of the cuticle, which may act as a geared pump pushing particles deeper into hair follicles than smaller sized compounds, at the same time decelerating their removal by sebum excretion.

4.2.2 Multiphoton microscopy for the investigation of dermal penetration of nanoparticle-borne drugs

The study 'Multiphoton microscopy for the investigation of dermal penetration of nanoparticle-borne drugs' describes the application of multiphoton microscopy (MPM) to a non-invasive, high-resolution three-dimensional (3D) visualization of fluorescence labelled NP on excised human skin. It allowed to simultaneously localize the NP and to study the release, accumulation, and penetration of a model drug which was incorporated into the NP, thereby even discriminating between particle-bound and released compound.

Major challenge of those investigations was the development of an appropriate NP model consisting of a carrier labelled by means of a fluorescence dye and a drug to be released. Since most pharmaceutical substances are basically non-fluorescent it was reasonable to use a second fluorescence dye as fluorescent drug model. The fluorescence label had to meet the demands (i) stable labelling in case of the dye for the NP cores, (ii) release from the NP in case of the model drug, (iii) different excitation and emission wavelengths, and (iv) preferably small cross-talk. In order to meet these criteria, the fluorescent PLGA NP formulation described in chapter 4.1 was advanced. FA-PLGA was used as a polymer for NP preparation employing a single emulsion method. Thereby, the second fluorescence dye Texas Red[®], chosen as a model drug, was physically dissolved in the polymer matrix. The fluorescence dyes exhibited excitation and emission maxima at 485 and 510 nm in case of the green polymer bound dye FA, and at 596 and 615 nm in case of the red dye Texas Red.

The mean size of two-colour labelled NP was 290 ± 5 nm (Figure 10A). Via SPM homogeneity, spherical shape and a smooth surface of the particles was verified (Figure 10B).

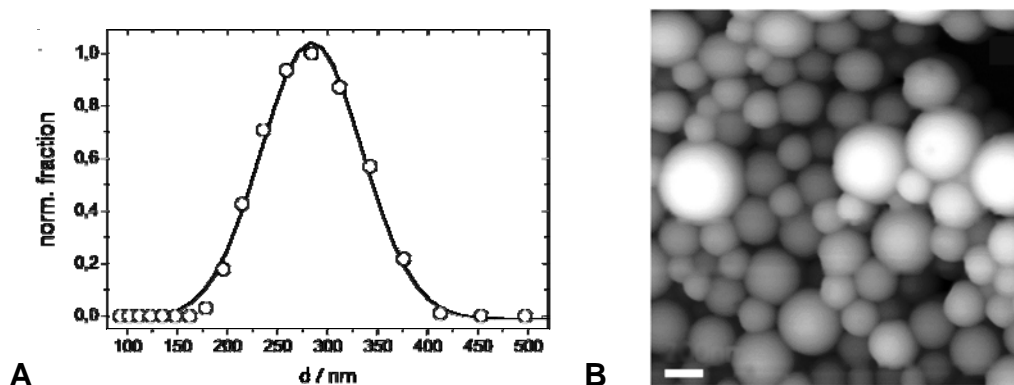


Figure 10: Histogram of the particle diameter d obtained by PCS (the line is a Gaussian fit to the data) (A) and a $2 \times 2 \mu\text{m}$ SPM topography image of two-colour fluorescence labelled NP (B) (bar = 200 nm).¹⁵⁵

In preliminary experiments, successful nanoencapsulation and different release characteristics of both fluorescence dyes were confirmed: simultaneous fluorescence imaging after excitation at 488 and 568 nm using CLSM revealed the same pattern of red and green fluorescent NP; it further indicated a release of the red label Texas Red, whereas the green label FA appeared to remain NP-bound.

Multiphoton fluorescence imaging enabled 3D tracing of individual NP, embedded in a 1.5% Natrosol[®] hydrogel, with diffraction-limited resolution and allowed detailed studies on the migration in the skin. Due to the significant endogenous fluorescence of keratin under two-photon excitation at a wavelength of 800 nm the outermost layer of the stratum corneum could be imaged and hence, the dermal topography. Obviously, the fluorescence labelled NP were not able to penetrate the stratum corneum and stayed in the gel-filled dermatoglyphs over 5 h. This corresponds with findings described in chapter 4.2.3 where penetration of flufenamic acid loaded PLGA NP into human skin was not found. Via this imaging mode, changes in the background fluorescence intensity of the ointment matrix and the stratum corneum were not observed as a consequence of the release and accumulation of Texas Red. The reason for this result is the comparable low two-photon absorption cross-section of Texas Red at 800 nm while FA and keratin are efficiently excited.

To investigate the distribution of the model drug Texas Red as a function of time, two-photon spectral imaging was performed. Whereas the Texas Red content in the NP showed up to be low and basically constant, the concentration of Texas Red in the gel matrix dropped significantly with time starting already from the earliest measurement after 30 min. This result indicated that the vast fraction of Texas Red was taken up from

the gel to the stratum corneum surface almost immediately after application. Furthermore, the release of Texas Red from the NP to the matrix had obviously started well before application to the skin. An increase of Texas Red concentration in the deeper stratum corneum and stratum granulosum showed a slow penetration of the dye.

Finally, a multitracking experiment was performed in order to co-localize the distribution of Texas Red, FA and keratin fluorescence roughly 5 h after the application of fluorescence labelled NP. By this technique optical sections were recorded up to a depth of $-32\ \mu\text{m}$. Figure 11 shows an optical section in $-20\ \mu\text{m}$ depth.

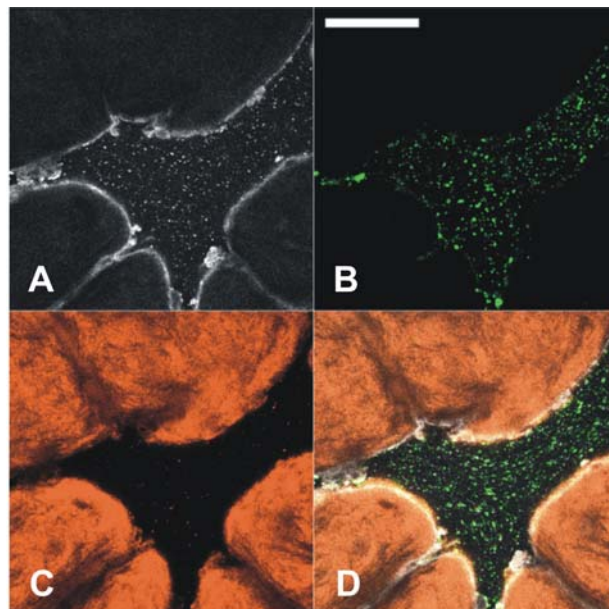


Figure 11: $325 \times 325\ \mu\text{m}^2$ optical sections in $-20\ \mu\text{m}$ depth obtained in multitracking experiments. Figure A represents a multiphoton excited image (predominantly keratin autofluorescence and FA), Figure B a 488 nm excited image (FA), and Figure C a 543 nm excited image (Texas Red). Figure D was obtained by an overlay of the images A, B, and C (bar = $100\ \mu\text{m}$).¹⁵⁵

The 488 nm excited image proves, that FA was strictly bound to the NP and not released during the time of observation. In chapter 4.1 a leaking of fluorescent degradation products from particles of the same polymer FA-PLGA was shown. However, in this study, no such phenomenon was found. In the 543 nm excited images the distribution of Texas Red, which penetrated the skin and accumulated in the stratum corneum, is visible. The predominant fraction of the dye was found within the skin, but the particles were also slightly observable. Obviously, there was still a certain amount of the dye stored in the NP, though the release process had proceeded far.

In conclusion, MPM combined with spectral imaging was found to allow non invasive long term studies of the penetration of a particle-borne drug-model into skin with sub cellular resolution. Due to virtually no out-of-focus effects of the scanning laser beam,¹⁵⁶ this technique is considered as gentle for *in vitro* and *in vivo* studies. By dual colour labelling a clear discrimination between particle-bound and released drug-model was possible. Due to the excitation of endogenous fluorophores of the skin by multiphoton excitation and the correlation of the resulting autofluorescence image to the drug fluorescence pattern the identification of accumulative spots and penetration pathways was possible with sub-cellular resolution.^{157, 158}

4.2.3 Influence of nanoencapsulation on human skin transport of flufenamic acid

In the subsequent studies, the influence of nanoencapsulation on the permeation and penetration of the lipophilic model drug flufenamic acid (FFA) into excised human skin was investigated. Therefore, PLGA NP were chosen as a valuable carrier system and the NP mediated transport of FFA was compared with the transport of the free drug.

For the preparation of flufenamic acid nanoparticles (FFA NP), a single emulsion method was studied to be most appropriate resulting in a drug entrapment of 64% (w/w). FFA NP were in the size order of 330 nm and narrowly distributed (PI = 0.16). By means of SPM imaging spherical particle shape and smooth surface were confirmed (Figure 12A). In order to increase the viscosity of the preparations applied on the skin, FFA NP were incorporated in a 1.5% Natrosol[®] hydrogel. SPM imaging evidenced homogeneous distribution and conserved integrity of FFA NP in the hydrogel (Figure 12B).

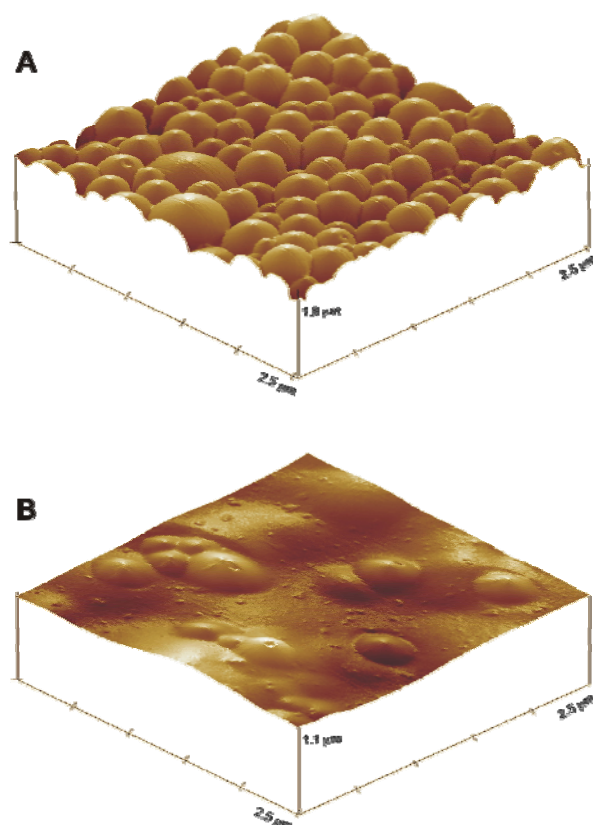


Figure 12: 3D SPM topography images of FFA NP in aqueous solution (A) and incorporated into a Natrosol hydrogel (B).

Comparing the transport of FFA derived from a NP hydrogel with that from a hydrogel containing the same concentration of free drug, two different *in vitro* test systems were employed. Thereby, excised human skin from abdominal plastic surgery was used for all penetration and permeation experiments: For monitoring drug penetration, the Saarbruecken model¹⁵⁹ was used where the skin itself acts as a receptor compartment. A tape stripping technique followed by cryosectioning of the deeper skin layers allowed quantification of the penetrated drug amount. Drug release from the formulation and drug permeation through the epidermis were studied using a static Franz diffusion cell technique. No difference in drug transport into the stratum corneum was found between nanoencapsulated and free drug. The drug accumulation in the deeper skin layers and the drug transport across human epidermis was slightly delayed for the nanoencapsulated drug compared to the free drug after shorter incubation times (< 12 h). In contrast, after longer incubation times (> 12 h) the nanoencapsulated drug showed a statistically significantly enhanced transport and accumulation ($P < 0.05$).

The mechanisms by which NP increased the amount of FFA in deeper skin layers at longer incubation times remained unclear. However, it may be speculated that the degradation of NP leads to some release of acidic compounds (lactic and glycolic acid). The acidification of particles and their surroundings might favour the non-ionised form of FFA, thus exhibiting improved penetration in the stratum corneum. PH changes of PLGA particles as consequence of degradation have also been reported by Fu et al.¹⁶⁰ earlier. Another explanation might be that NP were able to cross the stratum corneum as described by Kohli et al.¹⁶¹ after a certain incubation time, subsequently, leading to an increase in the drug amount taken up.

To verify the presence and to visualize the distribution of the applied NP on the skin, MPM was used after an incubation time of 30 min. As expected, structure and autofluorescence of the skin corresponded to published data.¹⁵⁶ FFA NP were found homogeneously distributed on the skin surface and within the dermatoglyphs, but no NP were detected within or between the corneocytes. No hair follicles or sweat glands were observed. Consequently, possible transport of nanoparticles by transappendageal routes such as previously reported by several authors^{8, 43, 162} could not be confirmed in this study. However, visualization of drug transport processes of NP especially using longer incubation times (>12 h) is still ongoing and subject of further investigations.

4.3 Surface biotinylated nanoparticles for coupling of versatile ligands

Generally, nanoparticulate drug targeting systems may bear different functionalities. The inner functionality is reflected by the NP core which encapsulates the active moiety, thus acting as a stabilizer and controlling drug release. Complementarily, the outer functionality of a NP is represented by the NP surface which may establish specific and non-specific interactions with the target. However, in most cases, common preparation techniques of polymeric NP need to be specifically arranged for each compound to be entrapped or attached. The aim of the study 'Coupling of biotin-(polyethyleneglycol)amine to poly(D,L-lactide-co-glycolide) nanoparticles for versatile surface modification' was to develop a procedure for surface functionalization of preformed NP, which may eventually already contain active pharmacological ingredients, for subsequent versatile conjugation of targeting ligands and fluorescence dyes under mild conditions. For such purpose, the avidin-biotin

system was chosen as avidin (Av) and its homologues streptavidin (SAv) and NeutrAvidin™ (NAv) exhibit very high affinities ($K_d = 10^{-13} - 10^{-16}$ M) and a rapid and stable binding to biotin.^{163, 164} Taking into consideration the presence of free carboxylic acid groups on the surface of NP made of poly(estere)s, it was opted for an approach where biotin-(polyethyleneglycol)amine (BPEG) functionalized NP (BPEG PLGA NP) bind to conjugates of Av (or homologues). Consequently, both targeting moieties as well as fluorescence labels can be easily linked to the surface of thus functionalized NP as long as they are available as conjugates of Av (or homologues) (Figure 13A).

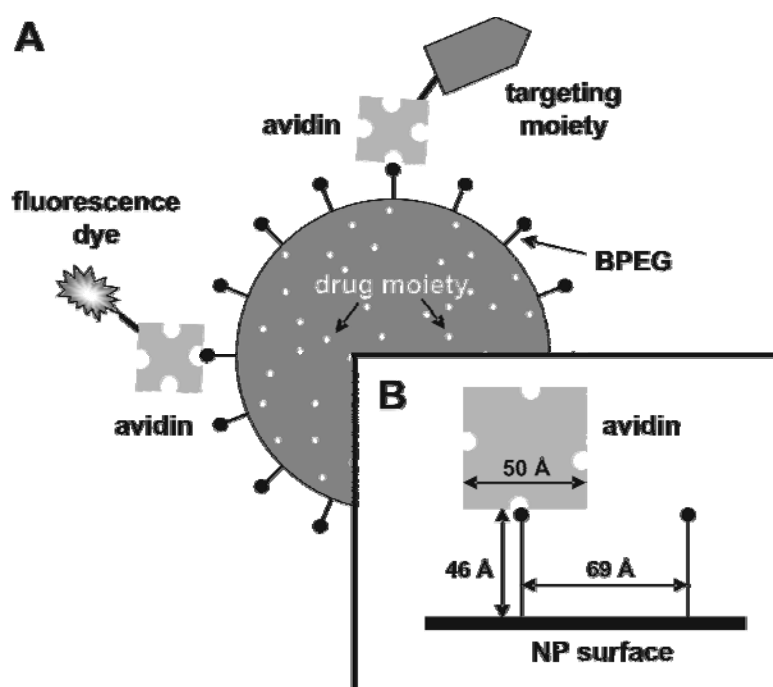


Figure 13: Schematic illustration of a surface modified PLGA NP by means of BPEG. Figure 13A gives an overview of the aims of the study. Versatile binding of targeting moieties is realized employing avidin (and homologues) conjugates. Binding of fluorescence dye conjugated avidin opens the possibility of an additional fluorescence labelling of the NP. Figure 13B represents a virtual zoom into the NP surface. Assuming homogenous distribution of the BPEG molecules on the NP surface, the mean distance is calculated to 69 Å. The length of the BPEG molecule is determined to roughly 46 Å. The size of avidin is reported to 50 Å × 50 Å × 40 Å with the biotin binding sites in a distance of 29.5 and 20 Å.¹⁶⁵

PLGA NP in the size of 210 nm were prepared by the classic oil-in-water method. Subsequently, BPEG PLGA NP were generated via a triazine-promoted amidation of the carboxylic acid groups present on the PLGA NP surface. The technique has been frequently described in the literature;¹⁶⁶⁻¹⁶⁸ here it was adapted to surface modification of PLGA NP. Such functionalization did not involve an increase in size, i.e. any change in the hydrodynamic diameter was beneath the detection limit. The zeta potential

changed from -32 mV to -23 mV after surface functionalization. The negative surface charge of both particle species is attributed to the presence of carboxyl end groups deriving from PLGA chain ends. However, in case of the BPEG PLGA NP, the particle surface was partially shielded owing to covalent modification of the carboxyl groups by means of BPEG molecules. The amount of surface associated biotin was determined to 850 pmol per mg polymer corresponding to roughly 2,650 biotin molecules on the surface of one single average-sized (210 nm) BPEG PLGA NP. Assuming that BPEG chains are evenly distributed on the NP surface, the mean distance of two chains would be 69 Å. The length of the BPEG chains was calculated to maximally 46 Å. In solution, one would expect the BPEG molecule to adopt a more or less coiled conformation, here however, to roughly estimate surface conditions it was deliberately assumed that the molecule exists in a stretched conformation. The size of Av is reported to $50 \text{ Å} \times 50 \text{ Å} \times 40 \text{ Å}$ with the biotin binding sites being in a distance of 29.5 and 20 Å to each other.¹⁶⁹ The dimensions of such a BPEG functionalized NP surface is drawn to scale in Figure 13B indicating that each single BPEG graft on the NP surface should be well accessible to Av.

SPM studies showed that surface modification of PLGA NP and binding of Av to BPEG PLGA NP did not lead to changes in particle shape and surface structure. Obviously, those modifications resulted in changes of elasticity or adhesion of the cantilever tip. By resonant mirror measurements the binding of BPEG PLGA NP with a NAv functionalized surface was studied (total binding) (Figure 14). A clear response was obtained, however the binding curve did not reach equilibrium during the measurement, possibly due to particle rearrangement on the NAv coated surface. Non-specific binding was studied by blocking the biotin binding sites of the same cuvette by free BPEG; it resulted only in a small response. The extent of specific binding of BPEG PLGA NP to the NAv surface is described by a calculated curve, which was obtained by subtracting the curve representing the non-specific binding from the curve representing the total binding.

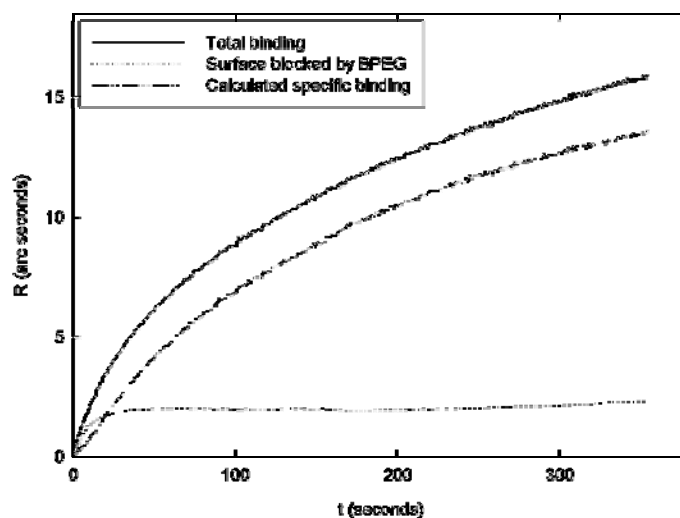


Figure 14: Results of resonant mirror adhesion studies: interactions of BPEG PLGA NP with a NAv surface and a NAv surface with BPEG blocked biotin binding sites. An additional curve calculated as the difference of both binding curves represents the extent of specific binding.¹⁶⁵

Aiming for a quantification of protein binding to BPEG PLGA NP and PLGA NP, an inverse setup was applied in order to determine the non-particle associated amounts of FITC-NAv and horse radish peroxidase-streptavidin after incubation with BPEG PLGA NP and PLGA NP. In the course of this work, it was found that this method is not suited for such purposes as BPEG grafts may be sheared off the NP cores when separating the particles. Further complicating, the fluorescence intensity of FITC-NAv was studied to be dependent on the concentration of biotin and BPEG in the assay. Hence, applying a gentle NP separation method combined with a direct determination of particle bound proteins may represent a possibly successful alternative.

For the first evaluation in a biological system, fluorescence labelled BPEG PLGA NP were used to demonstrate differences in binding and uptake behaviour between flat squameous epithelial cells from the alveolar epithelium (A549) in comparison to the relatively thick columnar epithelial cells from the intestinal mucosa (Caco-2). Dependent on the staining of the cell membranes NP decorated with different fluorescent NAv conjugates were applied, thus demonstrating the ease of versatile fluorescence labelling of BPEG PLGA NP.

5 References

1. W. C. Chan, Bionanotechnology progress and advances. *Biol Blood Marrow Transplant*: 12, 87-91 (2006)
2. O. Salata, Applications of nanoparticles in biology and medicine. *J Nanobiotechnology*: 2, 3-9 (2004)
3. R. Alvarez-Roman, A. Naik, Y. N. Kalia, R. H. Guy and H. Fessi, Enhancement of topical delivery from biodegradable nanoparticles. *Pharm Res*: 21, 1818-1825 (2004)
4. A. Lamprecht, N. Ubrich, H. Yamamoto, U. F. Schaefer, H. Takeuchi, C. M. Lehr, P. Maincent and Y. Kawashima, Design of rolipram-loaded nanoparticles: comparison of two preparation methods. *J Control Release*: 71, 297-306 (2001)
5. O. Kayser, A. Lemke and N. Hernandez-Trejo, The impact of nanobiotechnology on the development of new drug delivery systems. *Curr Pharm Biotechnol*: 6, 3-5 (2005)
6. I. Brigger, C. Dubernet and P. Couvreur, Nanoparticles in cancer therapy and diagnosis. *Adv Drug Deliv Rev*: 54, 631-651 (2002)
7. M. V. Yezhelyev, X. Gao, Y. Xing, A. Al-Hajj, S. Nie and M. O'Regan R, Emerging use of nanoparticles in diagnosis and treatment of breast cancer. *Lancet Oncol*: 7, 657-667 (2006)
8. R. Alvarez-Roman, A. Naik, Y. N. Kalia, R. H. Guy and H. Fessi, Skin penetration and distribution of polymeric nanoparticles. *J Control Release*: 99, 53-62 (2004)
9. J. M. Koziara, P. R. Lockman, D. D. Allen and R. J. Mumper, Paclitaxel nanoparticles for the potential treatment of brain tumors. *J Control Release*: 99, 259-269 (2004)
10. A. Lamprecht, U. F. Schaefer and C. M. Lehr, Size-dependent bioadhesion of micro- and nanoparticulate carriers to the inflamed colonic mucosa. *Pharm Res*: 18, 788-793 (2001)
11. I. Bala, S. Hariharan and M. N. Kumar, PLGA nanoparticles in drug delivery: the state of the art. *Crit Rev Ther Drug Carrier Syst*: 21, 387-422 (2004)
12. M. Higaki, T. Ishihara, N. Izumo, M. Takatsu and Y. Mizushima, Treatment of experimental arthritis with poly(D, L-lactic/glycolic acid) nanoparticles encapsulating betamethasone sodium phosphate. *Ann Rheum Dis*: 64, 1132-1136 (2005)
13. Y. N. Konan-Kouakou, R. Boch, R. Gurny and E. Allemann, In vitro and in vivo activities of verteporfin-loaded nanoparticles. *J Control Release*: 103, 83-91 (2005)
14. M. Yokoyama, Drug targeting with nano-sized carrier systems. *J Artif Organs*: 8, 77-84 (2005)
15. S. M. Cannizzaro, R. F. Padera, R. Langer, R. A. Rogers, F. E. Black, M. C. Davies, S. J. Tendler and K. M. Shakesheff, A novel biotinylated degradable polymer for cell-interactive applications. *Biotechnol Bioeng*: 58, 529-535 (1998)
16. R. Gref, P. Couvreur, G. Barratt and E. Mysiakine, Surface-engineered nanoparticles for multiple ligand coupling. *Biomaterials*: 24, 4529-4537 (2003)
17. S. Balthasar, K. Michaelis, N. Dinauer, H. von Briesen, J. Kreuter and K. Langer, Preparation and characterisation of antibody modified gelatin nanoparticles as drug carrier system for uptake in lymphocytes. *Biomaterials*: 26, 2723-2732 (2005)

References

18. J. Vandervoort and A. Ludwig, Biocompatible stabilizers in the preparation of PLGA nanoparticles: a factorial design study. *Int J Pharm*: 238, 77-92 (2002)
19. M. F. Zambaux, F. Bonneaux, R. Gref, E. Dellacherie and C. Vigneron, Preparation and characterization of protein C-loaded PLA nanoparticles. *J Control Release*: 60, 179-188 (1999)
20. S. Galindo-Rodriguez, E. Allemann, H. Fessi and E. Doelker, Physicochemical parameters associated with nanoparticle formation in the salting-out, emulsification-diffusion, and nanoprecipitation methods. *Pharm Res*: 21, 1428-1439 (2004)
21. G. Tosi, F. Rivasi, F. Gandolfi, L. Costantino, M. A. Vandelli and F. Forni, Conjugated poly(D,L-lactide-co-glycolide) for the preparation of in vivo detectable nanoparticles. *Biomaterials*: 26, 4189-4195 (2005)
22. B. D. Chithrani, A. A. Ghazani and W. C. Chan, Determining the size and shape dependence of gold nanoparticle uptake into mammalian cells. *Nano Lett*: 6, 662-668 (2006)
23. A. Tanimoto and S. Kuribayashi, Application of superparamagnetic iron oxide to imaging of hepatocellular carcinoma. *Eur J Radiol*: 58, 200-216 (2006)
24. D. Williams, Quantum dots in medical technology. *Med Device Technol*: 17, 8-9 (2006)
25. C. M. Keck and R. H. Muller, Drug nanocrystals of poorly soluble drugs produced by high pressure homogenisation. *Eur J Pharm Biopharm*: 62, 3-16 (2006)
26. P. Kocbek, S. Baumgartner and J. Kristl, Preparation and evaluation of nanosuspensions for enhancing the dissolution of poorly soluble drugs. *Int J Pharm*: 312, 179-186 (2006)
27. S. Khandavilli and R. Panchagnula, Nanoemulsions as Versatile Formulations for Paclitaxel Delivery: Peroral and Dermal Delivery Studies in Rats. *J Invest Dermatol*, doi: 10.1038/sj.jid.5700485 (2006)
28. G. Sharma, S. Anabousi, C. Ehrhardt and M. N. Ravi Kumar, Liposomes as targeted drug delivery systems in the treatment of breast cancer. *J Drug Target*: 14, 301-310 (2006)
29. L. O. Cinteza, T. Y. Ohulchanskyy, Y. Sahoo, E. J. Bergey, R. K. Pandey and P. N. Prasad, Diacyllipid micelle-based nanocarrier for magnetically guided delivery of drugs in photodynamic therapy. *Mol Pharm*: 3, 415-423 (2006)
30. J. Lademann, H. Richter, U. F. Schaefer, U. Blume-Peytavi, A. Teichmann, N. Otberg and W. Sterry, Hair follicles - a long-term reservoir for drug delivery. *Skin Pharmacol Physiol*: 19, 232-236 (2006)
31. Q. Z. Zhang, L. S. Zha, Y. Zhang, W. M. Jiang, W. Lu, Z. Q. Shi, X. G. Jiang and S. K. Fu, The brain targeting efficiency following nasally applied MPEG-PLA nanoparticles in rats. *J Drug Target*: 14, 281-290 (2006)
32. A. Vila, A. Sanchez, C. Evora, I. Soriano, O. McCallion and M. J. Alonso, PLA-PEG particles as nasal protein carriers: the influence of the particle size. *Int J Pharm*: 292, 43-52 (2005)
33. S. Sakuma, R. Sudo, N. Suzuki, H. Kikuchi, M. Akashi and M. Hayashi, Mucoadhesion of polystyrene nanoparticles having surface hydrophilic polymeric chains in the gastrointestinal tract. *Int J Pharm*: 177, 161-172 (1999)
34. K. Manjunath and V. Venkateswarlu, Pharmacokinetics, tissue distribution and bioavailability of clozapine solid lipid nanoparticles after intravenous and intraduodenal administration. *J Control Release*: 107, 215-228 (2005)

References

35. J. Hadgraft, Skin deep. *Eur J Pharm Biopharm*: 58, 291-299 (2004)
36. J. Hadgraft, Skin, the final frontier. *Int J Pharm*: 224, 1-18 (2001)
37. J. Cazares-Delgadillo, A. Naik, Y. N. Kalia, D. Quintanar-Guerrero and A. Ganem-Quintanar, Skin permeation enhancement by sucrose esters: a pH-dependent phenomenon. *Int J Pharm*: 297, 204-212 (2005)
38. S. Tokumoto, N. Higo and K. Sugibayashi, Effect of electroporation and pH on the iontophoretic transdermal delivery of human insulin. *Int J Pharm*: 326, 13-19 (2006)
39. S. K. Rastogi and J. Singh, Effect of chemical penetration enhancer and iontophoresis on the in vitro percutaneous absorption enhancement of insulin through porcine epidermis. *Pharm Dev Technol*: 10, 97-104 (2005)
40. C. M. Heard, D. Kung and C. P. Thomas, Skin penetration enhancement of mefenamic acid by ethanol and 1,8-cineole can be explained by the 'pull' effect. *Int J Pharm*: 321, 167-170 (2006)
41. A. Copovi, O. Diez-Sales, J. V. Herraiez-Dominguez and M. Herraiez-Dominguez, Enhancing effect of alpha-hydroxyacids on "in vitro" permeation across the human skin of compounds with different lipophilicity. *Int J Pharm*: 314, 31-36 (2006)
42. R. Alvarez-Roman, A. Naik, Y. N. Kalia, H. Fessi and R. H. Guy, Visualization of skin penetration using confocal laser scanning microscopy. *Eur J Pharm Biopharm*: 58, 301-316 (2004)
43. R. Toll, U. Jacobi, H. Richter, J. Lademann, H. Schaefer and U. Blume-Peytavi, Penetration profile of microspheres in follicular targeting of terminal hair follicles. *J Invest Dermatol*: 123, 168-176 (2004)
44. A. Teichmann, U. Jacobi, M. Ossadnik, H. Richter, S. Koch, W. Sterry and J. Lademann, Differential stripping: determination of the amount of topically applied substances penetrated into the hair follicles. *J Invest Dermatol*: 125, 264-269 (2005)
45. A. Teichmann, M. Ossadnik, H. Richter, W. Sterry and J. Lademann, Semiquantitative determination of the penetration of a fluorescent hydrogel formulation into the hair follicle with and without follicular closure by microparticles by means of differential stripping. *Skin Pharmacol Physiol*: 19, 101-105 (2006)
46. J. Shim, H. Seok Kang, W. S. Park, S. H. Han, J. Kim and I. S. Chang, Transdermal delivery of mixnoxidil with block copolymer nanoparticles. *J Control Release*: 97, 477-484 (2004)
47. M. Simeonova, R. Velichkova, G. Ivanova, V. Enchev and I. Abrahams, Poly(butylcyanoacrylate) nanoparticles for topical delivery of 5-fluorouracil. *Int J Pharm*: 263, 133-140 (2003)
48. V. Jennings and S. H. Gohla, Encapsulation of retinoids in solid lipid nanoparticles (SLN). *J Microencapsul*: 18, 149-158 (2001)
49. V. Jennings, A. Gysler, M. Schafer-Korting and S. H. Gohla, Vitamin A loaded solid lipid nanoparticles for topical use: occlusive properties and drug targeting to the upper skin. *Eur J Pharm Biopharm*: 49, 211-218 (2000)
50. S. A. Wissing and R. H. Muller, The influence of solid lipid nanoparticles on skin hydration and viscoelasticity--in vivo study. *Eur J Pharm Biopharm*: 56, 67-72 (2003)
51. C. Santos Maia, W. Mehnert, M. Schaller, H. C. Korting, A. Gysler, A. Haberland and M. Schafer-Korting, Drug targeting by solid lipid nanoparticles for dermal use. *J Drug Target*: 10, 489-495 (2002)

References

52. S. K. Jain, M. K. Chourasia, R. Masuriha, V. Soni, A. Jain, N. K. Jain and Y. Gupta, Solid lipid nanoparticles bearing flurbiprofen for transdermal delivery. *Drug Deliv*: 12, 207-215 (2005)
53. V. Jenning, M. Schafer-Korting and S. Gohla, Vitamin A-loaded solid lipid nanoparticles for topical use: drug release properties. *J Control Release*: 66, 115-126 (2000)
54. C. Song and S. Liu, A new healthy sunscreen system for human: solid lipid nanoparticles as carrier for 3,4,5-trimethoxybenzoylchitin and the improvement by adding Vitamin E. *Int J Biol Macromol*: 36, 116-119 (2005)
55. S. A. Wissing and R. H. Muller, Solid lipid nanoparticles as carrier for sunscreens: in vitro release and in vivo skin penetration. *J Control Release*: 81, 225-233 (2002)
56. H. Chen, X. Chang, D. Du, W. Liu, J. Liu, T. Weng, Y. Yang, H. Xu and X. Yang, Podophyllotoxin-loaded solid lipid nanoparticles for epidermal targeting. *J Control Release*: 110, 296-306 (2006)
57. Z. Mei, H. Chen, T. Weng, Y. Yang and X. Yang, Solid lipid nanoparticle and microemulsion for topical delivery of triptolide. *Eur J Pharm Biopharm*: 56, 189-196 (2003)
58. M. Higaki, M. Kameyama, M. Udagawa, Y. Ueno, Y. Yamaguchi, R. Igarashi, T. Ishihara and Y. Mizushima, Transdermal delivery of CaCO₃-nanoparticles containing insulin. *Diabetes Technol Ther*: 8, 369-374 (2006)
59. M. Uner, S. A. Wissing, G. Yener and R. H. Muller, Skin moisturizing effect and skin penetration of ascorbyl palmitate entrapped in solid lipid nanoparticles (SLN) and nanostructured lipid carriers (NLC) incorporated into hydrogel. *Pharmazie*: 60, 751-755 (2005)
60. M. Ricci, C. Puglia, F. Bonina, C. Di Giovanni, S. Giovagnoli and C. Rossi, Evaluation of indomethacin percutaneous absorption from nanostructured lipid carriers (NLC): in vitro and in vivo studies. *J Pharm Sci*: 94, 1149-1159 (2005)
61. R. H. Muller, M. Radtke and S. A. Wissing, Solid lipid nanoparticles (SLN) and nanostructured lipid carriers (NLC) in cosmetic and dermatological preparations. *Adv Drug Deliv Rev*: 54 Suppl 1, S131-155 (2002)
62. A. Vogt, B. Combadiere, S. Hadam, K. M. Stieler, J. Lademann, H. Schaefer, B. Aufran, W. Sterry and U. Blume-Peytavi, 40 nm, but not 750 or 1,500 nm, nanoparticles enter epidermal CD1a+ cells after transcutaneous application on human skin. *J Invest Dermatol*: 126, 1316-1322 (2006)
63. Z. Cui and R. J. Mumper, Topical immunization using nanoengineered genetic vaccines. *J Control Release*: 81, 173-184 (2002)
64. Z. Cui, L. Baizer and R. J. Mumper, Intradermal immunization with novel plasmid DNA-coated nanoparticles via a needle-free injection device. *J Biotechnol*: 102, 105-115 (2003)
65. N. Hussain, V. Jaitley and A. T. Florence, Recent advances in the understanding of uptake of microparticulates across the gastrointestinal lymphatics. *Adv Drug Deliv Rev*: 50, 107-142 (2001)
66. Y. Dong and S. S. Feng, Poly(d,l-lactide-co-glycolide)/montmorillonite nanoparticles for oral delivery of anticancer drugs. *Biomaterials*: 26, 6068-6076 (2005)
67. Z. Li, S. Zhu, K. Gan, Q. Zhang, Z. Zeng, Y. Zhou, H. Liu, W. Xiong, X. Li and G. Li, Poly-L-lysine-modified silica nanoparticles: a potential oral gene delivery system. *J Nanosci Nanotechnol*: 5, 1199-1203 (2005)
68. M. P. Desai, V. Labhsetwar, G. L. Amidon and R. J. Levy, Gastrointestinal uptake of biodegradable microparticles: effect of particle size. *Pharm Res*: 13, 1838-1845 (1996)

References

69. J. F. Hillyer and R. M. Albrecht, Gastrointestinal persorption and tissue distribution of differently sized colloidal gold nanoparticles. *J Pharm Sci*: 90, 1927-1936 (2001)
70. M. Shakweh, M. Besnard, V. Nicolas and E. Fattal, Poly (lactide-co-glycolide) particles of different physicochemical properties and their uptake by peyer's patches in mice. *Eur J Pharm Biopharm*: 61, 1-13 (2005)
71. P. Jani, G. W. Halbert, J. Langridge and A. T. Florence, Nanoparticle uptake by the rat gastrointestinal mucosa: quantitation and particle size dependency. *J Pharm Pharmacol*: 42, 821-826 (1990)
72. F. Delie, Evaluation of nano- and microparticle uptake by the gastrointestinal tract. *Adv Drug Deliv Rev*: 34, 221-233 (1998)
73. S. Hariharan, V. Bhardwaj, I. Bala, J. Sitterberg, U. Bakowsky and M. N. Ravi Kumar, Design of estradiol loaded PLGA nanoparticulate formulations: a potential oral delivery system for hormone therapy. *Pharm Res*: 23, 184-195 (2006)
74. M. H. El-Shabouri, Positively charged nanoparticles for improving the oral bioavailability of cyclosporin-A. *Int J Pharm*: 249, 101-108 (2002)
75. C. M. Lehr, J. A. Bouwstra, W. Kok, A. B. Noach, A. G. de Boer and H. E. Junginger, Bioadhesion by means of specific binding of tomato lectin. *Pharm Res*: 9, 547-553 (1992)
76. I. Ezpeleta, M. A. Arangoa, J. M. Irache, S. Stainmesse, C. Chabenat, Y. Popineau and A. M. Orecchioni, Preparation of Ulex europaeus lectin-gliadin nanoparticle conjugates and their interaction with gastrointestinal mucus. *Int J Pharm*: 191, 25-32 (1999)
77. M. A. Arangoa, G. Ponchel, A. M. Orecchioni, M. J. Renedo, D. Duchene and J. M. Irache, Bioadhesive potential of gliadin nanoparticulate systems. *Eur J Pharm Sci*: 11, 333-341 (2000)
78. N. Hussain and A. T. Florence, Utilizing bacterial mechanisms of epithelial cell entry: invasin-induced oral uptake of latex nanoparticles. *Pharm Res*: 15, 153-156 (1998)
79. G. F. Dawson and G. W. Halbert, The in vitro cell association of invasin coated polylactide-co-glycolide nanoparticles. *Pharm Res*: 17, 1420-1425 (2000)
80. C. T. Lee, C. P. Huang and Y. D. Lee, Synthesis and characterizations of amphiphilic poly(l-lactide)-grafted chondroitin sulfate copolymer and its application as drug carrier. *Biomol Eng*, doi: 10.1016/j.bioeng.2006.05.010 (2006)
81. C. Pimienta, V. Lenaerts, C. Cadieux, P. Raymond, J. Juhasz, M. A. Simard and C. Jolicoeur, Mucoadhesion of hydroxypropylmethacrylate nanoparticles to rat intestinal ileal segments in vitro. *Pharm Res*: 7, 49-53 (1990)
82. K. Yoncheva, S. Gomez, M. A. Campanero, C. Gamazo and J. M. Irache, Bioadhesive properties of pegylated nanoparticles. *Expert Opin Drug Deliv*: 2, 205-218 (2005)
83. G. Sandri, M. C. Bonferoni, S. Rossi, F. Ferrari, S. Gibin, Y. Zambito, G. Di Colo and C. Caramella, Nanoparticles based on N-trimethylchitosan: Evaluation of absorption properties using in vitro (Caco-2 cells) and ex vivo (excised rat jejunum) models. *Eur J Pharm Biopharm*, doi: 10.1016/j.ejpb.2006.07.016 (2006)
84. G. P. Carino, J. S. Jacob and E. Mathiowitz, Nanosphere based oral insulin delivery. *J Control Release*: 65, 261-269 (2000)

References

85. C. M. Adeyeye, J. D. Bricker, V. D. Vilivalam and W. I. Smith, Acute gastrointestinal toxic effects of suspensions of unencapsulated and encapsulated ibuprofen in rats. *Pharm Res*: 13, 784-793 (1996)
86. S. Sakuma, M. Hayashi and M. Akashi, Design of nanoparticles composed of graft copolymers for oral peptide delivery. *Adv Drug Deliv Rev*: 47, 21-37 (2001)
87. M. S. Mesiha, M. B. Sidhom and B. Fasipe, Oral and subcutaneous absorption of insulin poly(isobutyrylcyanoacrylate) nanoparticles. *Int J Pharm*: 288, 289-293 (2005)
88. F. Qian, F. Cui, J. Ding, C. Tang and C. Yin, Chitosan graft copolymer nanoparticles for oral protein drug delivery: preparation and characterization. *Biomacromolecules*: 7, 2722-2727 (2006)
89. Z. Ma, T. M. Lim and L. Y. Lim, Pharmacological activity of peroral chitosan-insulin nanoparticles in diabetic rats. *Int J Pharm*: 293, 271-280 (2005)
90. Y. Luo, D. Chen, L. Ren, X. Zhao and J. Qin, Solid lipid nanoparticles for enhancing vinpocetine's oral bioavailability. *J Control Release*: 114, 53-59 (2006)
91. J. W. Simecka, Mucosal immunity of the gastrointestinal tract and oral tolerance. *Adv Drug Deliv Rev*: 34, 235-259 (1998)
92. M. A. Conway, L. Madrigal-Estebas, S. McClean, D. J. Brayden and K. H. Mills, Protection against *Bordetella pertussis* infection following parenteral or oral immunization with antigens entrapped in biodegradable particles: effect of formulation and route of immunization on induction of Th1 and Th2 cells. *Vaccine*: 19, 1940-1950 (2001)
93. M. Bivas-Benita, M. Laloup, S. Versteheyhe, J. Dewit, J. De Braekeleer, E. Jongert and G. Borchard, Generation of *Toxoplasma gondii* GRA1 protein and DNA vaccine loaded chitosan particles: preparation, characterization, and preliminary in vivo studies. *Int J Pharm*: 266, 17-27 (2003)
94. J. L. Chew, C. B. Wolfowicz, H. Q. Mao, K. W. Leong and K. Y. Chua, Chitosan nanoparticles containing plasmid DNA encoding house dust mite allergen, Der p 1 for oral vaccination in mice. *Vaccine*: 21, 2720-2729 (2003)
95. A. T. Florence and N. Hussain, Transcytosis of nanoparticle and dendrimer delivery systems: evolving vistas. *Adv Drug Deliv Rev*: 50 Suppl 1, S69-89 (2001)
96. A. Lamprecht, N. Ubrich, H. Yamamoto, U. Schafer, H. Takeuchi, P. Maincent, Y. Kawashima and C. M. Lehr, Biodegradable nanoparticles for targeted drug delivery in treatment of inflammatory bowel disease. *J Pharmacol Exp Ther*: 299, 775-781 (2001)
97. H. Nakase, K. Okazaki, Y. Tabata, S. Uose, M. Ohana, K. Uchida, Y. Matsushima, C. Kawanami, C. Oshima, Y. Ikada and T. Chiba, Development of an oral drug delivery system targeting immune-regulating cells in experimental inflammatory bowel disease: a new therapeutic strategy. *J Pharmacol Exp Ther*: 292, 15-21 (2000)
98. A. Lamprecht, H. Yamamoto, H. Takeuchi and Y. Kawashima, Nanoparticles enhance therapeutic efficiency by selectively increased local drug dose in experimental colitis in rats. *J Pharmacol Exp Ther*: 315, 196-202 (2005)
99. Y. Meissner, Y. Pellequer and A. Lamprecht, Nanoparticles in inflammatory bowel disease: particle targeting versus pH-sensitive delivery. *Int J Pharm*: 316, 138-143 (2006)
100. R. A. Jain, The manufacturing techniques of various drug loaded biodegradable poly(lactide-co-glycolide) (PLGA) devices. *Biomaterials*: 21, 2475-2490 (2000)
101. A. Goepferich, Mechanism of polymer degradation and erosion. *Biomaterials*: 17, 103-114 (1996)

References

102. K. M. Huh, Y. W. Cho and K. Park, PLGA-PEG Block Copolymers for Drug Formulations. *Drug Delivery Technology*: 3 (2003)
103. F. von Burkersroda, L. Schedl and A. Goepferich, Why degradable polymers undergo surface erosion or bulk erosion. *Biomaterials*: 23, 4221-4231 (2002)
104. J. Panyam, W. Z. Zhou, S. Prabha, S. K. Sahoo and V. Labhasetwar, Rapid endo-lysosomal escape of poly(DL-lactide-co-glycolide) nanoparticles: implications for drug and gene delivery. *Faseb J*: 16, 1217-1226 (2002)
105. U. Bilati, E. Allemann and E. Doelker, Poly(D,L-lactide-co-glycolide) protein-loaded nanoparticles prepared by the double emulsion method--processing and formulation issues for enhanced entrapment efficiency. *J Microencapsul*: 22, 205-214 (2005)
106. D. Quintanar-Guerrero, E. Allemann, H. Fessi and E. Doelker, Pseudolatex preparation using a novel emulsion-diffusion process involving direct displacement of partially water-miscible solvents by distillation. *Int J Pharm*: 188, 155-164 (1999)
107. J. W. Vanderhoff, M. S. El-Aasser and J. Ugelstad, Polymer emulsification process. US Patent 4177177 (1979)
108. D. Quintanar-Guerrero, H. Fessi, E. Allemann and E. Doelker, Influence of stabilizing agents and preparative variables on the formation of poly(D,L-lactic acid)nanoparticles by an emulsification-diffusion technique. *Int J Pharm*: 143, 133-141 (1996)
109. A. Lamprecht, N. Ubrich, M. Hombreiro Perez, C. Lehr, M. Hoffman and P. Maincent, Biodegradable monodispersed nanoparticles prepared by pressure homogenization-emulsification. *Int J Pharm*: 184, 97-105 (1999)
110. Y. N. Konan, R. Cerny, J. Favet, M. Berton, R. Gurny and E. Allemann, Preparation and characterization of sterile sub-200 nm meso-tetra(4-hydroxyphenyl)porphyrin-loaded nanoparticles for photodynamic therapy. *Eur J Pharm Biopharm*: 55, 115-124 (2003)
111. H. Fessi, F. Puisieux, J. P. Devissaguet, N. Ammoury and S. Benita, Nanocapsule formation by interfacial polymer deposition following solvent displacement. *Int J Pharm*: 55, R1-R4 (1989)
112. U. Bilati, E. Allemann and E. Doelker, Development of a nanoprecipitation method intended for the entrapment of hydrophilic drugs into nanoparticles. *Eur J Pharm Sci*: 24, 67-75 (2005)
113. U. Bilati, E. Allemann and E. Doelker, Nanoprecipitation versus emulsion-based techniques for the encapsulation of proteins into biodegradable nanoparticles and process-related stability issues. *AAPS PharmSciTech*: 6, E594-604 (2005)
114. W. Abdelwahed, G. Degobert and H. Fessi, Investigation of nanocapsules stabilization by amorphous excipients during freeze-drying and storage. *Eur J Pharm Biopharm*: 63, 87-94 (2006)
115. M. Chacon, J. Molpeceres, L. Berges, M. Guzman and M. R. Aberturas, Stability and freeze-drying of cyclosporine loaded poly(D,L lactide-glycolide) carriers. *Eur J Pharm Sci*: 8, 99-107 (1999)
116. M. Ueda, A. Iwara and J. Kreuter, Influence of the preparation methods on the drug release behaviour of loperamide-loaded nanoparticles. *J Microencapsul*: 15, 361-372 (1998)
117. K. S. Soppimath, T. M. Aminabhavi, A. R. Kulkarni and W. E. Rudzinski, Biodegradable polymeric nanoparticles as drug delivery devices. *J Control Release*: 70, 1-20 (2001)

References

118. H. S. Yoo, J. E. Oh, K. H. Lee and T. G. Park, Biodegradable nanoparticles containing doxorubicin-PLGA conjugate for sustained release. *Pharm Res*: 16, 1114-1118 (1999)
119. G. Dalwadi, H. A. Benson and Y. Chen, Comparison of diafiltration and tangential flow filtration for purification of nanoparticle suspensions. *Pharm Res*: 22, 2152-2162 (2005)
120. M. C. Venier-Julienne and J. P. Benoit, Preparation, purification and morphology of polymeric nanoparticles as drug carriers. *Pharm Acta Helv*: 71, 121-128 (1996)
121. L. Mu and S. S. Feng, PLGA/TPGS nanoparticles for controlled release of paclitaxel: effects of the emulsifier and drug loading ratio. *Pharm Res*: 20, 1864-1872 (2003)
122. W. K. Lee, J. Y. Park, E. H. Yang, H. Suh, S. H. Kim, D. S. Chung, K. Choi, C. W. Yang and J. S. Park, Investigation of the factors influencing the release rates of cyclosporin A-loaded micro- and nanoparticles prepared by high-pressure homogenizer. *J Control Release*: 84, 115-123 (2002)
123. J. Panyam, M. M. Dali, S. K. Sahoo, W. Ma, S. S. Chakravarthi, G. L. Amidon, R. J. Levy and V. Labhasetwar, Polymer degradation and in vitro release of a model protein from poly(D,L-lactide-co-glycolide) nano- and microparticles. *J Control Release*: 92, 173-187 (2003)
124. M. Dunne, I. Corrigan and Z. Ramtoola, Influence of particle size and dissolution conditions on the degradation properties of polylactide-co-glycolide particles. *Biomaterials*: 21, 1659-1668 (2000)
125. U. Westedt, L. Barbu-Tudoran, A. K. Schaper, M. Kalinowski, H. Alfke and T. Kissel, Deposition of nanoparticles in the arterial vessel by porous balloon catheters: localization by confocal laser scanning microscopy and transmission electron microscopy. *AAPS PharmSci*: 4, E41 (2002)
126. S. Prabha, W. Z. Zhou, J. Panyam and V. Labhasetwar, Size-dependency of nanoparticle-mediated gene transfection: studies with fractionated nanoparticles. *Int J Pharm*: 244, 105-115 (2002)
127. C. C. Müller-Goymann, Physicochemical characterization of colloidal drug delivery systems such as reverse micelles, vesicles, liquid crystals and nanoparticles for topical administration. *Eur J Pharm Biopharm*: 59, 343-356 (2004)
128. R. H. Müller and R. Schuhmann, Teilchengrößenmessung in der Laborpraxis. *WVG, Stuttgart* 1996: p. 25
129. nitioncom/en/products/zeecom_s.htm, accessed on 21/08/06
130. Z. Zhang and S. S. Feng, The drug encapsulation efficiency, in vitro drug release, cellular uptake and cytotoxicity of paclitaxel-loaded poly(lactide)-tocopheryl polyethylene glycol succinate nanoparticles. *Biomaterials*: 27, 4025-4033 (2006)
131. N. Csaba, L. Gonzalez, A. Sanchez and M. J. Alonso, Design and characterisation of new nanoparticulate polymer blends for drug delivery. *J Biomater Sci Polym Ed*: 15, 1137-1151 (2004)
132. J. S. Hrkach, M. T. Peracchia, A. Domb, N. Lotan and R. Langer, Nanotechnology for biomaterials engineering: structural characterization of amphiphilic polymeric nanoparticles by ¹H NMR spectroscopy. *Biomaterials*: 18, 27-30 (1997)
133. C. Chen, C. H. Yu, Y. C. Cheng, P. H. Yu and M. K. Cheung, Biodegradable nanoparticles of amphiphilic triblock copolymers based on poly(3-hydroxybutyrate) and poly(ethylene glycol) as drug carriers. *Biomaterials*: 27, 4804-4814 (2006)

References

134. A. M. Layre, P. Couvreur, H. Chacun, C. Aymes-Chodur, N. E. Ghermani, J. Poupaert, J. Richard, D. Requier and R. Gref, Busulfan loading into poly(alkyl cyanoacrylate) nanoparticles: Physicochemistry and molecular modeling. *J Biomed Mater Res B Appl Biomater*: (2006)
135. O. Sanli, N. Ay and N. Isiklan, Release characteristics of diclofenac sodium from poly(vinyl alcohol)/sodium alginate and poly(vinyl alcohol)-grafted-poly(acrylamide)/sodium alginate blend beads. *Eur J Pharm Biopharm*, doi: 10.1016/j.ejpb.2006.08.004 (2006)
136. K. Nam, T. Kimura and A. Kishida, Preparation and characterization of cross-linked collagen-phospholipid polymer hybrid gels. *Biomaterials*: 28, 1-8 (2007)
137. T. R. Noel, R. Parker, G. J. Brownsey, I. A. Farhat, W. MacNaughtan and S. G. Ring, Physical aging of starch, maltodextrin, and maltose. *J Agric Food Chem*: 53, 8580-8585 (2005)
138. A. Saez, M. Guzman, J. Molpeceres and M. R. Aberturas, Freeze-drying of polycaprolactone and poly(D,L-lactic-glycolic) nanoparticles induce minor particle size changes affecting the oral pharmacokinetics of loaded drugs. *Eur J Pharm Biopharm*: 50, 379-387 (2000)
139. W. Abdelwahed, G. Degobert and H. Fessi, A pilot study of freeze drying of poly(epsilon-caprolactone) nanocapsules stabilized by poly(vinyl alcohol): formulation and process optimization. *Int J Pharm*: 309, 178-188 (2006)
140. A. Lamprecht, N. Ubrich, H. Yamamoto, U. F. Schaefer, H. Takeuchi, P. Maincent, Y. Kawashima and C. M. Lehr, Biodegradable nanoparticles for targeted drug delivery in treatment of inflammatory bowel disease. *J Pharmacol Exp Ther*: 299, 775-781 (2001)
141. E. Horisawa, K. Kubota, I. Tuboi, K. Sato, H. Yamamoto, H. Takeuchi and Y. Kawashima, Size-dependency of DL-lactide/glycolide copolymer particulates for intra-articular delivery system on phagocytosis in rat synovium. *Pharm Res*: 19, 132-139 (2002)
142. B. Weiss, U. F. Schaefer, J. Zapp, A. Lamprecht, A. Stallmach and C.-M. Lehr, Nanoparticles made of fluorescence-labelled PLGA: preparation, stability and biocompatibility. *J Nanosci Nanotechnol*: 6, 3048-3056 (2006)
143. N. Ubrich, P. Bouillot, C. Pellerin, M. Hoffman and P. Maincent, Preparation and characterization of propranolol hydrochloride nanoparticles: a comparative study. *J Control Release*: 97, 291-300 (2004)
144. P. Ahlin, J. Kristl, A. Kristl and F. Vrecer, Investigation of polymeric nanoparticles as carriers of enalaprilat for oral administration. *Int J Pharm*: 239, 113-120 (2002)
145. V. Saxena, M. Sadoqi and J. Shao, Indocyanine green-loaded biodegradable nanoparticles: preparation, physicochemical characterization and in vitro release. *Int J Pharm*: 278, 293-301 (2004)
146. S. Bozdog, K. Dillen, J. Vandervoort and A. Ludwig, The effect of freeze-drying with different cryoprotectants and gamma-irradiation sterilization on the characteristics of ciprofloxacin HCl-loaded poly(D,L-lactide-glycolide) nanoparticles. *J Pharm Pharmacol*: 57, 699-707 (2005)
147. D. Quintanar-Guerrero, A. Ganem-Quintanar, E. Allemann, H. Fessi and E. Doelker, Influence of the stabilizer coating layer on the purification and freeze-drying of poly(D,L-lactic acid) nanoparticles prepared by an emulsion-diffusion technique. *J Microencapsul*: 15, 107-119 (1998)
148. F. De Jaeghere, E. Allemann, J. C. Leroux, W. Stevels, J. Feijen, E. Doelker and R. Gurny, Formulation and lyoprotection of poly(lactic acid-co-ethylene oxide) nanoparticles: influence on physical stability and in vitro cell uptake. *Pharm Res*: 16, 859-866 (1999)

References

149. M. Vert, S. Li and H. Garreau, New insights on the degradation of bioresorbable polymeric devices based on lactic and glycolic acids. *Clin Mater*: 10, 3-8 (1992)
150. G. A. Simon and H. I. Maibach, The pig as an experimental animal model of percutaneous permeation in man: qualitative and quantitative observations-an overview. *Skin Pharmacol Appl Skin Physiol*: 13, 229-234 (2000)
151. J. Lademann, H. Richter, A. Teichmann, N. Otberg, U. Blume-Peytavi, J. Luengo, B. Weiss, U. F. Schaefer, C.-M. Lehr, R. Wepf and W. Sterry, Nanoparticles - an efficient carrier for drug delivery into the hair follicles. *Eur J Pharm Biopharm*, doi: 10.1016/j.ejpb.2006.10.019 (2006)
152. S. S. Biel, K. Kawaschinski, K. P. Wittern, U. Hintze and R. Wepf, From tissue to cellular ultrastructure: closing the gap between micro- and nanostructural imaging. *J Microsc*: 212, 91-99 (2003)
153. H. Weigmann, J. Lademann, H. Meffert, H. Schaefer and W. Sterry, Determination of the horny layer profile by tape stripping in combination with optical spectroscopy in the visible range as a prerequisite to quantify percutaneous absorption. *Skin Pharmacol Appl Skin Physiol*: 12, 34-45 (1999)
154. J. Lademann, H. Weigmann, C. Rickmeyer, H. Barthelmes, H. Schaefer, G. Mueller and W. Sterry, Penetration of titanium dioxide microparticles in a sunscreen formulation into the horny layer and the follicular orifice. *Skin Pharmacol Appl Skin Physiol*: 12, 247-256 (1999)
155. F. Stracke, B. Weiss, C. M. Lehr, K. König, U. F. Schaefer and M. Schneider, Multiphoton Microscopy for the Investigation of Dermal Penetration of Nanoparticle-Borne Drugs. *J Invest Dermatol*: 126, 2224-2233 (2006)
156. K. König and I. Riemann, High-resolution multiphoton tomography of human skin with subcellular spatial resolution and picosecond time resolution. *J Biomed Opt*: 8, 432-439 (2003)
157. B. Yu, K. Hean Kim, P. T. So, D. Blankschtein and R. Langer, Topographic heterogeneity in transdermal transport revealed by high-speed two-photon microscopy: determination of representative skin sample sizes. *J Invest Dermatol*: 118, 1085-1088 (2002)
158. B. Yu, K. H. Kim, P. T. So, D. Blankschtein and R. Langer, Visualization of oleic acid-induced transdermal diffusion pathways using two-photon fluorescence microscopy. *J Invest Dermatol*: 120, 448-455 (2003)
159. H. Wagner, K. H. Kostka, C. M. Lehr and U. F. Schaefer, Drug distribution in human skin using two different in vitro test systems: comparison with in vivo data. *Pharm Res*: 17, 1475-1481 (2000)
160. K. Fu, D. W. Pack, A. M. Klibanov and R. Langer, Visual evidence of acidic environment within degrading poly(lactic-co-glycolic acid) (PLGA) microspheres. *Pharm Res*: 17, 100-106 (2000)
161. A. K. Kohli and H. O. Alpar, Potential use of nanoparticles for transcutaneous vaccine delivery: effect of particle size and charge. *Int J Pharm*: 275, 13-17 (2004)
162. J. Lademann, H. Schaefer, N. Otberg, A. Teichmann, U. Blume-Peytavi and W. Sterry, [Penetration of microparticles into human skin]. *Hautarzt*: 55, 1117-1119 (2004)
163. N. M. Green, Avidin. *Adv Protein Chem*: 29, 85-133 (1975)
164. N. M. Green, Avidin and streptavidin. *Methods Enzymol*: 184, 51-67 (1990)

References

165. B. Weiss, M. Schneider, S. Taetz, D. Neumann, U. F. Schaefer and C.-M. Lehr, Coupling of biotin-(polyethyleneglycol)amine to poly(D,L-lactide-co-glycolide) nanoparticles for versatile surface modification. *submitted to Bioconjug Chem (2006)*
166. A. J. Bradley and M. D. Scott, Separation and purification of methoxypoly(ethylene glycol) grafted red blood cells via two-phase partitioning. *J Chromatogr B Analyt Technol Biomed Life Sci*: 807, 163-168 (2004)
167. H. Rayle and L. Fellmeth, Development of a Process for Triazine-Promoted Amidation of Carboxylic Acids. *Org Proc Res Dev*: 3, 172-176 (1999)
168. S. M. Moghimi, Chemical camouflage of nanospheres with a poorly reactive surface: towards development of stealth and target-specific nanocarriers. *Biochim Biophys Acta*: 1590, 131-139 (2002)
169. L. Pugliese, A. Coda, M. Malcovati and M. Bolognesi, Three-dimensional structure of the tetragonal crystal form of egg-white avidin in its functional complex with biotin at 2.7 Å resolution. *J Mol Biol*: 231, 698-710 (1993)

6 Forthcoming publications

The following publications resulted from the present thesis (the corresponding chapter is indicated within parenthesis):

B. Weiss, U.F. Schaefer, J. Zapp, A. Lamprecht, A. Stallmach, C.-M. Lehr, Nanoparticles made of fluorescence-labelled poly(L-lactide-co-glycolide): preparation, stability, and bio-compatibility. *J Nanosci Nanotechnol*: 6, 3048-3056 (2006) (6.1)

J. Lademann, H. Richter, A. Teichmann, N. Otberg, U. Blume-Peytavi, J. Luengo, B. Weiss, U.F. Schaefer, C.-M. Lehr, R. Wepf, W. Sterry, Nanoparticles – an efficient carrier for drug delivery into the hair follicles. *Eur J Pharm Biopharm* doi: 10.1016/j.ejpb.2006.10.019 (2006) (6.2)

F. Stracke, B. Weiss, C.-M. Lehr, K. König, U.F. Schaefer, M. Schneider, Multiphoton Microscopy for the Investigation of Dermal Penetration of Nanoparticle-Borne Drugs. *J Invest Dermatol*: 126, 2224-2233 (2006) (6.3)

J. Luengo, B. Weiss, M. Schneider, A. Ehlers, F. Stracke, K. König, K.-H. Kostka, C.-M. Lehr, U.F. Schaefer, Influence of nanoencapsulation on human skin transport of flufenamic acid. *Skin Pharmacol Physiol*: 19, 190-197 (2006) (6.4)

B. Weiss, M. Schneider, S. Taetz, D. Neumann, U.F. Schaefer, C.-M. Lehr, Coupling of biotin-(polyethyleneglycol)amine to poly(D,L-lactide-co-glycolide) nanoparticles for versatile surface modification. *submitted to Bioconjug Chem* (2006) (6.5)



Nanoparticles Made of Fluorescence-Labelled PLGA: Preparation, Stability, and Biocompatibility

Barbara Weiss¹, Ulrich F. Schaefer¹, Josef Zapp², Alf Lamprecht³, Andreas Stallmach⁴, and Claus-Michael Lehr^{1,*}

¹Department of Biopharmaceutics and Pharmaceutical Technology, Saarland University, Saarbruecken, Germany

²Department of Pharmaceutical Biology, Saarland University, Saarbruecken, Germany

³Laboratory of Pharmaceutical Engineering, University of Franche-Comté, Besançon Cedex, France

⁴Department of Gastroenterology, Hepatology and Infectiology, Friedrich-Schiller-University, Jena, Germany

Nanoparticles have recently been demonstrated in a rat model to be a promising tool for targeting inflamed areas of the intestinal mucosa in inflammatory bowel diseases whilst concentrating anti-inflammatory drugs at their site of action. Still, however, this novel concept has to be proven *in vivo* in humans. As a first step biodegradable and biocompatible fluorescent nanoparticles were prepared and characterized to serve as markers for successful inflammation targeting in future clinical trials. To achieve stable fluorescence labelling, fluoresceinamine was covalently bound to poly(L-lactide-co-glycolide) (PLGA) as described by Horisawa et al. The modification rate of carboxyl-end groups of the PLGA chains determined by ¹H NMR was 65%. From this modified polymer, nanoparticles (FA-PLGA nanoparticles) of approximately 270 nm size were prepared via nanoprecipitation. Apart from an initial burst effect, most of the label (>88%) appeared to be strongly bound and was leaked only slowly from the particles. In contrast, we found an immediate leakage of encapsulated sodium fluorescein with nanoparticles prepared by a double emulsion method. In degradation experiments we studied and visualized the changes in morphology and elastic properties of the FA-PLGA nanoparticles within 15 weeks using atomic force microscopy. When FA-PLGA nanoparticles were applied on an *in vitro* model of the intestinal mucosa (Caco-2 cell culture), only minor amounts of their fluorescent degradation products (~0.02% after 6 h) were transported. In a cytotoxicity study with Caco-2 cells, FA-PLGA nanoparticles yielded an IC₅₀ value as for plain PLGA nanoparticles. In conclusion, the polymer modification method allows to prepare fluorescently labelled nanoparticles from a well-known biodegradable pharmaceutical polymer with sufficient stability to be monitored over a period of several days. Some initial leakage of fluorescence label appears to be unavoidable but negligible with respect to potential absorption and cytotoxicity when applied *in vivo*.

Keywords: Fluoresceinamine, PLGA Modification, Atomic Force Microscopy, Caco-2 Cells, Cytotoxicity, NMR.

1. INTRODUCTION

In the recent years, polymeric nanoparticles have turned out to be a promising tool for the targeted delivery of drugs to specific anatomical sites. Nanoparticles may exhibit significant interactions with the intestine,¹ the skin,^{2,3} the blood brain barrier,⁴ and various other tissues of interest. In general, drug targeting at the cellular or tissue level appears to be size-dependent.⁵ Smaller particles seem to be taken up to a higher degree than larger ones, representing a crucial advantage of nanoparticles over microparticles.

Concerning the intestine, polymeric particulate carrier systems have potential for targeting of inflamed areas of the gut mucosa in inflammatory bowel diseases (IBD).

Previously, some size dependent accumulation and prolonged retention of orally administered micro- and nanoparticles in the affected regions of the large intestine have been studied in rats, suggesting that the smaller the particle size the better the binding to the inflamed tissue.¹ The standard treatment of IBD involves the frequent intake of anti-inflammatory drugs at high doses. In general, these drugs are administered orally and become systemically bioavailable, often leading to strong adverse effects. Thus, targeting the inflamed areas of the intestine and, hence, concentrating the drug at its site of action can reduce possible systemic adverse effects. This has previously been demonstrated in a rat colitis model by our group⁶ using rolipram as an anti-inflammatory model drug. Furthermore, as generally known, polymeric nanoparticles can be

* Author to whom correspondence should be addressed.

designed to control drug release. Therefore, the use of nanoparticles also implicates the possibility to reduce the dosage frequency.

Considering these promising results in animals, a proof of concept for this novel targeting approach in IBD must be provided in humans. For such purpose, drug-free but fluorescence-labelled nanoparticles are needed to show their accumulation in inflamed areas of the colonic mucosa in IBD patients by fluorescence microscopy. At the same time non-toxicity and biocompatibility of the nanoparticles are essential requirements, and as a consequence the choice of their components is rather restricted. Among the pharmaceutical polymers, poly(D,L-lactide-co-glycolide) (PLGA) appears as most suitable because this material is biocompatible, biodegradable, and part of several registered and marketed drug and medicinal products even for parenteral applications.⁷⁻¹⁰ As a fluorescence marker, fluorescein is well common, being also applied in high doses for diagnostic purposes, e.g., the usual dose for retinal angiography in adults is the equivalent of 500 mg given by rapid intravenous injection.¹¹

However, it is still crucial for intended studies that the fluorescence label remains firmly associated with the nanoparticles over an appreciable period of time i.e., a burst effect and a subsequent leakage of the fluorescent label must be minimized as far as possible. Though, this is not trivial when dealing with nanoparticles made of a biodegradable polymer.

In the present study, fluorescent biodegradable and biocompatible nanoparticles for the purpose of future *in vivo* endoscopic investigations of IBD in humans were prepared. The fluorescein derivative 5-fluoresceinamine (FA) was chemically bound to PLGA by a simple one-step reaction.¹² Nanoparticles made from this modified polymer (FA-PLGA nanoparticles) were characterized for their *in vitro* leakage of fluorescence marker, size, charge, and morphology. For comparison, fluorescently labelled nanoparticles were also prepared by nano-encapsulation of sodium fluorescein with non-modified PLGA using a double emulsion method (FC-PLGA nanoparticles). The morphology of nanoparticles was imaged within long-term particle degradation using atomic force microscopy and the development of the surface structure as well as the changes of the physical parameter elasticity during degradation were monitored. Furthermore, nanoparticles were applied to Caco-2 cell monolayers in order to evaluate the interaction with intestinal epithelial cells, addressing absorption of degradation products and potential cytotoxicity.

2. METHODS AND MATERIALS

2.1. Materials

Poly(L-lactide-co-glycolide) (PLGA) (Resomer RG 50:50 H; inherent viscosity 0.31 dl/g) was kindly provided by Boehringer Ingelheim (Boehringer Ingelheim GmbH

& Co., KG, Ingelheim, GE). 5-Fluoresceinamine (FA), sodium fluorescein (FC), and 1-ethyl-3-(3-Dimethylaminopropyl)-carbodiimide hydrochloride (DMAP) were obtained from Sigma (Sigma Chemical Co., St. Louis, MO, USA). Polyvinylalcohol (PVA) (Mowiol 4-88) was purchased from Kuraray (Kuraray Specialities GmbH, Frankfurt am Main, GE). Dulbecco's modified Eagle's medium (DMEM), non-essential aminoacids (NeAA), and fetal bovine serum (FBS) were provided by GIBCO (Invitrogen Corp., Carlsbad, CA, USA). All other chemicals were of analytical grade. Hank's balanced salt solution (HBSS) was composed of: NaCl 8.000 g/L, KCl 0.400 g/L, NaHCO₃ 0.358 g/L, Na₂HPO₄ 0.048 g/L, KH₂PO₄ 0.06g/L, glucose 1.000 g/L, HEPES (C₈H₁₈N₂O₄S) 2.388 g/L, CaCl₂ 0.140 g/L, MgCl₂ 0.047 g/L, MgSO₄ × 7 H₂O 0.100 g/L. Phosphate buffered solution pH 7.4 (PBS) was composed of KCl 0.20 g/L, NaCl 8.00 g/L, KH₂PO₄ 0.20 g/L, Na₂HPO₄ × 2H₂O 1.44 g/L. Graphs were fitted using SigmaPlot 8.0 (SPSS Inc., Chicago, IL, USA) and results are expressed as mean ± SD or as range.

2.2. Preparation of Nanoparticles

2.2.1. Polymer Labeling and Preparation of FA-PLGA Nanoparticles

FA bound PLGA (FA-PLGA) was prepared based upon the method described by Horisawa et al.¹² Briefly, PLGA (3.07 g) and FA (0.0583 g) were dissolved entirely in 30 ml of acetonitrile with 0.0408 g of DMAP and incubated at room temperature for 24 h under light protection and gentle stirring. The resulting FA-PLGA was precipitated by the addition of purified water and separated by centrifugation. The polymer was rinsed from excessive reagents (repeated dissolution in acetone and precipitation with ethanol) and then lyophilized (Alpha 2-4 LSC, Martin Christ Gefriertrocknungsanlagen GmbH, Osterode, GE).

FA-PLGA nanoparticles were prepared by interfacial polymer deposition (nanoprecipitation) as described by Fessi et al.¹³ 100 mg of FA-PLGA were dissolved in 16 ml of acetone at room temperature. After addition of 3 ml of ethanol, the polymer solution (final concentration 5.3 mg/ml) was pumped into 25 ml of a 0.5% PVA solution in purified water in order to induce polymer precipitation and thus particle formation. Thereby, the system was gently stirred with a magnetic stirrer. Finally, the residual organic solvent was removed using a rotary evaporator and the nanoparticles were lyophilized. Nanoparticles were prepared with a total of $n = 4$.

2.2.2. Preparation of FC-PLGA Nanoparticles

FC-PLGA nanoparticles were prepared employing a double emulsion (W₁/O/W₂) method.^{14,15} The first emulsion (W₁/O) was formed between an organic polymer solution

(100 mg PLGA in 5 ml ethyl acetate) and an aqueous solution, which was 100 μ l HBSS containing 0.5 mg/ml of FC, under stirring on a magnetic stirrer for one hour. Then, the W_1/O emulsion was emulsified into 5 ml of 1% PVA solution. Stirring was continued for two more hours resulting in a $W_1/O/W_2$ double emulsion which was then homogenized using an Ultra-Turrax[®] T 25 Mixer (Janke und Kunkel GmbH & Co., Staufen, GE) at 13,500 rpm. Organic solvent was again removed by a rotary evaporator. Nanoparticles were dialyzed using a standard dialysis tube (cellulose ester, cut-off 14,000 Da) against 2 l of demineralized water for 24 h and immediately lyophilized.

The FC content of FC-PLGA nanoparticles was determined after dissolution in 0.1 N NaOH. Samples were diluted in PBS, the fluorescence was quantified using a Cytofluor II fluorescence reader (PerSeptive Biosystems, Wiesbaden-Norderstedt, GE) and the mean FC content per mg of nanoparticles was calculated. FC-PLGA nanoparticles were prepared and analyzed with a total of $n = 3-5$.

2.2.3. Preparation of PLGA Nanoparticles

PLGA nanoparticles were prepared from non-labelled polymer according to the procedure described in 2.2.1 using a 5.3 mg/ml PLGA and a 0.5% PVA solution.

2.3. FA-PLGA Labelling Efficiency

The polymer labelling efficiency, i.e., the average percentage of modified PLGA chains by a covalent coupling of FA, was determined via ¹H NMR. About 30 mg of a FA-PLGA sample were dissolved in 0.6 ml DMSO- d_6 (99.9% D) and a ¹H NMR spectrum (500 MHz) was measured using the standard pulse program for protons. 256 scans were used to get an adequate signal-to-noise ratio especially for the protons of the FA moiety. The relaxation delay was set to 10 s to allow the magnetization to achieve equilibrium. To calculate the PLGA-FA ratio the integrals of the six xanthene protons (6.4 to 6.8 ppm) of FA and those of the three H atoms of the methine and methylene groups of the lactide-glycolide dimer of PLGA were defined. The polymer labelling efficiency was determined with $n = 5$ different polymer batches. All measurements were performed at 298 K using a Bruker Avance 500 spectrometer (Bruker BioSpin GmbH, Rheinstetten, GE). Chemical shifts are given in parts per million (ppm) on the δ scale referenced to the DMSO- d_6 solvent peak at 2.50 ppm.

2.4. Physicochemical Characterization of the Nanoparticles

2.4.1. Particle Size and Surface Charge (Zeta Potential)

For determination of particle size and zeta potential, the nanoparticle dispersions were 100 fold diluted in

demineralized water and analyzed using a Zetasizer 3000 (Malvern Instruments, Malvern, U.K.). The measurement of the nanoparticle size was based upon photon correlation spectroscopy (PCS). This technique yields the particle mean diameter and the polydispersity index (PI) which is a dimensionless measure for the broadness of the particle size distribution. The zeta potential was analyzed by laser doppler electrophoresis (LDE) within a range from pH 2 to pH 10 using the automatic titration device MPT-1 (Malvern Instruments, Malvern, U.K.).

2.4.2. Morphology Studies of FA-PLGA Nanoparticles

Nanoparticle surface and shape were imaged by atomic force microscopy (AFM). For sample preparation, a drop of a freshly prepared nanoparticle suspension was mounted on a silicon wafer and air-dried. Imaging was performed by a Bioscope[™] AFM and a Nanoscope IV[™] controller (Veeco Instruments, Santa Barbara, CA, USA) in a vibration-free environment. For all measurements, Tapping mode[™] was employed using a commercially available pyramidal tip (silicon, Ultrasharp, MikroMasch, Tallinn, EST) on a cantilever with a length of 230 μ m. The resonance frequency was approximately 170 kHz, the nominal force constant 40 N/m, and the scan frequency between 0.1 and 1 Hz.

2.4.3. In Vitro Leakage of Fluorescence Markers

Lyophilized nanoparticles (10–25 mg) were suspended in a flask containing 100 ml of PBS and incubated in a horizontal oscillating water bath at 120 rpm and 37 °C. 1.0 ml samples were withdrawn at appropriate time intervals and centrifuged for 10 min at 23147 ± 66 g. The supernatant was removed and assayed for the leakage of fluorescence markers from FA-PLGA and FC-PLGA nanoparticles, respectively. In pre-experiments, a separation of nanoparticles in the size order of 270 nm under these centrifugation conditions has been confirmed (no nanoparticles in the supernatant detectable by PCS). Nanoparticle suspensions were filled up to 100 ml again with fresh PBS at each sample point. The amount of leaked fluorescence marker was evaluated by fluorescence spectroscopy using excitation and emission wavelengths of 485 nm and 510 nm, respectively. The loss of nanoparticles and fluorescence marker due to sampling was calculated and accounted for the results. References were lyophilized nanoparticles which were dissolved in 0.1 N NaOH and then diluted in PBS in case of FA-PLGA nanoparticles, and a FC solution in PBS in case of FC-PLGA nanoparticles. Linearity was given from 0.5 to 26.5 μ g/ml of FA-PLGA nanoparticles ($R^2 > 0.995$) and from 3.13 to 50.0 ng/ml of FC ($R^2 > 0.999$). The whole experiment was performed under protection from light and with a total of $n = 6$.

2.4.4. Thin Layer Chromatography (TLC)

Approximately 2 μl of each test substance and reference was spotted on a silica gel 60 TLC plate (Merck, Darmstadt, GE). Plates were developed in a chamber by the ascending technique and solvent ascend was fixed at the height of 9 cm. After development, the plates were withdrawn from the chambers and dried at room temperature. The developed plates were analyzed via fluorescence detection at 366 nm. Test substance was a 1 mg/ml particle suspension. Thereby, 0.1 N NaOH was used as a solvent in order to accelerate particle degradation. After incubation at room temperature for 12 h, the test substance was centrifuged for 10 min at 23147 ± 66 g and the supernatant was used for TLC. Reference was a 2 mg/ml FA solution in ethanol. The mobile phase consisted of a mixture of isopropanol-acetic acid (15:2, v/v).

2.4.5. FA-PLGA Nanoparticle Degradation

The physical stability of aqueous FA-PLGA nanoparticle formulations was assessed over 15 weeks. The nanoparticle suspension was dialyzed against PBS at room temperature and under gentle agitation. A dialysis membrane with a cut-off of 100,000 Da (Spectra Por[®] CE, Carl Roth GmbH, Karlsruhe, GE) was used and the buffer was renewed every week. Samples were withdrawn from the dialysis tube at appropriate time intervals and the effect of dialysis time on nanoparticle size and morphology was assessed using PCS and AFM, respectively.

2.5. Caco-2 Cell Culture

Caco-2 cells, clone C2BBel1, were purchased at passage 60 from American Tissue Culture Collection (ATCC; Manassas, VA, USA) and used at passages 70 to 91. Cells were grown to a confluency of approximately 90% in 75 cm² T-flasks with DMEM supplemented with 10% FBS and 1% NeAA. Thereby, the culture medium was changed every second day and the temperature was 37 °C in an atmosphere of around 85% relative humidity and 5% CO₂.

2.5.1. Cytotoxicity

After trypsinization, Caco-2 cells were seeded on 96-well tissue culture plates with flat bottom (Greiner Bio-One GmbH; Frickenhausen, GE) at a density of roughly 60,000 cells/cm² and grown for 7 days. Cytotoxicity was evaluated after 8 h incubation with a test substance by the quantification of plasma membrane damage leading to a release of the cytosolic enzyme LDH. It was then determined using the cytotoxicity LDH kit as described by Roche Diagnostics (Roche Diagnostics GmbH, Mannheim, GE). Experiments were performed with $n = 6$ replications for each concentration using FA-PLGA nanoparticles, PLGA nanoparticles and FC as test substances.

2.5.2. Transport Assay

Cells were trypsinized and seeded on top of Transwell permeable filter inserts (pore size 0.4 μm , 4.67 cm², Corning Incorp., Life Sciences, Acton, MA, USA) at a density of roughly 60,000 cells/cm². 21 to 25 days after seeding, Caco-2 monolayers with a transepithelial electrical resistance (TEER) > 350 $\Omega \cdot \text{cm}^2$ (background subtracted) were used for transport studies. The transport was assessed in absorptive (apical to basolateral) direction.

Prior to the transport experiments, the monolayers were incubated (30 min) with freshly prepared HBSS (pH 7.4, 37 °C) on both sides. Subsequently, starting at $t = 0$ min, a solution or suspension of the test substance was added to the donor compartment and blank HBSS to the receiver compartment.

Throughout the experiments, monolayers were agitated using an orbital shaker (IKA[®]-Werke GmbH & CO., KG; Staufen, GE) at 100 rpm. Samples were taken after 30, 60, 120, 180, 240, and 360 min from the receiver compartment and the fluorescence was determined using the Cytofluor II fluorescence reader. After each sampling, an equal volume of fresh transport buffer was added to the receiver compartment. To ensure integrity of the monolayers, TEER values were measured before the experiment, after the 30 minutes of pre-incubation, and at the end of the experiment. Maximum flux was determined from a minimum of 4 data points using the steady-state part of the permeated mass per cm² versus time curve.

Test substances for the transport studies were (A) lyophilized FA-PLGA nanoparticles freshly suspended in HBSS at a concentration of 2 mg/ml, (B) lyophilized FA-PLGA nanoparticles suspended in HBSS at a concentration of 2 mg/ml and incubated at room temperature for 24 h (partially degraded FA-PLGA nanoparticles), and (C) the degradation products of FA-PLGA nanoparticles under the conditions of (B) (supernatant of the partially degraded FA-PLGA nanoparticles after centrifugation for 10 min at 23147 ± 66 g). Furthermore, a (D) 12 $\mu\text{g}/\text{ml}$ FC solution in HBSS and a (E) 12 $\mu\text{g}/\text{ml}$ solution of FC in HBSS containing additionally 2 mg/ml of PLGA nanoparticles were used. All experiments were performed at 37 °C with $n = 8$ –10 replications.

3. RESULTS

3.1. FA-PLGA Labelling Efficiency

As described by Horisawa et al.,¹² FA was bound covalently to the terminal carboxyl groups of the PLGA chains by amide formation. By integration of well defined protons of the PLGA polymer and those of the FA component (see Section 2.3) the PLGA-FA ratio was found to be $1:220 \pm 13$. Considering the mean molecular weight of the polymer, which was 34,000 Da (according to the informations of the manufacturer) a modification rate of approximately 65% carboxyl-end groups could be estimated.

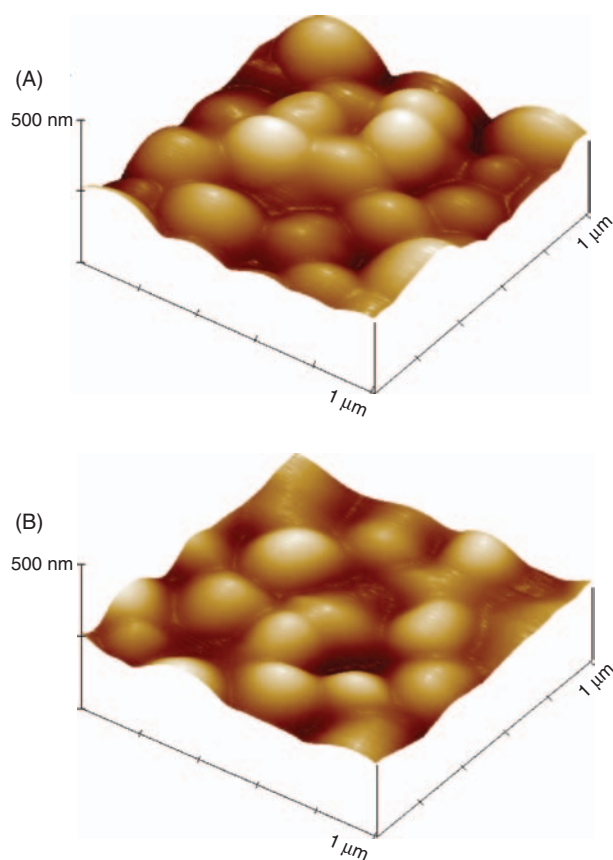


Fig. 1. $1 \times 1 \mu\text{m}$ AFM topography images of FA-PLGA nanoparticles in the size order of 270 nm (A) and FC-PLGA nanoparticles in the size order of 250 nm (B) in 3D view.

This corresponds to a mean FA content of roughly 6000 ppm (w/w).

3.2. Physicochemical Properties

3.2.1. FA-PLGA Nanoparticles

PCS measurements showed that the mean particle size was 269.5 ± 21.1 nm with a PI of 0.13 to 0.21. FA-PLGA nanoparticle shape and surface properties were visualized by AFM. Figure 1A exhibits an AFM topography image of the nanoparticles in the size order of 270 nm in 3D view. The nanoparticle sample is prepared as a dense layer on the silicon wafer. It is clearly visible that nanoparticles are of spherical shape and feature a smooth surface without any visible pores. The zeta potential of FA-PLGA nanoparticles remained constant at -1.4 ± 0.5 mV in the pH range from 2 to 9 (data not shown).

3.2.2. FC-PLGA Nanoparticles

In case of FC-PLGA nanoparticles, we determined a particle size of 249.3 ± 8.5 nm (PI 0.01–0.16). As shown in the AFM topography image (Fig. 1B) the shape and surface properties of FC-PLGA nanoparticles do not differ from

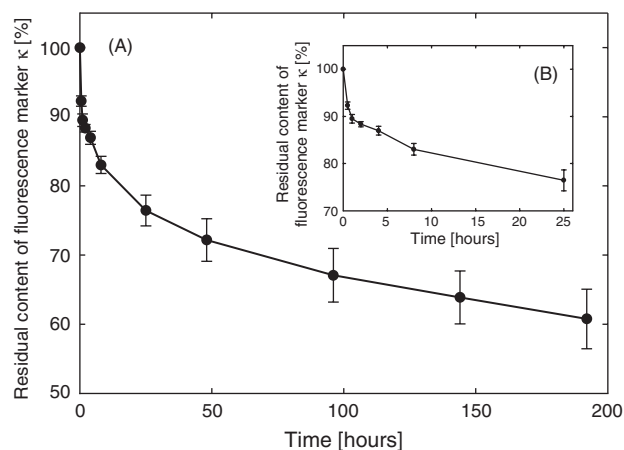


Fig. 2. Residual content of fluorescence marker (κ) in FA-PLGA nanoparticles over 192 h (A) and 25 h (B). The experiment was performed in PBS at 37 °C. Data are shown as mean \pm SD ($n = 6$).

those of FA-PLGA nanoparticles. The mean FC content was found to be 180 ± 30 ppm (w/w).

3.2.3. PLGA Nanoparticles

PLGA nanoparticles exhibited a size of 187.6 ± 14.3 nm (PI 0.06–0.10). Also, PLGA nanoparticles were spherical and had a smooth surface (data not shown).

3.3. Leakage of Fluorescence Marker

3.3.1. FA-PLGA Nanoparticles

Decomposition of the FA-PLGA nanoparticles led to different fluorescent degradation products and was assessed via TLC where various fluorescent bands besides the FA band could be detected (data not shown).

Figure 2 shows the *in vitro* leakage profile of FA-PLGA nanoparticles in PBS, expressed as the percentage of fluorescence marker which is still nanoparticle bound with respect to the amount of FA initially associated with the nanoparticles (κ). Obviously, an initial burst effect occurred within the first 2 h (Fig. 2B) resulting in a loss of fluorescence marker of 11.7%, followed by a simple exponential decay of the form $\kappa(t) = \kappa_0 + A \cdot e^{-\beta t}$ with a time constant of $\beta = 0.01 \text{ s}^{-1}$. This function was fitted to the data shown in Figure 2A. After 8 days (192 h) of incubation, still 60.8% of fluorescence marker was nanoparticle bound (Fig. 2A).

3.3.2. FC-PLGA Nanoparticles

In contrast to FA-PLGA nanoparticles where the fluorescence label is covalently bound to the polymer, FC-PLGA nanoparticles obtained by nano-encapsulation of the low molecular weight label sodium fluorescein exhibited a fast leakage which was $82.6 \pm 15.7\%$ of FC after 30 min (Fig. 3).

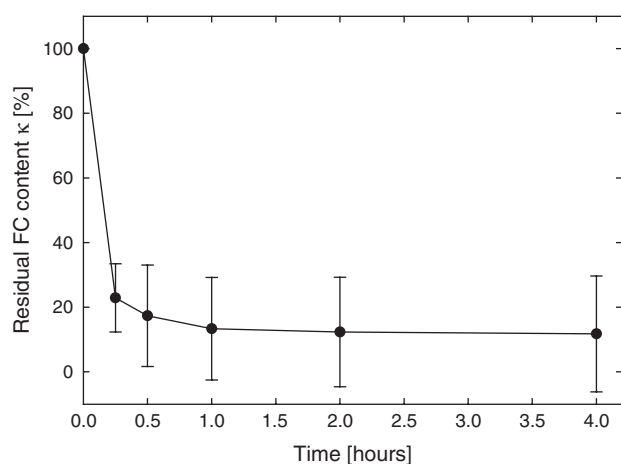


Fig. 3. Residual content of FC (κ) in FC-PLGA nanoparticles over 4 h. The experiment was performed in PBS at 37 °C. Data are shown as mean \pm SD ($n = 6$).

3.4. FA-PLGA Nanoparticle Degradation

Figure 4 presents the FA-PLGA nanoparticle morphology over 15 weeks of incubation in PBS at room temperature. The AFM topography images show the changes of the surface structure during the degradation process of the sample. The changes of the elastic properties become visible in the phase contrast images. At the beginning of the experiment, nanoparticles were spherical and exhibited a

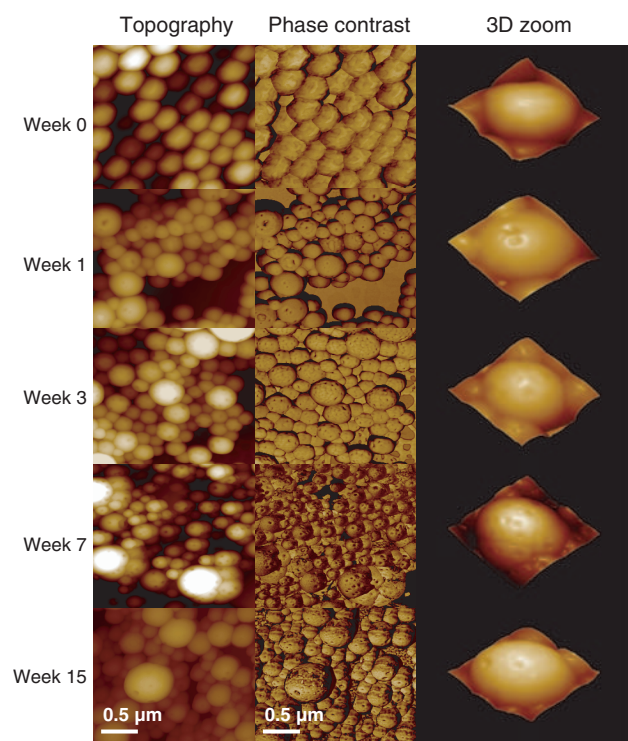


Fig. 4. AFM topography and phase contrast images of FA-PLGA nanoparticles and a 3 D zoom of a random nanoparticle in the size order of 280 nm. Nanoparticles were imaged after 0 weeks, 1 week, 3 weeks, 7 weeks, and 15 weeks of incubation in PBS at room temperature.

smooth surface. After one week of incubation, first pitting of the nanoparticle surface could be visualized. This effect progressively continued until week 3 when the particles were observed to develop a porous outer appearance. Until week 7 the number of indentations did not rise significantly whereas the depth of the indentations increased. This could also be detected by measuring the surface height properties in the AFM topography plot. In week 15, the outer appearance of the nanoparticles did not appear as porous any more. As indicated in the phase contrast images, general changes in the surface seemed to have occurred resulting in a smoothing of the surface. PCS analysis of the nanoparticles revealed that the mean particle size did not change notably. It was found to be in the range of 282 ± 8 nm in course of the incubation time (data not shown).

3.5. Cytotoxicity

For experiments in biological systems, either *in vitro* or *in vivo*, it is pivotal to obtain sufficient fluorescence signals at particle concentrations well below the level that causes any cytotoxic effects. Therefore, the cytotoxicity (tox) of FA-PLGA nanoparticles, PLGA nanoparticles, and FC solution was studied, as diagrammed in Figure 5. In these experiments, PLGA nanoparticles and FC were applied in concentration ranges referred to their calculated content within 0.02 to 64.00 mg/ml of FA-PLGA nanoparticles (see Section 3.1).

It is obvious that the plots for either FA-PLGA or PLGA nanoparticles are equally shaped and of the same scale, in contrast to the FC solution curve which is significantly shifted to lower values. A sigmoidal function of the form $\text{tox}(c) = \text{tox}_0 + ac^b / (IC_{50}^b + c^b)$ was fitted to each of the curves in Figure 5. The IC_{50} values were 10.4 ± 1.0 mg/ml in case of the FA-PLGA nanoparticles ($\text{tox}_{\max} = 99.0\%$),

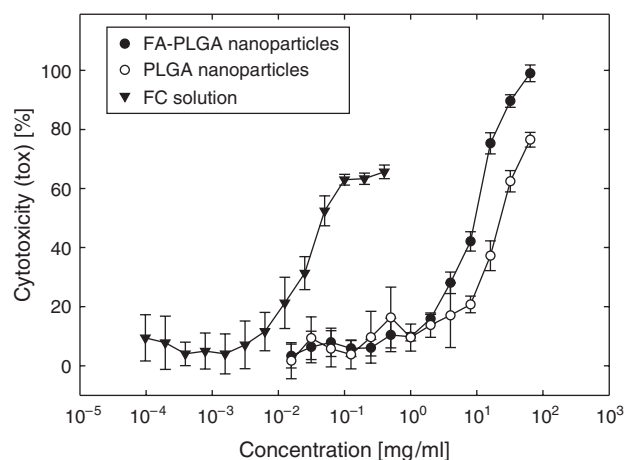


Fig. 5. Cytotoxicity (tox) of FA-PLGA nanoparticles (\bullet), PLGA nanoparticles (\circ), and sodium fluorescein (FC) solution (\blacktriangledown) on Caco-2 cells plotted against their concentrations. Data are shown as mean \pm SD ($n = 6$).

Table I. Flux and permeated amount of fluorescence marker after 6 h in transport experiments across Caco-2 monolayers ($n = 8-10$).

	Flux [$\mu\text{g}/\text{cm}^2/\text{min}$]	Permeated amount of fluorescence marker after 6 h [%]
(A) FA-PLGA nanoparticles	$1.58 \pm 0.59 \cdot 10^{-6}$	0.016 ± 0.006
(B) Partially degraded FA-PLGA nanoparticles	$1.24 \pm 0.41 \cdot 10^{-6}$	0.012 ± 0.004
(C) Degradation products of FA-PLGA nanoparticles	$0.97 \pm 0.26 \cdot 10^{-6}$	0.010 ± 0.002
(D) FC solution	$6.24 \pm 0.36 \cdot 10^{-4}$	4.767 ± 0.448
(E) FC solution containing PLGA nanoparticles	$4.75 \pm 0.96 \cdot 10^{-4}$	3.117 ± 0.780

20.5 ± 3.5 mg/ml with the PLGA nanoparticles ($\text{tox}_{\text{max}} = 76.5\%$), and 26.8 ± 2.3 $\mu\text{g}/\text{ml}$ with the FC solution ($\text{tox}_{\text{max}} = 65.6\%$).

A concentration of 2 mg/ml of FA-PLGA nanoparticles corresponding to 2 mg/ml of PLGA nanoparticles and to 12 $\mu\text{g}/\text{ml}$ of FC (see Section 3.1) was chosen for transport studies.

3.6. Transport Studies

Comparing the transport of the test substances across Caco-2 monolayers, (A) FA-PLGA nanoparticles, (B) partially degraded FA-PLGA nanoparticles, and (C) degradation products exhibited a maximum flux between $0.97 \pm 0.26 \cdot 10^{-6}$ and $1.58 \pm 0.59 \cdot 10^{-6}$ $\mu\text{g}/\text{cm}^2/\text{min}$ and the permeated amount of the fluorescence marker FA after 6 h was in the range of 0.010 ± 0.002 to $0.016 \pm 0.006\%$ (Table I). Both values were found to be roughly 500 fold lower than with the (C) FC solution and the (D) FC solution containing PLGA nanoparticles, respectively. These test substances exhibited a maximum flux of $4.75 \pm 0.96 \cdot 10^{-4}$ to $6.24 \pm 0.36 \cdot 10^{-4}$ $\mu\text{g}/\text{cm}^2/\text{min}$. 3.117 ± 0.780 to $4.767 \pm 0.448\%$ of the fluorescence marker FC were permeated after 6 h (Table I). All permeated mass per cm^2 versus time curves run linear over 8 h (data not shown).

A centrifugation of the solutions in the acceptor compartment in case of the test substances (A) FA-PLGA nanoparticles and (B) partially degraded FA-PLGA nanoparticles did not lead to any lowering of fluorescence.

4. DISCUSSION

PLGA nanoparticles are well appreciated because of their biocompatibility and biodegradability offering a wide range of useful applications in the field of advanced drug delivery. However, drug encapsulation especially in case of hydrophilic compounds still encounters difficulties namely rapid diffusion out of the polymer. Several approaches can be found in the literature in order to overcome this problem.

Recently, it has been demonstrated that a wide range of organic solvents with different polarities can be used when employing the nanoprecipitation method and thus enabling also the entrapment of hydrophilic drugs.¹⁶ Furthermore, PLGA is not only available in an end-capped

form but also with free carboxy end groups which opens the possibility of a covalent coupling of hydrophilic compounds prior to nanoparticle formation. Fluorescein-linked PLGA nanoparticles are used for various studies, amongst others in biological systems.^{17,18} For that purpose different coupling methods have been described in the literature. Recently, Tosi et al. reported a polymer preparation technique based on a covalent coupling of carboxy-fluorescein to PLGA after activation with dicyclohexylcarbodiimide and *N*-hydroxysuccinimide for the preparation of *in vivo* detectable nanoparticles in a rat model.¹⁷ Moreover, fluorescein derivatives have been used for PLGA coupling such as fluorescein cadaverine¹⁸ and fluoresceinamine.¹² The method described by Horisawa et al.¹² has been applied in the present study because of its simplicity and reproducibility, i.e., an amino derivative of sodium fluorescein was bound to the carboxy function of PLGA via a one-step reaction. From this modified polymer, particles with a mean diameter of 269.5 nm were prepared. In regard to an *in vivo* application of the nanoparticles in IBD, this size order is expected to be adequate for the detection of even single particles in biological tissue whilst still likely to display an enhanced accumulation and retention in inflamed mucosal areas. The leakage of fluorescence marker occurred in a strongly delayed manner. The initial burst effect led to a 11.7% loss of fluorescence marker within 2 h (Fig. 2B) which is most likely due to starting polymer degradation after re-hydration of the freeze dried nanoparticles. As generally known from PLGA devices, polymer swelling occurs under aqueous conditions leading to a subsequent polymer chain cleavage. After 8 days 60.8% of fluorescence marker was still nanoparticle bound (Fig. 2A). We found by means of TLC analysis that polymer degradation led to different fluorescent products which we expected to be fluoresceinamine-linked PLGA fragments. The FA-PLGA degradation products, however, were not identified in this study.

Alternatively to a covalent coupling to the polymer, the standard method for the entrapment of hydrophilic drugs is a W/O/W emulsification process, encapsulating the drugs within little aqueous droplets inside the polymeric nanoparticles. In the present study this method has been employed for the purpose of comparison with FA-PLGA nanoparticles, using FC which is strongly hydrophilic.

In contrast to FA-PLGA nanoparticles, it could be shown that the release of encapsulated fluorescence marker from those particles was very fast: 82.6% were released immediately after 30 min as outlined in Figure 3. Via AFM it was studied that this effect was not associated with any surface phenomena i.e., shape and surface appearance of FC-PLGA nanoparticles did not differ from those of FA-PLGA nanoparticles (Fig. 1). Possible explanations for the fast FC release are that either the hydrophilic compound diffuses out of the nanoparticle core very fast or that the W/O/W emulsification method led to an imperfect encapsulation due to the instable nature of the emulsion droplets during the preparation process. Sampath et al. described this burst release as an immediate dissolution of the adsorbed drug onto the nanoparticle surface and as a consequence of a big and more variable surface of smaller particles.¹⁹ Also, our results are in accordance with the literature where hydrophilic drugs are described to be released more or less rapidly when encapsulated into PLGA nanoparticles using the W/O/W method. In case of the hydrophilic low molecular weight model drug propranolol-HCl, Ubrich et al.⁵ reported a release up to 45% from their propranolol-HCl nanoparticles over 8 hours. Ahlin et al.²⁰ detected a release of 60 to 70% of enalaprilat encapsulated into nanoparticles in different physiological release media even at room temperature after 1 min. Saxena et al. encapsulated indocyanine green, a tricyanocyanine dye. In their release experiments, they found a liberation of 78% over the first 8 h.²¹ In conclusion, FC-PLGA nanoparticles, in contrast to FA-PLGA nanoparticles, do not appear to be suitable for particle visualization studies over a larger period of time due to a rapid loss and a rather low and probably insufficient residual amount of encapsulated compound. However, in future studies the W/O/W emulsion technology might also be further improved in order to achieve a more stable FC entrapment.

Generally, highly negative zeta potential values are expected for pure polyester nanoparticles from non-end capped PLGA due to the presence of carboxyl groups on the polymeric chain extremities.²² However, in this study we used PLGA with around 65% of chain end groups being modified by a covalent bonding of FA. This modification led to the less negative surface charge of -1.4 mV. Another factor can be residual PVA from the preparation process. It is reported that this polymer may create a shield between the nanoparticle surface and the surrounding medium and thus is masking possible charged groups existing on the particle surface²² whilst protecting the nanoparticles from aggregation.

Degradation of insoluble, biodegradable polymers in aqueous medium follows two main mechanisms, either surface erosion, bulk erosion or both. Poly(α -hydroxy esters) like PLGA have been shown to predominantly erode in bulk up to a relatively large size including nano- and microparticulate drug carriers.²³ Moreover, the PLGA

degradation rate is influenced by several parameters like the polymer molecular weight, polydispersity index, crystallinity, and glass transition temperature.²⁴ Furthermore, it is described in the literature that larger polymeric devices show a greater degradation rate than smaller ones. This is due to an accumulation of acidic degradation products in the inner regions of a polymeric device which further accelerates polymer decomposition (autocatalysis).²⁵ Therefore, the degradation process described for microparticles e.g., by Dunne et al.²⁴ and Fu et al.²⁶ can not be transferred without limitations to the size of nanoparticles.

Bulk erosion is characterized by the formation of pores enabling water to penetrate into the particles followed by a random cleavage of the ester bonds. During that process, the particle core and size generally remain constant.

This also complies with our size measurements in the nanoparticle degradation experiment. We visualized the progression of pore formation via AFM (Fig. 4). In our case, pore development was already apparent after week 1 proceeding until week 7. In association with pore formation and degradation, we found a change in the elastic properties which can be explained by a swelling process. This might also be a possible explanation for the particle surface smoothening found after 15 weeks of degradation.

Comparing the transport properties of (A) FA-PLGA nanoparticles across Caco-2 monolayers with those of (B) partially degraded FA-PLGA nanoparticles and (C) their degradation products (Table I), it is highly probable that the fluorescence signal detected in the receiver compartment reflects the transport of released FA-PLGA degradation products. This was further confirmed by the result that centrifugation of the receptor solutions did not lead to any decrease of fluorescence. Flux values of the three test substances were in the same size range. However we observed a slightly decreased flux for the (C) FA-PLGA nanoparticle degradation products which can be explained by a decreasing concentration gradient during the experiment due to a lack of FA-PLGA nanoparticles in the donor compartment. No additional transport mechanism except diffusion seems to be activated. Moreover, it was shown that these degradation products were transported only to a very small extent, approximately 500 times less than the low permeability marker FC (Table I). This result might be due to a high molecular weight when FA is additionally bound to short lactide-glycolide chains.

Different problems arise when comparing the three test substances (A) FA-PLGA nanoparticles, (B) partially degraded FA-PLGA nanoparticles, and the (C) degradation products:

One point is particle degradation during the transport experiments which results in a concentration increase of free FA-PLGA degradation products in the donor compartment in case of the test substances (A) FA-PLGA nanoparticles and (B) partially degraded FA-PLGA nanoparticles.

Another point is that fluorescent degradation products of FA-PLGA, which we expect to be fluoresceinamine-bound

short PLGA chains, are likely to undergo further degradation during the experiments. However, by a comparison of the transport properties of (A) FA-PLGA nanoparticles and (B) partially degraded FA-PLGA nanoparticles it was shown that this degradation does not affect the transport.

In terms of an *in vivo* application in a clinical study in humans, FA-PLGA nanoparticles were assayed for their cytotoxic effects on human intestinal epithelial cells (Caco-2). The IC₅₀ value was shown to be 10 mg/ml. It was in the same order as found with nanoparticles from pure PLGA which is well-known for its excellent biocompatibility. Apparently, covalent labelling of PLGA with FA did not affect the cytotoxic potential of the nanoparticles. Compared to the non-toxic compound FC, FA-PLGA nanoparticles exhibited an even 750 fold higher IC₅₀ (Fig. 5). This means that the nanoparticles are significantly less cytotoxic than this small molecular weight fluorescent molecule which is obviously non-toxic *in vivo*, as can be judged from its common use in high doses as a diagnostic agent in man. With respect to a potential absorption of FA-PLGA nanoparticles from the lumen of the intestine, our results from the Caco-2 transport experiments indicate that only the degradation products are transported across the intestinal epithelial barrier. Even if absorption due to a compromised barrier function of the intestinal mucosa under conditions of IBD might occur to some extent, a progressive shortening of the polymer chains would facilitate their elimination.

5. CONCLUSION

From the present study, it is evident that a covalent coupling of FA to PLGA using carbodiimide as an activating agent represents a simple, reproducible, and efficient method for polymer labelling. Nanoparticles from FA-PLGA exhibited a much better labelling stability compared to nanoparticles prepared by FC encapsulation using the classic W/O/W method. Due to well-known biocompatibility and biodegradability of PLGA, FA-PLGA nanoparticles appear as valuable tool to study their potential to target inflamed mucosal areas in IBD patients. In experiments with intestinal epithelial cells the cytotoxicity was found to be low. Moreover, there was no detectable nanoparticle transport across Caco-2 cell monolayers and only an extremely small transport of FA-PLGA degradation products.

Acknowledgments: Generous financial support by the DFG (grant number Sta 295/6-1) is gratefully acknowledged. Boehringer Ingelheim is kindly acknowledged for

providing the polymer. Concerning practical support, we would like to thank Prof. M. N. V. Ravi Kumar and Prof. U. Bakowsky for their kind scientific advices.

References and Notes

1. A. Lamprecht, U. F. Schaefer, and C. M. Lehr, *Pharm. Res.* 18, 788 (2001).
2. R. Alvarez-Roman, A. Naik, Y. N. Kalia, R. H. Guy, and H. Fessi, *Pharm. Res.* 21, 1818 (2004).
3. J. Luengo, B. Weiss, M. Schneider, A. Ehlers, F. Stracke, K. Koenig, K.-H. Kostka, C.-M. Lehr, and U. F. Schaefer, *Skin Pharm. Phys.* (2006), in press.
4. J. M. Koziara, P. R. Lockman, D. D. Allen, and R. J. Mumper, *J. Control. Rel.* 99, 259 (2004).
5. N. Ubrich, P. Bouillot, C. Pellerin, M. Hoffman, and P. Maincent, *J. Control. Rel.* 97, 291 (2004).
6. A. Lamprecht, N. Ubrich, H. Yamamoto, U. F. Schaefer, H. Takeuchi, P. Maincent, Y. Kawashima, and C. M. Lehr, *J. Pharmacol. Exp. Ther.* 299, 775 (2001).
7. J. Panyam, S. K. Sahoo, S. Prabha, T. Bargar, and V. Labhasetwar, *Int. J. Pharm.* 262, 1 (2003).
8. I. Bala, S. Hariharan, and M. N. Kumar, *Crit. Rev. Ther. Drug Carrier Syst.* 21, 387 (2004).
9. J. Vandervoort and A. Ludwig, *Int. J. Pharm.* 238, 77 (2002).
10. M. N. Ravi Kumar, U. Bakowsky, and C. M. Lehr, *Biomaterials* 25, 1771 (2004).
11. S. C. Sweetman (ed.), in Martindale, Pharmaceutical Press, Grayslake (2002), p. 334–7.
12. E. Horisawa, K. Kubota, I. Tuboi, K. Sato, H. Yamamoto, H. Takeuchi, and Y. Kawashima, *Pharm. Res.* 19, 132 (2002).
13. H. Fessi, F. Puisieux, J. P. Devissaguet, N. Ammoury, and S. Benita, *Int. J. Pharm.* 55, R1 (1998).
14. R. Alex and R. Bodmeier, *J. Microencapsul.* 7, 347 (1990).
15. S. Cohen, T. Yoshioka, M. Lucarelli, L. H. Hwang, and R. Langer, *Pharm. Res.* 8, 713 (1991).
16. U. Bilati, E. Allemann, and E. Doelker, *Eur. J. Pharm. Sci.* 24, 67 (2005).
17. G. Tosi, F. Rivasi, F. Gandolfi, L. Costantino, M. A. Vandelli, and F. Forni, *Biomaterials* 26, 4189 (2005).
18. A. Weissenboeck, E. Bogner, M. Wirth, and F. Gabor, *Pharm. Res.* 21, 1917 (2004).
19. S. S. Sampath, K. Garvin, and D. H. Robinson, *Int. J. Pharm.* 78, 165 (1992).
20. P. Ahlin, J. Kristl, A. Kristl, and F. Vrečer, *Int. J. Pharm.* 239, 113 (2002).
21. V. Saxena, M. Sadoqi, and J. Shao, *Int. J. Pharm.* 278, 293 (2004).
22. Y. N. Konan, R. Cerny, J. Favet, M. Berton, R. Gurny, and E. Allemann, *Eur. J. Pharm. Biopharm.* 55, 115 (2003).
23. F. von Burkersroda, L. Schedl, and A. Goepferich, *Biomaterials* 23, 4221 (2002).
24. M. Dunne, I. Corrigan, and Z. Ramtoola, *Biomaterials* 21, 1659 (2000).
25. I. Grizzi, H. Garreau, S. Li, and M. Vert, *Biomaterials* 16, 305 (1995).
26. K. Fu, D. W. Pack, A. M. Klibanov, and R. Langer, *Pharm. Res.* 17, 100 (2000).

Received: 5 December 2005. Accepted: 8 February 2006.

Unpublished results

1 Introduction

The publication 'Nanoparticles made of fluorescence labelled PLGA: preparation, stability and biocompatibility' describes the development of drug-free but fluorescence labelled non-toxic NP to study their interaction with inflamed areas of the colonic mucosa of patients with irritable bowel disease (IBD) in a future clinical study. This approach is based on recent findings in an animal model where NP were demonstrated to exhibit enhanced accumulation and prolonged retention in inflamed intestinal tissue whilst concentrating anti-inflammatory drugs at their site of action.¹⁻³

From the publication, it is evident that a covalent coupling of 5-fluoresceinamine (FA) to PLGA represents a simple, reproducible, and efficient method for polymer labelling. There, the labelling efficiency of FA-modified PLGA (FA-PLGA) was determined and NP made of FA-PLGA were characterized for their size, zeta potential, morphology, stability, and leakage of fluorescence marker. In experiments with intestinal epithelial cells the cytotoxicity and the transport of NP across Caco-2 cell monolayers was studied.

The first part of the present chapter provides physicochemical characterizations of FA-PLGA and FA-PLGA NP which have not been included in the study 'Nanoparticles made of fluorescence labelled PLGA: preparation, stability and biocompatibility'. This additional information contributes to a more precise specification of such systems. First, the glass transition temperature of FA-PLGA was determined to investigate if this special attribute of polymers has been changed due to modification. Second, the density of FA-PLGA NP was determined to enable a more conceivable quantification of particles when applied in biological systems. Finally, lyophilisation of FA-PLGA NP was studied since re-suspendability of those particles after lyophilisation becomes highly important in the context of a future clinical study when lyophilised particles are re-constituted directly before application to patients.

The second part of this chapter focuses on a first proof of determining FA-PLGA NP in intestinal tissue. After administration of FA-PLGA NP formulations to IBD patients, particles should be well visualisable by confocal laser scanning microscopy when accumulating in inflamed areas of the intestinal mucosa. Moreover, in case of taking biopsies of such tissue, the tissue attached particle amount should be quantifiable with

low analytical detection limit. In the following, both approaches have been studied using porcine intestine from the abattoir as a model.

2 Materials and methods

2.1 Materials

FA-PLGA NP were prepared as described in the publication 'Nanoparticles made of fluorescence labelled PLGA: preparation, stability and biocompatibility'. Excised porcine intestine was obtained from the abattoir. The tissue was rinsed with water and frozen at -20°C until use. Ammonium chloride buffer pH 9.5 was composed as described in the European Pharmacopoeia 5. Phosphate buffered solution pH 7.4 (PBS) was composed of KCl 0.20 g/l, NaCl 8.00 g/l, KH₂PO₄ 0.20 g/l, Na₂HPO₄ x 2H₂O 1.44 g/l.

2.2 Extended physicochemical characterization of FA-PLGA nanoparticles

2.2.1 Differential scanning calorimetry investigation of FA-PLGA

The glass transition temperature (T_g) of FA-PLGA was determined by differential scanning calorimetry (DSC) using a differential scanning calorimeter DSC Q100 (Waters GmbH, TA Instruments, Eschborn, GE). The instrument calibration was carried out with an indium standard. Amounts between 5 and 10 mg of lyophilised polymer were qualitatively analyzed in an air tight aluminium pan. Samples were scanned from -50°C to 200°C at a rate of 10°C/min. Results are expressed as mean \pm SD and the number of replicates was $n = 6$ (polymer derived from 2 batches).

2.2.2 Determination of the density of FA-PLGA nanoparticles

The density of lyophilised FA-PLGA NP ρ_p was determined after re-suspension of the particles in demineralised water using a water pycnometer at 23°C. The calculation was performed according to the formula:

$$\rho_p = \frac{m_p \cdot \rho_w}{M + m_p - M'}$$

where ρ_w is the density of demineralised water at 23°C, m_p the mass of lyophilised particles applied, M the mass of the pycnometer when completely filled with degassed demineralised water, and M' the mass of the water-filled pycnometer additionally containing the FA-PLGA NP. The experiment was performed with a number of $n = 2$ replicates.

2.2.3 Lyophilisation of FA-PLGA nanoparticles

FA-PLGA nanoparticles were lyophilised by means of an Alpha 2-4 LSC freeze-dryer (Martin Christ Gefriertrocknungsanlagen GmbH, Osterode, GE). Samples were entirely frozen at -40°C. Main drying was performed at 20°C and 0.05 mbar for 24 h. Then, the pressure was decreased to 0.001 mbar and drying was continued for another 2 h. After lyophilisation particles were stored in sealed vessels and under protection from light until being re-hydrated (within less than 10 days). Nanoparticle size and polydispersity index (PI) were determined before and after lyophilisation. The ratios of the final particle size and PI (after lyophilisation) to the initial size and PI (before lyophilisation) were expressed as S_f/S_i and PI_f/PI_i , respectively. The number of replicates was $n = 3$.

2.3 Detection of FA-PLGA nanoparticles in intestinal tissue

2.3.1 Visualization by confocal laser scanning microscopy

Confocal laser scanning microscopy (CLSM) was performed at a sample depth of 15 μm (from the luminal side) using a Bio-Rad MRC-1024 CLSM (Bio-Rad Laboratories, Hercules, CA, USA) equipped with an argon/krypton laser. The objective used was an oil immersion objective 40 \times NA=1.3. Green fluorescence was collected with a band pass filter (Zeiss: 520/35) and red fluorescence was collected with a long pass filter (Zeiss: LP585) after excitation at 488 nm and 568 nm, respectively. Imaging was performed after washing a piece of thawed excised porcine intestine twice with PBS and incubating it with a 10 mg/ml suspension of FA-PLGA NP of average size (270 nm) for 15 min.

2.3.2 Determination of the analytical detection limit

Pieces of 14 mm² were punched out from thawed porcine intestine. 4 ml of FA-PLGA NP suspension in ammonium chloride buffer pH 9.5 were added to each punch and incubated at room temperature for 24 h under protection from light until complete decomposition of the particles. Then, the preparations were centrifuged at 222 g in order to remove the tissue material, and the fluorescence of the supernatant was determined using a fluorescence spectrophotometer at an excitation and emission wavelength of 485 and 510 nm, respectively. In preliminary experiments it was confirmed that porcine tissue material without NP, however treated analogously, did not exhibit significant fluorescence under these conditions. The particle concentrations applied ranged from 0 to 1.06 mg/ml. The experiment was performed with n = 2 repeats.

3 Results and discussion

3.1 Differential scanning calorimetry results

The mean T_g of FA-PLGA designated as the inflexion point of the curve in the thermograms was $28.8 \pm 3.1^\circ\text{C}$. At a temperature above 100°C the polymer was degraded. Figure 1 shows a typical DSC thermogram of FA-PLGA.

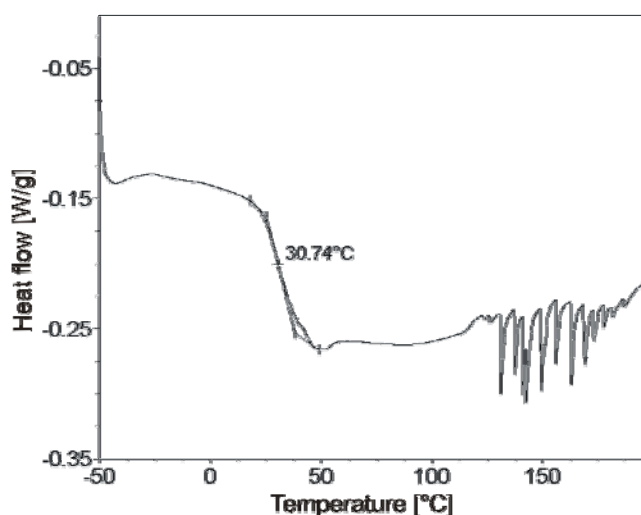


Figure 1: DSC thermogram of a representative FA-PLGA sample; the heat flow is plotted against the temperature (exo up). The inflexion point of the curve represents the glass transition temperature. At a temperature above 100°C the polymer was degraded.

In literature, PLGA polymers made of D,L-PLA and PGA with a content of less than 70% (w/w) are described to be amorphous in nature.⁴ Generally, amorphous polymers are characterized by their T_g which is the transition point between a highly viscous brittle structure called glass and a less viscous, more mobile, rubbery state. The T_g can be modified by blending with a small amount of a low molecular weight substance resulting in either plasticization or anti-plasticization of the polymer and, thus, a decrease or increase of the T_g .⁵ According to the information of the manufacturer, the T_g of blank PLGA (poly(D,L-lactide-co-glycolide), Resomer RG 50:50 H, inherent viscosity 0.31 dl/g) used for the preparation of FA-PLGA is 43°C. In case of FA-PLGA, the T_g was roughly 29°C indicating a decrease of T_g as consequence of polymer modification. There are two possible explanations for this result. First, polymer modification may have led to irregularities in polymer structure i.e. polymer chains may be more flexible and mobile due to the binding of FA to its carboxylic acid end groups. Second, lyophilisation of FA-PLGA may not have resulted in a complete removal of water which was, thus, acting as a plasticizer. The recent speculation is based on findings of Blasi et al.⁵ who reported the presence of water residues in larger amounts to become visible in the appearance of ice melting peaks in the thermograms, whereas water closely associated with the polymer matrix only gives influence on T_g .

3.2 Density of FA-PLGA nanoparticles

The density of FA-PLGA NP ρ_p was determined to a mean of 1.46 ± 0.04 g/ml. It did not differ relevantly from the density of pure PLGA applied for FA-PLGA NP preparation which the manufacturer reported to roughly 1.25 - 1.3 g/ml. By means of the density of FA-PLGA NP a number of roughly $6.6 \cdot 10^{13}$ particles of mean size (270 nm) could be calculated to correspond to 1 g.

3.3 Lyophilisation of FA-PLGA nanoparticles

The ratios of particle size S_f/S_i and polydispersity index PI_f/PI_i were 1.06 ± 0.05 and 1.76 ± 0.50 . After re-constitution of the lyophilised FA-PLGA NP the Tyndall effect was maintained. The particle size ratio shows only minor increase of NP size as consequence of lyophilisation whereas the PI ratio indicates a broadening of the size

distribution. However, the maximum PI was 0.21 still indicating a narrow particle size distribution in all cases.

Lyophilisation is one of the most suitable methods in order to stabilize and to facilitate the handling of nanoparticulate systems which, stored as suspensions, would suffer alteration in a brief period of time.⁶ Several authors have claimed that additives like saccharides, polyalcohols and high molecular weight compounds are necessary in order to prevent PLGA NP from aggregation during lyophilisation and to maintain the integrity after re-hydration of the lyophilised samples.⁶⁻⁹ Saez et al. reported that only an addition of 20% of sucrose or 20% of glucose exerted sufficient lyoprotection of NP from blank PLGA resulting in a S_f/S_i of roughly 1.5.⁶ Chacón et al.⁸ found that at least 5% of the cryoprotectants glucose and trehalose were essential to keep the initial size of PLGA NP still resulting in particle aggregation. In contrast, in the present study it was found that NP from FA-PLGA maintained their size and still showed narrow size distribution when lyophilised without any additives. In literature, this behaviour was described as an effect of the stabilizer PVA used for the preparation of NP¹⁰⁻¹² forming a stable thick layer on the particle surface.¹⁰ Even after repeated washing, a fraction of PVA generally remains well associated with the particle surface.^{13, 14} The reasons for that effect are a fixation of the hydroxyl groups of PVA molecules to the acetyl groups of PLGA via hydrophobic bonding¹³ and/or a interpenetration of PVA and PLGA during particle preparation.¹¹ It has been suggested that stabilization of NP during lyophilisation only requires their maintenance in a vitrified state.¹⁵ Similar to other cryoprotectants, PVA is described to form a glassy state at low temperature due to hydrogen bonding between the polymer and the water molecules, thus stabilizing NP during lyophilisation and preventing particle aggregation.¹¹

With respect to a future administration in a clinical study FA-PLGA NP may be easily lyophilised and re-suspended without any significant changes in particle size and size distribution. Thereby, an addition of cryoprotectants, which may possibly interfere with other ingredients of the final formulation to be applied to patients, or at least increase the osmolarity does not appear as necessary.

3.4 Visualization and analytical quantification of FA-PLGA NP in porcine intestinal tissue

For a first evaluation of particle visualization and quantification in intestinal tissue, excised intestine from pig was used as a model without confirming the maintenance of the intestinal integrity. To ascertain the traceability of FA-PLGA NP, the tissue was imaged by CLSM after incubation with such particles. Green fluorescent NP could be well visualized by imaging in different depths of the tissue. Slight red fluorescence derives from the autofluorescence of the tissue. Figure 2 represents an image at a sample depth of 15 μm .

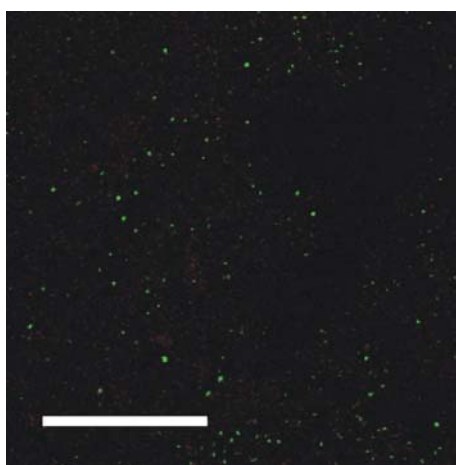


Figure 2: CLSM image of porcine intestinal tissue at a sample depth of 15 μm after 5 min incubation with FA-PLGA NP. Particles are green fluorescent. Slight red fluorescence derives from the autofluorescence of the tissue. (bar = 100 μm)

The approach to determine the detection limit of FA-PLGA NP in intestinal tissue is based on the idea of an analytical quantification of tissue attached particles in biopsies taken from patients with IBD in a future clinical study. For that purpose, a decomposition of FA-PLGA NP in alkaline buffer in the presence of porcine intestinal tissue and a determination of the fluorescence of the tissue-free supernatant were opted. Linearity was given within the applied particle concentration range (0 - 1.06 mg/ml; $R^2 > 0.999$). The detection limit, which was determined at a FA-PLGA NP concentration exhibiting a fluorescence signal of 10fold the background fluorescence, was 3 $\mu\text{g/ml}$ corresponding to a total number of $9.2 \cdot 10^8$ NP with the experimental setup applied. To enable an efficient absorption of nutrients, the surface of the intestinal mucosa exhibits wrinkles and villi, thus leading to a surface increase up to 600fold (e.g. in case of healthy tissue from the small intestine). Assuming a mono-particular occupation of such tissue, a number of $9.2 \cdot 10^8$ NP would cover a real surface area of

0.6% on a 14 mm² tissue punch. In inflamed intestinal tissue physiological conditions may be strongly different, however, perforation of the inflamed mucosa may even enhance particle accumulation.

4 Conclusion

The present study fortified that NP made of FA-PLGA may represent a powerful tool to investigate their potential to target inflamed mucosal areas in IBD patients in a clinical study. In regard to a clinical application, it was shown that FA-PLGA NP lyophilized without addition of cryoprotectants may be easily re-constituted without any alteration of size or size distribution before administration to patients. In preliminary investigations with porcine intestinal tissue, FA-PLGA NP turned out to be well visualisable by CLSM indicating good aspects of such technique *in vivo* in humans. Furthermore, it was shown that extraction of biopsies taken from IBD patients may represent an easy method to quantify particle accumulation in inflamed intestinal tissue with low detection limit.

5 References

1. A. Lamprecht, U. F. Schaefer and C. M. Lehr, Size-dependent bioadhesion of micro- and nanoparticulate carriers to the inflamed colonic mucosa. *Pharm Res*: 18, 788-793 (2001)
2. A. Lamprecht, N. Ubrich, H. Yamamoto, U. F. Schaefer, H. Takeuchi, C. M. Lehr, P. Maincent and Y. Kawashima, Design of rolipram-loaded nanoparticles: comparison of two preparation methods. *J Control Release*: 71, 297-306 (2001)
3. A. Lamprecht, N. Ubrich, H. Yamamoto, U. F. Schaefer, H. Takeuchi, P. Maincent, Y. Kawashima and C. M. Lehr, Biodegradable nanoparticles for targeted drug delivery in treatment of inflammatory bowel disease. *J Pharmacol Exp Ther*: 299, 775-781 (2001)
4. D. M. Gilding and A. M. Reed, Biodegradable polymers for use in surgery. Poly(glycolic)/poly(lactic acid) homo and copolymers. *Polymer*: 20, 1459-1464 (1979)
5. P. Blasi, S. S. D'Souza, F. Selmin and P. P. DeLuca, Plasticizing effect of water on poly(lactide-co-glycolide). *J Control Release*: 108, 1-9 (2005)
6. A. Saez, M. Guzman, J. Molpeceres and M. R. Aberturas, Freeze-drying of polycaprolactone and poly(D,L-lactic-glycolic) nanoparticles induce minor particle size changes affecting the oral pharmacokinetics of loaded drugs. *Eur J Pharm Biopharm*: 50, 379-387 (2000)
7. P. Ahlin, J. Kristl, A. Kristl and F. Vrečer, Investigation of polymeric nanoparticles as carriers of enalaprilat for oral administration. *Int J Pharm*: 239, 113-120 (2002)
8. M. Chacon, J. Molpeceres, L. Berges, M. Guzman and M. R. Aberturas, Stability and freeze-drying of cyclosporine loaded poly(D,L lactide-glycolide) carriers. *Eur J Pharm Sci*: 8, 99-107 (1999)
9. S. Bozdog, K. Dillen, J. Vandervoort and A. Ludwig, The effect of freeze-drying with different cryoprotectants and gamma-irradiation sterilization on the characteristics of ciprofloxacin HCl-loaded poly(D,L-lactide-glycolide) nanoparticles. *J Pharm Pharmacol*: 57, 699-707 (2005)
10. D. Quintanar-Guerrero, A. Ganem-Quintanar, E. Allemann, H. Fessi and E. Doelker, Influence of the stabilizer coating layer on the purification and freeze-drying of poly(D,L-lactic acid) nanoparticles prepared by an emulsion-diffusion technique. *J Microencapsul*: 15, 107-119 (1998)
11. W. Abdelwahed, G. Degobert and H. Fessi, A pilot study of freeze drying of poly(epsilon-caprolactone) nanocapsules stabilized by poly(vinyl alcohol): formulation and process optimization. *Int J Pharm*: 309, 178-188 (2006)
12. F. De Jaeghere, E. Allemann, J. C. Leroux, W. Stevels, J. Feijen, E. Doelker and R. Gurny, Formulation and lyoprotection of poly(lactic acid-co-ethylene oxide) nanoparticles: influence on physical stability and in vitro cell uptake. *Pharm Res*: 16, 859-866 (1999)
13. H. Murakami, M. Kobayashi, H. Takeuchi and Y. Kawashima, Preparation of poly(DL-lactide-co-glycolide) nanoparticles by modified spontaneous emulsification solvent diffusion method. *Int J Pharm*: 187, 143-152 (1999)
14. S. K. Sahoo, J. Panyam, S. Prabha and V. Labhasetwar, Residual polyvinyl alcohol associated with poly (D,L-lactide-co-glycolide) nanoparticles affects their physical properties and cellular uptake. *J Control Release*: 82, 105-114 (2002)
15. S. de Chasteigner, G. Cavé, H. Fessi, J. P. Devissaguet and F. Puisieux, Freeze-drying of itraconazole-loaded nanosphere suspensions: a feasibility study. *Drug Dev Res*: 38, 116-124 (1996)

6.1 Nanoparticles made of fluorescence-labelled poly(L-lactide-co-glycolide): preparation, stability, and biocompatibility

ACCEPTED MANUSCRIPT

**NANOPARTICLES - AN EFFICIENT CARRIER FOR DRUG DELIVERY INTO THE
HAIR FOLLICLES**

Juergen Lademann^{1*}, Heike Richter¹, Alexa Teichmann¹, Nina Otberg¹, Ulrike Blume-Peytavi¹, Javiana Luengo^{2,3}, Barbara Weiß², Ulrich F. Schaefer², Claus-Michael Lehr², Roger Wepf⁴, Wolfram Sterry¹

¹ Charité-Universitätsmedizin Berlin, Department of Dermatology, Center of Experimental and Applied Cutaneous Physiology (CCP), Berlin, Germany

² Saarland University, Department of Biopharmaceutics and Pharmaceutical Technology, Saarbruecken, Germany

³ Universidad de Concepción, Facultad de Farmacia, Concepción, Chile

⁴ Beiersdorf AG, 20245 Hamburg, Germany

Keywords: Particles, hair follicles, percutaneous penetration, reservoir function, drug delivery

Corresponding author:

* Prof. Dr. Juergen Lademann
Center of Experimental and Applied
Cutaneous Physiology,
Department of Dermatology
Charité-Universitätsmedizin Berlin
Charitéplatz 1
10117 Berlin
Tel.: ++49 30 450 518 100
Fax: ++49 30 450 518 918
E-mail: juergen.lademann@charite.de

Abstract

The penetration and storage behavior of dye containing nanoparticles (diameter 320 nm) into the hair follicles was investigated. The results were compared to the findings obtained with the same amount of dye in the non-particle form.

In the first part of the experiments, the penetration of the dye into the hair follicles was investigated *in vitro* on porcine skin, which is an appropriate model for human tissue. It was found that the nanoparticles penetrate much deeper into the hair follicles than the dye in the non-particle form, if a massage had been applied. Without massage, similar results were obtained for both formulations.

Subsequently, the storage behavior of both formulations in the hair follicles was analyzed *in vivo* on human skin by differential stripping. Using the same application protocol, the nanoparticles were stored in the hair follicles up to 10 days, while the non-particle form could be detected only up to 4 days.

Taking into consideration the surface structure of the hair follicles, it was assumed that the movement of the hairs may act as a pumping mechanism pushing the nanoparticles deep into the hair follicles.

Introduction

The knowledge of the penetration efficacy of topically applied substances into and through the skin is important for the development and optimization of cosmetic products and drugs. Whilst in the last decades, the penetration of topically applied substances through the skin barrier (stratum corneum) was assumed to be diffusion inside the lipid layers surrounding the corneocytes [1-3], recent investigations have attributed that the hair follicles perform a significant part in skin penetration [4-7]. Several *in vivo* and *in vitro* investigations have revealed a significant influence of the hair follicles on the penetration process [8-11]. Feldmann and Maibach [8] showed

higher absorption rates in skin areas with higher follicle density. Hueber et al. [9] and Tenjarla et al.[10] found a decrease in percutaneous absorption of appendage-free scarred skin compared to normal skin.

Barry[11] explored a novel in vitro technique by comparing drug delivery through epidermal membranes with penetration through a sandwich model, assuming that the top epidermal membrane essentially blocks all shunts in the lower membrane.

Furthermore, the hair follicles represent an efficient reservoir for topically applied substances, which is comparable to the reservoir of the stratum corneum on a number of body sites [12]. The highest volume of hair follicles can be found on the scalp, calf and forehead regions. In contrast to the reservoir of the stratum corneum, which is located in the uppermost cell layers of the horny layer (approx. 5 μm)[13], the reservoir of the hair follicles is usually extended deep into the tissue up to 2,000 μm [14]. Here, dendritic cells and a close network of blood capillaries surround the hair follicles. Whilst the storage of substances in the stratum corneum is rather short, due to its high turnover, the reservoir of the hair follicles can be depleted only by penetration into living tissue, or by leaving the hair follicles, with sebum flow and active hair growth [6]. Actually, the hair follicles appear to be an efficient long-term reservoir for topically applied substances; especially particles play an important role in follicular penetration [6, 14]. If the size of the particles is higher than 5 μm , they do not penetrate into the lipid layers of the stratum corneum but only into the infundibula of the hair follicles [15]. TiO_2 particles with a diameter of approx. 100 nm, often used in sunscreens, penetrate into the hair follicles but do not pass out of the follicles into living tissue [16]. Additionally, 100-nm-particles do not penetrate into all hair follicles, but it must be distinguished between “open” and “closed” hair follicles. Closed hair follicles are covered by a plug, which can easily be removed by cyanoacrylate surface biopsy or by peeling [17, 18]. Toll et al.[14] used this procedure to open all

follicles of excised human skin samples, and investigated the penetration efficacy into the hair follicles of fluorescent dye-labeled microspheres in different sizes (1.5 μm – 0.75 μm). Small particles at a diameter of approx. 750 nm penetrated most efficiently into the follicles, a process which could even be enhanced by mechanical massage of the particles into the skin.

The aim of the present investigation was the comparison of the efficacy of the penetration and storage of substances in particle and non-particle form into hair follicles. Penetration experiments were carried out using the fluorescent dye sodium fluorescein in vitro on porcine ear-skin, because of the necessity to analyze a high number of biopsies. Porcine skin is a highly suitable substitute for human tissue [19]. Subsequently, the storage behavior of substances in particle and non-particle form was investigated in vivo on human skin, using the recently developed method of differential stripping [20].

Additionally, the structure of the hair surface and the hair follicles was analyzed to explain the observed differences in penetration and storage behavior of particle and non-particle formulations.

Materials and Methods

Formulations

The Department of Biopharmaceutics and Pharmaceutical Technology, University of Saarland, Saarbruecken prepared two formulations based on the same hydrogel. The formulations of both, the particle and non-particle form, contained the same concentration of the fluorescent dye, sodium fluorescein. This food dye was used on account of its good fluorescent properties and efficient penetration into and through the skin, depending on the formulation [21].

Fluorescent particles: nanoparticles (average diameter 320 nm, PI 0.06) were prepared from Resomer® RG 50:50H (Boehringer Ingelheim, Ingelheim, Germany) covalently labeled with 5-fluoresceinamine (Sigma Chemical Co., St. Louis, MO, USA).

The polymer dissolved in acetone was pumped into a 0.5% solution of polyvinylalcohol (PVA) Mowiol® 4-88 (Kuraray Specialities Europe GmbH, Frankfurt, Germany) and stirred during nanoprecipitation. Organic solvent was removed using a rotary evaporator. Particles were freeze-dried.

Fluorescent particle-containing hydrogel: a 1% suspension of fluorescein labeled nanoparticles (average diameter 320 nm, PI 0.06) was prepared in water. A 3% hydroxyethylcellulose hydrogel (Natrosol® type 250 M pharma, Aqualon, Duesseldorf, Germany) was prepared separately. The polymer was dispersed in water under vigorous stirring (800 rpm) until it was homogeneously distributed; later on, the polymer was allowed to swell under low speed stirring (100 rpm) overnight. Both preparations were mixed at a proportion 1:1 and shaken until a homogeneous distribution of the particles in the gel was obtained, resulting in a nanoparticle 0.5% w/w hydrogel.

Fluorescein-containing hydrogel: a 0.003% sodium fluorescein containing hydrogel (equivalent to the fluoresceinamine amount linked to the polymer) was prepared by dissolution of the dye in water and addition of the polymer under stirring. Again, the preparation was stirred overnight with low speed (100 rpm) to allow swelling of the polymer. Both gels showed similar viscosities.

Pre-treatment of volunteers / porcine skin

The in vivo experiments were performed on the calves of six volunteers, and the in vitro investigations on ear skin of 12 freshly slaughtered pigs (6-month-old, German domestic pigs). The calves of the volunteers and the ear skin of the pigs were prepared by washing, drying with soft tissue, and abscising the hairs; defined skin areas of 10 cm x 4 cm were demarcated using a permanent marker. Approval for this study had been obtained from the Ethics Committee of the Charité and from the Veterinary Board of Control, Berlin, Treptow-Köpenick. The study was conducted according to the ethical rules stated in the Declaration of Helsinki Principles. The volunteers participating in the study had given their written consent.

Study designs

- Study design A: In vitro investigation of the follicular penetration depth of a topically applied dye in particle and non-particle form by analyzing biopsies.
- Study design B: In vivo analysis of the storage effect of the topically applied dye in particle and non-particle form by differential stripping

Study design A

Application

2 mg/cm² of each of the two formulations were applied homogeneously onto the ear skin of 12 pigs. In the case of six pig ears, the formulations were massaged into the tissue for 3 min by means of a massage appliance (Massage Gerät PC60, Petra electric, Burgau, Germany). In the case of the other six pig ears, the formulations were applied lightly without massage.

Biopsies and Microscopy

After a penetration time of 1 h, biopsies were taken from the pretreated porcine tissue, using 3 mm punch biopsies. Subsequently, the samples were frozen and histological sections were obtained. These were analyzed using a laser scanning microscope LSM 2000 (Carl Zeiss, Jena, Germany). The samples were measured in the transmission and the fluorescent modus. By superposition of the images, it was possible to investigate the distribution of the fluorescent dye inside the hair follicles as previously described by Toll et al [14]. Fifty hair follicles from skin areas treated with the particle-containing formulation and fifty hair follicles from skin areas treated with the non-particle formulation were investigated. The penetration depths of the fluorescence were measured; mean values and standard deviations were calculated and compared.

Study design B

Application

2 mg/cm² of both formulations were applied homogeneously on the calves of six volunteers. The formulations were massaged into the skin for 3 min by means of a massage appliance.

Differential stripping

After increasing penetration times of 24, h, 72 h and 120 h, differential stripping was applied on adjacent pretreated skin areas of each volunteer as described previously by Teichmann et al. [20]. Therefore, the upper part of the stratum corneum, which serves as a reservoir for topically applied substances, was removed by tape stripping as described by Weigmann et al. [22]. A roller was used to press the adhesive film (*tesa* Film No. 5529, Beiersdorf, Hamburg, Germany). During the rolling movement, the skin became stretched and the adhesive film was in contact with the flat skin

surface. In this way, the influence of the furrows and wrinkles of the skin surface on the tape stripping procedure could be avoided [23]. Fifteen to twenty tapes strips were removed from the skin. The tape strips were checked using a laser scanning microscope, in order to ensure that the fluorescent dye had been removed completely from the stratum corneum and was located only in the orifices of the hair follicles. Subsequently, a drop of superglue (UHU GmbH & Co. KG, Brühl, Germany) was placed on the surface of the treated skin and covered with a glass slide under slight pressure. After polymerization (approx. 2 min), the cyanoacrylate was strongly linked with the upper layers of the stratum corneum, the hair shafts and the content of the follicular infundibula and was removed with one quick movement. After removal, the cyanoacrylate skin surface biopsies were checked microscopically to make sure that the dye was only located in the casts of the hair follicles.

Afterwards, the samples were punched to a constant size of 15 mm in diameter and were extracted in ethanol (Uvasol, Merck, Darmstadt, Germany) using ultrasound (Sonorex Super RK102H, Bandelin Electronic, Berlin, Germany) and centrifugation (at 4,000 rpm for 10 min at 20°C, Centrifuge MR1812, Jouan GmbH, Unterhaching, Germany). Then, the solvents were analyzed in the fluorescence spectrometer LS50B (Perkin Elmer Instruments GmbH, Überlingen, Germany). The fluorescence of the dye was excited in the maximum of the absorption band at 450 nm; the fluorescence signal was detected in the spectral region from 520 to 650 nm. The intensity of the fluorescence signal was used as a measure for the concentration of the dye penetrated into the hair follicles.

Statistical analysis

Statistical analysis was performed with the software program SPSS® 12.0. Based on non-significant results ($p > 0.05$) of the Kolomogorov-Smirnov test, mean values and standard deviations were calculated using the software program Microsoft® Excel 2003.

In the case of study design A, the Wilcoxon test was utilized to analyze the penetration depth of the fluorescent dye in particle and non-particle form and with and without massage appliance affording a significance $p < 0.05$.

Results

Study design A:

In the case of study design A, the follicular penetration depth of the topically applied fluorescein in particle and non-particle form was determined by analyzing biopsies of porcine skin. In figure 1, the penetration of the fluorescent dye in the particle and non-particle form into the hair follicles of porcine skin, after the application of massage, is demonstrated by the superposition of a transmission and fluorescent image. The distribution of the fluorescent dye in the hair follicles is depicted in white. Figure 1a shows the penetration into the hair follicles of the fluorescent dye in the particle form, whilst figure 1b demonstrates the penetration of the fluorescent dye in the non-particle form. Significant differences can be observed: the particles penetrate much deeper into the hair follicles than the non-particle form if massage is applied.

Figure 2 represents the mean values and standard deviations of the follicular penetration depths of the fluorescent dye in particle and non-particle form. The results were obtained at an average on 50 hair follicles. The penetration depth was significantly deeper ($p < 0.05$), if the fluorescent dye had been applied in the particle form.

On the skin of six further pig ears, the same two formulations were gently applied to the skin without massage. Typical results can be seen in figure 3, where the superposition of fluorescent and transmission images are presented. The penetration depth of the two formulations is nearly identical ($p > 0.05$). The average penetration depth determined for the non-particle formulation was $300.74 \pm 65.37 \mu\text{m}$, for the particle formulation $297.45 \pm 71.6 \mu\text{m}$ (figure 4). For both formulations, the penetration depth was significantly lower for non-massage appliance than in the case of a massage being applied ($p < 0.05$).

Study design B

In the case of study design B, the concentration of the fluorescent dye, applied in particle and non-particle form by means of massage, penetrated into the hair follicle infundibula of the calf region of volunteers, was analyzed quantitatively utilizing differential stripping. The concentration of the fluorescent dye was analyzed at different time points after application. The obtained results are summarized in figure 5.

As the absolute amounts of fluorescein detected after one day in the hair follicles of different volunteers varied by a factor of 3, the concentration values determined after one day were standardized to 100% for better comparison of the mean values and standard deviations. The concentration of the dye decreased in time. If the skin had been treated with the formulation containing the fluorescent dye in the non-particle form, the dye could be detected only up to 4 days in the hair follicles. In contrast, the fluorescent dye in the particle form could still be detected 10 days after application.

Discussion

Follicular penetration is an important and promising pathway for selective dermatotherapy. To optimize penetration and storage of topically applied molecules, innovative formulations are conceived. These approaches are mainly focused on nano- or microsphere technology.

In the present study, we were able to demonstrate the superiority of particles versus non-particle formulations, not only for penetration but also for storage behavior. Interestingly, penetration of particle-containing formulations was enhanced by mechanical massage, reaching significant deeper penetration depths than without massage. However, without any mechanical manipulation on the skin surface, no significant differences between the two formulations were observed.

Regarding the storage behavior of human hair follicles, striking results could be obtained: the nanoparticles remained in the hair follicles much longer than the non-particle substances.

These results appear to be surprising, as it could be expected that the small amounts of non-particle substances, with their relatively small size, penetrate better into the small hair follicles than the much larger particles. The results obtained show the opposite effect, but only in the case of a massage being applied. Possibly, apart from fluid mixing, this effect can be explained by the structure of the hairs and the hair follicles, which are very similar in porcine and human skin. The stratum corneum extends deeply into the hair follicles. From the structure analysis of hair surface and hair follicles, it is known that the cuticle produced by keratinocyte desquamation forms a structured surface, which can be approximated by a zigzag relief [24]. This relief is determined by the thickness of the keratin cells, which is between 500 and 800 nm. If the hairs are moved by massage, the cuticle cells may act as a geared pump. Particles, comparable in size to the surface structure of the hairs and

hair follicles are probably pushed into the follicles by means of the pump movement of the hairs.

These findings are in agreement with the results obtained by Toll et al. [14], the microparticles with a diameter of 750 nm penetrated better into the hair follicles of excised human skin than larger particles, when a massage had been applied.

Under in vivo conditions, this assumed pump mechanism also occurs without a massage, on account of the continuous movement of the body, which is able to stimulate the pump mechanism of the terminal and vellus hairs. This in vivo movement is less than in the case of a massage, but it occurs continuously.

The in vivo storage experiments demonstrated that the penetration into the hair follicles is a fast process (1 hour), in comparison to the release of the nanoparticles out of the follicles, which continues for some days. The penetration process into the hair follicles is determined by the concentration gradient of the topically applied substances. If the reservoir of the skin surface and the stratum corneum, as the source of the penetration into the hair follicles, is depleted by textile contact and desquamation, the sebum production seems to be mainly responsible for the penetration of the substances out of the hair follicles. The non-particle substances are quickly moved out by the sebum production, probably, because they are not inhibited by the surface structures of the follicles and the hairs, whereas, the movement of the particles out of the hair follicles is assumed to be retarded by the surface structure. Taking into consideration the experiments concerning the follicle penetration of TiO₂ microparticles [16], it can be expected that all particles at a size of >100 nm, which penetrate into the hair follicles, will also be moved out after some time on account of the sebum production not having reached the living cells.

Conclusions

Nanoparticles are well suited to penetrate efficiently into the hair follicles, reaching deeper functional structures, where they can be stored for some days. In the case of non-particle substances, such a long-term effect cannot be observed, either in the hair follicles or in the stratum corneum. In principle, the stratum corneum is not suited as a long-term reservoir of topically applied substances, as these substances are mainly located on the skin surface or in the upper-cell layers after topical application [13]. These upper-cell layers are later continuously scuffed by desquamation. Therefore, the hair follicles are the only long-term reservoir for topically applied substances; consequently, they are important targets for drug delivery, as they are surrounded by a close network of blood capillaries and dendritic cells (Langerhans cells). Additionally, the hair follicles contain stem cells. Selecting the correct size of particles as drug carriers, thus, an efficient selective drug delivery and storage of topically applied substances into hair follicles is possible, which is important for selective dermatotherapy.

Acknowledgments:

We would like to thank the Universidad de Concepción and Proyecto MECESUP UCO 0202 (Ministerio de Educación – Gobierno de Chile) for their financial support.

References

- [1] J. Bouwstra, G. Pilgram, G. Gooris, H. Koerten, M. Ponec, New aspects of skin barrier organization, *Skin Pharmacol. Appl. Skin Physiol.* 14 (2001) 52-62.
- [2] E.H. Choi, S.H. Lee, S.K. Ahn, S.M. Hwang, The pretreatment effect of chemical skin penetration enhancers in transdermal drug delivery using iontophoresis, *Skin Pharmacol. Appl. Skin Physiol.* 12 (1999) 326-335.
- [3] J. Hadgraft, Modulation of the barrier function of the skin, *Skin Pharmacol. Appl. Skin Physiol.* 14 (2001) 72-81.
- [4] A.C. Lauer, L.M. Lieb, C. Ramachandran, G.L. Flynn, N.D. Weiner, Transfollicular Drug Delivery, *Pharm. Res.* 12 (2) (1995) 179-186.
- [5] H. Schaefer, J. Lademann, The role of follicular penetration, *Skin Pharmacol. Appl. Skin Physiol.* 14 (2001) 23-27.
- [6] J. Lademann, N. Otberg, H. Richter, H.J. Weigmann, U. Lindemann, H. Schaefer, W. Sterry, Investigation of follicular penetration of topically applied substances, *Skin Pharmacol. Appl. Skin Physiol.* 14 (2001) 17-22.
- [7] T. Ogiso, T. Shiraki, K. Okajima, T. Tanino, M. Iwaki, T. Wada, Transfollicular drug delivery: Penetration of drugs through human scalp and comparison of penetration between scalp and abdominal skins in vitro, *J. Drug Target.* 10 (5) (2002) 369-378.

- [8] R.J. Feldmann, H.I. Maibach, Regional variation in percutaneous penetration of ¹⁴C cortisol in man, *J. Invest. Dermatol.* 48 (1967) 181-183.
- [9] F. Hueber, M. Besnard, H. Schaefer, J. Wepierre, Percutaneous absorption of estradiol and progesterone in normal and appendage-free skin of the hairless rat: Lack of importance of nutritional blood flow, *Skin Pharm. Appl. Skin Phys.* 7 (1994) 245-256.
- [10] S.N. Tenjarla, R. Kasina, P. Puranajoti, M.S. Omar, W.T. Harris, Synthesis and evaluation of N-acetylprolinate esters – Novel skin penetration enhancers, *Int. J. Pharm.* 192 (1999) 147-158.
- [11] B.W. Barry, Drug delivery routes in skin: a novel approach, *Adv. Drug Deliv. Rev.* 54 (2002) 31-40.
- [12] N. Otberg, H. Richter, H. Schaefer, U. Blume-Peytavi, W. Sterry, J. Lademann, Variations of hair follicle size and distribution in different body sites, *J. Invest. Dermatol.* 122 (2004) 14-19.
- [13] H.J. Weigmann, J. Lademann, S. Schanzer, U. Lindemann, R. v. Pelchrzim, H. Schaefer, W. Sterry, Correlation of the local distribution of topically applied substances inside the stratum corneum determined by tape stripping to differences in bioavailability, *Skin Pharm. Appl. Skin Phys.* 14 (2001) 93-103.

- [14] R. Toll, U. Jacobi, H. Richter, J. Lademann, H. Schaefer, U. Blume-Peytavi, Penetration profile of microspheres in follicular targeting of terminal hair follicles, *J. Invest. Dermatol.* 123 (2004) 168-176.
- [15] H. Schaefer and T.E. Redelmeier, In: *Skin Barrier: Principles of Percutaneous Absorption*. Basel / Freiburg / Paris / London / New Dehli / Bangkok / Singapore / Tokyo / Sydney: Karger, 1996, 82-86.
- [16] J. Lademann, H.J. Weigmann, C. Rickmeier, H. Barthelmes, H. Schaefer, G. Mueller, W. Sterry, Penetration of titanium dioxide microparticles in a sunscreen formulation into the horny layer and the follicular orifice, *Skin Pharm. Appl. Skin Phys.* 12 (1999) 247-56.
- [17] N. Otberg, H. Richter, A. Knuettel, H. Schaefer, W. Sterry, J. Lademann, Laser spectroscopic methods for the characterization of open and closed follicles, *Laser Phys. Lett.* 1(1) (2004) 46–49.
- [18] N. Otberg, H. Richter, U. Jacobi, U. Blume-Peytavi, H. Schaefer, W. Sterry, J. Lademann, In vivo method to assess active and inactive hair follicles, *JDDG* 2 (6) (2004) 501.
- [19] G.A. Simon, H.I. Maibach, The pig as an experimental animal model of percutaneous permeation in man: qualitative and quantitative observations – An overview, *Skin Pharmacol. Appl. Skin Physiol.* 13 (2000) 229-234.

- [20] A. Teichmann, U. Jacobi, M. Ossadnik, H. Richter, S. Koch, W. Sterry, J. Lademann, Differential Stripping: Determination of the amount of topically applied substances penetrated into the hair follicles, *J. Invest. Dermatol.* 125 (2) (2005) 264-69.
- [21] U. Jacobi, E. Waibler, W. Sterry, J. Lademann, In vivo determination of the long term reservoir of the horny layer using laser scanning microscopy, *J. Laser Physics*; in press
- [22] H.J. Weigmann, J. Lademann, H. Meffert, H. Schaefer, W. Sterry, Determination of the horny layer profile by tape stripping in combination with optical spectroscopy in the visible range as a prerequisite to quantify percutaneous absorption, *Skin Pharmacol. Appl. Skin Physiol.* 12 (1999) 34-45.
- [23] J. Lademann, H.J. Weigmann, S. Schanzer, H. Richter, H. Audring, C. Antoniou G. Tsikrikas, H. Gers-Barlag, W. Sterry, Disturbing influences of furrows and wrinkles quantifying penetration of drugs and cosmetics by tape stripping. *J. Biomed. Opt.*, in press
- [24] S.Biel, K. Kawaschinski, K.P. Wittern, U. Hintze, R. Wepf, From tissue to cellular ultrastructure: closing the gap between micro- and nanostructural imaging, *J. Microsc.* 212 (2003) 91-9.

Figure legends

Figure 1

Superposition of a transmission and fluorescent image, demonstrating the in vitro penetration of the dye-containing formulation into the hair follicles of porcine skin after application of a massage

A: dye in particle form

B: dye in non-particle form

Figure 2

Average penetration depth of the particle and non-particle containing formulations after massage appliance (porcine skin). Significant differences ($p < 0.05$) are indicated with *.

Figure 3

Superposition of a transmission and fluorescent image, demonstrating the in vitro penetration of the dye containing formulation into the hair follicles of porcine skin without massage

A: dye in particle form

B: dye in non-particle form

Figure 4

Average penetration depth of the particle and non-particle containing formulations without massage appliance (porcine skin). Significant differences ($p < 0.05$) are indicated with *.

Figure 5

Semi-quantitative determination of the fluorescent dye in the hair follicle infundibula by cyanoacrylate skin surface biopsy at different time points after application (calves of 6 volunteers, mean values and standard deviations)

Figure 1

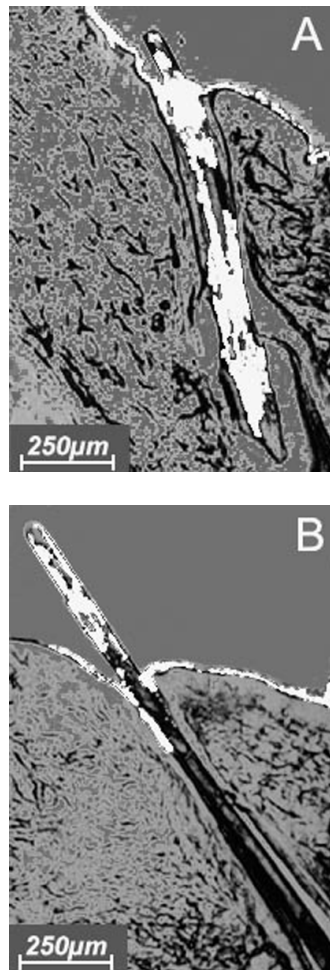
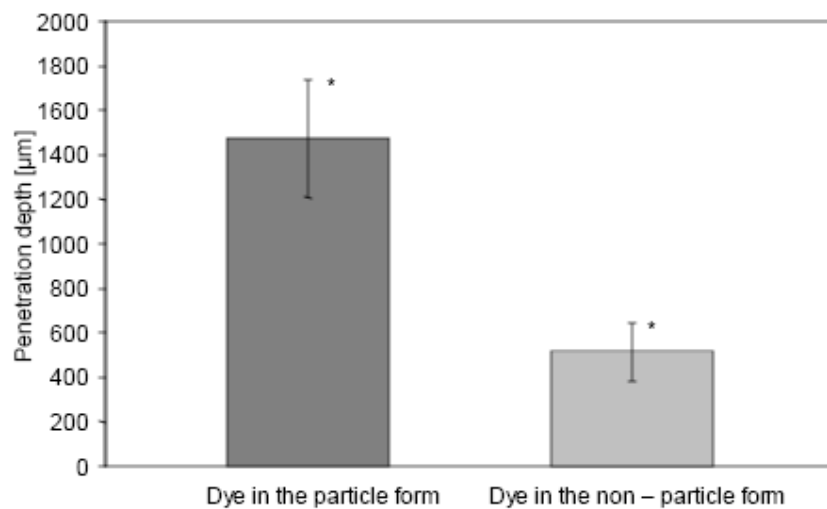
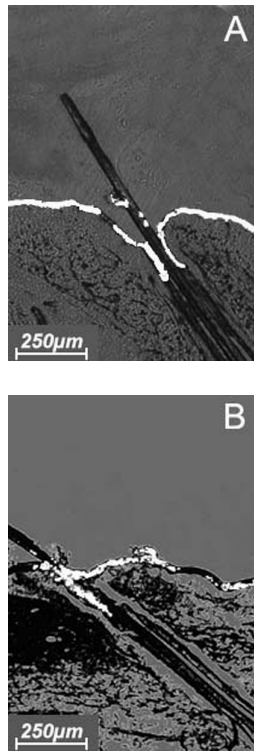


Figure 2



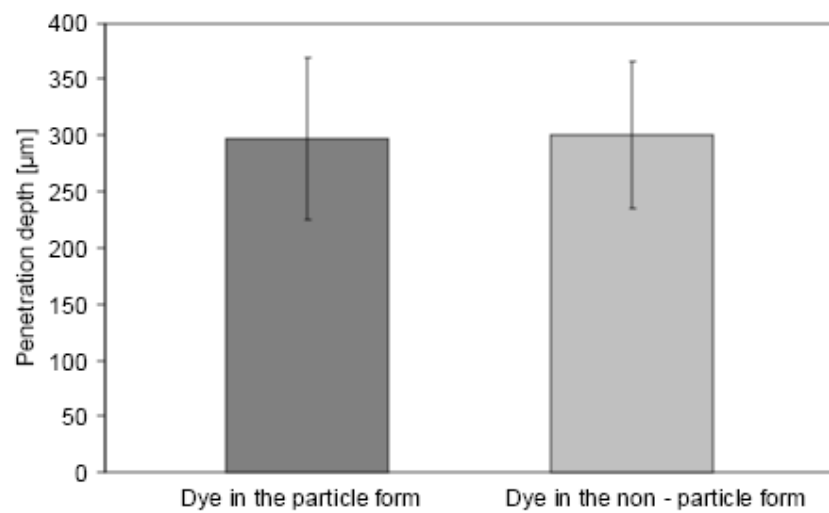
ACCEPTED MANUSCRIPT

Figure 3



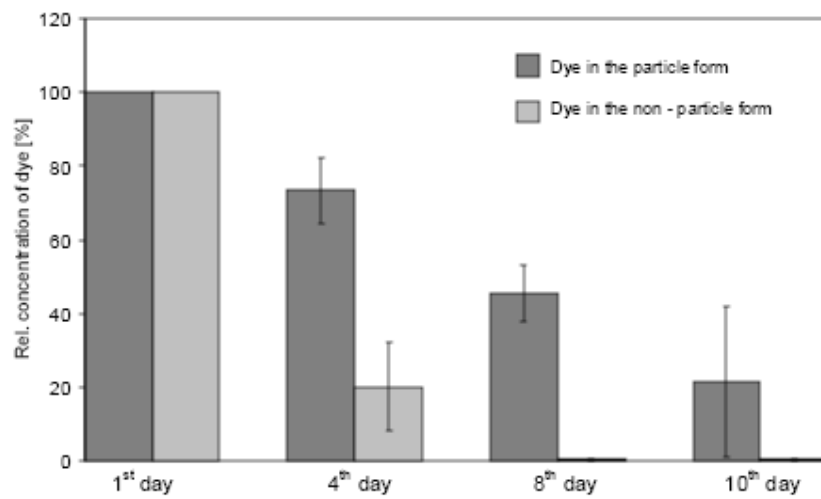
ACCEPTED MANUSCRIPT

Figure 4



ACCEPTED MANUSCRIPT

Figure 5



ACCEPTED MANUSCRIPT

Multiphoton Microscopy for the Investigation of Dermal Penetration of Nanoparticle-Borne Drugs

Frank Stracke¹, Barbara Weiss², Claus-Michael Lehr², Karsten König¹, Ulrich F. Schaefer² and Marc Schneider²

Multiphoton microscopy (MPM) of a dually fluorescence-labeled model system in excised human skin is employed for high-resolution three-dimensional (3D) visualization in order to study the release, accumulation, and penetration properties of drugs released from nanoscale carrier particles in dermal administration. Polymer particles were covalently labeled with fluorescein, whereas Texas Red as a drug-model was dissolved in the particles to be released to the formulation matrix. Single nanoparticles on skin could easily be localized and imaged with diffraction-limited resolution. The temporal evolution of the fluorescent drug-model concentration in various skin compartments over more than 5 hours was investigated by multiphoton spectral imaging of the same area of the specimen. The 3D penetration profile of the drug model in correlation with skin morphology and particle localization information is obtained by multiple laser line excitation experiments. MPM combined with spectral imaging was found to allow noninvasive long-term studies of particle-borne drug-model penetration into skin with subcellular resolution. By dual color labeling, a clear discrimination between particle-bound and released drug model was possible. The introduced technique was shown to be a powerful tool in revealing the dermal penetration properties and pathways of drugs and nanoscale drug vehicles on microscopic level.

Journal of Investigative Dermatology (2006) **126**, 2224–2233. doi:10.1038/sj.jid.5700374; published online 18 May 2006

INTRODUCTION

The encapsulation of active substances is a common pharmaceutical strategy to modify the transport and release properties of a drug. Especially to nanoparticulate systems, great potential is attributed in the field of drug delivery. This is partly due to the fact that sensitive drugs can be hidden from degradation in the particles (Volodkin *et al.*, 2004; Daniels, 2006). Further powerful properties of nanoscale drug carriers are the sustained release (El-Samaligy *et al.*, 1986; Daniels, 2006) of the active substances, resulting in an extended activity or enhanced uptake (Alvarez-Roman *et al.*, 2004c; Lombardi Borgia *et al.*, 2005) and the possible reduction of adverse effects (Lamprecht *et al.*, 2001). Functional coatings of the particles may allow the targeted accumulation and release of drugs at their therapeutic sites (Wartlick *et al.*, 2004; Dinauer *et al.*, 2005; Kotrotsiou *et al.*, 2005).

Widely used nanoparticle formulations are based on poly(lactic acid) (PLA), poly(glycolic acid) (PGA), and their co-polymers, poly(lactide-co-glycolide) (PLGA), which are known for their good biocompatibility and degradability through natural pathways (Brannon-Peppas, 1995). In oral and parenteral applications, these solid biodegradable polymeric nanoparticles have already shown their advantage over liposomes by their increased stability (Soppimath *et al.*, 2001; Hans and Lowman, 2002; Ravi Kumar *et al.*, 2003). Nanoscale polymeric drug vehicles have also been proposed for transdermal delivery (Kohli and Alpar, 2004; Alvarez-Roman *et al.*, 2004c; Lombardi Borgia *et al.*, 2005; Luengo *et al.*, 2006). Penetration (Alvarez-Roman *et al.*, 2004c; Luengo *et al.*, 2006), permeation (Luengo *et al.*, 2006), and accumulation (Toll *et al.*, 2004) of some particle-borne drugs and drug models after topical application have been investigated by conventional techniques and confocal microscopy of single stained particles.

Established methods for the investigation of drug penetration into the skin are mostly destructive: a representative sample of a defined skin layer is isolated and extracted for chemical analysis (tape stripping method, cryo-sectioning) (Wagner *et al.*, 2001; Brain *et al.*, 2002). The result of such an experiment is an area-averaged depth profile of the drug in the skin to a certain time (Luengo *et al.*, 2006). The depth profiles for different incubation times have to be investigated with different samples, neglecting the individual characteristics of biological specimens. To evaluate and optimize novel dermal drug delivery strategies using nanoscale drug

¹Fraunhofer Institute for Biomedical Technology, St Ingbert, Germany and

²Department of Biopharmaceutics & Pharmaceutical Technology, Saarland University, Saarbrücken, Germany

Correspondence: Dr Frank Stracke, Fraunhofer Institute for Biomedical Technology, Ensheimer Str. 48, 66386 St Ingbert, Germany.

E-mail: frank.stracke@ibmt.fraunhofer.de

Abbreviations: FA, fluoresceinamine; MPM, multiphoton microscopy; PLGA, polylactide-co-glycolide; PMT, photomultiplier tube; PVA, polyvinylalcohol; ROI, region of interest; x, y, lateral dimensions; z, normal dimension/subsurface depth

Received 17 February 2006; accepted 27 March 2006; published online 18 May 2006

carriers, more versatile techniques are required. Such a technique must allow the discrimination between free and carrier-bound drugs, the tracing of the carrier nanoparticles, the allocation of microscopic delivery pathways to specific dermal sites, and time studies on the same skin area. After application of nanoparticles as topical vehicles, one can imagine different routes of drug delivery. It could be assumed that the whole nanoparticulate system is taken up without being destroyed (Kohli and Alpar, 2004) or that the nanocarrier is decomposed close to the skin surface and thereafter the active substance penetrates depending on the local environment (acidification or absorption of drug/nanoparticle-complexes) as speculated in Luengo *et al.* for the enhanced long-term uptake of flufenamic acid (Luengo *et al.*, 2006). Furthermore, a direct diffusion from the carrier into the stratum corneum is reasonable as described by Bouwstra *et al.* (Meuwissen *et al.*, 1998; Van Kuijk-Meuwissen *et al.*, 1998a). In any case, it is essential to distinguish between particles, particle-bound drug, and released drug. Herein we describe how multiphoton laser scanning microscopy (MPM) and confocal laser scanning microscopy can be very beneficial tools in order to meet all these demands in one experiment. In particular, multiphoton microscopy enables repeated noninvasive investigations of skin tissue down to the dermis with virtually no out-of-focus effects of the scanning laser beam (König and Riemann, 2003). Owing to multiple labeling techniques in combination with multiphoton spectral imaging or selective excitation of the labels, a clear discrimination between particles and free drug model is possible, as well as tracking of single particles. Owing to the excitation of endogenous fluorophores of the skin by multiphoton excitation and the correlation of the resulting autofluorescence image with the drug fluorescence pattern, the identification of accumulative spots and penetration pathways is possible with subcellular resolution (Yu *et al.*, 2002, 2003). MPM provides several considerable advantages over conventional fluorescence and confocal microscopy (Xu *et al.*, 1996; König, 2000). Three of which are relevant to the present investigation: the concentration of all light-matter interactions to the focal volume, the convenient separation of fluorescence from scattered excitation light due to the large blueshift of fluorescence, and the capability to excite compounds that else require ultraviolet excitation, in particular native fluorophores as nicotinic adenine dinucleotide (hydrogenated form, NADH) and keratin (Huang *et al.*, 2002; König and Riemann, 2003; Pena *et al.*, 2005). The confined interaction volume at the focal point is due to the I^n -dependence of n -photon absorption processes on the illumination intensity I . Hence, already two-photon absorptions are confined to a sub-femtoliter focal volume, in which the illumination intensity is sufficiently high. As the excitation with near infrared lasers matches the optical window of biological matter (700–1100 nm), virtually no single-photon absorptions occur in the illumination cones. As a consequence, no fluorescence is generated outside the focal volume and, therefore, three-dimensional spatial resolution is an inherent feature of multiphoton laser scanning microscopy. Furthermore, out-of-focus photo-damage

is drastically reduced and light penetration depth into tissue is significantly enhanced (Centonze and White, 1998; König and Riemann, 2003).

As most pharmaceutical substances are basically non-fluorescent, the usage of appropriate fluorescent model compounds is reasonable. Such a model compound has to match the molecular size, charge, membrane permeability, distribution, and diffusion coefficients as good as possible. A fluorescent label fixed to the actual drug molecule changes these properties and, thus, the penetration behavior considerably. Hence labeling makes sense only if specific interactions of the drug to certain sites are investigated. In contrast, the nonsuperficial fluorescent labeling of the nanoscale carrier particles does not change the particle's pharmacokinetics significantly. In addition, the fate of the nanocarrier itself and its role in the changed uptake behavior may be investigated. In this work, a two-color labeling technique was used to trace the migration of the nanoparticles and to observe the release and uptake of the drug-model compound. To this end, fluoresceinamine (FA) was covalently linked to the polymeric particle material and Texas Red was physically resolved in the particle matrix. It is shown that individual subdiffraction sized nanoparticles can be localized, traced, and spectrally analyzed. Owing to the two-color staining, a clear discrimination between free and particle-bound dye was achieved. The method turned out to allow stable measurements on excised human skin over hours with no significant drift of the specimen.

RESULTS

Multiphoton fluorescence imaging

The multiphoton optical sections were recorded from the skin surface down to the bottom of the shown dermatoglyph at $z = -42 \mu\text{m}$ over 5 hours under identical conditions (Figure 1). It was found that the subdiffraction-limit-sized particles can easily be detected and localized, as long as their mean distance is well above this limit. They appear as lateral diffraction-limited spots with widths of about $0.5 \mu\text{m}$, which is in reasonable agreement with theoretical predictions for the minimum achievable full-width half-maximum of 302 nm. (The theoretical full-width half-maximum was calculated by convolution of a sphere profile of $d = 290 \text{ nm}$ with the squared intensity point spread function IPSF^2 . The IPSF^2 was derived according to Zipfel *et al.* (2003).) A typical fluorescence profile of two particles *in situ* is displayed in Figure 2. The minimal fluorescence spot size may be broadened by Brownian motion and distorted by flux motions of the gel in the dermatoglyphs. In the case of the bright spots, the detector went into saturation, which additionally caused a considerable broadening of the spot size. The mean distance between the nanoparticles in the present formulation is of the order of $5 \mu\text{m}$. Three-dimensional tracing of individual particles is easily possible under the outlined conditions and allows detailed studies on the migration of nanoscale drug carriers in the skin.

The significant endogenous fluorescence of keratin under two-photon excitation enables imaging of the outermost layer of the stratum corneum and hence the dermal topography.

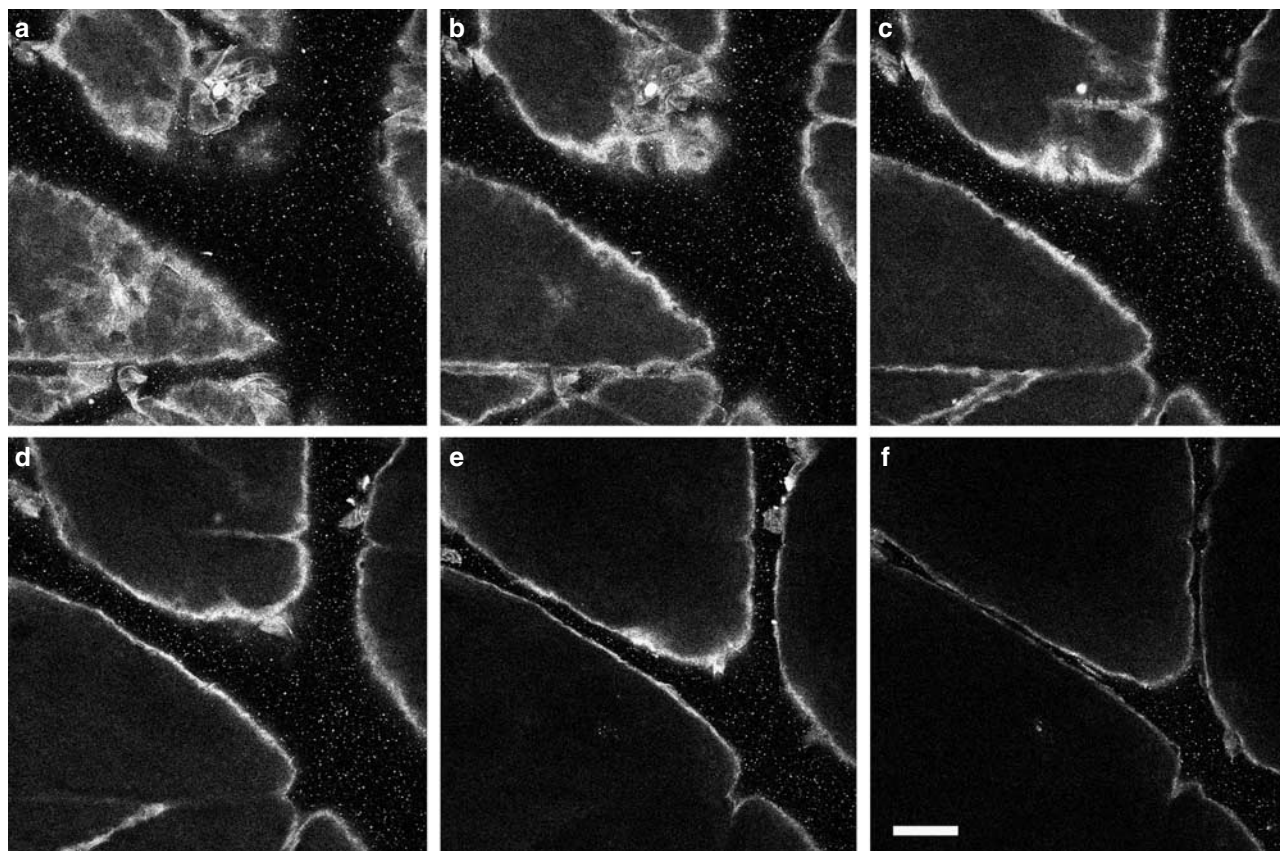


Figure 1. $325 \times 325 \mu\text{m}^2$ multiphoton optical sections of human skin treated with a hydrogel suspension of two-color-labeled nanoparticles. The subsurface depths of the displayed images are (a) $-6 \mu\text{m}$, (b) $-9 \mu\text{m}$, (c) $-12 \mu\text{m}$, (d) $-15 \mu\text{m}$, (e) $-24 \mu\text{m}$, and (f) $-33 \mu\text{m}$. The keratin autofluorescence clearly shows the surface of the dermatoglyphs. The excitation power for the multiphoton optical sections was $P_{\text{EX}} = 5 \text{ mW}$, the pixel acquisition time $t_{\text{px}} = 3.2 \mu\text{s}$ (Bar = $50 \mu\text{m}$).

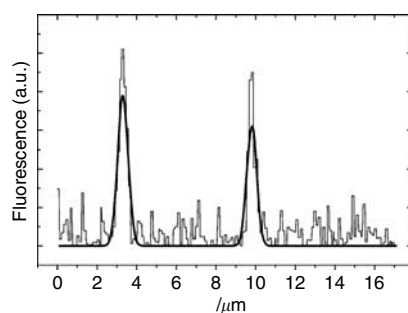


Figure 2. Fluorescence intensity profile of two multiphoton excited nanoparticles *in situ*. The bimodal fit yields a full-width at half-maximum of $0.5 \mu\text{m}$. This is a reasonable value for the diffraction-limited resolution of nanoscale particles under the present conditions.

The PLGA particles are obviously not able to penetrate the stratum corneum, and stay in the gel-filled dermatoglyphs over the entire observation time (Figure 3). This corresponds with former findings of the authors in which no penetration of PLGA particles loaded with flufenamic acid into the human skin could be observed (Luengo *et al.*, 2006). It is noteworthy that even after more than 5 hours, swelling, shrinking, and

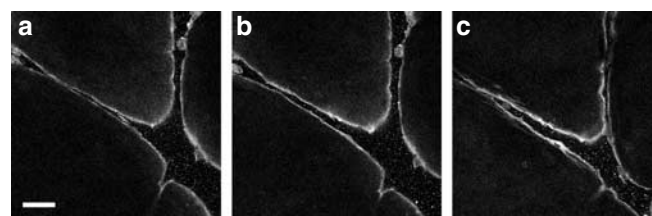


Figure 3. $325 \times 325 \mu\text{m}^2$ multiphoton optical sections at a depth of $-27 \mu\text{m}$ (a) 15, (b) 50, and (c) 315 minutes after application of the nanoparticulate formulation. (Bar = $50 \mu\text{m}$).

stress relaxation motions of the skin sample lead only to minute deformations within the field of view. No drift of the specimen occurred.

No significant changes in the background fluorescence intensity of the gelly suspension matrix or in the stratum corneum as a consequence of the Texas Red release and accumulation were observed in the multiphoton fluorescence mode. The reason for this finding is the comparable low two-photon absorption cross-section of Texas Red at $\lambda = 800 \text{ nm}$ (Figure 4), whereas fluorescein and keratin are efficiently excited.

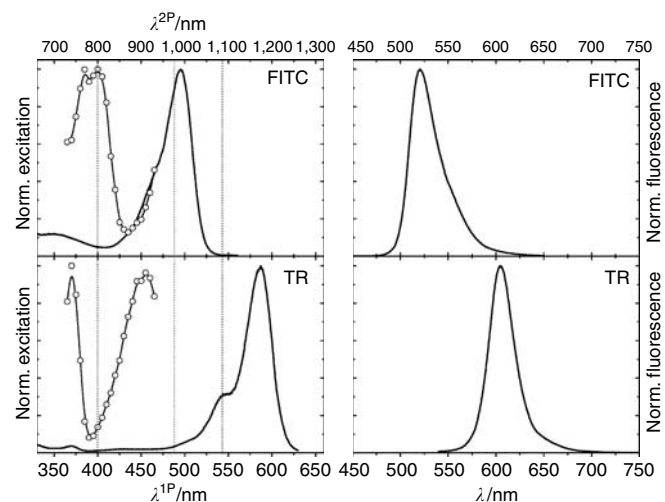


Figure 4. One- (solid line) and two-photon (open circles plus B-spline fit) excitation spectra are displayed in the left panels. The right panels show the related fluorescence spectra of (a) FITC dextran and (b) Texas Red. All spectra are normalized, the one- and two-photon abscissa are aligned for equal transition energies. One- and two-photon excitation spectra may differ considerably because of the converse selection rules of the related absorption processes. The excitation wavelengths at $\lambda^{1P} = 488$ nm and 543 nm as well as at $\lambda^{2P} = 800$ nm are accentuated by dotted vertical lines.

Multiphoton spectral imaging

In order to investigate the distribution of the drug-model Texas Red as a function of time, two-photon spectral imaging was applied. In this technique, the luminescence signal from the specimen is spectrally resolved and the spectrum is stored for each pixel or voxel, respectively. From these data, fluorescence spectra for arbitrary regions of interest can be calculated. The laser wavelength of 800 nm leads to an image, which is dominated by the fluorescein emission and the endogenous fluorescence of the stratum corneum. However, owing to the different sensitivity spectrum of the META detector array, the sensitivity loss in the red spectral range is less drastic than for the photomultiplier tubes. Even faint contributions of the Texas Red fluorescence to any pixel or region of interest (ROI) of the image can now be isolated from the other emissions by spectral separation. In the present study, a $145 \times 145 \mu\text{m}^2$ area from the middle of Figure 1 was investigated. The spectral images were recorded to similar times as that of the optical sections. In Figure 5a, a typical example of such a spectral image is displayed in true color mode. The nanoparticles appear clearly green, indicating that their fluorescence originates predominantly from the covalently bound fluorescein. The outermost layer of the stratum corneum shows a heterogeneous distribution of colors. For an interpretation, the fluorescence spectrum of the respective region is taken (Figure 6a, ROI 2). The reddish color of the deeper skin is mainly caused by residual scattered excitation light beyond 700 nm (Figure 6a, ROI 3).

In Figure 5a, three regions of interest are indicated: ROI 1 contains the gel matrix including the nanoparticles, ROI 2 contains the keratinous surface layer of the stratum corneum,

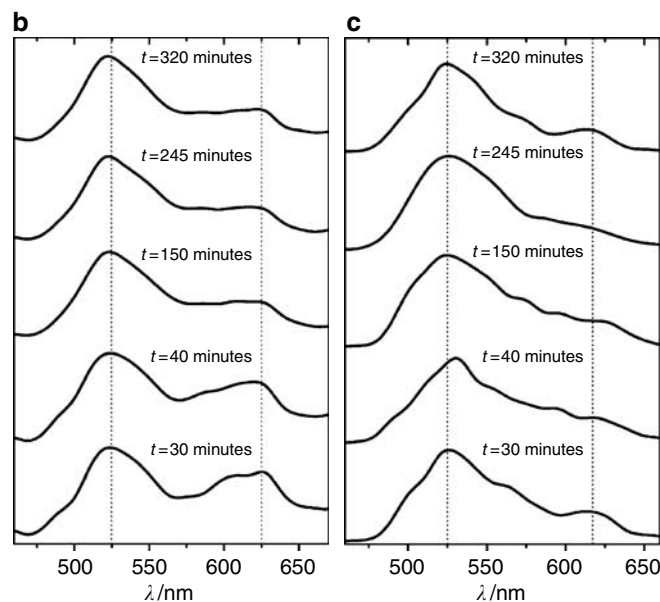
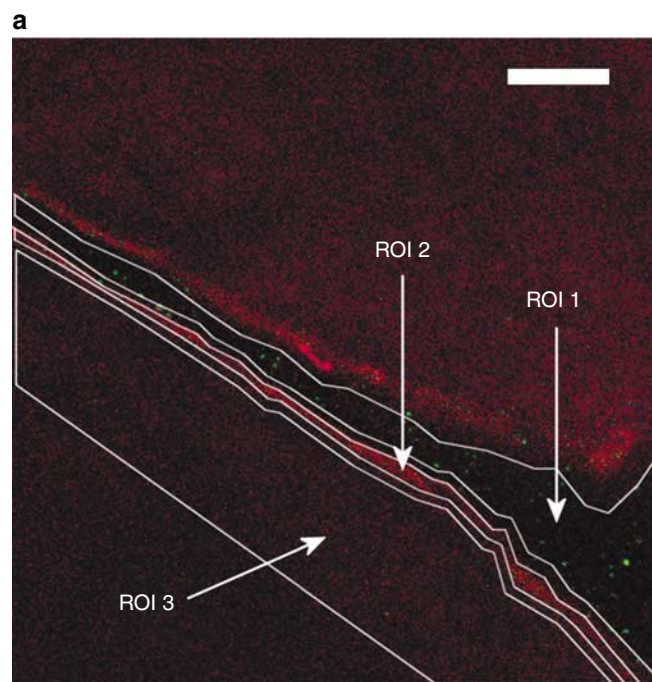


Figure 5. Multiphoton spectral imaging. (a) True color representation of a spectral image at $z = -21 \mu\text{m}$ with plots of the ROIs used for spectral analysis (Bar = $20 \mu\text{m}$). (b) Fluorescence spectra series of ROI 1 showing the decline of Texas Red in the gel matrix (including particles). The Texas Red content in the particles is low and shows no clear trend as depicted in the series of the average spectra of 15 particles per image in (c). As the Texas Red content of the particles does not change significantly, the decline of Texas Red in ROI 1 must occur in the gel matrix itself. The excitation power for the multiphoton spectral images was $P_{\text{EX}} = 15$ mW, the pixel acquisition time $t_{\text{px}} = 3.2 \mu\text{s}$.

and ROI 3 covers the deeper layers down to approximately $20 \mu\text{m}$. Average fluorescence spectra are calculated from the ROIs at different times to reveal the evolution of the Texas Red concentration in these regions. Owing to the small deformations of the specimen, especially in vertical direction,

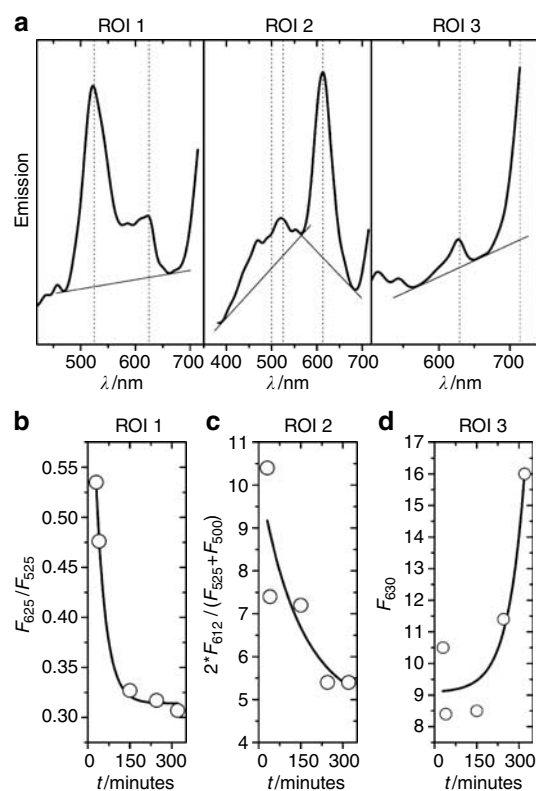


Figure 6. Quantitative spectral analysis of the Texas Red concentration in different skin compartments. Scheme (a) shows the baselines and spectral positions used for calculating the emission ratios for the determination of the relative contents of the drug-model Texas Red in the ROIs. (b–d) Temporal evolution of the emission ratios as a measure of Texas Red content in the ROIs. In ROI 2 the Texas Red emission at 612 nm is divided by the average keratin autofluorescence intensity at 500 and 525 nm because of the interference of the broad autofluorescence emission with noise effects around 500 nm.

the ROIs do not enclose exactly identical skin domains at the different times. This may be a cause for small discrepancies in the spectral analysis. However, as the ROIs were always chosen to enclose only skin compartments according to the definitions above, the spectral analysis will still reveal the accurate trends. To rule out errors due to varying offsets and fluctuations in the absolute signal, the Texas Red fluorescence is determined relative to an emission, which is expected to be constant in time. For ROI 1, the fluorescein emission from the nanoparticles at 525 nm is used, for ROI 2 the keratin autofluorescence around 510 nm, and for ROI 3 the back-scattered excitation light at 714 nm. Linear baselines are applied to reduce the influence of the background (Figure 6a). As in particular the autofluorescence in ROI 2 and the Texas Red emission in ROI 3 show only dim intensities, the determined intensity ratios for ROI 2 and ROI 3 have large uncertainties. However, the rough trends are visible in those plots.

Whereas the Texas Red content in the nanoparticles showed up to be low and basically constant already from the first measurement at $t = 30$ minutes (Figure 5c), the concentration of Texas Red in the gel matrix drops significantly with time (Figures 5b and 6b). The Texas Red concentration in

the superficial layer of the stratum corneum is also declining, but less rapidly (Figure 6c). The observation of declining concentration in this compartment from the earliest measurement at $t = 30$ minutes on means that the vast fraction of Texas Red was taken up from the gel to the stratum corneum surface almost immediately after application. Furthermore, the release of Texas Red from the nanoparticles to the matrix started well before application to the skin. Probably, the predominant fraction was released to the solvent even before suspension of the particles to the hydrogel. As the concentration of the released dye is decreasing in the gel-filled dermatoglyphs and in the stratum corneum surface, it must have penetrated the skin (or metabolism of the dye occurred, which is unlikely). In fact, an increase of Texas Red concentration in the deeper stratum corneum and stratum granulosum is evident (Figure 6d), indicating a slow penetration of the dye. The fits to the plots are mono-exponential decays and growth, respectively. The fit curves have no theoretical pharmacokinetic background, but allow a convenient comparison of decay and rise times. Advanced interpretations of the release, uptake, and penetration of the dye will be possible only on the basis of an appropriate pharmacokinetic model. The decay times of the mono-exponential fits are $\tau_{ROI1} = 35 \pm 6$ minutes and $\tau_{ROI2} = 148 \pm 319$ minutes, and the rise time is $\tau_{ROI3} = 59 \pm 38$ minutes.

Multitracking studies

After 320 minutes, a multitracking experiment visualizes the distribution of Texas Red, fluorescein, and keratin fluorescence (Figure 7). In this technique, the signals from the different fluorophores are separated by their excitation spectra, not by their fluorescence spectra as performed in spectral imaging. As opposed to the spectral images, which are recorded with one excitation wavelength, herein the successive use of three excitation sources may lead to small mismatches between the channels. The vertical mismatch of the near infrared two-photon excitation image to the images excited by visible laser sources is due to chromatic aberrations of the objective. The small average lateral shift from the fluorescein image, excited by the 488 nm argon ion laser line, to the Texas Red image, excited by the 543 nm helium neon laser line, is due to the microscope optics and could be compensated by image processing. Furthermore, a multitracking experiment yields an overlay of successive scan images. If the specimen shows dynamics, any motion is reflected by shifts from one scan to the next. One must keep these mismatches in mind when performing colocalization studies on different dyes. In Figure 7d, an average lateral shift of about $6 \mu\text{m}$ is evident between the fluorescein image and the Texas Red image. The shift is not uniform for all particles, but varies owing to flux motions within the hydrogel during the acquisition times of the three single images of the multitracking experiment. The particle pattern in the two-photon excited image exhibits no correlation with the visibly excited images, indicating a vertical mismatch of the focal planes exceeding the normal size of the focal volumes (approximately $1 \mu\text{m}$). This mismatch is also evident in the missing congruency of the dermatoglyph borders in the two-

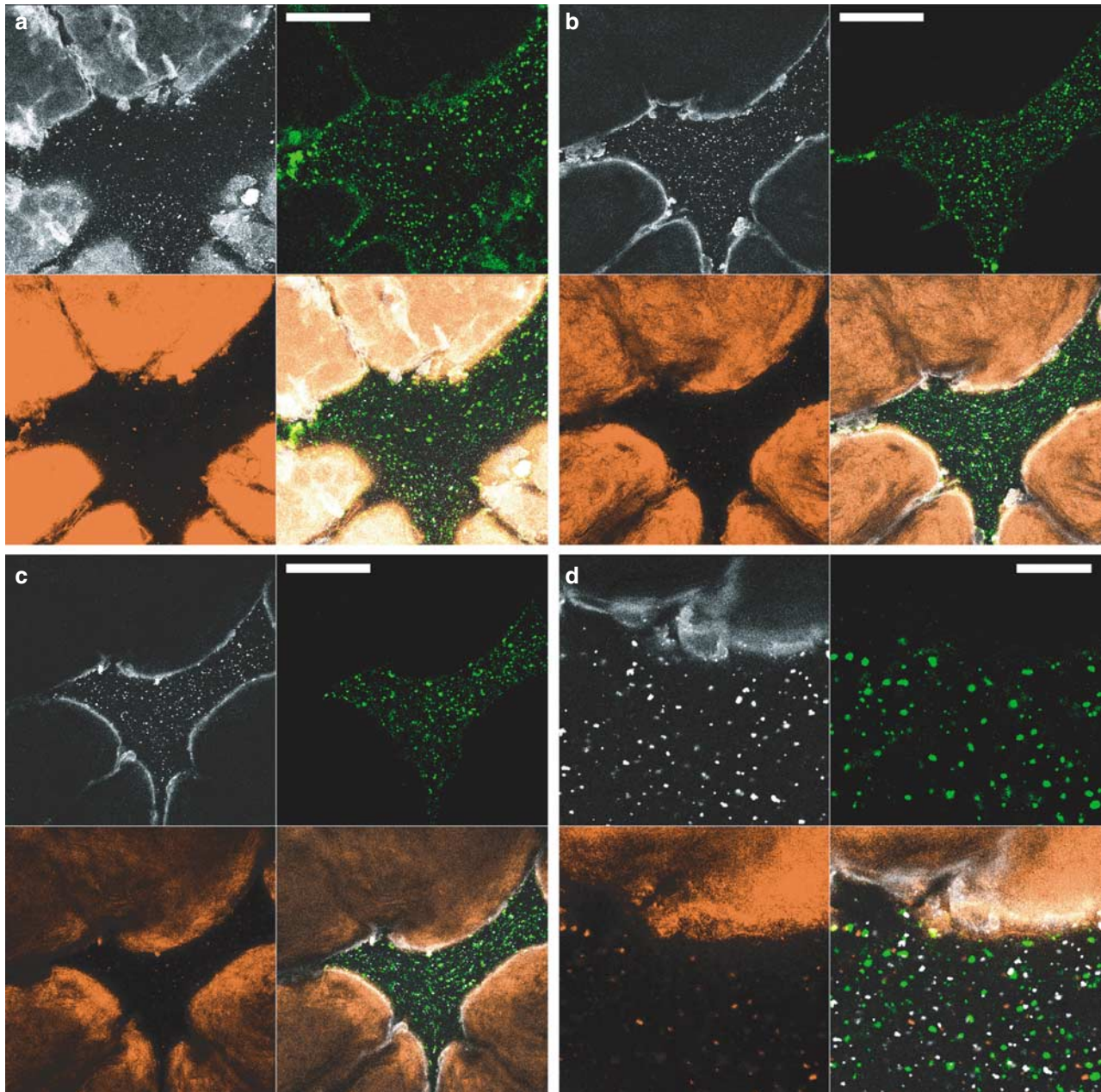


Figure 7. Multitracking experiments. (a–c) $325 \times 325 \mu\text{m}^2$ combined optical sections in -4 , -20 , and $-32 \mu\text{m}$ depth (Bar = $100 \mu\text{m}$). (d) A detailed image of particles and skin surface (Bar = $25 \mu\text{m}$). Each panel consists of a multiphoton excited image (predominantly keratin autofluorescence and fluorescein, gray scale, top left image), a 488 nm excited image (fluorescein, green scale, top right image) and a 543 nm excited image (Texas Red, orange scale, bottom left image), as well as an overlay of which (bottom right image). The excitation powers for the optical sections in the multitracking study were $P_{\text{EX}}(800 \text{ nm}) = 10 \text{ mW}$, $P_{\text{EX}}(488 \text{ nm}) = 50 \mu\text{W}$, and $P_{\text{EX}}(543 \text{ nm}) = 36 \mu\text{W}$, and the pixel acquisition time was always $t_{\text{px}} = 3.2 \mu\text{s}$.

photon excited image and the 543 nm excited image (Figure 7). The keratin autofluorescence seems to be located not at the surface of the Texas Red stained dermatoglyph, but some microns inside the skin. This is a consequence of the vertical mismatch between the near infrared and visible focus. Nevertheless, detailed distribution analysis for each isolated dye can be performed as well as a rough colocalization study, as fluorescein and keratin are not excited by the 543 nm laser line and Texas Red is virtually exclusively excited by this excitation source (Figure 4).

The 488 nm excited image (green) proves that FA is strictly bound to the particles and not released during the time of observation. Previous experiments showed that released fluorescein is rapidly bound to the keratinous layer of the stratum corneum. In the present study, no such accumulation was found. The fluorescence spots of the particles are mostly broadened owing to saturation. In the 543 nm excited images (orange), the distribution of Texas Red is visible. The predominant fraction of the dye is to be found within the skin, but the particles are also slightly observable. Obviously,

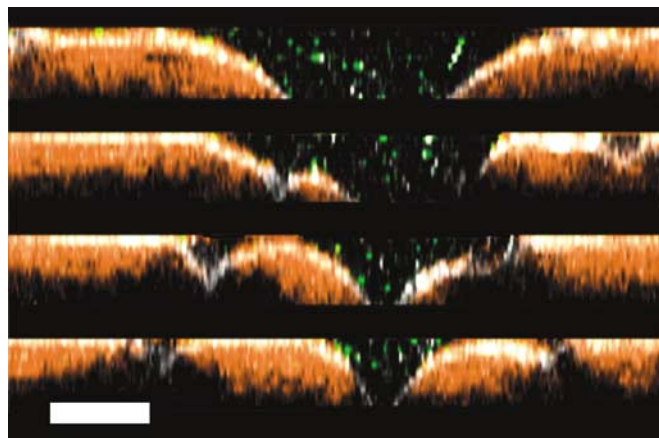


Figure 8. *xz*-Multitracking sections composed from a stack of *xy*-optical sections with 3 μm distance in between each. This representation nicely reveals the penetration profiles of Texas Red into the skin and the correlation of the penetration behavior with skin morphology. The color coding is in accordance with Figure 7 (Bar = 50 μm \times 10 μm).

there is still a certain amount of the dye stored in the nanoparticles, although the release process has proceeded far. The released Texas Red penetrated the skin and accumulated in the stratum corneum down to approximately 20 μm (Figure 7b). In Figure 7c, recorded at a depth of 32 μm , the penetration into deeper skin compartments can be recognized, as the walls of the dermatoglyph are steep enough to reveal the diffusion from the superficial layers inwards. The distribution of Texas Red in the skin is not uniform, but structured. It is conspicuous that the superficial accumulation is strongest, where the skin adjoins to large gel-filled spaces. Beneath the superficial layer, the distribution of the drug model is more uniform, which indicates faster diffusion of the compound in these skin compartments. The fundamental discrepancy between the visible excited images and the two-photon image proves that the visible skin structures from the two-photon image are predominantly due to keratin autofluorescence and not due to the superficial accumulation of Texas Red. *xz*-Sections can be extracted from the multitracking *z*-stacks, which nicely exhibit the concentration profile in normal direction (Figure 8). The highest concentrations of Texas Red in the deeper layers are found under superficial areas with pronounced keratin autofluorescence. This supports the hypothesis of a fast resorption of Texas Red from the hydrogel to the keratinous compartments and a slower diffusion from there to the skin tissue underneath. A vertical mismatch of several microns between the 543 nm excited Texas Red fluorescence and the multiphoton excited endogenous keratin fluorescence due to the chromatic aberration of the optics is apparent in all *xz*-sections.

DISCUSSION

A major challenge in the design of nanoscale drug delivery entities is the development of mechanisms that trigger the release of the drug when the nanoparticle attains its therapeutic site. For dermal applications, such mechanisms

may consist of an intrinsic recognition element for specific sites or compounds of the skin and thereby a controlled release step. Another approach to this end is to modify the particle surface in a way that they accumulate at the therapeutic site and to start the drug release by external stimuli like light illumination or the delayed application of a kick-off agent. A pure diffusive release of a drug from suspended particles starts at the moment of suspension, and after a certain storage time the drug is predominantly dissolved in the suspension matrix. Hence, this way of formulation compromises all advantages of nanoparticulate drug delivery. As so far no such intelligent trigger techniques are established for topical application of nanoscale drug carriers, the simple diffusive release mechanism is observed in the present work to demonstrate the capabilities of laser scanning microscopy in this field. As a consequence, it was found that the major fraction of Texas Red was already released to the gel matrix at the moment of the first measurement. This observation demonstrates that diffusive release of drugs from the particle cannot be employed for the practical use of nanoscale drug carriers and, in general, stresses the need for the design of intelligent nanocarriers with controllable release behavior. The three-dimensional microscopic and spectral resolution of the utilized techniques showed up to have a more versatile potential for the evaluation of such smart nanoparticle formulations than conventional penetration study methods.

In general, multiphoton and confocal microscopy of dually labeled nanoparticles in human skin biopsies have been demonstrated to be very suitable techniques to investigate the migration, accumulation, release, and penetration of nanoparticle-borne drugs in dermal application. By different fluorescence spectra of the covalently fixed and the physically dissolved dye, discrimination between particle-bound and released compounds is possible. By performing spectral imaging, the quantitative analysis of the release process is much less interfered by background emissions and crosstalk errors than in a conventional two detector channel study with a dichroic beamsplitter. Furthermore, an emission can be attributed to a certain compound with a high degree of accuracy by resolving the fluorescence spectrum.

It was shown that tracing of even single particles of about 300 nm diameter in the gel matrix inside the dermatoglyphs is not a difficult task. The observation depth of MPM even in turbid media is on the order of several hundred microns (Centonze and White, 1998) and is mostly limited by the working distance of the applied high numerical aperture objectives. Hence, single fluorescent nanoparticles should be observable within the skin down to the dermis. This is of particular importance if particles are investigated, which are able to penetrate the epidermal layers. No penetration of particles into the skin was found in the present study. Owing to the three-dimensional subcellular resolution and the possibility of repeated noninvasive investigations of the same skin area, detailed information on the penetration pathways of particle-bound and free drug models are accessible.

As confocal microscopy with visible excitation does not provide such enhanced observation depths, the multitracking

technique is primarily adequate for investigations on the upper skin layers. Problems may arise from possible lateral mismatches, the chromatic shift of the focal planes in case of strongly differing excitation wavelengths, and the time lag between the single scans. The influences of these interferences have to be carefully regarded in the interpretations of multitracking studies. Nevertheless, it can be a powerful tool if the applied fluorophores are basically excited exclusively by the chosen laser lines, as demonstrated in the present study.

The specimen mounting fulfilled the objectives of keeping the skin sample in place with an accuracy of few microns in three dimensions, to avoid desiccation and to minimize swelling and shrinking effects. In the present study, excised, frozen, and thawed human skin was used. The properties of a skin specimen treated accordingly will certainly differ from skin *in vivo* and freshly excised biopsies, as for example, the pH depth profile changes rapidly after excision (Wagner *et al.*, 2003) and the endogenous NADH fluorescence of the vital epidermal layers is virtually vanished after frozen storage. In spite of these physiological changes, permeation measurements did not exhibit a changed passage behavior for the investigated compounds after frozen storage of human skin, indicating that the nonvital superficial layer of the stratum corneum was the main penetration barrier (Wagner *et al.*, 2004). An MPM experiment on freshly excised human skin or *in vivo* could reveal even more detailed information on the drug penetration into the vital skin layers, as the cellular autofluorescence would allow the allocation of the drug pathways on single cell level.

By deliberate variation of the fluorescent drug-model, correlations of the microscopic penetration behavior with various physicochemical properties of the drug models could be investigated. An intelligent release mechanism providing for a defined initial time of release from the nanoscale drug carrier would allow to study the accurate evolution of drug concentrations in the diverse skin compartments and to derive a pharmacokinetic model of the drug uptake from nanoparticulate formulations.

Concluding, we demonstrated the benefits of multicolor labeling of biodegradable nanoparticles and the intriguing insights into the penetration behavior of particle-borne drugs due to the combination with MPM and confocal laser scanning microscopy. The usage of two fluorescent dyes of well-separated absorption and emission spectra enabled the investigation of the transport of a fluorescent drug model *in situ*. This might be extended to multiple loading of nanoparticles with two or more drug-models that differ in spectral and physicochemical properties for direct comparison. Furthermore, relevant pharmaceutical compounds with native fluorescence may be investigated as well as intelligent release mechanisms. The kinetics of the drug transport from the initial formulation to the subcutaneous compartments can be studied in elementary steps, as the enrichment of particles in certain dermal sites (Toll *et al.*, 2004), the release of the drug from the particles, its uptake into the stratum corneum, the diffusion into the deeper skin layers, etc. The determination of the enrichment in dependence of time as well as the

visualization of the 'structured' diffusion process into the skin envisages the potential of this approach. In addition, the covalent label to the nanoparticle itself enables the investigator to follow the fate of the nano-carrier, its uptake, accumulation, or decomposition. This might be very meaningful in particular for the exploration of the penetration function of hair shafts. First evidence was observed that these follicles might play an important role (Van Kuijk-Meuwissen *et al.*, 1998b; Toll *et al.*, 2004; Alvarez-Roman *et al.*, 2004b).

MATERIALS AND METHODS

Materials

Poly(L-lactide-co-glycolide) (Resomer RG 50:50 H) was kindly provided by Boehringer Ingelheim (Boehringer Ingelheim GmbH & Co. KG, Ingelheim, Germany). 5-Fluoresceinamine and 1-ethyl-3-(3-Dimethylaminopropyl)-carbodiimide hydrochloride were obtained from Sigma (Sigma Chemical Co., St Louis, MO, USA). Polyvinylalcohol (Mowiol 4-88) was purchased from Kuraray (Kuraray Specialities GmbH, Frankfurt am Main, Germany). Texas Red[®] was provided by Atto-Tec (Atto-Tec GmbH, Siegen, Germany). We gratefully acknowledge the kind provision of Natrosol[®] 250 M hydrogel (Aqualon, Hercules Inc., DE, USA) by J. Luengo. All other chemicals are of analytical grade.

Polymer labeling and preparation of dual color nanoparticles

FA-bound PLGA (FA-PLGA) was prepared based upon the method described by Horisawa *et al.* (Horisawa *et al.*, 2002). Briefly, PLGA (3.07 g) and FA (0.0583 g) were dissolved entirely in 30 ml of acetonitrile with 0.0408 g of 1-Ethyl-3-(3-dimethylaminopropyl)-carbodiimide hydrochloride and incubated at room temperature for 24 h under light protection and gentle stirring. The resultant FA-PLGA was precipitated by the addition of purified water and separated by centrifugation. The polymer was rinsed from excessive reagents (dissolution in acetone and precipitation with ethanol in terms) and then lyophilized (Alpha 2-4 LSC, Martin Christ Gefriertrocknungsanlagen GmbH, Osterode, Germany).

Texas Red nanoparticles were prepared from FA-PLGA, employing a single emulsion method (oil in water). The emulsion was formed between an organic FA-PLGA solution (2% (w/v) in ethyl acetate), which additionally contained 30 μ l of a saturated Texas Red solution and 5 ml of a polyvinylalcohol solution (1% in demineralized water) under stirring on a magnetic stirrer for 2 hours. Then the emulsion was homogenized using an Ultra-Turrax[®] T 25 Mixer (Janke und Kunkel GmbH & Co., Staufen, Germany) at 13,500 r.p.m. and the organic solvent was removed by a rotary evaporator. The mean particle size was determined to $d = 290 \pm 5$ nm using photo-correlation spectroscopy (Zetasizer[®] 3000HSA, Malvern Instruments GmbH, Herrenberg, Germany), and the homogeneity of the particles was verified using scanning probe microscopy (BioScope, Veeco, Santa Barbara, USA) (Figure 9). To prepare the gelly nanoparticle suspension, a Natrosol[®] gel (3% w/w) was mixed with an aqueous suspension of the nanoparticles in a 1:1 ratio.

Skin preparation

Excised human skin from Caucasian female patients who had undergone abdominal plastic surgery was used. The procedure was approved by the Ethical Committee of the Caritas-Traegergesellschaft, Trier, Germany (6 July 1998) and conducted according

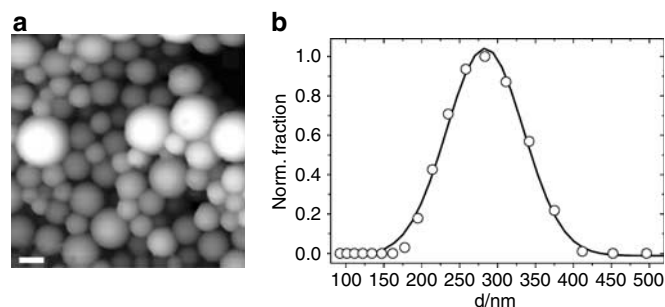


Figure 9. (a) $2 \times 2 \mu\text{m}^2$ scanning force microscopy image of an air-dried aqueous suspension of the PLGA nanoparticles on a glass substrate. The image was acquired in the tapping mode, 0.2 Hz scan speed. The topography from 180 nm to 550 nm altitude is encoded in the gray scale (Bar = 200 nm). (b) Histogram of the particle diameter d obtained by photocorrelation spectroscopy. The line is a Gaussian fit to the data.

to the Declaration of Helsinki Principles. Adequate health and no medical history of dermatological disease were required. After excision the skin was cut into $10 \times 10 \text{ cm}^2$ pieces, and the subcutaneous fatty tissue was removed from the skin specimen by using a scalpel. Afterwards the surface of each specimen was cleaned with water, wrapped in aluminum foil, and stored in polyethylene bags at -26°C until use. Previous investigations have shown that no change in the penetration characteristics occurs during the storage time of 6 months (Bronaugh *et al.*, 1986; Wagner *et al.*, 2004).

Laser scanning microscopy

The microscopy studies were performed on a versatile laser scanning microscope (LSM 510 NLO META, Carl Zeiss Jena GmbH, Germany) for conventional confocal microscopy with multiple excitation laser lines and multiphoton excitation microscopy. Herein, the 488 nm laser line of the internal argon ion laser and the 543 nm line of the internal helium neon laser were applied for confocal imaging. For MPM, a femtosecond pulsed titan:sapphire laser at $\lambda = 800 \text{ nm}$ with 90 fs pulse width and 80 MHz repetition rate (Vitesse, Coherent Inc., Santa Clara, USA) was coupled into the microscope.

The META scanning and detection module offers different ways to detect the fluorescence light. First, the complete emission is distributed between two sensitive photomultiplier tubes by means of neutral and dichroic mirrors. Second, the emission signal is spectrally dispersed by a diffraction grating and guided on a 32 channel photomultiplier array for spectral analysis. Each channel detects a spectral range of about 10 nm in this arrangement. Three different imaging modes were applied in the present study: (a) the multiphoton fluorescence mode for the cumulative detection of the emitted fluorescence. Here, the fluorescence intensity is recorded by one photomultiplier tube. The laser line is blocked by a 650 nm shortpass beamsplitter and a 685 nm shortpass filter. This detection mode is the most sensitive one, but any spectral information will be lost. (b) In the multiphoton spectral imaging mode, the emitted light is separated from the laser line by the 650 nm shortpass beamsplitter and recorded spectrally resolved by means of the grating and the detector array. Each pixel of a spectral image contains the data of the 32 detector channels, so that emission spectra for each pixel or for defined areas of the image are accessible. The displayed images are

true color coded. The spectral data are converted into appropriate RGB values. (c) The multitracking mode is actually an overlay of three fluorescence intensity images, subsequently acquired at different excitation wavelengths. An overlay procedure with two visible excitation laser lines was utilized on similar specimens by Alvarez-Roman *et al.* (2004a). The excitation wavelengths are chosen to be preferably absorbed by exclusively one fluorophore (Figure 4). The 488 nm argon ion laser line is predominantly absorbed by fluorescein, the 543 nm helium neon laser line by Texas Red exclusively. Two-photon excitation at 800 nm is strong for fluorescein and the endogenous fluorophore keratin, but poor for Texas Red.

Two-photon excitation spectra (Figure 4) were acquired according to a modified "excitation fingerprinting" procedure introduced by Dickinson *et al.* (2003). In contrast to the excitation fingerprinting technique, where the excitation power is kept constant for different wavelengths, herein the laser power calibration is adjusted for constant photon flux at different wavelengths to yield correct two-photon excitation spectra (Schneider *et al.*, 2005). One-photon excitation and fluorescence spectra were acquired with a Hitachi FL 4500 fluorometer using 50 μM aqueous solutions of FITC dextran and Texas Red. FITC dextran was used in order to investigate a compound preferably akin to FA-PLGA while showing good water solubility. The spectral properties of the fluorescein derivatives are almost unaffected by different substituents in the 5-position.

Sample preparation

For microscopy, discs of 0.8 cm diameter were punched out of frozen skin and placed surface-up on a microscopy slide inside a circular vertical spacer. After application of the gelly suspension to the skin surface, a cover slide was fixed onto the spacer by double-faced adhesive tape in a way that the skin surface was gently pressed against the cover slide. This setup provides constant specimen thickness and prevents desiccation of the skin sample. The observation was performed through the cover slide by means of a $40 \times / 1.3$ numerical aperture Oil Objective (Plan Neofluar, Carl Zeiss Jena GmbH, Germany).

CONFLICT OF INTEREST

The authors state no conflict of interest.

ACKNOWLEDGMENTS

This work is part of the PhD thesis of Ms. Barbara Weiss. We gratefully acknowledge the kind provision of Natrosol[®] hydrogel by J. Luengo and the supply of excised human skin samples by K.-H. Kostka (Department of Plastic and Hand Surgery, Caritaskrankenhaus, Lebach, Germany).

REFERENCES

- Alvarez-Roman R, Naik A, Kalia Y, Guy RH, Fessi H (2004a) Skin penetration and distribution of polymeric nanoparticles. *J Controlled Release* 99: 53–62
- Alvarez-Roman R, Naik A, Kalia YN, Fessi H, Guy RH (2004b) Visualization of skin penetration using confocal laser scanning microscopy. *Eur J Pharmaceut Biopharmaceut* 58:301–16
- Alvarez-Roman R, Naik A, Kalia YN, Guy RH, Fessi H (2004c) Enhancement of topical delivery from biodegradable nanoparticles. *Pharmaceut Res* 21:1818–25
- Brain KR, Walters KA, Watkinson AC (2002) Methods for studying percutaneous absorption. In: *Dermatol Transdermal Formulations* (Walters KA, ed), 1st ed. New York: Marcel Dekker Inc., 197

- Brannon-Peppas L (1995) Recent advances on the use of biodegradable microparticles and nanoparticles in controlled drug delivery. *Int J Pharmaceut* 116:1-9
- Bronaugh RL, Stewart RF, Simon M (1986) Methods for *in vitro* percutaneous-absorption studies. VII. Use of excised human-skin. *J Pharmaceut Sci* 75: 1094-7
- Centonze VE, White JG (1998) Multiphoton excitation provides optical sections from deeper within scattering specimens than confocal imaging. *Biophys J* 75:2015-24
- Daniels J (2006) How polymeric microspheres deliver the goods. *Pharmaceut Technol Europe* 18:30-2
- Dickinson ME, Waters CW, Fraser SE, Simbuerger E, Zimmermann B (2003) Multiphoton excitation spectra in biological samples. *J Biomed Opt* 8: 329-38
- Dinauer N, Von Briesen H, Balthasar S, Weber C, Kreuter J, Langer K (2005) Selective targeting of antibody-conjugated nanoparticles to leukemic cells and primary T-lymphocytes. *Biomaterials* 26:5898-906
- El-Samaligy MS, Rohdewald P, Mahmoud HA (1986) Polyalkyl cyanoacrylate nanocapsules. *J Pharmacy Pharmacol* 38:216-8
- Hans ML, Lowman AM (2002) Biodegradable nanoparticles for drug delivery and targeting. *Curr Opin Solid State Mater Sci* 6:319-27
- Horisawa E, Kubota K, Tuboi I, Sato K, Yamamoto H, Takeuchi H *et al.* (2002) Size-dependency of DL-lactide/glycolide copolymer particulates for intra-articular delivery system on phagocytosis in rat synovium. *Pharmaceut Res* 19:132-9
- Huang SH, Heikal AA, Webb WW (2002) Two-photon fluorescence spectroscopy and microscopy of NAD(P)H and flavoprotein. *Biophys J* 82:2811-25
- Kohli AK, Alpar HO (2004) Potential use of nanoparticles for transcutaneous vaccine delivery: effect of particle size and charge. *Int J Pharmaceut* 275: 13-7
- König K (2000) Multiphoton microscopy in life sciences. *J Microsc* 200:83-104
- König K, Riemann I (2003) High-resolution multiphoton tomography of human skin with subcellular spatial resolution and picosecond time resolution. *J Biomed Opt* 8:432-9
- Kotrotsiou O, Kotti K, Dini E, Kammona O, Kiparissides C (2005) Nanostructured materials for selective recognition and targeted drug delivery. *J Phys Conf Ser* 10:281-4
- Lamprecht A, Ubrich N, Yamamoto H, Schaefer UF, Takeuchi H, Maincent P *et al.* (2001) Biodegradable nanoparticles for targeted drug delivery in treatment of inflammatory bowel disease. *J Pharmacol Exp Therap* 299: 775-81
- Lombardi Borgia S, Regehly M, Sivaramakrishnan R, Mehnert W, Korting HC, Danker K *et al.* (2005) Lipid nanoparticles for skin penetration enhancement – correlation to drug localization within the particle matrix as determined by fluorescence and piezoelectric spectroscopy. *J Controlled Release* 110:151-63
- Luengo J, Weiss B, Schneider M, Ehlers A, Stracke F, König K *et al.* (2006) Influence of nanoencapsulation on human skin transport of flufenamic acid. *Skin Pharma Physiol* 19:191-8
- Meuwissen MEMJ, Junginger HE, Bouwstra JA, Janssen J, Cullander C (1998) A cross-section device to improve visualization of fluorescent probe penetration into the skin by confocal laser scanning microscopy. *Pharmaceut Res* 15:352-6
- Pena AM, Strupler M, Boulesteix T, Godeau G, Schanne-Klein MC (2005) Spectroscopic analysis of keratin endogenous signal for skin multiphoton microscopy. *Opt Express* 13:6667
- Ravi Kumar MNV, Sameti M, Kneuer C, Lamprecht A, Lehr C-M (2003) Polymeric nanoparticles for drug and gene delivery. In: *Encyclopedia of nanoscience and nanotechnology* (Nalwa HS, ed). American Scientific Publishers: Stevenson Ranch, CA, 1-19
- Schneider M, Barozzi S, Testa I, Faretta M, Diaspro A (2005) Two-photon activation and excitation properties of PA-GFP in the 720-920 nm region. *Biophys J* 89:1346-52
- Soppimath KS, Aminabhavi TM, Kulkarni AR, Rudzinski WE (2001) Biodegradable polymeric nanoparticles as drug delivery devices. *J Controlled Release* 70:1-20
- Toll R, Jacobi U, Richter H, Lademann J, Schaefer H, Blume-Peytavi U (2004) Penetration profile of microspheres in follicular targeting of terminal hair follicles. *J Invest Dermatol* 123:168-76
- Van Kuijk-Meuwissen MEMJ, Junginger HE, Bouwstra JA (1998a) Interactions between liposomes and human skin *in vitro*, a confocal laser scanning microscopy study. *Biochim Biophys Acta Biomembranes* 1371:31-9
- Van Kuijk-Meuwissen MEMJ, Mouglin L, Junginger HE, Bouwstra JA (1998b) Application of vesicles to rat skin *in vivo*: a confocal laser scanning microscopy study. *J Controlled Release* 56:189-96
- Volodkin DV, Sukhorukov GB, Larionova NI (2004) Protein encapsulation via porous CaCO₃ microparticles templating. *Biomacromolecules* 5: 1962-72
- Wagner H, Kostka K-H, Lehr C-M, Schaefer UF (2001) Interrelation of permeation and penetration parameters obtained from *in vitro* experiments with human skin and skin equivalents. *J Controlled Release* 75: 283-95
- Wagner H, Lehr C-M, Schaefer UF, Kostka K-H (2003) pH profiles in human skin: influence of two *in vitro* test systems for drug delivery testing. *Eur J Pharmaceut Biopharmaceut* 55:57-65
- Wagner H, Schaefer UF, Kostka K-H, Adelhardt W (2004) Effects of various vehicles on the penetration of flufenamic acid into human skin. *Eur J Pharmaceut Biopharmaceut* 58:121-9
- Wartlick H, Michaelis K, Balthasar S, Kreuter J, Langer K, Strebhardt K (2004) Highly specific HER2-mediated cellular uptake of antibody-modified nanoparticles in tumour cells. *J Drug Targeting* 12:461-71
- Xu C, Zipfel W, Shear JB, Williams RM, Webb WW (1996) Multiphoton fluorescence excitation: new spectral windows for biological nonlinear microscopy. *Proc Natl Acad Sci USA* 93:10763-8
- Yu B, Blankschtein D, Langer R, Kim KH, So PTC (2003) Visualization of oleic acid-induced transdermal diffusion pathways using two-photon fluorescence microscopy. *J Invest Dermatol* 120:448-55
- Yu B, Kim KH, So PTC, Blankschtein D, Langer R (2002) Topographic heterogeneity in transdermal transport revealed by high-speed two-photon microscopy: determination of representative skin sample sizes. *J Invest Dermatol* 118:1085-8
- Zipfel WR, Williams RM, Webb WW (2003) Nonlinear magic: multiphoton microscopy in the biosciences. *Nat Biotechnol* 21:1369-77

Influence of Nanoencapsulation on Human Skin Transport of Flufenamic Acid

J. Luengo^{a, b} B. Weiss^b M. Schneider^b A. Ehlers^c F. Stracke^c K. König^c
K.-H. Kostka^d C.-M. Lehr^b U.F. Schaefer^b

^aDepartamento de Farmacia, Universidad de Concepción, Concepción, Chile; ^bDepartment of Biopharmaceutics and Pharmaceutical Technology, Saarland University, Saarbrücken, ^cFraunhofer Institute for Biomedical Technology (IBMT), St. Ingbert and ^dDepartment of Plastic and Hand Surgery, Caritaskrankenhaus, Lebach, Germany

Key Words

Poly(lactide-co-glycolide) nanoparticles · Drug permeation · Drug penetration · Drug delivery system · Multiphoton fluorescence microscopy

Abstract

The effect of the inclusion of flufenamic acid in poly(lactide-co-glycolide) nanoparticles on the transport of flufenamic acid into excised human skin was investigated. Penetration and permeation data were acquired using two different *in vitro* test systems: the Saarbrücken penetration model, where the skin acts as its own receptor medium, and the Franz diffusion cell, where the receptor medium is a buffer solution. For the stratum corneum, no differences were found between nanoencapsulated and free drug. Drug accumulation in the deeper skin layers and drug transport across human epidermis were slightly delayed for the nanoencapsulated drug compared to the free drug after shorter incubation times (<12 h). In contrast, after longer incubation times (>12 h), the nanoencapsulated drug showed a statisti-

cally significantly enhanced transport and accumulation ($p < 0.05$). Additionally, nanoencapsulated flufenamic acid was visualized by multiphoton fluorescence microscopy. Particles were found homogeneously distributed on the skin surface and within the dermatoglyphs, but no nanoparticles were detected within or between the corneocytes.

Copyright © 2006 S. Karger AG, Basel

Introduction

Due to its special structure, the skin provides the main barrier between the body and the environment, at the same time limiting the drug delivery along this route [1–5]. Many strategies have been employed to improve the dermal and transdermal delivery of drugs, e.g. increasing the effective concentration of the drug in the vehicle, improving the partitioning between the formulation and the skin, the use of chemical penetration enhancers and different physical enhancement methods like iontophoresis, electroporation and microneedles [5, 6]. Furthermore, carrier systems like liposomes, microparticles or nanoparticles (NP) [7–9] have been explored. For microparticles, some targeting to the hair follicles has been shown by Toll

The PhD theses of Ms. Luengo and Ms. Weiss have equally contributed to the present work.

KARGER

Fax +41 61 306 12 34
E-Mail karger@karger.ch
www.karger.com

© 2006 S. Karger AG, Basel
1660–5527/06/0194–0190\$23.50/0

Accessible online at:
www.karger.com/spp

Ulrich F. Schaefer
Im Stadtwald
Geb. 8.1, PO Box 151150
DE-66041 Saarbrücken (Germany)
Tel. +49 681 302 2019, Fax +49 681 302 4677, E-Mail ufs@mx.uni-saarland.de

et al. [10], using polystyrene microspheres in a range of 0.75–6 μm , and Lademann et al. [11], using titanium dioxide particles in a range of 0.1–0.3 μm also resulting in an enhanced delivery to the deeper skin layers. Studies on solid lipid NP [12–14] also showed increased transdermal drug delivery induced by their occlusive effects. Alvarez-Román et al. [15] reported preferential accumulation of non-biodegradable drug-free polymeric NP in the hair follicle opening of pig skin. In addition, the same authors reported an increased level within the stratum corneum of the pig ear of the highly lipophilic sun-protecting agent, octyl methoxycinnamate, when nanoencapsulated in the biodegradable polymer poly(ϵ -caprolactone) [16].

Some of the most widely used polymers in the NP formulation are poly(lactic acid), poly(glycolic acid), and their co-polymer, poly(lactide-*co*-glycolide) (PLGA), which are known for their good biocompatibility and resorbability through natural pathways [17]. In oral and parenteral applications, solid biodegradable polymeric NP based on PLGA have shown their advantage over liposomes by their increased stability [18–20], but in the field of dermal delivery their potential appears to be rather unexplored.

The objective of this study was to investigate the influence of nanoencapsulation on the permeation and penetration of the lipophilic model drug flufenamic acid (FFA) into skin using PLGA as carrier polymer. In order to monitor drug penetration, the Saarbrücken model [21] (SB-M) was used in which the skin itself acts as a receptor compartment. A tape stripping technique followed by cryosectioning of the deeper skin layers allows to quantify the penetrated drug amount. Drug release from the formulation and drug permeation through the epidermis were studied using the static Franz diffusion cell (FD-C) technique. Due to the size differences between the hair follicles of pig skin and of human skin [22], which may play an important role in the results, we decided to use excised human skin from abdominal plastic surgery instead of pig skin. As polymer PLGA was chosen in view of its excellent biocompatibility and the availability of various methods to prepare drug-loaded NP from this polymer. To verify the presence and to visualize the distribution of the applied NP on the skin, multiphoton fluorescence imaging was used. This technique allows to excite the natural fluorescence of the FFA in non-polar surroundings ($\lambda_{\text{max}} = 420 \text{ nm}$) by a two-photon absorption process. Two-photon excitation induced with femtosecond near-infrared laser pulses offers the possibility of high-resolution 3-dimensional imaging of the skin [23].

Materials and Methods

Materials

Natrosol[®] 250 M (Aqualon, Hercules Inc., Del., USA), FFA, modification II (Kali-Chemie Pharma, Hannover, Germany), poly(*D,L*-lactide-*co*-glycolide) (50:50) with a molecular weight of 40,000–75,000 Da (Sigma Chemical Co., St. Louis, Mo., USA), polyvinyl alcohol Mowiol[®] 4-88 (Kuraray Specialities Europe GmbH, Frankfurt, Germany), Ringer solution, McIlvaine citric acid-phosphate buffer (pH 2.2), sodium hydroxide solution (0.05 *M*) (all components from Merck, Darmstadt, Germany), Plastibase[®] (Heiden GmbH, München, Germany), methanol Chromasolv[®] (Sigma-Aldrich GmbH, Seelze, Germany), Tesa Film kristall-klar 19 mm (Tesa AG, Hamburg, Germany), ethyl acetate (Fluka Chemie GmbH, Buchs, Switzerland), and cellulose membrane MWCO 12,000–14,000 Da (Medicell International Ltd., London, UK) were used as obtained from the suppliers.

Equipment

High-performance liquid chromatography (HPLC) system was used: Chromeleon[™] version 6.5 SP2, build 968; P580 pump; ASI-100 automated sample injector; STH 585 column oven; UVD 170S detector (Dionex Softro GmbH, Germering, Germany); FD-C type 4G-01-00-15 (Perme Gear, Riegelsville, Pa., USA); cryomicrotome HR Mark II, model 1978 (Slee, Mainz, Germany); centrifuge Sigma 3E-1 (Sigma, Aichach, Germany); high-speed homogenizer Ultra-Turrax[®] T25 (Jahnke & Kunkel GmbH & Co. KG, Staufen, Germany); atomic force microscope nanoscope IV Bioscope[™] (Veeco Instruments, Santa Barbara, Calif., USA); freeze-drier Alpha 2-4 LSC (Christ, Osterode, Germany); Rotavapor[®] R-205 (Büchi, Flawil, Switzerland); Zetasizer[®] 3000 HS A (Malvern Instruments GmbH, Herrenberg, Germany); for multiphoton fluorescence imaging, the femtosecond laser imaging system DermalInspect[®] (JenLab GmbH, Jena, Germany), equipped with a Chameleon laser system (Coherent Inc., Santa Clara, Calif., USA) and a Hamamatsu PMT(H7732) detector (Hamamatsu Photonics Deutschland GmbH, Herrsching am Ammersee, Germany), was used.

Methods

NP Preparation and Characterization

PLGA NP loaded with FFA (FFA NP) were prepared using a solvent extraction method. Thirty milligrams of FFA were dissolved in a solution of 600 mg of PLGA in 20 ml of ethyl acetate. This organic phase was added dropwise into 20 ml of an aqueous phase, containing 1% of polyvinyl alcohol as a quasi-emulsifier, under stirring with a magnetic stirring bar. The resulting o/w emulsion was homogenized with a high-speed homogenizer at 13,500 rpm for 10 min. To complete the precipitation, water was added up to 200 ml under stirring with a magnetic bar. Organic solvent was then removed using a rotating evaporator. The resulting NP suspension was freeze-dried and stored until use.

For reference, standard drug-free NP were prepared in the same way.

Size and surface morphology of the FFA NP were determined using photon correlation spectroscopy and atomic force microscopy (AFM). For the AFM measurements, a drop of the NP suspension and hydrogel (HG), respectively, were air-dried on a silica wafer. Imaging was done using a silicon cantilever with a spring constant of approximately 40 N/m and a resonance frequency of about 170 kHz. The scan speed applied was 0.2 Hz. The resolution

was 512×512 pixels. In order to avoid generating sample artefacts, the tip loading force was minimized.

The content of FFA in the particles was determined using the following equation:

$$FFA_{NP} = FFA_{Total} - FFA_{Free}$$

Whereas FFA_{Free} was determined in the supernatant obtained from a centrifuged suspension (23,147 g), FFA_{Total} was obtained after a proper extraction of the NP suspension using 0.05 M sodium hydroxide solution. The obtained drug entrapment was 63.6% w/w.

Gel Preparation

FFA Natrosol HG was prepared with FFA dissolved in water under vigorous stirring. Afterwards, Natrosol was added in a proportion equivalent to 1.5% (w/w) and stirred overnight until the polymer was completely swollen. The absence of crystals was determined by microscopic inspection of the gels.

To prepare an FFA NP HG, a Natrosol gel (3% w/w) was mixed with an aqueous suspension of the NP in a 1:1 ratio to obtain the same concentration as in FFA HG. The presence and integrity of the particles in the gel were confirmed by AFM (fig. 1). In addition, the FFA concentration in each gel was verified by HPLC.

In the same way, an HG containing drug-free NP was prepared.

Penetration and permeation experiments were carried out using FFA HG and FFA NP HG, each with a drug concentration of 0.12 mg/g.

Skin Preparation

Excised human skin from Caucasian female patients, who had undergone abdominal plastic surgery, was used. The procedure was approved by the Ethics Committee of the Caritas Trägergesellschaft, Trier, Germany (July 6, 1998). Adequate health and no medical history of dermatological disease were required. After excision, the skin was cut into 10×10 cm² pieces and the subcutaneous fatty tissue was removed from the skin specimen using a scalpel. Afterwards the surface of each specimen was cleaned with water, wrapped in aluminium foil and stored in polyethylene bags at -26°C until use. Previous investigations have shown that no change in the penetration characteristics occurs during the storage time of 6 months [8, 24].

Disks of 25 mm in diameter were punched out from frozen skin, thawed, cleaned with Ringer solution, and either transferred directly into the SB-M or used to prepare heat-separated epidermis sheets for the FD-C experiment.

Heat-Separated Epidermis Preparation

The epidermis was separated placing the thawed and cleaned skin disc in water at 60°C for 90 s. After that, the skin was removed from the water and placed, dermal side down, on a filter paper. The epidermal layer was peeled off from the skin using forceps. Before use in the FD-C, the epidermal membrane was prehydrated for 1 h.

Permeation Experiments

Using an FD-C, experiments were carried out using heat-separated epidermis mounted on a cellulose membrane disc. The membrane was positioned between the donor and acceptor compartment. As donor 750 μl of preparation and as receptor 12.1 ml of Sørensen phosphate buffer (pH 7.4) were used. The donor compart-

ment was sealed with aluminium foil and the system was maintained at $32 \pm 1^\circ\text{C}$ in a water bath. The acceptor fluid was stirred using magnetic bars at 500 rpm. At predetermined time intervals, samples of 1.0 ml were collected from the acceptor medium and replaced immediately with fresh buffer solution. Samples were collected for 29 h and analysed by HPLC.

Release experiments were done in the same way but using a cellulose membrane to separate donor and receptor compartment.

Penetration Experiments

Using a SB-M apparatus, a full-thickness skin disc was transferred into the cavity of a Teflon block on filter paper soaked with Ringer solution to prevent any change in the hydration state of the skin. The cavity of the upper Teflon punch was filled with the drug preparation and fixed in position. The gap between the two Teflon parts was sealed with Plastibase to avoid water loss from the skin. The whole apparatus was transferred into an oven at $32 \pm 1^\circ\text{C}$ for a predetermined incubation time. For details, see Wagner et al. [21].

Skin Segmentation

After the incubation time, all the skin specimens investigated with SB-M were segmented using the tape stripping and cryosectioning methods. For detailed descriptions, the reader is referred to Wagner et al. [21].

Tape Stripping Method. The samples obtained were pooled according to the following scheme: No. 1 = 1 strip, No. 2 = 1 strip, No. 3 = 3 strips and No. 4–6 = 5 strips.

Cryosectioning. After tape stripping, the skin was rapidly frozen in a stream of expanding carbon dioxide. A specimen of 13 mm in diameter was punched out from the stripped area and transferred into a cryomicrotome. The sections were pooled using the following scheme: No. 1 = incomplete cuts, No. 2–5 = 2×25 μm , No. 6–10 = 4×25 μm , No. 11–15 = 6×25 μm , No. 16 = 8×25 μm , No. 17 = rest of skin.

Sample Extraction

The pooled samples were extracted with 0.05 M sodium hydroxide solution and shaken during 2 h at room temperature. After that, tape stripping samples were separated from the solid content and directly transferred to the HPLC system. The samples of cryosectioning were centrifuged at 456 g for 30 min; afterwards the supernatant was separated and transferred to the HPLC system.

HPLC Method

All the samples were analysed using the following HPLC conditions: column LiChrospher 100 RP-18, 5 μm , 125×4 mm (Merck); mobile phase: McIlvaine buffer pH 2.2, methanol (20:80); flow rate: 1.2 ml/min; wavelength: 284 nm; injection volume: 20 μl ; retention time: 3.5 ± 0.2 min. This method has been previously validated by Wagner et al. [21].

Area under the Penetration Curve

The area under the penetration curve (AUPC) was calculated from the curves of the penetrated amount per cubic centimetre of skin ($C = \mu\text{g}/\text{cm}^3$) versus depth ($d = \mu\text{m}$) obtained from the SB-M experiments, using the following equation:

$$AUPC(d_i) = \sum_{i=1}^n C_i (d_i - d_{i-1})$$

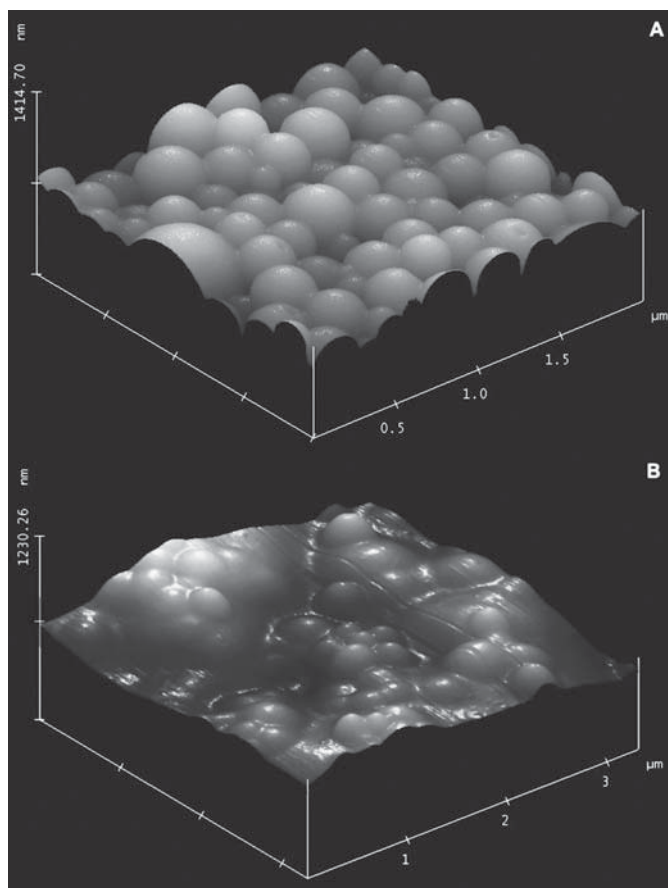


Fig. 1. AFM images of FFA containing NP. **A** Aqueous suspension. **B** Incorporated into Natrosol HG.

Statistical Evaluation

For statistical evaluation, SigmaStat 3.0.1 was used.

Multiphoton Fluorescence Imaging

Skin samples were punched out, thawed and cleaned before gel application and image acquisition. Plain Natrosol HG, HG containing non-loaded NP or containing FFA-loaded NP were applied to the skin and imaged using multiphoton fluorescence imaging with a $40\times/NA\ 1.3$ (oil) objective, at an excitation wavelength of $\lambda = 720\text{ nm}$ (pulse length 170 fs, repetition rate 90 MHz) and an average power of 13 mW. Images were acquired in less than 30 min after application of the gel onto the skin. Acquisition time was chosen to be 25 s for a 512×512 pixel image. Starting at the skin surface ($z = 0\ \mu\text{m}$) every $2.3\ \mu\text{m}$ an image was recorded to finally obtain a $200 \times 200 \times 46\ \mu\text{m}^3$ stack. The focal plane was varied by a piezo-driven objective, allowing to survey the entire epidermis down to the stratum basale.

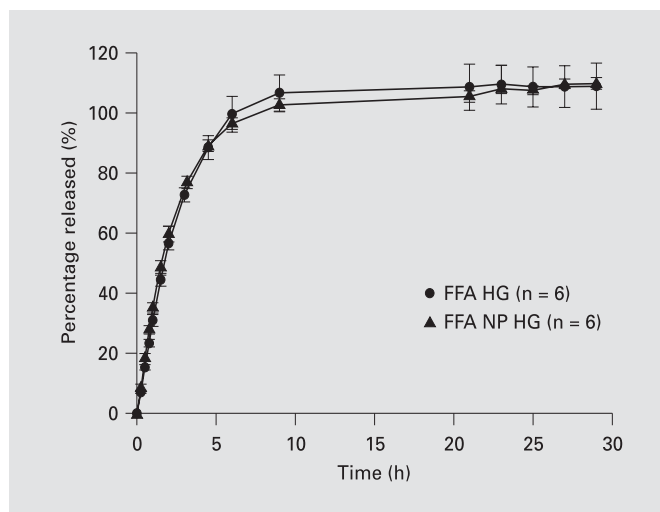


Fig. 2. Percentage of FFA released from FFA HG and FFA NP HG.

Results

To avoid any interindividual variability of human skin, all penetration and permeation experiments were carried out with skin from the same donor and repeated 6 times. Only for visualization studies was skin from a different donor used.

As shown by AFM in figure 1, the incorporation of NP (mean size 328.2 nm, PI 0.16) into a hydroxyethyl cellulose gel has no influence on shape and size distribution of the particles, confirming that the HG contained undamaged NP.

Release Experiments

Release experiments have shown very similar profiles for free and nanoencapsulated drug (fig. 2).

Penetration Experiments

Stratum corneum

Between the free and the nanoencapsulated drug, no statistically significant difference in the amount of FFA accumulated in the stratum corneum, expressed as AUPC, was detected at any incubation time. Furthermore, it is remarkable that there was a slight decrease of the AUPC for both formulations with increasing incubation time (fig. 3A).

Deeper Skin Layers (Viable Epidermis and Dermis)

For these layers, statistically significant differences in the FFA amounts between the 2 formulations (t test, $p <$

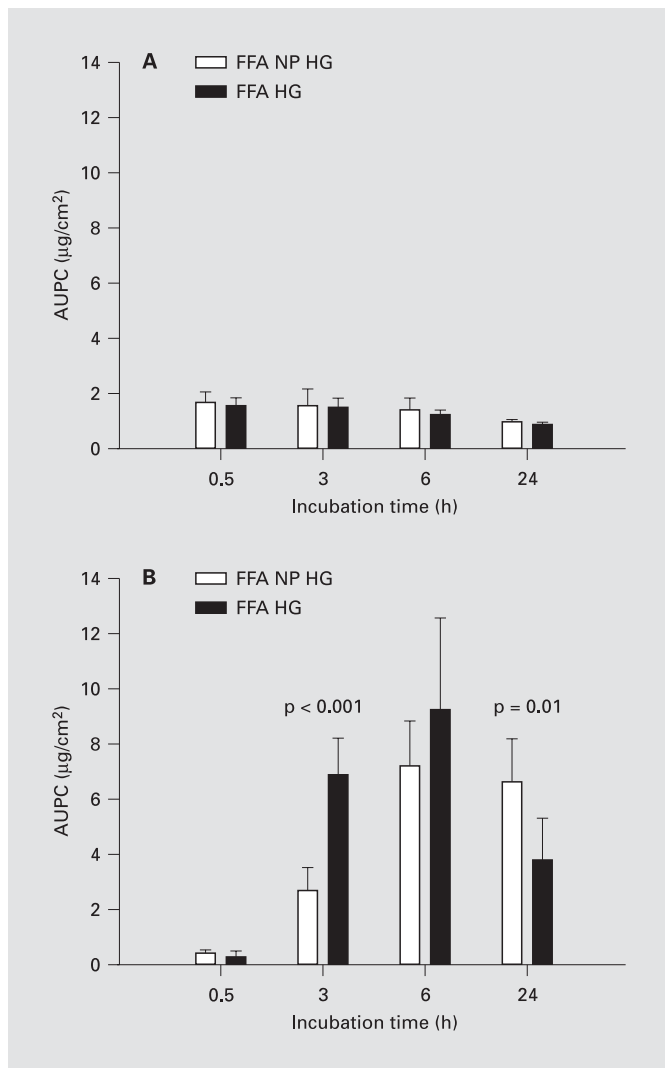


Fig. 3. AUPC of FFA penetrated into human skin using the SB-M at different incubation times (n = 6). **A** Stratum corneum. **B** Deep skin layers.

0.05) were observed at 3 and 24 h of incubation time, respectively. Interestingly, after 3 h, higher levels were found for the preparation containing the free drug than for the NP formulation. In contrast, after 24 h, this relation was inverted, i.e. a considerably higher amount of drug has penetrated from NP compared to the free drug (fig. 3B). In addition, a decrease compared with the 6-hour values was observed for both preparations, although the same preparations were used. This may be due to a radial diffusion in the SB-M. Considering that the drug was extracted only from samples obtained from a disc of 13 mm (in diameter) of the stripped area, not all the drug can be

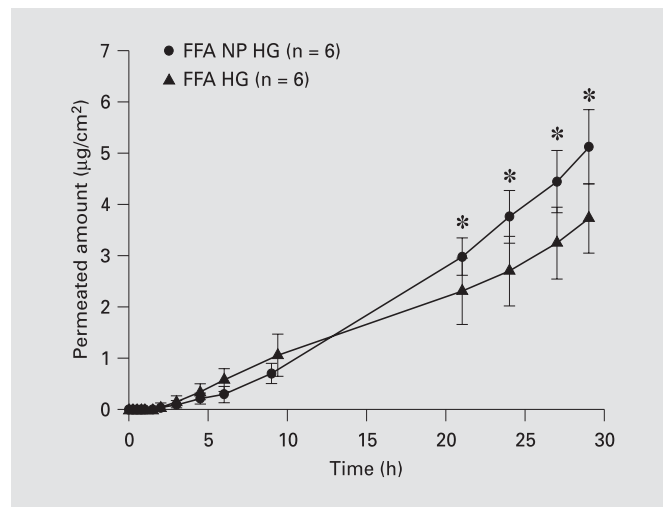


Fig. 4. Permeation of the FFA amount through heat-separated human epidermis using the FD-C system (asterisks indicate statistically significant differences).

detected. For both preparations, FFA was detected in the filter paper under the skin, indicating that the sink conditions, which favour the vertical diffusion of the drug, were not maintained completely and therefore could have influenced the obtained results. However, one can assume that for both experimental series the effect occurs in the same magnitude. Therefore, direct comparison of the nanoencapsulated drug preparation and the free drug preparation at this incubation time is still justified.

Permeation Experiments

For better comparison, the same time points as chosen in the penetration studies (SB-M) were used in the permeation experiments (FD-C). At shorter incubation times (<12 h), there were no significant differences in the permeated amount of the drug. The levels of the free drug formulation tended to be slightly increased, but the differences were not statistically significant (fig. 4). However, for longer incubation times (24 h and later), there was a statistically significant inversion of the drug amount permeated, i.e. more drug had permeated from the nanoencapsulated drug formulation compared to the free drug formulation.

Visualization Experiments

Multiphoton fluorescence imaging experiments were carried out using a particle-free HG, an HG containing drug-free NP and an HG with FFA NP. As expected, the skin shows an autofluorescence and structure correspond-

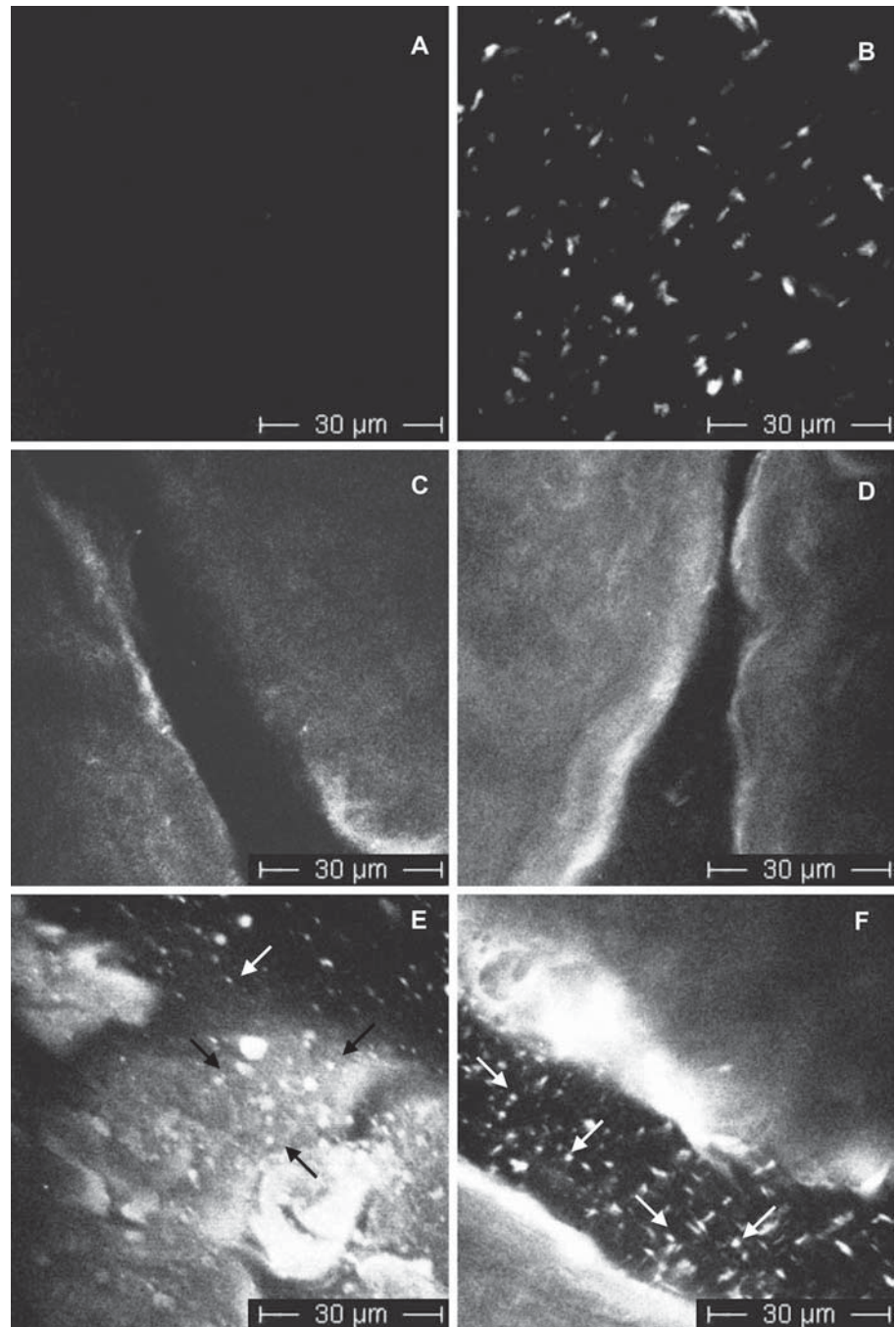


Fig. 5. Multiphoton fluorescence imaging of plain HG (**A**), FFA NP HG (**B**), skin with plain HG (**C**), skin with drug-free NP HG (**D**), skin with FFA NP HG distributed on the surface (**E**) and skin with FFA NP HG in the dermatoglyphs at a depth of 16 μm (**F**).

ing to published data [23]. In preliminary studies, it was found that neither FFA in solution nor FFA crystals could be visualized in the HG by this technique. However, nanoencapsulated FFA yielded a fluorescence signal probably due to the fact that the fluorescence of the drug is favoured by the non-polar and acidic environment of the polymer (fig. 5) [25]. The ostensive size of some of the

NP in the multiphoton images on the order of a few micrometres is due to (1) the system resolution ($dx = dy =$ approx. $0.4 \mu\text{m}$, $dz =$ approx. $1 \mu\text{m}$); (2) partial aggregation, and (3) the Brownian motion of the subdiffraction-limit-sized particles during image acquisition. Transversal drift of the particles led to stretched shapes of their fluorescence spots.

The multiphoton sections taken at different relative depths (0–50 μm) to the surface of the human epidermis after treatment with the FFA NP formulation showed a consistent lateral and normal uniform distribution of particles on the skin surface and within the dermatoglyphs. However, no particles were detected within and between the corneocytes (fig. 5E, F). The particle distribution was not indicative of accumulation in any skin structure at least after 30 min of incubation.

Discussion

Using the SB-M, no differences in drug transport into the stratum corneum could be detected for the nanoencapsulated compared to the free drug (fig. 3). Normally for infinite dose experiments, it would be expected that the drug amount in the stratum corneum reaches a plateau while in the deep skin layers the drug amount increases. In our experiments, it is remarkable that a slight decrease of drug amounts for both preparations is visible for the stratum corneum. The reason might be a radial spreading of the preparation on the skin specimen surface.

For the deep skin layers, the permeation of the drug appeared lower when delivered by NP in comparison to the free drug preparation in both test systems for relatively short incubation times (<12 h).

In contrast to the results obtained at short incubation times, the proportion of drug transported into the deep skin layers was inverted after longer incubation times (>12 h). A statistically significantly higher level of drug was found for the nanoencapsulated drug compared to the free drug with both techniques, the FD-C and SB-M (fig. 3, 4). The mechanisms how NP increase the amount of FFA in the deep skin layers at longer incubation times remain unclear. Since the overall concentration of the FFA in the FFA HG and in FFA NP HG is equal, this should not affect the drug transport. However, it may be speculated that the degradation of the particles leads to some release of acidic compounds (lactic and glycolic acid). This acidification of the particles and their surroundings favours the non-ionized form of FFA which penetrates the stratum corneum better. pH changes of the PLGA particles due to the degradation has been previously reported by Fu et al. [26]. Furthermore, if particles were able to cross the stratum corneum [9] after a certain incubation time, this could also increase the amount taken up. However, multiphoton fluorescence imaging does not give any hint to this mechanism, at least not after a short incubation time (30 min).

Our attempts to visualize drug transport into the skin by multiphoton fluorescence microscopy were restricted to the nanoencapsulated drug, while the free FFA did not yield any fluorescence signal. The distribution of NP applied to the skin appeared to be homogeneous within the HG and followed the structure of the skin surface and the dermatoglyphs. No hair follicles or sweat glands were observed, so that possible transport of NP along these structures such as previously reported by others [10, 11, 15] could not be confirmed by this study. At least after the relatively short incubation time of 30 min, no particles were detected within or in between the corneocytes. The visualization of drug transport processes for NP after longer incubation times (>12 h) is still ongoing and subject of further investigations.

In summary, while there were no differences between free and nanoencapsulated drug in the stratum corneum, such differences became visible at the level of the deep skin layers. After shorter incubation times (<12 h), a significantly higher penetration was obtained with the free drug preparation, suggesting that nanoencapsulation causes a slight delay of drug transport, whereas, for longer incubation times (>12 h), the result was inverted and up to 50% more of drug was transported into the deep skin layers by the NP compared to the free drug formulation.

Conclusion

In this study, the effect of the nanoencapsulated FFA on the skin transport was investigated at different incubation times using permeation and penetration systems (FD-C and SB-M, respectively). For shorter incubation times (<12 h), a slight delay in the skin transport was observed. In contrast, for longer incubation times (>12 h), the drug transport was enhanced for the nanoencapsulated drug compared to the free drug. Although not yet fully understood, such observation underscores the potential of nanotechnology for transdermal drug delivery.

Acknowledgments

Universidad de Concepción and Proyecto MECESUP UCO 0202 (Ministerio de Educación – Gobierno de Chile) are thanked by their financial support.

References

- 1 US Environmental Protection Agency: Dermal exposure assessment: principles and applications. Washington, United States Environmental Protection Agency, Office of Health and Environmental Assessment, 1992.
- 2 Hadgraft J: Skin deep. *Eur J Pharm Biopharm* 2004;58:291–299.
- 3 Hadgraft J: Skin, the final frontier. *Int J Pharm* 2001;224:1–18.
- 4 Walters KA, Roberts MS: The structure and function of the skin; in Walters KA (ed): *Dermatological and Transdermal Formulations. Drugs and the Pharmaceutical Sciences*. New York, Dekker, 2002, vol 119, pp 1–39.
- 5 Cleary GW: Transdermal and transdermal-like delivery system opportunities: today and the future. *Drug Deliv Technol* 2003;3:35–40.
- 6 Barry BW: *Dermatological Formulations. Percutaneous Absorption: Drugs and the Pharmaceutical Sciences*. New York, Dekker, 1983, vol 18.
- 7 Williams AC, Barry BW: Penetration enhancers. *Adv Drug Deliv Rev* 2004;56:603–618.
- 8 Wagner H, Kostka K-H, Adelhardt W, Schaefer UF: Effects of various vehicles on the penetration of flufenamic acid into human skin. *Eur J Pharm Biopharm* 2004;58:121–129.
- 9 Kohli AK, Alpar HO: Potential use of nanoparticles for transcutaneous vaccine delivery: effect of particle size and charge. *Int J Pharm* 2004;275:13–17.
- 10 Toll R, Jacobi U, Richter H, Lademann J, Schaefer H, Blume-Peytavi U: Penetration profile of microspheres in follicular targeting of terminal hair follicles. *J Invest Dermatol* 2004;123:168–176.
- 11 Lademann J, Schaefer H, Otberg N, Blume-Peytavi U, Sterry W: Penetration von Mikropartikeln in die menschliche Haut. *Hautarzt* 2004;55:1117–1119.
- 12 Jenning V, Gysler A, Schafer-Korting M, Gohla SH: Vitamin A-loaded solid lipid nanoparticles for topical use: occlusive properties and drug targeting to the upper skin. *Eur J Pharm Biopharm* 2000;49:211–218.
- 13 Jenning V, Schafer-Korting M, Gohla S: Vitamin A-loaded solid lipid nanoparticles for topical use: drug release properties. *J Control Release* 2000;66:115–126.
- 14 Santos Maia C, Mehnert W, Schafer-Korting M: Solid lipid nanoparticles as drug carriers for topical glucocorticoids. *Int J Pharm* 2000;196:165–167.
- 15 Alvarez-Román R, Naik A, Kalia YN, Guy RH, Fessi H: Skin penetration and distribution of polymeric nanoparticles. *J Control Release* 2004;99:53–62.
- 16 Alvarez-Román R, Naik A, Kalia YN, Guy RH, Fessi H: Enhancement of topical delivery from biodegradable nanoparticles. *Pharm Res* 2004;21:1818–1825.
- 17 Brannon-Peppas L: Recent advances on the use of biodegradable microparticles and nanoparticles in controlled drug delivery. *Int J Pharm* 1995;116:1–9.
- 18 Hans ML, Lowman AM: Biodegradable nanoparticles for drug delivery and targeting. *Curr Opin Solid State Mater Sci* 2002;6:319–327.
- 19 Soppimath KS, Aminabhavi TM, Kulkarni AR, Rudzinski WE: Biodegradable polymeric nanoparticles as drug delivery devices. *J Control Release* 2001;70:1–20.
- 20 Ravi Kumar MNV, Sameti M, Kneuer C, Lamprecht A, Lehr C-M: Polymeric nanoparticles for drug and gene delivery; in Nalwa HS (ed): *Encyclopedia of Nanoscience and Nanotechnology*. American Scientific Publishers, 2003, vol 10, pp 1–19.
- 21 Wagner H, Kostka K-H, Lehr C-M, Schaefer UF: Drug distribution in human skin using two different in vitro test systems: comparison with in vivo data. *Pharm Res* 2000;17:1475–1481.
- 22 Dick IP, Scott RC: Pig ear skin as an in vitro model for human skin permeability. *J Pharm Pharmacol* 1992;44:640–645.
- 23 König K, Riemann I: High-resolution multiphoton tomography of human skin with subcellular spatial resolution and picosecond time resolution. *J Biomed Opt* 2003;8:432–439.
- 24 Bronaugh RL, Stewart RF, Morton S: Methods of in vitro percutaneous absorption studies VII: use of excised human skin. *J Pharm Sci* 1986;75:1094–1097.
- 25 Abignente E, De Caprariis P: Flufenamic Acid. *Analytical Profiles of Drug Substances*. In Florey K (ed), Academic Press, 1982, vol 11, pp 313–346.
- 26 Fu K, Pack DW, Klivanov AM, Langer R: Visual evidence of acidic environment within degrading poly(lactic-co-glycolic acid) (PLGA) microspheres. *Pharm Res* 2000;17:100–106.

Coupling of biotin-(polyethyleneglycol)amine to poly(D,L-lactide-co-glycolide) nanoparticles for versatile surface modification

Running title: Versatile surface modification of nanoparticles

Barbara Weiss ‡, Marc Schneider ‡, Sebastian Taetz ‡, Dirk Neumann §, Ulrich F. Schaefer ‡, Claus-Michael Lehr ‡*

‡ Biopharmaceutics and Pharmaceutical Technology, Saarland University, Saarbruecken, Germany

§ Junior Research Group Drug Transport, Center for Bioinformatics, Saarland University, Saarbruecken, Germany

* Correspondence: Prof. Dr. Claus-Michael Lehr, Biopharmaceutics and Pharmaceutical Technology, Saarland University, 66123 Saarbruecken, Germany
Tel: +49-681-302-3039; Fax: +49-681-302-4677; email: lehr@mx.uni-saarland.de

Abstract

Generally, polymeric nanoparticles (NP) for drug targeting are designed to entrap the drug moiety in the core and to present the targeting moiety on the surface. However, in most cases, common preparation techniques of polymeric NP need to be specifically arranged for each compound to be entrapped or attached. In the present work we introduce a method for versatile conjugation of targeting moieties to the surface of preformed, polymeric NP. Moreover, due to taking advantage of biotin-avidin interactions, our regime opens the additional possibility of a rapid fluorescence labelling of NP.

Poly(D,L-lactide-co-glycolide) (PLGA) NP in the size of 210 nm were prepared by the classic oil-in-water method. Such NP were functionalized with biotin-(polyethyleneglycol)amine (BPEG) by means of cyanuric chloride chemistry. The amount of surface associated biotin was 850 pmol per mg polymer corresponding to roughly 2,650 molecules biotin per NP. When drawn to scale, such surface coating appeared to be well suited for subsequent binding of avidin or avidin-linked ligands. By resonant mirror measurements we could prove specific binding of biotinylated NP to a NeutrAvidin (NAv) coated surface. Furthermore, after coupling of NAv-linked fluorescence dyes to BPEG functionalized NP, differences in binding and uptake could be demonstrated using two epithelial cell lines (Caco-2, A549).

Keywords: biotin, fluorescence dye, cyanuric chloride, neutravidin, PLGA

1 Introduction

Polymeric nanoparticles (NP) have turned out to be a promising carrier system for a number of active pharmacological ingredients (API) because they allow controlled release, drug targeting, and overcoming certain biological barriers such as the blood brain barrier (1-4), the skin (5-9), or the intestinal mucosa (10-13).

In this context, biocompatible and biodegradable polymers are highly preferred as they are eliminated from the body as small non-toxic fragments after having served their intended purpose (14). Well-known examples of such polymers are the aliphatic poly(esters) poly(lactic acid) (PLA), poly(glycolic acid) (PGA), and their copolymers poly(lactic acid-co-glycolic acid) (PLGA); they have been extensively used since the 1970s for biomedical applications like sutures, fibres, fracture repairs, implants, and vascular grafts (15). Later, mainly PLA and PLGA have also been applied for the preparation of NP (4, 6, 16-21) which resulted in a variety of well established methods for preparation and drug entrapment (14, 15). Nowadays, a major interest of research is the synthesis of novel biodegradable polymers for the preparation of NP with different drug loading properties, controlled release, and predictable degradation (22-28). Most of them are block-copolymers (22, 23, 26) or polymer blends (27) often also containing PLGA or PLA subunits (26-28).

Generally, nanoparticulate drug targeting systems may bear different functionalities. The inner functionality is reflected by the NP core encapsulating the active moiety, small drug molecules (6, 8, 29-32), or therapeutic proteins (16, 33-35). The active compound is stabilized towards the physiological environment and its release can be controlled by the composition and structure of the polymer matrix. Complementarily, the outer functionality of a NP is represented by the NP surface which may establish specific and non-specific interactions with the target, e.g. some particular cells, tissues, or organs. In regard of drug targeting, specific interactions between NP and the target cells or tissues are favoured, requiring a sufficient number of targeting ligands on the NP surface to be available for such interaction (36-38).

The aim of this study was to develop a procedure for surface functionalization of preformed NP, which may eventually already contain an API, for subsequent versatile conjugation of targeting ligands and fluorescence dyes under mild conditions. For such purpose we chose the avidin-biotin system as avidin (Av) and its homologues

streptavidin (SAv) and NeutrAvidin™ (NAv) exhibit very high affinities ($K_d = 10^{-13} - 10^{-16}$ M) and a rapid and stable binding to biotin (39, 40). Taking into consideration the presence of free carboxylic acid groups on the surface of NP made of poly(esters) like PLA, PLGA, PGA and diverse lactide and/or glycolide containing blends and block-copolymers (23, 26, 27) we have opted for an approach where surface biotinylated NP bind to conjugates of avidin (or homologues). Consequently, both targeting moieties (antibodies, Fab fragments, etc.) as well as fluorescence labels can be easily linked to the surface of thus functionalized NP as long as they are available as conjugates of avidin (or homologues) (Figure 1A).

In the present study an effective surface biotinylation of preformed PLGA NP cores could be demonstrated. PLGA NP were characterized for their size, zeta potential and surface characteristics before and after biotin functionalization. The particle associated biotin amount was determined to scale. Resonant mirror measurements gave evidence for specific binding of biotinylated NP to a NAv surface. For first evaluation in a biological system, differences in binding and uptake of NP were studied in two epithelial cell lines after labelling the NP with Av linked fluorescence dyes.

2 Methods and materials

2.1 Materials

Poly(D,L-lactide-co-glycolide) (PLGA) (Resomer RG 50:50 H; inherent viscosity 0.31 dl/g) was kindly provided by Boehringer Ingelheim (Boehringer Ingelheim GmbH & Co. KG, Ingelheim, GE). Biotin-(polyethyleneglycol)amine (BPEG) was obtained from Sigma (Sigma Chemical Co., St. Louis, MO, USA). Polyvinylalcohol (PVA) (Mowiol 4-88) was bought from Kuraray (Kuraray Specialities GmbH, Frankfurt am Main, GE). NeutrAvidin™ Biotin-Binding Protein (NAv), avidin - FITC conjugate (FITC-Av), streptavidin - FITC conjugate (FITC-SAv), and NeutrAvidin™ - FITC conjugate (FITC-NAv) were purchased from Pierce (Perbio Science Deutschland GmbH, Bonn, GE). NeutrAvidin™ - Rhodamin Red™ – X conjugate (Rho-NAv) was obtained from Invitrogen (Molecular Probes, Inc., Eugene, OR, USA). Rhodamine ricinus communis agglutinin I (Rho-RCA) and fluorescein wheat germ agglutinin (FITC-WGA) were obtained from Vector (Vector Laboratories, Inc., Burlingame, CA, USA). Dulbecco's modified Eagle's medium (DMEM), RPMI-1640, non-essential amino acids (NeAA) and fetal bovine serum (FBS) were bought from GIBCO (Invitrogen Corp., Carlsbad, CA, USA). All other chemicals were of analytical grade. Phosphate buffered solution pH 7.4 (PBS) was composed of KCl 0.20 g/l, NaCl 8.00 g/l, KH₂PO₄ 0.20 g/l, Na₂HPO₄ × 2H₂O 1.44 g/l.

2.2 Preparation of biotin-(polyethyleneglycol)amine coated PLGA nanoparticles

PLGA NP were prepared by a single emulsion method (41). Briefly, 100 mg of PLGA were dissolved in 5 ml of ethyl acetate and emulsified into a 1% PVA solution. The system was stirred at room temperature for 2 h at 800 rpm on a magnetic stirrer and then homogenized for 10 min using an Ultra-Turrax® T 25 Mixer (Janke und Kunkel GmbH & Co., Staufen, GE) at 13,500 rpm. The volume was filled up to 50 ml with demineralised water and the organic solvent was evaporated using a rotary evaporator. BPEG coated PLGA NP (BPEG PLGA NP) were generated from PLGA NP via a triazine-promoted amidation of the carboxylic acid groups present on the PLGA NP surface. The technique has been frequently described in the literature (42-44); here it was adapted to surface modification of PLGA NP. The carboxylic acid groups formed activated intermediates with cyanuric chloride and, subsequently, the desired carboxyl amides in a single one-step reaction (Figure 2). The amino groups for the amidation

reaction derived from BPEG. 1 ml of PLGA NP suspension was supplemented with 1 ml of saturated cyanuric chloride solution and 50 μ l of 10 mg/ml BPEG solution and incubated at room temperature for 24 h under gentle shaking on a horizontal shaker. BPEG PLGA NP were rinsed from excessive reagents by dialysis against 2 l of demineralised water for 24 h using a dialysis membrane with a cut-off of 100,000 Da (Spectra Por[®] CE, Carl Roth GmbH, Karlsruhe, GE). The dialysis water was renewed after 8 h of dialysis time. In case blank PLGA NP were used for comparison, they were also dialysed as described above. The NP concentration was determined via the residue of a defined volume of NP suspension after lyophilization. NP were prepared with a total of n = 3 to 5 batches.

2.3 Physicochemical characterization of the nanoparticles

2.3.1 Particle size and surface charge (zeta potential)

For determination of particle size and zeta potential, the NP suspensions were 100 fold diluted in demineralised water and analysed using a Zetasizer Nano ZS (Malvern Instruments, Malvern, UK). The measurement of the NP size was based upon photon correlation spectroscopy (PCS). This technique yields the particle mean diameter and the polydispersity index (PI) which is a dimensionless measure for the broadness of the particle size distribution. The zeta potential was analysed by laser doppler anemometry using the same instrument in appropriate settings. Results are expressed as mean \pm SD.

2.3.2 Morphology study

NP shape and surface properties were imaged by means of Scanning probe microscopy (SPM). NP samples were prepared as dense layers by mounting a drop of a freshly prepared NP suspension on a silicon wafer and air-drying. Imaging was performed using a Bioscope[™] SPM and a Nanoscope IV[™] controller (Veeco Instruments, Santa Barbara, CA, USA) in a vibration-free environment. For all measurements, Tapping mode[™] was employed using a commercially available pyramidal tip (silicon, Ultrasharp, MikroMasch, Tallinn, EST) on a cantilever with a length of 230 μ m. The resonance frequency was approximately 170 kHz, the nominal force constant 40 N/m, and the scan frequency between 0.1 and 1 Hz.

2.4 Particle associated biotin amount

The amount of biotin on BPEG PLGA NP was determined by means of FluoReporter® Biotin Quantitation Assay (Molecular Probes™, Invitrogen GmbH, Karlsruhe, GE). This assay uses Biotective™ Green reagent which consists of Av labelled with a fluorescence dye and with quencher dye ligands occupying the biotin binding sites. The ligand quenches the fluorescence through fluorescence resonance energy transfer. By addition of any biotin the ligand is displaced from Biotective™ Green reagent, yielding fluorescence proportional to the amount of added biotin. The assay was performed according to the protocol of the manufacturer. NP suspensions were used in concentrations between 0.49 and 0.88 mg/ml and experiments were performed with 3 batches and with a total of $n = 2$ to 3 samples each. The background was subtracted. Results are expressed as mean \pm SD.

2.5 Modelling of biotin-(polyethyleneglycol)amine

To determine the dimensions of BPEG we built a single stretched molecule using the program HyperChem Professional 7.1 (ScienceServe, Pegnitz, GE). The geometry optimization was performed on a personal computer employing the MM + force field. For the energy minimization we used a conjugate gradient method with a termination value of the root mean square gradient of 0.1 kcal/mol/Å according to the HyperChem manual.

2.6 Resonant mirror system (RMS) adhesion studies

The interaction of BPEG PLGA NP and PLGA NP with two differently modified surfaces was examined by means of a RMS (IAsys, Cambridge, UK). First, the interaction of the NP with a NAv coated surface was investigated.

In a second run, the binding sites of NAv were blocked using a 0.02 mg/ml BPEG solution (incubation time \sim 4.5 min) to study possible non-specific binding of NP with this surface.

Briefly, NP suspensions were added to the coated sensor chip and allowed to bind to the surface. The adhesion process was monitored and the measurements were stopped after 5 to 10 min. The vertical displacement of the vibrostirrer was set to 0.425 mm and the temperature of the instrument was set to 25°C.

The concentrations of BPEG PLGA NP and PLGA NP were 0.5 and 1.2 mg/ml, respectively. The NAv functionalized surface was generated by incubating a biotin coated cuvette (Thermo Electron LED GmbH, Langenselbold, GE) with NAv as described in the IAsys standard immobilization protocol. All reactions were performed in PBS.

2.7 Cell culture

2.7.1 Caco-2 cells

Caco-2 cells, clone C2BBE1, were purchased at passage 60 from American Tissue Culture Collection (ATCC; Manassas, VA, USA) and used at passages 70 to 91. Cells were grown to a confluency of approximately 90 % in 75 cm² T-flasks with DMEM supplemented with 10 % FBS and 1 % NeAA. Thereby, the culture medium was changed every second day and the temperature was 37°C in an atmosphere of around 85 % relative humidity and 5 % CO₂.

2.7.2 A549 cells

A549 cells (ATCC No. CCL-185) were purchased at passage 82 from ATCC (American Type Culture Collection, Manassas, VA, USA) and used at passages 88 to 110. Cells were grown to a confluency of approximately 90% in 75 cm² T-flasks with RPMI-1640 supplemented with 10% FBS. Thereby, the culture medium was changed every second day and the temperature was 37°C in an atmosphere of around 85% relative humidity and 5% CO₂.

2.7.3 Uptake studies

After trypsinization Caco-2 and A549 cells were seeded on LAB-TEK[®] chamber slides (Nalge Nunc International, Rochester, NY, USA) at a density of roughly 20,000 and 12,500 cells / ml, respectively, and grown for 3 days. Uptake of test substances was evaluated after 6 and 24 h of incubation with a test substance at 37°C under protection from light. In case of the 24 h incubation time the supernatant was replaced by cell culture medium after 6 h. For localization of fluorescent NP cell membranes were stained using Rho-RCA and FITC-WGA, respectively, by incubation with a 5 µg/ml solution in PBS for 10 min at 37°C under protection from light. Cells were washed twice

with PBS and fixed by 10 min of incubation with 4% formaldehyde solution at room temperature under protection from light. Again, cells were washed twice and, then, subjected to confocal laser scanning microscopy (CLSM) which was performed using a Bio-Rad MRC-1024 CLSM (Bio-Rad Laboratories, Hercules, CA, USA) equipped with an argon/krypton laser. The objective used was an oil immersion objective 40× NA=1.3. Green fluorescence was collected with a band pass filter (Zeiss: 520/35) and red fluorescence was collected with a long pass filter (Zeiss: LP585) after excitation at 488 nm and 568 nm, respectively. For each set of samples the same detector settings were chosen. Test substances were: (i) 0.5 mg/ml BPEG PLGA NP which were pre-incubated with FITC-NAv or Rho-NAv in excess for 30 min, dialysed in order to remove unbound proteins, and 1:1 diluted with the respective growth medium and (ii) a 25 µg/ml FITC-NAv or Rho-NAv solution in the respective growth medium. The concentrations of the FITC-NAv and Rho-NAv solutions were well above the maximum of NP associated fluorescent proteins in a 0.25 mg/ml BPEG PLGA NP solution when all biotin molecules bound to one FITC-NAv or Rho-NAv molecule. References were only with the respective lectin conjugated fluorescence dye stained cells without incubating them with particles.

3 Results

3.1 Physicochemical properties of biotinylated nanoparticles

PCS measurements showed that size and PI of BPEG PLGA NP and PLGA NP were practically the same, i.e. there was no measurable increase in size of the original PLGA NP after functionalization with BPEG. Particle size distributions were monodisperse. However, the zeta potential changed from -32 mV to -23 mV (Table 1). Figure 3 presents SPM images of PLGA NP, BPEG PLGA NP and BPEG PLGA NP with associated FITC-Av. Before subjection to SPM measurements successful binding of FITC-Av to BPEG PLGA NP was confirmed via CLSM. The SPM topography images show the particle shape and surface structure. Obviously, all samples exhibited a spherical particle shape and a smooth surface irrespective of any surface modifications as in case of the BPEG PLGA NP and the BPEG PLGA NP with associated FITC-Av. However, clear differences were observed in the phase images of those samples, in contrast to the original PLGA NP. These alterations suggest changes of the elastic or adhesive properties as consequence of surface biotinylation of PLGA NP and also due to the binding of FITC-Av to thus modified surface.

FluoReporter[®] Biotin Quantitation Assay was used to quantitatively analyse the extent of surface modification of PLGA NP resulting in BPEG PLGA NP. By that method an amount of 845 ± 145 pmol of biotin attached to the surface of 1 mg of BPEG PLGA NP was determined. Assuming a particle density of 1.25 g/ml (which corresponds to the real density of PLGA according to the information of the manufacturer) an approximate number of 2,600 biotin molecules on the surface of one single average-sized (210 nm) BPEG PLGA NP could be calculated. Assuming that BPEG chains are evenly distributed on the NP surface, the mean distance of two chains would be 69 Å. The length of the BPEG chains was calculated to maximally 46 Å. In solution, we would expect the BPEG molecule to adopt a more or less coiled conformation, here however, to roughly estimate surface conditions we deliberately assumed the molecule to exist in a stretched conformation. The size of Av is reported to $50 \text{ Å} \times 50 \text{ Å} \times 40 \text{ Å}$ with the biotin binding sites being in a distance of 29.5 and 20 Å to each other (45). The dimensions of such a BPEG functionalized NP surface is drawn to scale in Figure 1B

indicating that each single BPEG graft on the NP surface should be well accessible to Av.

3.2 Selection of suitable avidin homologues for further functionalization

Each of the three proteins FITC-Av, FITC-SAv and FITC-NAv bound to BPEG PLGA NP, whereas only FITC-Av and FITC-SAv exhibited binding to blank PLGA NP, obviously due to non-specific interactions. In these cases we could visualize green fluorescent single NP or particle aggregates by means of CLSM. In contrast, we did not find binding of NAv-FITC to PLGA NP. Consequently, due to apparently weak non-specific particle binding, we chose NAv for further RMS measurements and ligand coupling.

3.3 RMS measurements

Using RMS, we first studied the binding of BPEG PLGA NP with a NAv functionalized surface (total binding) (Figure 4). We obtained a clear response, however, the binding curve did not reach equilibrium during the measurement, possibly due to particle rearrangement on the NAv coated surface. There was no observable NP dissociation and particles could not be washed easily from the surface indicating a strong binding. In a second experiment, non-specific binding was studied by blocking the biotin binding sites of a NAv functionalized cuvette using free BPEG. Here, we received only a small response. The extent of specific binding of BPEG PLGA NP to the NAv surface is described by a calculated curve, which was obtained by subtracting the curve representing the non-specific binding from the curve representing the total binding. Again, the curve did not reach equilibrium for reasons described above. For comparison, we also investigated the binding behaviour of non-functionalized PLGA NP to a NAv surface. Here, the equilibrium response was very small and readily established after approximately 100 s.

3.4 Uptake studies

Figure 5 shows xz-cross sections from a stack of confocal laser scans of Rho-RCA stained A549 cells, Rho-RCA stained Caco-2 cells, and FITC-WGA stained Caco-2 cells after 6 and 24 h incubation with fluorescent NP formulations. In order to investigate and visualise binding and uptake, we applied FITC-NAv labelled NP if the cell

membranes were stained with Rho-RCA, and Rho-NAv labelled NP if the membranes were stained with FITC-WGA.

In case of A549 cells, NP appeared in close association with the cell membranes after 6 h of incubation whereas we found a clear NP uptake after 24 h. In case of Caco-2 cells, there was no particle uptake even after 24 h of incubation. However, particles were attached to the cell membranes.

These results in Caco-2 cells were found with both FITC-NAv and Rho-NAv labelled BPEG PLGA NP, thus evidencing the suitability of this approach for rapid versatile fluorescence labelling.

In all cases employing plain FITC-NAv and Rho-NAv solutions (i.e. not coupled to NP), we did not find any fluorescence within the cells or at the membranes which had derived from the protein solutions (images not shown).

4 Discussion

The overall goal of this study was the evaluation of a procedure for surface functionalization of preformed NP made from biodegradable polymers such as PLGA. Surface modified NP are intended to be used for subsequent versatile conjugation of targeting moieties and for rapid fluorescence labelling under mild conditions.

Preformed PLGA NP were modified by easy covalent binding of a biotin derivative via a short PEG spacer (Figure 2). The biotinylated particle surface forms a platform for further specific binding of Av (and homologues) conjugated compounds, which may either be targeting moieties or fluorescence dyes, by brief incubation in aqueous medium (Figure 1A). By this NP modification method, harsh preparation conditions like shearing, heating or the presence of organic solvents are avoided. Another benefit of this technique concerns the detachment of compounds from the NP surface for potential targeting purposes. If NP are made from functionalized polymers (46-48), ongoing polymer erosion may uncover further active groups, thus leading to a subsequent re-binding of detached proteins. In contrast, with our approach, the NP core will not provide further biotin groups as soon as they are cleaved from the surface i.e. specific re-binding is most unlikely.

Regarding the biocompatibility of BPEG PLGA NP, biotin is a natural vitamin, and both substances, PEG and PLGA, may be considered as non-toxic (as they are part of FDA approved drug products for parenteral administration).

Surface functionalization of PLGA NP to yield BPEG PLGA NP did not involve an increase in size as determined by PCS, i.e. any change in the hydrodynamic diameter was beneath the detection limit (Table 1). As evidenced in SPM studies surface modification of PLGA NP and binding of Av to BPEG PLGA NP did not lead to changes in particle shape and surface structure (Figure 3). Obviously, however, as indicated in the phase images those modifications resulted in changes of elasticity or adhesion of the cantilever tip.

We found a decrease in the zeta potential for the BPEG PLGA NP in comparison to non-modified PLGA NP (Table 1). The negative surface charge of both particle species is attributed to the presence of carboxyl end groups deriving from PLGA chain ends. However, in case of the BPEG PLGA NP, the particle surface was partially shielded owing to covalent modification of the carboxyl groups by means of BPEG molecules. The PEG chain linking the biotin compound with the NP core consisted of 10 ethylene

oxide subunits and was conceived to facilitate the surface modification reaction by provision of amino groups and, at the same time, to increase biotin flexibility whilst protein binding.

Studying the binding specificity of Av and its homologues to BPEG PLGA NP and PLGA NP, we found specific binding to BPEG PLGA NP only in case of NAv. This finding has to be attributed to the character of the proteins: Av and its bacterially produced counterpart SAv represent positively charged glycoproteins with well known tendency of non-specific interactions with negatively charged compounds e.g. PLGA NP. NAv is manufactured from Av by deglycosylation, consequently, reducing charge and non-specific binding (49).

The binding specificity was confirmed in RMS measurements where BPEG PLGA NP showed specific binding to a NAv surface (Figure 4). Attachment of BPEG PLGA NP to the NAv surface did not reach equilibrium during the measurement which probably is to be attributed to particle rearrangement; in contrast minor non-specific binding of PLGA NP was completed rapidly.

For drug delivery applications, investigation and imaging of NP in biological systems, their penetration pathways, and their final localization at cellular or tissue level is of major interest (9, 18, 50). Common strategies represent the entrapment of fluorescence markers or visualisable drugs and the imaging of NP by fluorescence, confocal, or multiphoton microscopy (6, 9, 50, 51). The present work illustrates the application of fluorescence-labelled BPEG PLGA NP to demonstrate differences in binding and uptake behaviour between flat squameous epithelial cells from the alveolar epithelium (A549) in comparison to the relatively thick columnar epithelial cells from the intestinal mucosa (Caco-2) (Figure 5). Moreover, dependent on the staining of the cell membranes we applied NP decorated with different fluorescent NAv conjugates, thus demonstrating the ease of versatile fluorescence labelling of BPEG PLGA NP.

From calculations to scale of the surface of BPEG PLGA NP we hypothesized that particles are optimally covered by BPEG molecules. Presumably, those molecules are able to reach each site on the particle surface due to the flexibility of their PEG spacer in order to mediate specific binding of Av (and homologues). Considering Av and homologues being tetrameric with four biotin binding sites it is evident that this fact may lead to binding of biotin molecules deriving from several NP and subsequently to cross-linking. Nowadays, in order to overcome this cross-linking problem, one can find

different approaches in literature. Active monomeric Av and SAv mutants have been produced by means of biotechnological methods (52, 53). Since monomerization of those proteins generally involves loss of biotin binding affinity a SAv tetramer with only one functional biotin binding subunit was recently developed (54).

Those protein mutants would help to avoid particle cross-linking, whereas the choice of NAv as biotin binding protein can further minimize non-specific binding. Such refinement of our approach by using monovalent NAv appears well possible, however, this is still subject to ongoing research.

5 Conclusion

Successful surface biotinylation of preformed PLGA NP, representing a model for NP from any other polymer exhibiting free carboxylic acid groups, could be demonstrated. Without interfering with or being dependent on the methods of NP preparation and drug loading our approach allows versatile surface decoration with targeting moieties and fluorescence labels under mild conditions, provided they are available as conjugates of NAv. Binding studies and calculations to scale of the surface conditions of biotinylated NP revealed optimal conditions for subsequent specific binding of Av conjugated ligands. In a first biological evaluation with A549 and Caco-2 cells, BPEG PLGA NP enabled us to demonstrate differences in binding and uptake.

6 Acknowledgements

Boehringer Ingelheim is kindly acknowledged for providing the polymer. We would like to thank Jens Schaefer (Department of Pharmaceutics and Biopharmacy, Philipps-University Marburg) for his help with the Zetasizer measurements. D. Neumann is financially supported by the Deutsche Forschungsgemeinschaft (DFG grant BIZ 4/1).

7 References

- (1) Koziara, J. M., Lockman, P. R., Allen, D. D. and Mumper, R. J. (2004) Paclitaxel nanoparticles for the potential treatment of brain tumors. *J. Control. Release.* *99*, 259-269
- (2) Ambruosi, A., Gelperina, S., Khalansky, A., Tanski, S., Theisen, A. and Kreuter, J. (2006) Influence of surfactants, polymer and doxorubicin loading on the anti-tumour effect of poly(butyl cyanoacrylate) nanoparticles in a rat glioma model. *J. Microencapsul.* *23*, 582-592
- (3) Aktas, Y., Yemisci, M., Andrieux, K., Gursoy, R. N., Alonso, M. J., Fernandez-Megia, E., Novoa-Carballal, R., Quinoa, E., Riguera, R., Sargon, M. F., Celik, H. H., Demir, A. S., Hincal, A. A., Dalkara, T., Capan, Y. and Couvreur, P. (2005) Development and brain delivery of chitosan-PEG nanoparticles functionalized with the monoclonal antibody OX26. *Bioconjug. Chem.* *16*, 1503-1511
- (4) Costantino, L., Gandolfi, F., Tosi, G., Rivasi, F., Vandelli, M. A. and Forni, F. (2005) Peptide-derivatized biodegradable nanoparticles able to cross the blood-brain barrier. *J. Control. Release.* *108*, 84-96
- (5) Alvarez-Roman, R., Naik, A., Kalia, Y. N., Guy, R. H. and Fessi, H. (2004) Enhancement of topical delivery from biodegradable nanoparticles. *Pharm. Res.* *21*, 1818-1825
- (6) Luengo, J., Weiss, B., Schneider, M., Ehlers, A., Stracke, F., Konig, K., Kostka, K. H., Lehr, C. M. and Schaefer, U. F. (2006) Influence of nanoencapsulation on human skin transport of flufenamic acid. *Skin Pharmacol. Physiol.* *19*, 190-197
- (7) Shim, J., Seok Kang, H., Park, W. S., Han, S. H., Kim, J. and Chang, I. S. (2004) Transdermal delivery of minoxidil with block copolymer nanoparticles. *J. Control. Release.* *97*, 477-484
- (8) Simeonova, M., Velichkova, R., Ivanova, G., Enchev, V. and Abrahams, I. (2003) Poly(butylcyanoacrylate) nanoparticles for topical delivery of 5-fluorouracil. *Int. J. Pharm.* *263*, 133-140
- (9) Stracke, F., Weiss, B., Lehr, C. M., Konig, K., Schaefer, U. F. and Schneider, M. (2006) Multiphoton Microscopy for the Investigation of Dermal Penetration of Nanoparticle-Borne Drugs. *J. Invest. Dermatol.* *126*, 2224-2233
- (10) Lamprecht, A., Schaefer, U. F. and Lehr, C. M. (2001) Size-dependent bioadhesion of micro- and nanoparticulate carriers to the inflamed colonic mucosa. *Pharm. Res.* *18*, 788-793
- (11) Borges, O., Borchard, G., Verhoef, J. C., de Sousa, A. and Junginger, H. E. (2005) Preparation of coated nanoparticles for a new mucosal vaccine delivery system. *Int. J. Pharm.* *299*, 155-166
- (12) Shakweh, M., Besnard, M., Nicolas, V. and Fattal, E. (2005) Poly (lactide-co-glycolide) particles of different physicochemical properties and their uptake by peyer's patches in mice. *Eur. J. Pharm. Biopharm.* *61*, 1-13
- (13) Weiss, B., Schaefer, U. F., Zapp, J., Lamprecht, A., Stallmach, A. and Lehr, C.-M. (2006) Nanoparticles made of fluorescence-labelled PLGA: preparation, stability and biocompatibility. *J. Nanosci. Nanotechnol.* *6*, 3048-3056
- (14) Bala, I., Hariharan, S. and Kumar, M. N. (2004) PLGA nanoparticles in drug delivery: the state of the art. *Crit. Rev. Ther. Drug Carrier Syst.* *21*, 387-422
- (15) Jain, R. A. (2000) The manufacturing techniques of various drug loaded biodegradable poly(lactide-co-glycolide) (PLGA) devices. *Biomaterials.* *21*, 2475-2490
- (16) Bilati, U., Allemann, E. and Doelker, E. (2005) Poly(D,L-lactide-co-glycolide) protein-loaded nanoparticles prepared by the double emulsion method--processing and formulation issues for enhanced entrapment efficiency. *J. Microencapsul.* *22*, 205-214

6.5 Coupling of biotin-(polyethyleneglycol)amine to poly(D,L-lactide-co-glycolide) nanoparticles for versatile surface modification

- (17) Higaki, M., Ishihara, T., Izumo, N., Takatsu, M. and Mizushima, Y. (2005) Treatment of experimental arthritis with poly(D, L-lactic/glycolic acid) nanoparticles encapsulating betamethasone sodium phosphate. *Ann. Rheum. Dis.* 64, 1132-1136
- (18) Horisawa, E., Kubota, K., Tuboi, I., Sato, K., Yamamoto, H., Takeuchi, H. and Kawashima, Y. (2002) Size-dependency of DL-lactide/glycolide copolymer particulates for intra-articular delivery system on phagocytosis in rat synovium. *Pharm. Res.* 19, 132-139
- (19) Kristl, A., Allemann, E. and Gurny, R. (1996) Formulation and evaluation of zinc phthalocyanine-loaded poly(DL-lactic acid) nanoparticles. *Acta Pharm.* 46, 1-12
- (20) McClean (1998) Binding and uptake of biodegradable poly-DL-lactide micro- and nanoparticles in intestinal epithelia. *Eur. J. Pharm. Sci.* 6, 153-163
- (21) Nobs, L., Buchegger, F., Gurny, R. and Allemann, E. (2004) Poly(lactic acid) nanoparticles labeled with biologically active Neutravidin for active targeting. *Eur. J. Pharm. Biopharm.* 58, 483-490
- (22) Shenoy, D., Little, S., Langer, R. and Amiji, M. (2005) Poly(ethylene oxide)-modified poly(beta-amino ester) nanoparticles as a pH-sensitive system for tumor-targeted delivery of hydrophobic drugs: part 2. In vivo distribution and tumor localization studies. *Pharm. Res.* 22, 2107-2114
- (23) Duan, Y., Sun, X., Gong, T., Wang, Q. and Zhang, Z. (2006) Preparation of DHAQ-loaded mPEG-PLGA-mPEG nanoparticles and evaluation of drug release behaviors in vitro/in vivo. *J. Mater. Sci. Mater. Med.* 17, 509-516
- (24) Lescure, F., Seguin, C., Breton, P., Bourrinet, P., Roy, D. and Couvreur, P. (1994) Preparation and characterization of novel poly(methylidene malonate 2.1.2.)-made nanoparticles. *Pharm. Res.* 11, 1270-1277
- (25) Akagi, T., Higashi, M., Kaneko, T., Kida, T. and Akashi, M. (2006) Hydrolytic and enzymatic degradation of nanoparticles based on amphiphilic poly(gamma-glutamic acid)-graft-L-phenylalanine copolymers. *Biomacromolecules.* 7, 297-303
- (26) Farokhzad, O. C., Cheng, J., Teply, B. A., Sherifi, I., Jon, S., Kantoff, P. W., Richie, J. P. and Langer, R. (2006) Targeted nanoparticle-aptamer bioconjugates for cancer chemotherapy in vivo. *Proc. Natl. Acad. Sci. U S A.* 103, 6315-6320
- (27) Dong, Y. and Feng, S. S. (2006) Nanoparticles of poly(D,L-lactide)/methoxy poly(ethylene glycol)-poly(D,L-lactide) blends for controlled release of paclitaxel. *J Biomed. Mater. Res. A.* 78, 12-19
- (28) Lee, C. T., Huang, C. P. and Lee, Y. D. (2006) Synthesis and characterizations of amphiphilic poly(l-lactide)-grafted chondroitin sulfate copolymer and its application as drug carrier. *Biomol. Eng.* in press
- (29) Ahlin, P., Kristl, J., Kristl, A. and Vrečer, F. (2002) Investigation of polymeric nanoparticles as carriers of enalaprilat for oral administration. *Int. J. Pharm.* 239, 113-120
- (30) Ubrich, N., Bouillot, P., Pellerin, C., Hoffman, M. and Maincent, P. (2004) Preparation and characterization of propranolol hydrochloride nanoparticles: a comparative study. *J. Control. Release.* 97, 291-300
- (31) Yoo, H. S., Oh, J. E., Lee, K. H. and Park, T. G. (1999) Biodegradable nanoparticles containing doxorubicin-PLGA conjugate for sustained release. *Pharm. Res.* 16, 1114-1118
- (32) Polakovic, M., Gorner, T., Gref, R. and Dellacherie, E. (1999) Lidocaine loaded biodegradable nanospheres. II. Modelling of drug release. *J. Control. Release.* 60, 169-177
- (33) Raghuvanshi, R. S., Katare, Y. K., Lalwani, K., Ali, M. M., Singh, O. and Panda, A. K. (2002) Improved immune response from biodegradable polymer particles entrapping tetanus toxoid by use of different immunization protocol and adjuvants. *Int. J. Pharm.* 245, 109-121

6.5 Coupling of biotin-(polyethyleneglycol)amine to poly(D,L-lactide-co-glycolide) nanoparticles for versatile surface modification

- (34) Zambaux, M. F., Bonneaux, F., Gref, R., Dellacherie, E. and Vigneron, C. (1999) Preparation and characterization of protein C-loaded PLA nanoparticles. *J. Control. Release.* 60, 179-188
- (35) Sanchez, A., Tobio, M., Gonzalez, L., Fabra, A. and Alonso, M. J. (2003) Biodegradable micro- and nanoparticles as long-term delivery vehicles for interferon-alpha. *Eur. J. Pharm. Sci.* 18, 221-229
- (36) Dinauer, N., Balthasar, S., Weber, C., Kreuter, J., Langer, K. and von Briesen, H. (2005) Selective targeting of antibody-conjugated nanoparticles to leukemic cells and primary T-lymphocytes. *Biomaterials.* 26, 5898-5906
- (37) Gupta, P. N., Mahor, S., Rawat, A., Khatri, K., Goyal, A. and Vyas, S. P. (2006) Lectin anchored stabilized biodegradable nanoparticles for oral immunization 1. Development and in vitro evaluation. *Int. J. Pharm.* 318, 163-173
- (38) Weissenbock, A., Wirth, M. and Gabor, F. (2004) WGA-grafted PLGA-nanospheres: preparation and association with Caco-2 single cells. *J. Control. Release.* 99, 383-392
- (39) Green, N. M. (1975) Avidin. *Adv. Protein. Chem.* 29, 85-133
- (40) Green, N. M. (1990) Avidin and streptavidin. *Methods Enzymol.* 184, 51-67
- (41) Quintanar-Guerrero, D., Fessi, H., Allemann, E. and Doelker, E. (1996) Influence of stabilizing agents and preparative variables on the formation of poly(D,L-lactic acid)nanoparticles by an emulsification-diffusion technique. *Int. J. Pharm.* 143, 133-141
- (42) Bradley, A. J. and Scott, M. D. (2004) Separation and purification of methoxypoly(ethylene glycol) grafted red blood cells via two-phase partitioning. *J. Chromatogr. B Analyt. Technol. Biomed. Life Sci.* 807, 163-168
- (43) Rayle, H. and Fellmeth, L. (1999) Development of a Process for Triazine-Promoted Amidation of Carboxylic Acids. *Organic Process Research & Development.* 3, 172-176
- (44) Moghimi, S. M. (2002) Chemical camouflage of nanospheres with a poorly reactive surface: towards development of stealth and target-specific nanocarriers. *Biochim. Biophys. Acta.* 1590, 131-139
- (45) Pugliese, L., Coda, A., Malcovati, M. and Bolognesi, M. (1993) Three-dimensional structure of the tetragonal crystal form of egg-white avidin in its functional complex with biotin at 2.7 Å resolution. *J Mol Biol.* 231, 698-710
- (46) Cannizzaro, S. M., Padera, R. F., Langer, R., Rogers, R. A., Black, F. E., Davies, M. C., Tendler, S. J. and Shakesheff, K. M. (1998) A novel biotinylated degradable polymer for cell-interactive applications. *Biotechnol. Bioeng.* 58, 529-535
- (47) Gref, R., Couvreur, P., Barratt, G. and Mysiakine, E. (2003) Surface-engineered nanoparticles for multiple ligand coupling. *Biomaterials.* 24, 4529-4537
- (48) Tosi, G., Rivasi, F., Gandolfi, F., Costantino, L., Vandelli, M. A. and Forni, F. (2005) Conjugated poly(D,L-lactide-co-glycolide) for the preparation of in vivo detectable nanoparticles. *Biomaterials.* 26, 4189-4195
- (49) Molecular Probes. (2002) Avidin and NeutrAvidin™ Biotin-Binding Proteins and Conjugates. *Product information.*
- (50) Weissenboeck, A., Bogner, E., Wirth, M. and Gabor, F. (2004) Binding and uptake of wheat germ agglutinin-grafted PLGA-nanospheres by caco-2 monolayers. *Pharm. Res.* 21, 1917-1923
- (51) Saxena, V., Sadoqi, M. and Shao, J. (2004) Indocyanine green-loaded biodegradable nanoparticles: preparation, physicochemical characterization and in vitro release. *Int. J. Pharm.* 278, 293-301

6.5 Coupling of biotin-(polyethyleneglycol)amine to poly(D,L-lactide-co-glycolide) nanoparticles for versatile surface modification

(52) Laitinen, O. H., Nordlund, H. R., Hytonen, V. P., Uotila, S. T., Marttila, A. T., Savolainen, J., Airene, K. J., Livnah, O., Bayer, E. A., Wilchek, M. and Kulomaa, M. S. (2003) Rational design of an active avidin monomer. *J. Biol. Chem.* 278, 4010-4014

(53) Qureshi, M. H., Yeung, J. C., Wu, S. C. and Wong, S. L. (2001) Development and characterization of a series of soluble tetrameric and monomeric streptavidin muteins with differential biotin binding affinities. *J. Biol. Chem.* 276, 46422-46428

(54) Howarth, M., Chinnapen, D. J., Gerrow, K., Dorrestein, P. C., Grandy, M. R., Kelleher, N. L., El-Husseini, A. and Ting, A. Y. (2006) A monovalent streptavidin with a single femtomolar biotin binding site. *Nat. Methods.* 3, 267-273

8 Captions

Table 1: Size, polydispersity index (PI) and zeta potential of PLGA NP and BPEG PLGA NP ($n = 3 - 5$).

Figure 1: Schematic illustration of a surface modified PLGA NP by means of BPEG. Figure 1A gives an overview of the aims of the study. Versatile binding of targeting moieties is realized employing avidin (and homologues) conjugates. Binding of fluorescence dye conjugated avidin (and homologues) opens the possibility of an additional fluorescence labelling of the NP. Figure 1B represents a virtual zoom into the NP surface. Assuming homogenous distribution of the BPEG molecules on the NP surface, the mean distance is calculated to 69 Å. The length of the BPEG molecule is determined to roughly 46 Å. The size of avidin is reported to 50 Å × 50 Å × 40 Å with the biotin binding sites in a distance of 29.5 and 20 Å.

Figure 2: Reaction of chemical surface modification of PLGA NP resulting in BPEG PLGA NP.

Figure 3: SPM topography and phase images of PLGA NP, BPEG PLGA NP, and BPEG PLGA NP with associated FITC-Av. (bar = 250 nm)

Figure 4: Results of resonant mirror system (RMS) adhesion studies: interactions of BPEG PLGA NP with a NeutrAvidin (NAv) surface and a NAv surface with BPEG blocked biotin binding sites. An additional curve calculated as the difference of both binding curves represents the extent of specific binding.

Figure 5: xz-Cross sections from a stack of confocal laser scans (apical up) of Rho-RCA stained A549 cells (A), Rho-RCA stained Caco-2 cells (B), and FITC-WGA stained Caco-2 cells (C). Cells were imaged after 6 and 24 h incubation with FITC-NAv labelled BPEG PLGA NP (in case of Rho-RCA stained A549 and Caco-2 cells) and Rho-NAv labelled BPEG PLGA NP (in case of FITC-WGA stained Caco-2 cells). (bar = 50 μm × 5 μm)

6.5 Coupling of biotin-(polyethyleneglycol)amine to poly(D,L-lactide-co-glycolide) nanoparticles for versatile surface modification

Table 1: Size, polydispersity index (PI) and zeta potential of PLGA NP and BPEG PLGA NP.

	Size [nm]	PI	Zeta potential [mV]
PLGA NP	207 ± 4	0.042 ± 0.017	-32.0 ± 3.6
BPEG PLGA NP	207 ± 2	0.051 ± 0.004	-23.0 ± 4.1

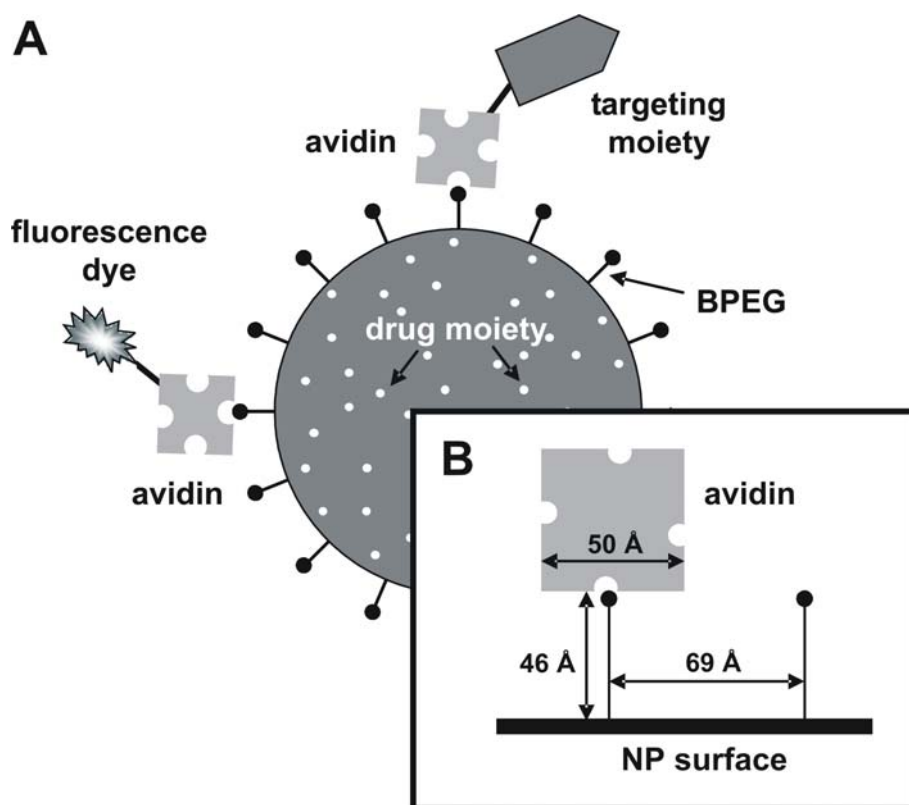


Figure 1: Schematic illustration of a surface modified PLGA NP by means of BPEG. Figure 1A gives an overview of the aims of the study. Versatile binding of targeting moieties is realized employing avidin (and homologues) conjugates. Binding of fluorescence dye conjugated avidin (and homologues) opens the possibility of an additional fluorescence labelling of the NP. Figure 1B represents a virtual zoom into the NP surface. Assuming homogenous distribution of the BPEG molecules on the NP surface, the mean distance is calculated to 69 Å. The length of the BPEG molecule is determined to roughly 46 Å. The size of avidin is reported to 50 Å × 50 Å × 40 Å with the biotin binding sites in a distance of 29.5 and 20 Å.

6.5 Coupling of biotin-(polyethyleneglycol)amine to poly(D,L-lactide-co-glycolide) nanoparticles for versatile surface modification

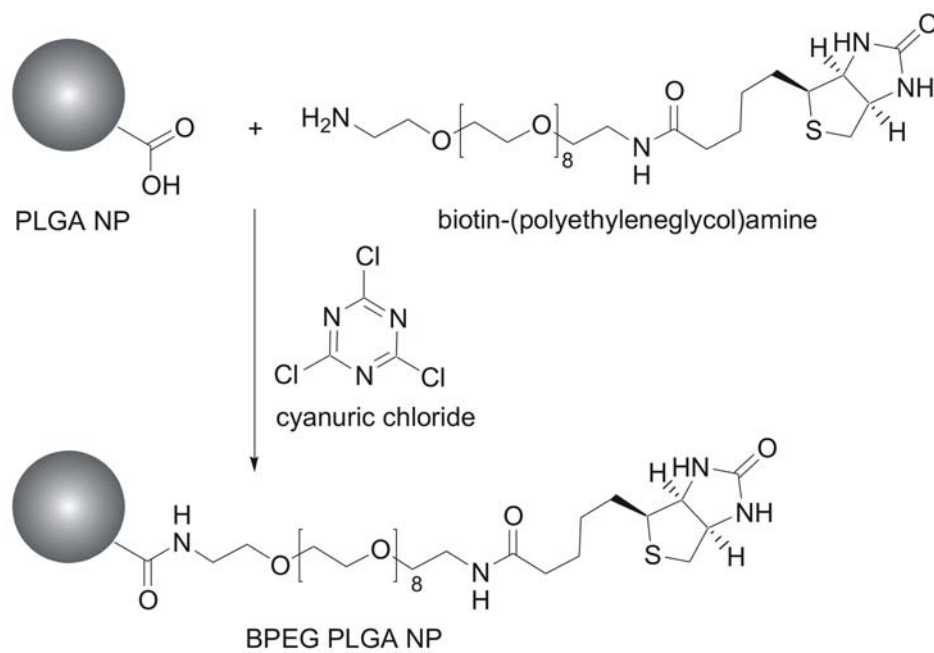


Figure 2: Reaction of chemical surface modification of PLGA NP resulting in BPEG PLGA NP.

6.5 Coupling of biotin-(polyethyleneglycol)amine to poly(D,L-lactide-co-glycolide) nanoparticles for versatile surface modification

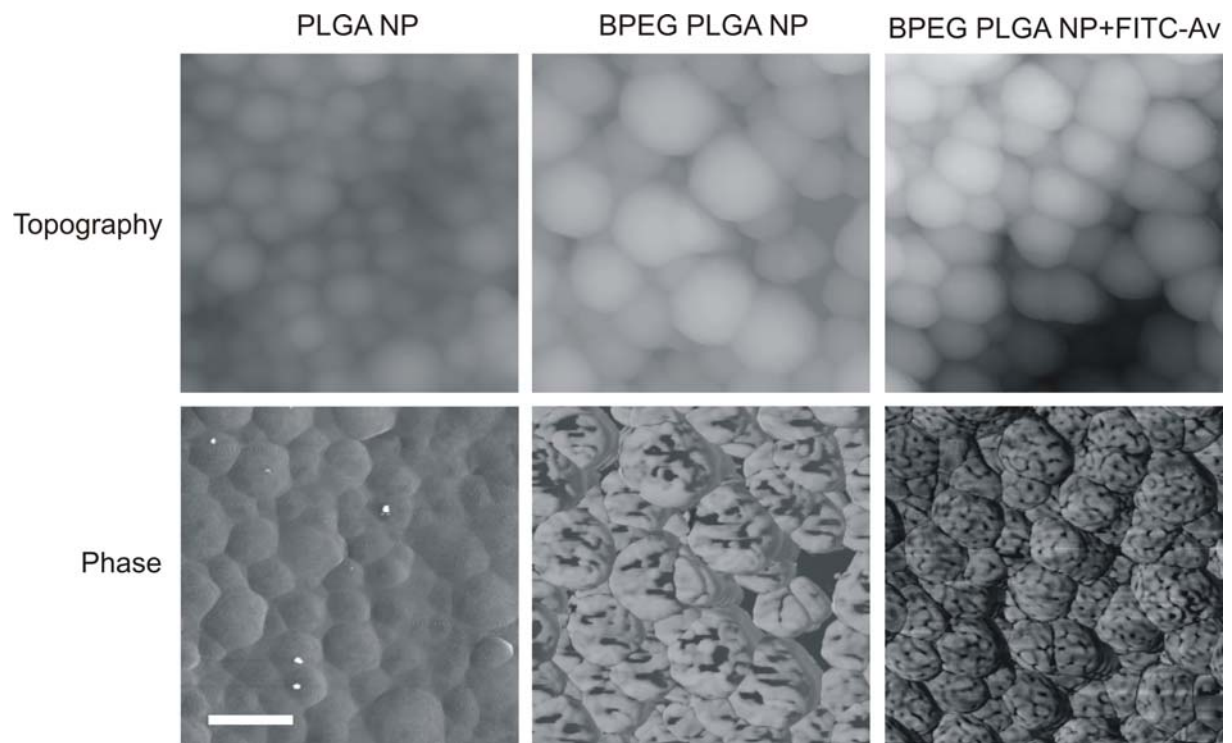


Figure 3: SPM topography and phase images of PLGA NP, BPEG PLGA NP, and BPEG PLGA NP with associated FITC-Av. (bar = 250 nm)

6.5 Coupling of biotin-(polyethyleneglycol)amine to poly(D,L-lactide-co-glycolide) nanoparticles for versatile surface modification

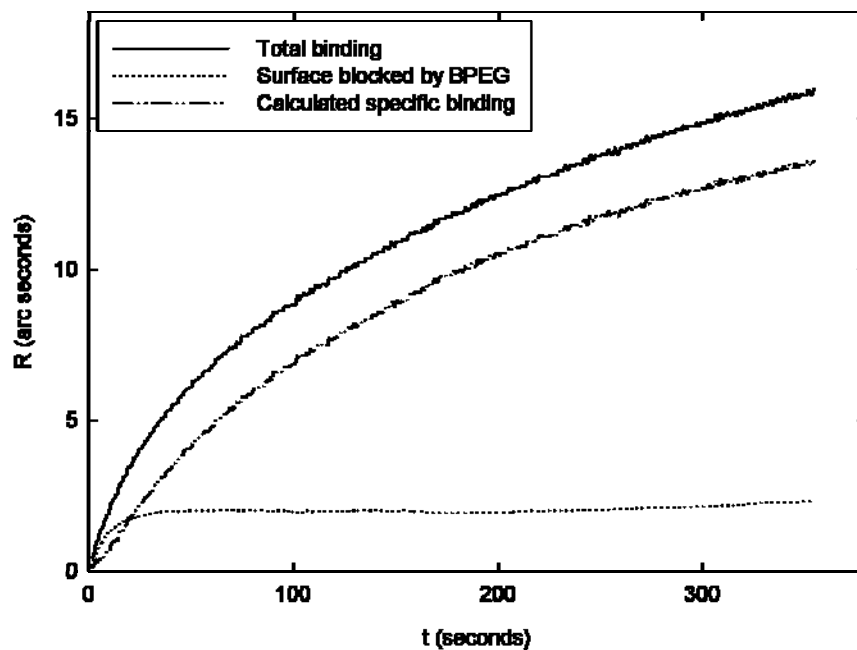


Figure 4: Results of resonant mirror system (RMS) adhesion studies: interactions of BPEG PLGA NP with a NeutrAvidin (NAv) surface and a NAv surface with BPEG blocked biotin binding sites. An additional curve calculated as the difference of both binding curves represents the extent of specific binding.

6.5 Coupling of biotin-(polyethyleneglycol)amine to poly(D,L-lactide-co-glycolide) nanoparticles for versatile surface modification

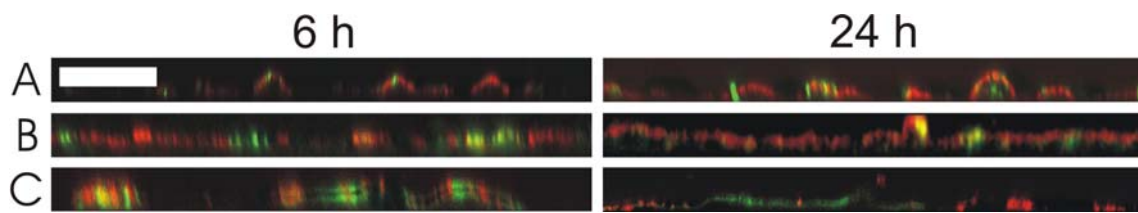


Figure 5: xz-Cross sections from a stack of confocal laser scans (apical up) of Rho-RCA stained A549 cells (A), Rho-RCA stained Caco-2 cells (B), and FITC-WGA stained Caco-2 cells (C). Cells were imaged after 6 and 24 h incubation with FITC-NAv labelled BPEG PLGA NP (in case of Rho-RCA stained A549 and Caco-2 cells) and Rho-NAv labelled BPEG PLGA NP (in case of FITC-WGA stained Caco-2 cells). (bar = $50 \mu\text{m} \times 5 \mu\text{m}$)

Unpublished results

1 Introduction

As described in detail in the publication 'Coupling of biotin-(polyethylene-glycol)amine to poly(D,L-lactide-co-glycolide) nanoparticles for versatile surface modification', a procedure for surface functionalization of preformed NP was developed aiming for subsequent versatile conjugation of targeting ligands and fluorescence dyes under mild conditions. For this purpose, the avidin-biotin system was chosen such that biotin-(polyethyleneglycol)amine (BPEG) modified poly(D,L-lactide-co-glycolide) (PLGA) NP (BPEG PLGA NP) bind to conjugates of avidin (Av) and its homologues streptavidin (SAv) and NeutrAvidin (NAv). Consequently, both targeting moieties and fluorescence labels may be easily linked to the surface of thus functionalized NP by brief incubation in aqueous medium as long as they are available as conjugates of Av (or homologues). Such method may be well applicable to NP made from any other aliphatic polyester like PLA, PGA, or block-copolymers¹⁻³ which may eventually already contain active pharmacological ingredients. Thereby, harsh preparation conditions like shearing, heating, or the presence of organic solvents can be avoided.

In the publication, binding studies and calculations to scale of the surface of BPEG PLGA NP revealed optimal conditions for subsequent specific binding of Av linked compounds. Successful fluorescence labelling of BPEG PLGA NP was confirmed employing diverse NAv linked fluorescence dyes. In a first biological evaluation, such fluorescent NP were shown to be well suitable to study differences in binding and uptake using two epithelial cell lines (Caco-2, A549).

Objectives of the present chapter were based on the results of the publication 'Coupling of biotin-(polyethylene-glycol)amine to poly(D,L-lactide-co-glycolide) nanoparticles for versatile surface modification'.

First, the fluorescence labelling of BPEG PLGA NP by means of FITC-NeutrAvidin (FITC-NAv) was studied. This has already been qualitatively been proven in the publication, aiming for a quantification of the labelling efficiency. Second, the surface binding of horse radish peroxidase- streptavidin (HRP-SAv) as a model protein conjugate was examined. HRP-SAv may be replaced by any Av (or homologues) linked proteinogenic

targeting moiety (e.g. lectins or antibodies) which may be easily produced by covalent cross-linking^{4, 5} or by biotechnological methods.⁶ In the context of those binding experiments and in order to illuminate the results, additional studies on the effect of biotin and BPEG in solution on the fluorescence and enzymatic activity of FITC-NAv and HRP-SAv, respectively, were performed.

2 Materials and methods

2.1 Materials

BPEG PLGA NP and blank PLGA NP were prepared as described in the publication 'Coupling of biotin-(polyethylene-glycol)amine to poly(D,L-lactide-co-glycolide) nanoparticles for versatile surface modification'. 3,3',5,5'-Tetramethylbenzidine (TMB), biotin-(polyethyleneglycol)amine (BPEG), and biotin were obtained from Sigma (Sigma Chemical Co., St. Louis, MO, USA). FITC-NeutrAvidin™ conjugate (FITC-NAv) and horse radish peroxidase-streptavidin conjugate (HRP-SAv) were purchased from Pierce (Perbio Science Deutschland GmbH, Bonn, GE). All other chemicals were of analytical grade.

2.2 Binding of proteins to biotin-(polyethyleneglycol)amine modified nanoparticles

Binding studies were performed in an inverse setup. The fluorescence (FITC-NAv) or absorption (HRP-SAv) derived from a protein containing particle suspension and from the supernatant of a centrifuged protein containing particle suspension were determined with respect to the fluorescence or absorption derived from the overall protein amount applied in the assays. Thereby, the protein concentrations were chosen in order to provide at least one protein molecule per biotin binding site on the BPEG PLGA NP. For comparison, binding to non-modified PLGA NP was investigated analogously. Reference samples were particle-free, however, treatment was the same. All experiments were performed in demineralised water.

2.2.1 FITC-NeutrAvidin

150 µl of NP suspension were incubated with 150 µl of FITC-NAv (100 µg/ml) for 30 min at room temperature under gentle shaking and protection from light. From this

mixture, 100 μl of sample were withdrawn to determine the overall fluorescence. After centrifugation at 23,147 for 10 min, 100 μl of sample were withdrawn from the supernatant to determine the supernatant fluorescence. The fluorescence of all samples was measured using a Cytofluor II fluorescence reader (PerSeptive Biosystems, Wiesbaden-Norderstedt, GE); excitation and emission wavelengths were 485 and 530 nm, respectively. In preliminary experiments it was confirmed that blank BPEG PLGA NP and PLGA NP did not exhibit fluorescence under these conditions. The number of replicates was $n = 3$ and results are expressed as mean \pm SD. Statistical analysis was performed using SigmaStat 3.0 (Systat Software GmbH, Erkrath, GE).

2.2.2 Horse radish peroxidase-streptavidin

100 μl of NP suspension were incubated with 100 μl of HRP-SAv (2 $\mu\text{g}/\text{ml}$) solution for 30 min at room temperature under gentle shaking. From this mixture, 50 μl were withdrawn (overall sample). After centrifugation at 23,147 g for 10 min, 50 μl were withdrawn from the supernatant (supernatant sample). The samples were diluted 1:2000 until the concentrations were appropriate for subsequent reaction with TMB. Then, 100 μl of TMB was added to 50 μl of each diluted sample and incubated for 30 min under protection from light. After addition of 100 μl of 0.5 M H_2SO_4 , the formation of a bluish dye was determined at 450 nm using a Tecan SLT spectrophotometer (Tecan Deutschland GmbH, Crailsheim, GE). In preliminary experiments it was confirmed that blank BPEG PLGA NP and PLGA NP did not influence the formation of dye under these conditions. The number of replicates was $n = 3$ to 5 and results are expressed as mean \pm SD. Statistical analysis was performed using SigmaStat 3.0.

2.3 Effect of biotin and biotin-(polyethyleneglycol)amine on FITC-NeutrAvidin

BPEG and biotin solutions were 1:2 diluted with a 142 $\mu\text{g}/\text{ml}$ FITC-NAv solution in demineralised water and incubated for 10 min under gentle shaking and protection from light. Subsequently, fluorescence measurements were performed again using excitation and emission wavelengths of 485 and 530 nm, respectively.

Biotin and BPEG solutions were applied in concentrations from 0 to 28 $\mu\text{g}/\text{ml}$ and from 0 to 100 $\mu\text{g}/\text{ml}$, respectively. The concentrations were chosen to comprise the intervals of a possible saturation of one to four biotin binding sites of NAv. The experiments were

performed with $n = 3$ repeats. The results are expressed as relative fluorescence (mean \pm SD) i.e. the fluorescence of the BPEG and biotin solutions in regard to the fluorescence of a blank FITC-NAv solution of the same concentration.

2.4 Effect of biotin and biotin-(polyethyleneglycol)amine on horse radish peroxidase-streptavidin

BPEG and biotin solutions were 1:2 diluted with a $1 \cdot 10^{-9}$ mg/ml HRP-SAv solution in demineralised water and incubated for 10 min under gentle shaking. 100 μ l of TMB was added to 50 μ l of each sample and incubated for 30 min under protection from light. After addition of 100 μ l of 0.5 M H_2SO_4 the formation of a bluish dye was determined as described in 2.2.2.

Biotin and BPEG solutions were applied in concentrations from 0 to $1 \cdot 10^{-7}$ mg/ml and from 0 to $4 \cdot 10^{-7}$ mg/ml, respectively. The concentrations were chosen to comprise the intervals of a possible saturation of one to four biotin binding sites of SAv. Experiments were performed with $n = 3$ repeats. Results are expressed as relative absorption i.e. the absorption derived from of the BPEG and biotin solutions in regard to the absorption derived from a blank HRP-SAv solution of the same concentration catalyzing the formation of a bluish dye.

3 Results

3.1 Binding of FITC-NeutrAvidin

As outlined in Figure 1, there was no statistically significant difference between the relative fluorescence in the overall and in the supernatant samples of BPEG PLGA NP (ANOVA, $P = 0.48$). However, the difference between all other samples (ANOVA, $P < 0.05$) was statistically significant. In comparison to the reference, the relative fluorescence was increased in case of BPEG PLGA NP and PLGA NP. Moreover, centrifugation of the overall samples led to an obvious loss of fluorescence in case of the PLGA NP and the reference.

Since employing the same FITC-NAv amount, the overall BPEG PLGA NP, the overall PLGA NP, and both reference samples should have exhibited the same relative fluorescence. Moreover, assuming a specific binding of FITC-NAv to BPEG PLGA NP

and minor non-specific binding to PLGA NP the fluorescence in the supernatant should have been decreased when compared to the overall sample.

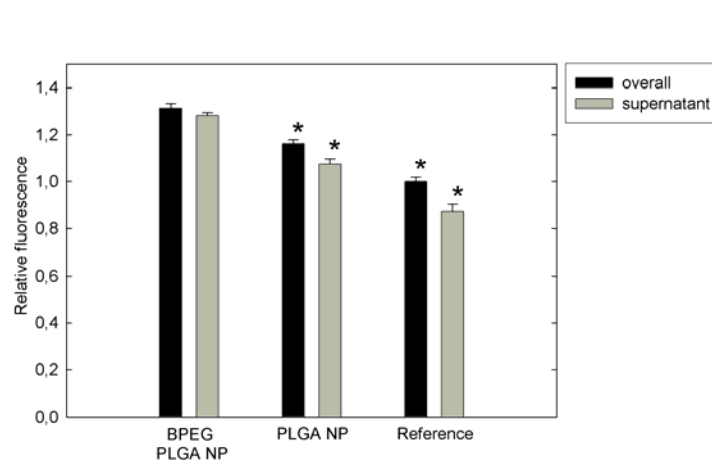


Figure 1: Fluorescence of the overall and of the supernatant samples relative to the fluorescence of the applied FITC-NAv amount in the assay. Test substances were BPEG PLGA NP and PLGA NP. References were particle-free, however, treated analogously.

3.2 Binding of horse radish peroxidase-streptavidin

The absorption at 450 nm which derived from the formation of a bluish dye catalyzed by HRP was practically the same in all samples (Figure 2). There was no statistically significant difference (ANOVA, $P = 0.985$).

In accordance to 3.1, a smaller relative absorption in the supernatant samples of both particle species than in the overall samples and in the reference samples was expected due to specific binding in case of BPEG PLGA NP and non-specific binding in case of PLGA NP.

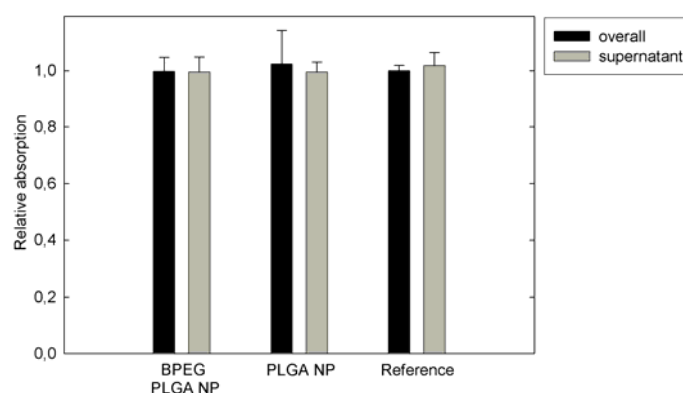


Figure 2: Absorption (450 nm) of the overall and of the supernatant samples relative to the absorption of the amount of HRP-SAv applied in the assay; absorption derived from the formation of a bluish dye catalyzed by HRP. Test substances were BPEG PLGA NP and PLGA NP. References were particle-free, however, treated analogously.

3.3 Effects of biotin and biotin-(polyethyleneglycol)amine on FITC-NeutrAvidin

3.3.1 Biotin

Figure 3A shows that different biotin concentrations led to altered fluorescence of a FITC-NAv solution. The initial increase of the relative fluorescence could be described by an asymptotic function of the form $y = a - b \cdot c^x$ ($a = 1.4$, $b = 0.38$, $c = 7.3 \cdot 10^{-7}$, $R^2 = 0.998$; an exponential fit of same quality was also possible) (Figure 3B). For concentrations between 0.21 and 0.90 $\mu\text{g/ml}$ the fluorescence reached a plateau, until, at higher concentration, the fluorescence decreased up to 31% with regard to a blank FITC-NAv solution. At a concentration of 1.4 $\mu\text{g/ml}$, biotin saturation of 4 potential biotin binding sites of all FITC-NAv molecules applied in the assay was theoretically possible.

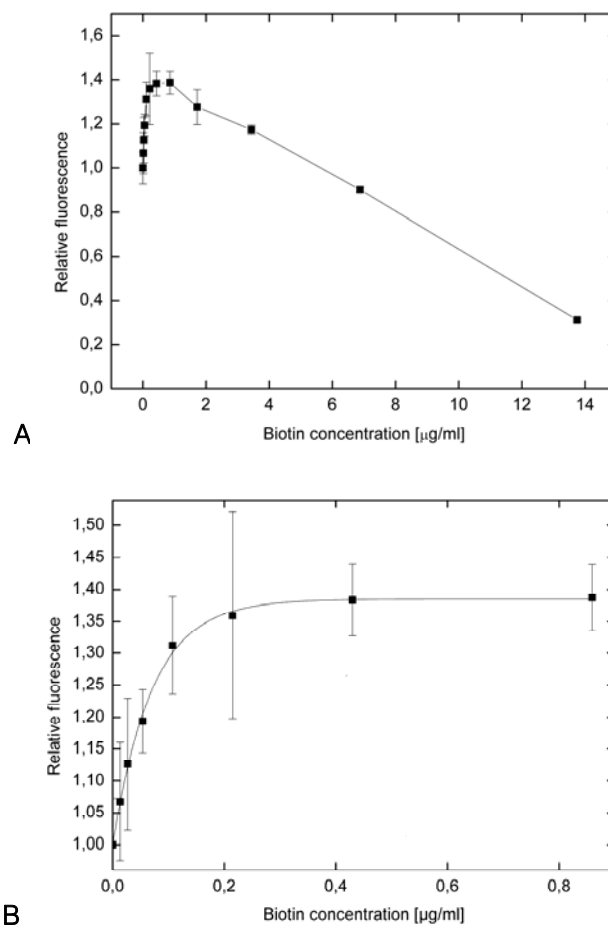


Figure 3: Fluorescence of a FITC-NAv solution containing different concentrations of biotin with regard to a blank FITC-NAv solution (A), and a zoom into A in a concentration range of 0 to 0.90 $\mu\text{g/ml}$ fitted by an asymptotic function (B).

3.3.2 Biotin-(polyethyleneglycol)amine

BPEG led to an increased fluorescence of a FITC-NAv solution (Figure 4A). As with biotin, the initial increase in the relative fluorescence could be described by an asymptotic function of the form $y = a \cdot b \cdot c^x$ ($a = 1.3$, $b = 0.36$, $c = 0.018$, $R^2 = 0.862$) (Figure 4B). For concentrations ranging from 0.49 to 6.30 $\mu\text{g/ml}$ the fluorescence reached a plateau. However, in contrast to the results obtained with biotin, at higher concentration, the fluorescence increased up to 263% with regard to a blank FITC-NAv solution. At a concentration of 3.9 $\mu\text{g/ml}$ BPEG, saturation of 4 potential biotin binding sites of all FITC-NAv molecules applied in the assay was theoretically possible.

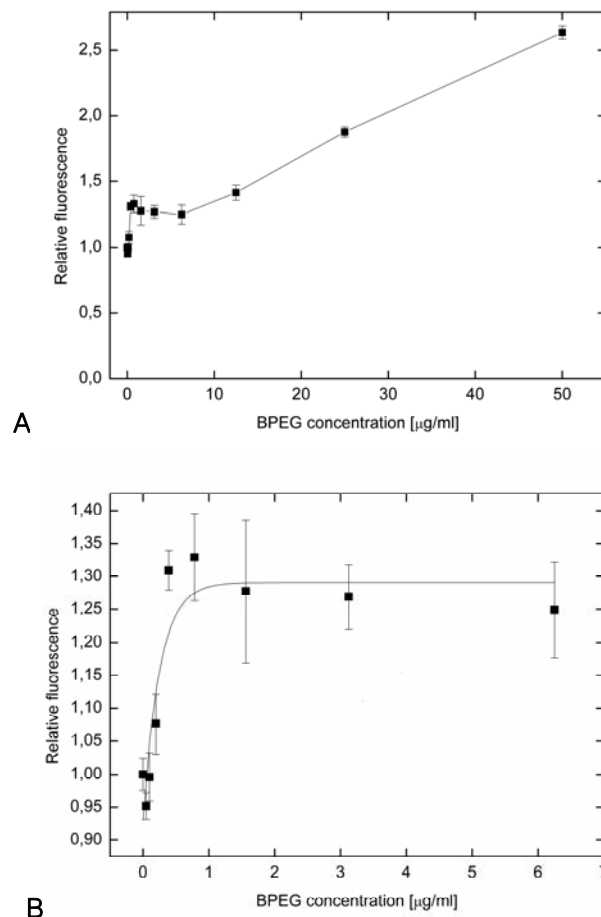


Figure 4: Fluorescence of a FITC-NAv solution containing different concentrations of BPEG with regard to a blank FITC-NAv solution (A), and a zoom into A in a concentration range of 0 to 6.30 $\mu\text{g/ml}$ fitted by an asymptotic function (B).

3.4 Effects of biotin and biotin-(polyethyleneglycol)amine on horse radish peroxidase-streptavidin

In contrast to FITC-NAv, biotin and biotin-(polyethyleneglycol)amine in different concentrations did not exhibit influence on HRP-SAv i.e. the formation of a bluish dye from TMB catalyzed by HRP was practically the same when compared to a blank HRP-SAv solution.

4 Discussion

Aiming for a quantification of particle bound proteins, first the interaction of BPEG PLGA NP and PLGA NP with FITC labelled NAv were studied. From those experiments a decrease in fluorescence of the supernatant samples was expected when compared to the overall samples being ascribed to a specific binding mediated by a number of roughly 2,600 biotin molecules surface associated to one single BPEG PLGA NP (see the publication 'Coupling of biotin-(polyethylene-glycol)amine to poly(D,L-lactide-co-glycolide) nanoparticles for versatile surface modification'), and due to a low non-specific binding in case of PLGA NP. However, with both NP species, an increase in fluorescence of the overall as well as the supernatant samples was found in regard to a blank FITC-NAv solution of the same concentration (Figure 1). To explain these results, the effects of BPEG and biotin on the fluorescence of FITC-NAv were investigated. Both biotin and BPEG containing FITC-NAv solutions showed an increase of fluorescence in regard to a blank FITC-NAv solution of the same concentration up to 140%. A plateau was reached close to concentrations where a saturation of all biotin binding sites of NAv is most likely (Figures 3A and 4A). At higher concentration, however, biotin decreased, whereas BPEG increased the fluorescence of FITC-NAv (Figures 3B and 4B), thus indicating a strong influence of the PEG chain on those effects.

The Av-biotin system is widely used in fluorescent immunoassays^{7, 8} where fluorescence labelled Av (and homologues) bind to a biotinylated primary antibody, whereas excessive reagents are generally removed by washing. Finally, the fluorescence of fluorescence labelled Av molecules in the same state, i.e. bound to an average number of biotin molecules linked to the primary antibody, is determined. In contrast, with the experimental setup applied, the overall fluorescence derived from free FITC-NAv as well as from biotin associated FITC-NAv. In the presence of different biotin concentrations,

FITC-NAv molecules may exist in different states and their fluorescence might be not comparable due to different interactions between Av and biotin (e.g. fluorescence amplification or quenching).

Considering the arrangement of the BPEG grafts on the surface of the NP, the PEG chain is connected to the particle core, whereas the biotin molecule may be directed versus the surrounding medium. It might be speculated that the effects of biotin - and not those of BPEG - can display the real effects of BPEG PLGA NP on FITC-NAv. However, in binding experiments FITC-NAv was applied in concentrations providing at least one protein molecule per each biotin binding site on the BPEG PLGA NP. Consequently, the concentration of biotin was in the range of the asymptotic increase of relative fluorescence of FITC-NAv, thus explaining the elevated relative fluorescence of a BPEG PLGA NP containing FITC-NAv solution, irrespective if the proteins finally interact with biotin or PEG linked biotin.

The elevated fluorescence of FITC-NAv in the presence of PLGA NP has not been explored in detail, however, it might be suggested that non-specific interactions can also influence the fluorescence of FITC-NAv, comparable to effects of the PEG chain.

The NP bound FITC-NAv amount was determined in an inverse setup in order to avoid quantification errors due to cross-linking of particles as with a direct method. Comparing the relative fluorescence of the overall and supernatant samples of BPEG PLGA NP, no statistically significant difference was detected (Figure 1). Obviously, either the NP bound amount of FITC-NAv was too small to be detected by the experimental setup, or, most likely, the BPEG chains had been sheared off the NP cores by high centrifugation forces when separating the NP from the supernatant. This theory is further confirmed by an increased relative fluorescence in case of BPEG PLGA NP which must have derived from binding of biotin to FITC-NAv resulting in effects as discussed above.

In case of PLGA NP there was a significant decrease of relative fluorescence in the supernatant samples (Figure 1) which might result from stronger non-specific binding of the proteins directly to the NP surface, hence, resisting high centrifugation forces. However, also an unexpected decrease of fluorescence in the supernatant samples of the reference was detected. This may only be attributed to either protein loss by adsorption to plastic material or by small protein aggregation and removal during

centrifugation, thus representing also a possible explanation for the findings with PLGA NP.

In the second study, commercially available HRP-SAv was employed as a model to investigate the binding of protein conjugates to the surface of NP. Thereby, HRP-SAv may be replaced by versatile proteinogenic targeting moieties as long as they are available as conjugates of Av (and homologues). As in case of FITC-NAv, in order to investigate both specific and non-specific binding BPEG PLGA NP and PLGA NP were employed. However, with the experimental setup applied, an evidence of HRP-SAv binding to each of the particle species could not be provided. The relative absorption representing the particle associated and free protein amount was not significantly different when comparing the supernatant, the overall, and the reference samples (Figure 2). In contrast to FITC-NAv, no influence of biotin and BPEG interaction with the biotin binding sites of the SAv compound on the activity of HRP could be determined. Analogous to the results with FITC-NAv, the results obtained with HRP-SAv suggest that the proteins either bound to the surface of both NP species in amounts below the detection limit, or that they were sheared off by high centrifugation forces when separating the NP from the supernatant. In conclusion, the present results are not sufficiently clarified, yet. Studies of the protein binding combined with an improvement of the experimental setup ought to be subject of further investigations.

5 Conclusion

Successful binding of FITC-NAv to BPEG PLGA NP was confirmed, however, quantification of the binding of FITC-NAv and HRP-SAv to BPEG PLGA NP and PLGA NP was not possible by means of the inverse experimental setup applied in this study. The fluorescence intensity of FITC-NAv turned out to be dependent on the concentration of biotin and BPEG indicating that the determination of the particle attached amounts of FITC-NAv might only be possible by a direct method like quantification of the particle bound protein amount instead of the protein amount in the supernatant of the assay. In case of HRP-SAv, no effects of biotin and BPEG on the HRP enzyme activity were found within the applied range of concentration. Centrifugation in order to separate NP from the supernatant, is assumed to result in

6.5 Coupling of biotin-(polyethyleneglycol)amine to poly(D,L-lactide-co-glycolide) nanoparticles for versatile surface modification

shearing off BPEG chains from the NP cores, thus strengthening the demand to apply a gentle method for particle separation in future.

6 References

1. D. Shenoy, S. Little, R. Langer and M. Amiji, Poly(ethylene oxide)-modified poly(beta-amino ester) nanoparticles as a pH-sensitive system for tumor-targeted delivery of hydrophobic drugs: part 2. In vivo distribution and tumor localization studies. *Pharm Res*: 22, 2107-2114 (2005)
2. Y. Duan, X. Sun, T. Gong, Q. Wang and Z. Zhang, Preparation of DHAQ-loaded mPEG-PLGA-mPEG nanoparticles and evaluation of drug release behaviors in vitro/in vivo. *J Mater Sci Mater Med*: 17, 509-516 (2006)
3. O. C. Farokhzad, J. Cheng, B. A. Teply, I. Sherifi, S. Jon, P. W. Kantoff, J. P. Richie and R. Langer, Targeted nanoparticle-aptamer bioconjugates for cancer chemotherapy in vivo. *Proc Natl Acad Sci U S A*: 103, 6315-6320 (2006)
4. B. Simons, H. Kaplan and M. A. Hefford, Novel cross-linked enzyme-antibody conjugates for Western blot and ELISA. *J Immunol Methods*: 315, 88-98 (2006)
5. T. Iwamasa, N. Ninomiya, T. Hamada and S. Fukuda, Immunohistochemical localization of acid alpha-glucosidase in rat liver. *J Histochem Cytochem*: 30, 378-384 (1982)
6. A. Stallmach, T. Marth, B. Weiss, B. M. Wittig, A. Hombach, C. Schmidt, M. Neurath, M. Zeitz, S. Zeuzem and H. Abken, An interleukin 12 p40-IgG2b fusion protein abrogates T cell mediated inflammation: anti-inflammatory activity in Crohn's disease and experimental colitis in vivo. *Gut*: 53, 339-345 (2004)
7. Q. P. Qin, T. Lovgren and K. Pettersson, Development of highly fluorescent detection reagents for the construction of ultrasensitive immunoassays. *Anal Chem*: 73, 1521-1529 (2001)
8. K. K. Sin, C. P. Chan, T. H. Pang, M. Seydack and R. Renneberg, A highly sensitive fluorescent immunoassay based on avidin-labeled nanocrystals. *Anal Bioanal Chem*: 384, 638-644 (2006)

7 Summary / Zusammenfassung

Summary

Subjects of the present thesis were the formulation, characterization, and evaluation of poly(lactic acid-co-glycolic acid) (PLGA) based nanoparticulate systems addressing the biological barriers intestine and skin.

This work was focussed on the following three main subjects:

- Preparation, characterization, and evaluation of fluoresceinamine labelled PLGA nanoparticles to study their interaction with inflamed intestinal tissue *in vivo* in humans
- Studies on skin permeation and penetration of fluorescent and drug containing nanoparticles *in vitro* and *in vivo*
- Development and evaluation of surface biotinylated nanoparticles for coupling of versatile ligands

Preparation, characterization, and evaluation of fluoresceinamine labelled PLGA nanoparticles

Previously, Alf Lamprecht and co-workers studied a size dependent accumulation and prolonged retention of orally administered micro- and nanoparticles (NP) in inflamed regions of the intestine - whilst concentrating anti-inflammatory drugs at their site of action - in an animal model. Based on these promising results, such novel concept has to be proven *in vivo* in a clinical study with patients suffering from inflammatory bowel diseases (IBD). For this purpose, drug-free but fluorescence labelled non-toxic NP were developed and evaluated to show their accumulation in inflamed areas of the intestinal mucosa in IBD patients by means of fluorescence microscopy.

For a stable fluorescence labelling, PLGA was covalently modified with 5-fluoresceinamine (FA), which was found to represent a simple, reproducible, and efficient method of polymer labelling (efficiency 65%). From such polymer (FA-PLGA),

fluorescent NP (FA-PLGA NP) in the size of 270 nm were prepared by means of nanoprecipitation. In regard to an *in vivo* application of the NP in IBD, this size order is expected to be adequate for the detection of even single particles in biological tissue, whilst still likely to display an enhanced accumulation and retention in inflamed mucosal areas. FA-PLGA NP were almost uncharged as consequence of polymer modification. Compared to NP prepared by encapsulation of FC using the classic water-in-oil-in-water method, NP from FA-PLGA exhibited a much better labelling stability which is crucial for the intended studies. In degradation experiments, increasing pore formation and changes in the elastic properties of FA-PLGA NP was shown with time; thereby, the NP size stayed unchanged. With respect to future application in a clinical study, FA-PLGA NP can be re-constituted without significant changes in size and size distribution after lyophilisation without cryoprotectants. Moreover, the NP were well to visualize and to quantify with low detection limit in preliminary experiments with porcine intestinal tissue.

In order to evaluate the interaction with intestinal epithelial cells, FA-PLGA NP were applied on an *in vitro* model of the intestinal mucosa (Caco-2 cell culture) addressing absorption and potential cytotoxicity. A transport of FA-PLGA NP across Caco-2 monolayers was not found, but transport of minor amounts of their fluorescent degradation products which, however, was approximately 500 times smaller than the transport of the low permeability marker FC. The cytotoxicity of FA-PLGA NP was studied to be significantly (750 fold) smaller than in case of the non-toxic diagnostic agent fluorescein sodium.

In conclusion, polymer modification allowed to prepare fluorescence labelled NP from a biodegradable polymer with sufficient stability to be monitored over a period of several days. Due to very low cytotoxicity and only negligible transport of NP degradation products over an *in vitro* cell culture model of the intestinal mucosa, FA-PLGA NP appear as valuable tool to study their interaction with inflamed intestinal tissue in IBD in terms of an *in vivo* application in a clinical study.

Studies on skin permeation and penetration of fluorescent and drug containing nanoparticles

Major subject of this part of the present thesis was to investigate and to visualize NP transport, storage and drug release in skin *in vitro* and *in vivo*, thereby, employing fluorescence labelled and drug containing NP from PLGA. The following three topics have been explored in detail:

Several studies have recently revealed significant influence of hair follicles on the penetration of topically applied substances into the skin, such as low molecular weight compounds and NP. Still, however, penetration and storage features of topically applied NP formulations needs to be explored in detail. Here, the penetration and storage of compounds in free and nanoencapsulated form in hair follicles was compared *in vitro* on porcine skin using FA-PLGA NP and a particle-free sodium fluorescein formulation of the same dye concentration. It was found that NP penetrated much deeper into the hair follicles than the dye derived from the particle-free formulations if a massage had been applied. Analyzing the storage behaviour of both formulations *in vivo* in humans, NP were shown to be stored in the hair follicles much longer (up to 10 days) than the particle-free formulation.

Explaining these results, it was hypothesized that the surface structure of the skin, in particular of the cuticle, may act as a geared pump pushing particles deeper into hair follicles than smaller sized compounds and, at the same time, decelerating particle removal by sebum excretion.

Multiphoton microscopy was employed to simultaneously study and visualize the penetration and drug release of NP - embedded in a gel matrix - in excised human skin. For that purpose, a dually fluorescence labelled nanoparticulate model system was developed, where the first fluorescence dye was stable entrapped in the polymer core and the second dye mimicked a drug to be released. The FA-PLGA NP formulation was advanced to an additional encapsulation of Texas Red as a model drug employing an oil-in-water method. Two-colour labelled NP exhibited a size of 290 nm, narrow size distribution, spherical shape, and a smooth surface.

Multiphoton fluorescence imaging enabling three-dimensional tracing of individual NP with diffraction-limited resolution indicated that fluorescence labelled NP were not able to penetrate the stratum corneum, but stayed in the gel-filled dermatoglyphs over 5 h. Two-photon spectral imaging was applied to investigate the distribution of the model drug Texas Red as a function of time. The Texas Red content in the NP turned out to be low and basically constant, whereas the concentration of Texas Red dropped in the gel matrix and increased in the deeper stratum corneum and stratum granulosum, indicating a slow penetration of the dye from the gel into the skin with time. Multitracking experiments after 5 h of incubation allowed a co-localization of FA which was strictly bound to the NP, Texas Red which was found to be penetrated into the skin to a predominant fraction, and keratin.

Concluding, multiphoton microscopy combined with spectral imaging was found to allow non invasive long term studies of the penetration of dually fluorescence labelled NP into skin with sub-cellular resolution, thereby, even discriminating between particle bound and released dye. Due to virtually no out-of-focus effects of the scanning laser beam, this technique is considered gentle for both *in vitro* and *in vivo* studies.

Subsequently, PLGA NP were chosen as a valuable carrier system to investigate the influence of nanoencapsulation on the permeation and penetration of the lipophilic model drug flufenamic acid (FFA) into excised human skin. It was found that an oil-in-water method was most appropriate to encapsulate FFA into PLGA NP. Resulting FFA NP were in the size order of 330 nm, had a narrow size distribution and a high drug entrapment. Moreover, the particles exhibited spherical shape and smooth surface which were even contained after incorporation in Natrosol hydrogel to give the final particle formulation. Penetration and permeation results were acquired using the Saarbrücken penetration model and Franz diffusion cells as *in vitro* test systems. Comparing the transport of a FFA NP formulation and FFA formulation with same drug content, no differences were found for the stratum corneum. Drug accumulation in the deeper skin layers and drug transport across the epidermis were slightly delayed in case of the nanoencapsulated FFA compared to free FFA after shorter incubation times (<12 h). However, after longer incubation times, nanoencapsulated FFA showed a statistically significantly enhanced transport and accumulation. The mechanisms for

such results remained unclear. It has been speculated that some acidification of the particles and their surroundings as a consequence of PLGA degradation may favour the non-ionized form of FFA, thus leading to enhanced penetration through the stratum corneum. When visualizing FFA NP on excised human skin, they were found to be homogeneously distributed on the skin surface and within the dermatoglyphs; no NP were within or between the corneocytes.

Development and evaluation of surface biotinylated nanoparticles

Generally, polymeric NP for drug targeting are designed to entrap the drug moiety in the core and to present the targeting moiety on the surface, thereby using specific techniques for each compound to be entrapped or attached.

The subject of the final part of this thesis was to develop a procedure for surface functionalization of preformed NP, which may eventually already contain active pharmacological ingredients, for subsequent versatile conjugation of targeting ligands and fluorescence dyes under mild conditions. For that purpose, an approach where surface biotinylated NP bind to conjugates of avidin (or its homologues streptavidin or NeutrAvidin) was opted. Consequently, both targeting moieties as well as fluorescence labels may be easily linked to the surface of thus functionalized NP as long as they are available as conjugates of avidin.

PLGA NP in the size of 210 nm were prepared by the classic oil-in-water method and, subsequently functionalized with biotin-(polyethyleneglycol)amine (BPEG) employing cyanuric chloride chemistry. By such method, an effective surface biotinylation of NP cores could be demonstrated which appeared to be well suited for subsequent binding of avidin or avidin linked ligands when described to scale. Surface modification did not involve an increase in size or alteration in shape and surface structure. However, functionalized PLGA NP (BPEG PLGA NP) were less negatively charged and exhibited changes in elastic or adhesive properties, which were even more significant after binding of avidin. So far, binding of avidin and homologues to BPEG PLGA NP could only be shown qualitatively, since the quantification of NP bound proteins was not possible using an inverse experimental setup. Specific binding to BPEG PLGA NP was

only given in case of NAv which was further confirmed by resonant mirror measurements.

For a first evaluation in biological systems, differences in binding and uptake of NP were studied in two epithelial cell lines after labelling BPEG PLGA NP with avidin linked fluorescence dyes.

Zusammenfassung

Das Thema der vorliegenden Dissertationsarbeit ist die Formulierung, Charakterisierung und Evaluierung von Nanopartikeln aus Polymilchsäure-co-glykolsäure (PLGA), die an den biologischen Barrieren Darm und Haut zum Einsatz kommen sollen.

Die Arbeit konzentrierte sich auf folgende drei Schwerpunkte:

- Herstellung, Charakterisierung und Evaluierung von fluoreszeinamin-markierten Nanopartikeln aus PLGA, die dazu bestimmt sind, die Wechselwirkung mit entzündeter Darmschleimhaut in einer *In-vivo*-Studie am Menschen zu untersuchen
- *In-vitro*- und *In-vivo*-Untersuchungen von Permeation und Penetration fluoreszierender oder Arzneistoff enthaltender Nanopartikel in die Haut
- Entwicklung und Evaluierung von mit Biotin oberflächenmodifizierten Nanopartikeln, an die vielfältig Liganden gebunden werden sollen

Herstellung, Charakterisierung und Evaluierung von fluoreszeinamin-markierten Nanopartikeln aus PLGA

Alf Lamprecht und Mitarbeiter fanden in Untersuchungen am Tiermodell eine größenabhängige Anreicherung und eine verlängerte Retention von oral verabreichten Mikro- und Nanopartikeln (NP) an der entzündeten Darmschleimhaut. Durch Anwendung partikulärer Systeme gelang es zudem, antientzündliche Wirkstoffe an ihrem Wirkort zu konzentrieren. Auf diese viel versprechenden Ergebnisse aufbauend soll nun ein solches neuartiges Konzept auch in einer klinischen Studie an Patienten mit chronisch-entzündlichen Darmerkrankungen überprüft werden.

Im Rahmen der vorliegenden Arbeit wurden fluoreszenz-markierte Nanopartikel formuliert, um damit in entzündetem Gewebe der Darmschleimhaut Partikelanreicherungen mittels Fluoreszenzmikroskopie aufzuzeigen. Zur stabilen Fluoreszenzmarkierung wurde PLGA kovalent mit 5-Fluoreszeinamin (FA) modifiziert. Diese Methode erwies sich als leicht durchführbar und reproduzierbar und führte zu

einer hohen Modifikationsrate (65%). Aus dem modifizierten Polymer (FA-PLGA) wurden durch Nanopräzipitation fluoreszierende NP (FA-PLGA NP) in der Größe von 270 nm hergestellt. Hinsichtlich einer *In-vivo*-Anwendung dieser NP bei chronisch-entzündlichen Darmerkrankungen ist von dieser Partikelgröße zu erwarten, dass sich einzelne NP gut detektieren lassen und dabei die am Tiermodell beschriebenen Effekte an der Darmschleimhaut zeigen. Infolge der Polymermodifikation waren die FA-PLGA NP nahezu ungeladen.

Im Vergleich zu NP, in die Fluoreszein-Natrium mittels der klassischen Wasser-in-Öl-in-Wasser-Methode verkapselt wurde, waren FA-PLGA NP wesentlich stabiler und setzten weniger Fluoreszenzmarker frei. Somit erschienen sie für eine zukünftige Studie als besser geeignet

In Partikel-Degradationsexperimenten wurde gezeigt, dass FA-PLGA NP mit der Zeit zunehmend Poren entwickeln und Änderungen in den viskoelastischen Eigenschaften erfahren. Die Partikelgröße bleibt dabei aber konstant. Im Hinblick auf eine Anwendung der fluoreszierenden NP in einer klinischen Studie ist es wichtig, dass die fluoreszierenden NP sich ohne Änderungen der Größe und der Größenverteilung nach der Gefriertrocknung rekonstituieren lassen. Dies wurde im Falle der FA-PLGA NP gezeigt, wobei ein Einsatz von Kryoprotektiva nicht notwendig war. In Vorexperimenten am Schweinedarm ließen sich die fluoreszierenden NP gut abbilden und zudem mit niedrigem Detektionslimit quantifizieren.

Um Wechselwirkungen mit epithelialen Darmzellen zu untersuchen, wurden die FA-PLGA NP in einem Zellkulturmodell der Darmschleimhaut (Caco-2-Zellen) auf ihre Absorption und Zytotoxizität geprüft. Ein Transport von NP selbst über den Zell-Monolayer fand nicht statt. Es trat jedoch ein Transport von sehr geringen Mengen ihrer fluoreszierenden Abbauprodukte (ca. 500mal weniger als der „low permeability marker“ Fluoreszein) auf. Die Zytotoxizität der FA-PLGA NP war signifikant geringer (ca. 750mal) als die des ungiftigen Diagnostikums Fluoreszein-Natrium.

Zusammenfassend lässt sich sagen, dass es mit Hilfe der Polymermodifikation gelang, fluoreszierende NP herzustellen, welche sich durch eine ausreichende Stabilität auszeichnen, um über einen Zeitraum von mehreren Tagen im Gewebe verfolgt werden zu können. Da die Partikel sich zudem als wenig zytotoxisch erwiesen und nur ein geringer Anteil ihrer Abbauprodukte im Zellkulturmodell transportiert wurde, scheinen

sie sich sehr gut dazu zu eignen, um in einer zukünftigen *In-vivo*-Studie Wechselwirkungen mit der entzündeten Darmschleimhaut an Patienten mit chronisch-entzündlichen Darmerkrankungen zu untersuchen.

Untersuchung von Permeation und Penetration fluoreszierender oder Arzneistoff enthaltender Nanopartikel in die Haut

Hauptschwerpunkt des zweiten Teils dieser Dissertation war es, den Transport, die Deposition sowie die Freisetzung von Arzneistoffen an der Haut *in vitro* und *in vivo* zu untersuchen und zu visualisieren. Dazu wurden fluoreszierende und arzneistoff-beladene NP eingesetzt. Folgende drei Thematiken wurden dabei bearbeitet:

Verschiedene Studien zeigten in jüngster Zeit, dass Haarfollikel einen bedeutenden Einfluss auf die Penetration von topisch angewendeten Substanzen, kleinen Molekülen wie NP, in die Haut besitzen. Dabei sind die Mechanismen der Penetration und Deposition von topisch applizierten NP noch relativ unklar. Diese wurden nun im Rahmen dieser Arbeit in Form eines Vergleichs zwischen fluoreszierenden FA-PLGA NP und einer partikelfreien Formulierung mit analoger Fluoreszein-Natrium-Konzentration *in vitro* auf Schweinehaut untersucht. Dabei wurde gezeigt, dass NP wesentlich tiefer in Haarfollikel penetrierten als der Fluoreszenzfarbstoff aus der partikelfreien Formulierung, jedoch nur, wenn eine Massage angewendet wurde. Die Untersuchung der *In-vivo*-Deposition beider Formulierungen auf der Haut am Menschen ergab, dass NP bedeutend länger (bis zu 10 Tagen) in den Haarfollikeln verblieben als der freie Fluoreszenzfarbstoff. Aus diesen Ergebnissen ließ sich die Hypothese ableiten, dass die Struktur der Kutikula der Haarschäfte mit einer Zahnradschleuse vergleichbar ist, die Partikel möglicherweise tiefer in Haarfollikel befördert als kleinere Substanzen und gleichzeitig ihren Abtransport im Zuge der Talgabscheidung verlangsamt.

Mittels Multiphotonen-Mikroskopie wurden simultan Penetration und Arzneistoff-freisetzung aus NP auf exzidiertem Humanhaut untersucht und visualisiert; die NP waren dabei in eine Gelmatrix eingebettet. Zu diesem Zweck wurde ein zweifach

fluoreszierendes nanopartikuläres Modellsystem entwickelt, bei dem ein Fluoreszenzfarbstoff stabil im Partikel eingebettet war und der zweite einen Arzneistoff imitierte, der freigesetzt wird. Die im ersten Teil beschriebene NP-Formulierung wurde hierfür weiter entwickelt; Texas Red wurde als Modellarzneistoff unter Anwendung einer Öl-in-Wasser-Methode in NP aus FA-PLGA eingearbeitet. Diese zweifach-fluoreszenzmarkierten NP besaßen eine Größe von 290 nm bei einer engen Größenverteilung. Zudem wiesen sie eine sphärische Form und eine glatte Oberfläche auf.

Multiphotonen-Fluoreszenzmessungen ermöglichten eine dreidimensionale Darstellung von einzelnen NP mit einer Größe unterhalb der Auflösungsgrenze. Es wurde gezeigt, dass die fluoreszenzmarkierten NP nicht in das Stratum Corneum penetrierten, sondern über einen Zeitraum von 5 Stunden in den mit Gel gefüllten Dermatoglyphen verblieben.

Durch spektrale Auswertung der Signale konnte die Verteilung des Modellarzneistoffs Texas Red in der Haut als Funktion der Zeit dargestellt werden. Hierbei war offensichtlich, dass der Texas Red-Gehalt der NP zwar relativ gering, dennoch aber konstant war. Die Texas Red-Konzentration im Gel nahm dagegen mit der Zeit ab, während sie im tieferen Stratum Corneum und im Stratum Granulosum zunahm, was auf eine langsame Penetration des Farbstoffs aus dem Gel in die Haut schließen ließ.

In „Multitracking“-Experimenten nach 5 Stunden Inkubation mit der fluoreszierenden NP-Formulierung ließen sich fluoreszierende Objekte co-lokalisieren: FA, das fest an die NP gebunden war, Texas Red, das zu einem großen Anteil in die Haut penetriert war, und Keratin.

Die Ergebnisse zeigten, dass es Multiphotonen-Mikroskopie mit spektraler Detektion ermöglichen, in Langzeitstudien nicht-invasiv die Penetration von zweifach-fluoreszenzmarkierten NP in die Haut mit hoher Auflösung zu untersuchen. Dabei konnte zwischen Partikel-gebundenem und freiem Farbstoff unterschieden werden. Da mit dieser Technik nahezu keine „Out-of-focus“-Effekte auftreten, erscheint sie geeignet für schonende *In-vitro*- und *In-vivo*-Untersuchungen.

In einer weiteren Studie auf Haut wurden PLGA NP eingesetzt, um den Einfluss von Nanoverkapselung auf die Permeation und Penetration des lipophilen Modellarzneistoffs Flufenaminsäure (FFA) in exzidierte Humanhaut zu untersuchen.

Um FFA in NP einzuarbeiten, erwies sich die Öl-in-Wasser-Methode als am besten geeignet. Die daraus resultierenden NP besaßen eine Größe von ca. 330 nm, eine enge Größenverteilung und eine hohe Verkapselungseffizienz. Sie waren sphärisch und hatten eine glatte Oberfläche, was auch noch in der endgültigen Formulierung, d.h. nach Einarbeitung in ein Hydrogel, gewährleistet war.

Die Penetrations- und Permeationsversuche wurden mit Hilfe der *In-vitro*-Testsysteme „Saarbrücker Penetrationsmodell“ und „Franz´sche Diffusionszelle“ durchgeführt. Dabei wurde ein Vergleich zwischen dem Transport des Arzneistoffs aus einer NP-Formulierung und dem aus einer Formulierung mit freiem Arzneistoff gleichen Gehalts angestellt. Für das Stratum Corneum zeigten sich keine Unterschiede. Die Arzneistoffanreicherung in tieferen Hautschichten sowie der Arzneistofftransport über die Epidermis erwiesen sich nach kurzen Inkubationszeiten (<12 Stunden) als leicht verzögert im Falle der nanoverkapselten FFA. Nach längeren Inkubationszeiten zeigte nanoverkapselte FFA jedoch signifikant höheren Transport und Anreicherung.

Die genauen Mechanismen, die zu diesen Ergebnissen führten, sind noch nicht vollständig geklärt. Es lässt sich jedoch vermuten, dass der Partikelabbau zur Anhebung des pH-Werts in den Partikeln und in ihrer Umgebung führt. Dadurch würde FFA bevorzugt in der nicht-ionisierten Form vorliegen, was die Penetration durch das Stratum Corneum fördern würde. Die Abbildung von FFA NP auf exzidierte Humanhaut zeigte eine homogene Verteilung auf der Hautoberfläche und in den Dermatoglyphen; es wurden jedoch keine NP in oder zwischen den Korneozyten gefunden.

Entwicklung und Evaluierung von mit Biotin oberflächenmodifizierten Nanopartikeln

Im allgemeinen sind NP aus Polymeren so aufgebaut, dass die aktive Komponente im Inneren der NP verkapselt ist, während die „Targeting“-Komponente auf der Oberfläche sitzt. Für jede Formulierung muss dabei jedoch ein eigenes Verfahren entwickelt werden.

Die Zielsetzung des letzten Teils dieser Arbeit war es, eine Methode zu entwickeln, um NP, die unter Umständen bereits eine pharmakologisch aktive Komponente enthalten, oberflächlich zu modifizieren. Diese NP sollen dann unter chemisch milden Bedingungen eine Bindung von vielfältigen „Targeting“-Komponenten und

Fluoreszenzfarbstoffen ermöglichen. Der Ansatz bestand darin, NP auf ihrer Oberfläche mit Biotin zu funktionalisieren, welches Konjugate von Avidin (und seinen Homologen Streptavidin und NeutrAvidin) binden kann. Folglich sollten damit sowohl „Targeting“-Komponenten als auch Fluoreszenzfarbstoffe an diese NP gebunden werden können, vorausgesetzt sie sind als Konjugate von Avidin verfügbar.

Mit Hilfe der klassischen Öl-in-Wasser-Methode wurden NP aus PLGA in einer Größe von 210 nm hergestellt und mit Biotin-(polyethylenglycol)amin (BPEG) unter Verwendung von Cyanurchlorid als Aktivierungsreagenz funktionalisiert. Es konnte gezeigt werden, dass mit dieser Methode eine effektive Biotinylierung der NP-Oberfläche möglich war, die bei maßstabsgetreuer Betrachtung optimale Bedingungen für eine Bindung von Avidin oder von mit Avidin verknüpften Liganden darstellte. Die Oberflächenmodifizierung führte zu keinen Veränderungen der Größe, Form oder Oberflächenstruktur der NP. Jedoch waren die mit BPEG funktionalisierten NP (BPEG PLGA NP) weniger negativ geladen und wiesen deutlich veränderte elastische und adhäsive Eigenschaften auf, was durch Bindung von Avidin noch verstärkt wurde.

Die Bindung von Avidin und Homologen an BPEG PLGA NP wurde im Rahmen dieser Arbeit qualitativ nachgewiesen; eine Quantifizierung der an die NP gebundenen Proteine war mit der verwendeten inversen Methode nicht möglich. Es wurde zudem deutlich, dass eine spezifische Bindung an BPEG PLGA NP nur im Falle von NeutrAvidin gegeben ist. Zur ersten Evaluation in biologischen Systemen wurden BPEG PLGA NP durch mit Avidin verbundenen Fluoreszenzfarbstoffen markiert. Mit diesen Partikeln konnten Unterschiede im Aufnahme- und im Adhäsionsverhalten an zwei epithelialen Zelllinien aufgezeigt werden.

Publication list

Papers in refereed journals

B. Weiss, M. Schneider, S. Taetz, D. Neumann, U.F. Schaefer, C.-M. Lehr, Coupling of biotin-(polyethyleneglycol)amine to poly(D,L-lactide-co-glycolide) nanoparticles for versatile surface modification. *submitted to Bioconjug Chem (2006)*

P. Li, F. Yu, B. Weiss, Ch. Baldes, E. Meese, F. Muecklich, C.-M. Lehr, U. Bakowsky, Effects of Micropatterning by Laser Interference Lithography on Inflammatory Gene Expression. *submitted to Biomaterials (2006)*

J. Lademann, H. Richter, A. Teichmann, N. Otberg, U. Blume-Peytavi, J. Luengo, B. Weiss, U.F. Schaefer, C.-M. Lehr, R. Wepf, W. Sterry, Nanoparticles – an efficient carrier for drug delivery into the hair follicles. *Eur J Pharm Biopharm* doi: 10.1016/j.ejpb.2006.10.019 (2006)

B. Weiss, U.F. Schaefer, J. Zapp, A. Lamprecht, A. Stallmach, C.-M. Lehr, Nanoparticles made of fluorescence-labelled PLGA: preparation, stability, and biocompatibility. *J Nanosci Nanotechnol*: 6, 3048-3056 (2006)

F. Stracke, B. Weiss, C.-M. Lehr, K. König, U.F. Schaefer, M. Schneider, Multiphoton Microscopy for the Investigation of Dermal Penetration of Nanoparticle-Borne Drugs. *J Invest Dermatol*: 126, 2224-2233 (2006)

J. Luengo, B. Weiss, M. Schneider, A. Ehlers, F. Stracke, K. König, K.-H. Kostka, C.-M. Lehr, U.F. Schaefer, Influence of nanoencapsulation on human skin transport of flufenamic acid. *Skin Pharmacol Physiol*: 19, 190-197 (2006)

A. Stallmach, T. Marth, B. Weiss, B.M. Wittig, A. Hombach, C. Schmidt, M. Neurath, M. Zeitz, S. Zeuzem, H. Abken, An interleukin 12 p40-IgG2b fusion protein abrogates T cell mediated inflammation: antiinflammatory activity in Crohn´s disease and experimental colitis *in vivo*. *Gut*: 53, 339-345 (2004)

Abstracts

B. Weiss, M. Schneider, D. Neumann, N. Daum, U.F. Schaefer, C.-M. Lehr, Surface-biotinylated biodegradable nanoparticles: characterization and evaluation. AAPS Annual Meeting, October 29 - November 2, 2006, San Antonio

B. Weiss, M. Schneider, U.F. Schaefer, C.-M. Lehr, Two-color fluorescent labelled nanoparticles for multiphoton microscopy studies. 33rd Annual Meeting & Exposition of the CRS, July 22-26, 2006, Vienna

M. Schneider, B. Weiss, J. Luengo, K. König, C.-M. Lehr, U.F. Schaefer, F. Stracke, Non-invasive Investigation of the Fate of Nanoparticles and their Payload Diffusing into Human Skin. 33rd Annual Meeting & Exposition of the CRS, July 22-26, 2006, Vienna

M. Schneider, F. Stracke, K. König, B. Weiss, J. Luengo, C.-M. Lehr, U.F. Schaefer, Double labeled nanoparticles on human skin: imaging with multiphoton microscopy. Workshop on Advanced Multiphoton and Fluorescence Lifetime Imaging Techniques, June 19-21, 2006, St. Ingbert

M. Schneider, F. Stracke, B. Weiss, J. Luengo, K. König, C.-M. Lehr, U.F. Schaefer, Investigation of dermal diffusion processes in the presence of nanoparticles with multiphoton microscopy. PPP, April 18-22, 2006, La Grande Motte

B. Weiss, M. Schneider, U.F. Schaefer, C.-M. Lehr, Evaluation of surface biotinylation of PLGA nanoparticles. CRS German Local Chapter Annual Meeting, February, 23-24, 2006, Jena

M. Schneider, J. Luengo, B. Weiss, F. Stracke, C.-M. Lehr, U.F. Schaefer, Interaction of human skin with biodegradable fluorescent nanoparticles. AAPS Annual Meeting, November 6-10, 2005, Nashville

J. Luengo, B. Weiss, M. Schneider, A. Ehlers, F. Stracke, K.-H. Kostka, C.-M. Lehr, U.F. Schaefer, Effect on the human skin penetration of a highly lipophilic drug incorporated into PLGA nanoparticles. European IP – Galenos Course "Cyclodextrins and their use in life sciences", September 5-14, 2005, Lisbon

J. Luengo, B. Weiss, C.-M. Lehr, U.F. Schaefer, Influence of PLGA-nanoparticles on human skin penetration and permeation of flufenamic acid *in vitro*. AAPS Annual Meeting, November 7-11, 2004, Baltimore

B. Weiss, J. Zapp, A. Lamprecht, A. Stallmach, U.F. Schaefer, C.-M. Lehr, Preparation and characterisation of nanoparticles from aminofluorescein-labelled PLGA. AAPS Annual Meeting, November 7-11, 2004, Baltimore

B. Weiss, A. Lamprecht, A. Stallmach, U.F. Schaefer, C.-M. Lehr, New approach for investigating colon targeting by fluorescent nanoparticles. DPhG Jahrestagung and Joint-Meeting, October 7-9, 2004, Regensburg

Curriculum vitae

Name: Barbara Weiß

Date of birth: September 27th, 1977

Place of birth: Nürnberg

Education

07/2003 – 11/2006	Dissertation on ‘The potential of nanoscale carriers for drug delivery to intestinal mucosa and skin’ Biopharmaceutics and Pharmaceutical Technology, Saarland University, Saarbrücken
06/2003	Certification as Pharmacist (‘Approbation’)
11/2002 – 04/2003	Internship at Novartis Institutes of BioMedical Research, Novartis Pharma AG, Basel Diploma Thesis on ‘Optimization of the microbial production of rec. h. CYP 2D6 expressed in <i>E.coli</i> and the reaction conditions for metabolite synthesis’
05/2002 – 10/2002	Internship at Ahorn Apotheke, Nürnberg
10/1997 – 04/2002	Study of Pharmacy, University of Regensburg, Pharmaceutical Examination
09/1995 – 06/1997	Martin - Behaim - Gymnasium Nürnberg Secondary High School, Abitur (A-levels)
09/1988 – 09/1995	Labenwolf - Gymnasium Nürnberg Secondary High School

Awards

2000 and 2002	Awards of the ‘Dr. August und Dr. Anni Lesmüller-Stiftung’
1997 – 2002	Scholarship of the ‘Begabtenförderung der Bayerischen Staatsregierung’
1997	Award of the ‘Fond der Chemischen Industrie’

Danksagung

Zuerst möchte ich mich bei **Prof. Claus-Michael Lehr** für die Bereitstellung des Themas, die ideenreiche Unterstützung und die Freiräume im Rahmen meiner Arbeit bedanken.

Mein besonderer Dank gilt **Dr. Ulrich Schäfer** für seine starke Betreuung, Hilfe und Unterstützung und für viele wertvolle Diskussionen und Informationen. Danke, dass du immer ein offenes Ohr hattest!

Dankeschön an **Prof. Alf Lamprecht**, der mir beim Einstieg in die Nanopartikel-Präparation geholfen hat und mir immer freundlich als Ansprechpartner zur Verfügung stand.

Herzlichen Dank auch an **Prof. Udo Bakowsky**, der mich in der Anfangszeit mit großer Geduld mit der Funktionsweise eines AFMs vertraut gemacht hat.

Bei **Prof. Andreas Stallmach** möchte ich mich für den Beitrag zur Finanzierung dieser Arbeit bedanken.

Ein großer Dank geht an die gesamte Arbeitsgruppe für den guten Zusammenhalt und das tolle Arbeitsklima!

Besonders bedanken möchte ich mich dabei bei:

Dr. Marc Schneider, fürs Korrekturlesen dieser Arbeit. Aber vor allem möchte ich mich bei dir bedanken für deine stetige Hilfsbereitschaft, für Ideen und Gespräche, die mich wirklich weiter gebracht haben und dafür, dass du mir an vielen Dingen die positiven Aspekte gezeigt hast,

Eva, die mir mit Rat und Tat bei Transportversuchen zur Seite stand,

Sebastian, für seine Hilfe und Einsatz bei „Uptake“-Versuchen,

Petra, für die nette Einführung in die Geheimnisse der Zellkultur,

Javiana, für die gute Zusammenarbeit im gemeinsamen Projekt,

Herrn Meiers, für die Unterstützung bei der Nanopartikel-Herstellung,

Leon, für die Weiterführung der Zellkultur-Experimente,

Herrn Leist, für Hilfe im Praktikum und Labor und für die Bereitstellung diversen Pflanzenmaterials,

Stephan, Sebastian, Katharina, Andi, Ping und Frank - ihr wart coole Bürokollegen! Danke für die nette Atmosphäre, fachliche Diskussionen und für den Spaß, mit dem sich einige Katastrophen des Doktorandenlebens leichter ertragen ließen!

Dann geht natürlich ein Dankeschön an die beiden Bioinformatiker:

Dr. Dirk Neumann, für seine Hilfe bei RMS-Messungen und für viele gute Gespräche und Tipps,

Thomas, den Retter bei AFM-Problemen.

Prof. Jürgen Lademann danke ich für gute Zusammenarbeit, die dieser Arbeit zu neuen Anwendungen verhalf.

Ein herzlicher Dank für gute Zusammenarbeit geht ebenfalls an **Dr. Frank Stracke**, der enorm zur Farbigkeit dieser Arbeit beigetragen hat.

Danke auch an **Dr. Josef Zapp** für seinen Beitrag zur Polymer-Charakterisierung.

Bei meinen **Eltern** möchte ich mich dafür bedanken, dass sie mir diesen Weg ermöglicht und mich mit stetiger Ermutigung begleitet haben. Danke für eure Unterstützung und Hilfe bei allen meinen Entscheidungen!

Abschließend möchte ich mich bei **Daniel** bedanken. Abgesehen von fachlicher Hilfe hast du mir persönlich sehr viel Kraft gegeben. Danke, dass du Höhen und Tiefen mit mir durchlebt hast und dass sich in deiner Nähe vieles relativiert!

Barbara

